5-30-2016 12:00 AM

State Space Modeling of Smart PV Inverter as STATCOM (PV-STATCOM) for Voltage Control in a Distribution System

Sridhar Bala Subramanian
The University of Western Ontario

Supervisor
Dr. Rajiv K. Varma
The University of Western Ontario

Graduate Program in Electrical and Computer Engineering
A thesis submitted in partial fulfillment of the requirements for the degree in Master of Engineering Science

Abstract

The grid integration of photovoltaic (PV) systems in distribution networks is facing challenges such as transient changes in voltage due to fluctuations in generated real power and tripping of PV systems. Smart PV inverters with functions such as dynamic reactive current injection and low voltage ride through are available to mitigate these challenges. This thesis shows that a better stable performance can be obtained if these functions are implemented using the novel patent-pending technology of PV system as a dynamic reactive power compensator (PV-STATCOM). A linearized state space model of PV-STATCOM is developed to show the benefits of PV-STATCOM controls over Smart PV inverter controls in the presence of control system interaction between dc-link voltage and point of common coupling voltage controllers. These benefits are further substantiated by comparing the performance of PV-STATCOM and Smart PV inverter to perform voltage control during system disturbances simulated by irradiance changes and faults.

Keywords

Photovoltaic (PV) System, Smart PV inverter, PV-STATCOM, Voltage Flicker, Transient Voltage Changes, Low Voltage Ride Through (LVRT), State Space Model, Dynamic Reactive Current Injection, DC-Link Voltage Control, Point of Common Coupling (PCC) voltage control.

Dedicated to my:

Spiritual Guru and Parents

Acknowledgments

I would like to express my sincere and deepest gratitude for my supervisor Dr. Rajiv K. Varma for his valuable and constructive guidance throughout the course of this research work. I am also immensely thankful for the constant support and motivation which he has provided me.

I would also like to express my sincere gratitude to my industry co-supervisor, Mr. Tim Vanderheide of Bluewater Power Generation Corporation for his kind support towards the completion of this research work. I would also like to thank Maureen Glaab for her support during my stay at Bluewater Power.

I would also like to thank Dr. Lyndon Brown, Dr. Jin Jiang, Dr. Hisham Mahmood and Dr. Mehrdad Kazerani for providing me with a good understanding of electrical and control engineering concepts required for my research through their courses.

I would like to acknowledge the financial support provided by the University of Western Ontario, Natural Sciences and Engineering Research Council of Canada (NSERC), Bluewater Power Generation Corporation and Ontario Centres of Excellence.

I would like to thank my colleagues Mohammad, Sibin, Ehsan, Reza, Hesam and Vishwajeet for all their help and support during the course of my graduate program. I would also like to thank all my friends for their support during my stay in London.

I would like to thank my parents and all family members for their constant support and encouragement during my stay in Canada.

SRIDHAR BALA SUBRAMANIAN

Table of Contents

List of Tables

List of Figures

List of Abbreviations

DG	:	Distributed Generator/Distributed Generation
EMTDC	:	Electromagnetic Transients including DC
HVRT	:	High Voltage Ride Through
IGBT	:	Insulated Gate Bipolar Transistor
LVRT	:	Low Voltage Ride Through
MPPT	:	Maximum Power Point Tracking
MV	:	Medium Voltage
PCC	:	Point of Common Coupling
PI	:	Proportional Integral
PLL	:	Phase Locked Loop
PSCAD	:	Power Systems Computer Aided Design
PV	:	Photovoltaic
RMS	:	Root Mean Square
SPWM	:	Sinusoidal Pulse Width Modulation
STATCOM	:	Static Synchronous Compensator
STC	:	Standard Test Conditions
VSC	:	Voltage Sourced Converter

List of Symbols

$\overrightarrow{f}$	:	General form of space phasor
C_{dc}	:	DC Link capacitance
C_x	:	Capacitance (x is used to denote appropriate quantity. For example: line, grid etc.)
$I_{SC(STC)}$	:	PV panel short circuit current at Standard Test Conditions (STC)
I_{pv}	:	PV array output current
$I_{pvpanel}$	:	Output current of a PV panel
I_{rated}	:	Rated current of VSC
K_i	:	Temperature coefficient of PV short circuit current
K_v	:	Temperature coefficient of PV open circuit voltage
L_x	:	Inductance (x is used to denote appropriate quantity. For example: line, grid etc.)
N_p	:	Number of panels in parallel
N_s	:	Number of panels in series
P_{VSC}	:	Active power of VSC
P_{rated}	:	Rated active power of the PV system
Q_{VSC}	:	Reactive power of VSC
R_s	:	Equivalent series resistance of each cell
R_{sh}	:	Equivalent shunt resistance of each cell

R_x	:	Resistance (x is used to denote appropriate quantity. For example: line, grid etc.)
T_s	:	Temperature at STC
V_{oc}	:	Open circuit voltage of a PV panel
V_x	:	Voltage (x is used to denote appropriate quantity. For example: line, grid etc.)
V_{xd}	:	d-axis voltage (x is used to denote appropriate quantity. For example: line, grid etc.)
V_{xq}	:	q-axis voltage (x is used to denote appropriate quantity. For example: line, grid etc.)
b_1,K_{pi1}, K_{pi2}, K_{ii1}, K_{ii2}, K_{pv}, K_{iv}, K_{pvs}, K_{ivs}, b_2, K_{droop}	:	Controller Gains of Current controller, DC-link voltage controller, PCC voltage controller and PLL.
f_s	:	Frequency of the grid supply (in Hz)
i_{xd}	:	d-axis current (x is used to denote appropriate quantity. For example: line, grid etc.)
i_{xq}	:	q-axis current (x is used to denote appropriate quantity. For example: line, grid etc.)
i_x	:	Current (x is used to denote appropriate quantity. For example: line, grid etc.)
m_d	:	d-axis modulation index
m_q	:	q-axis modulation index
n_p	:	Number of cells in parallel per panel

n_s	:	Number of cells in series per PV panel
u_d, u_q	:	Control Inputs of current controller
x_1	:	Substation transformer turns ratio
$x_3, x_4, x_5, x_6, x_7, x_8$	:	State Variables
$\tilde{y}, \tilde{u}, \tilde{x}$	:	Generalized form for linearized output, input and state variable.
$\tau_1, \tau_2, \tau_{Vdc}$	:	Time constants of filter
ω_o	:	Angular frequency of the grid supply at Steady State
L	:	Laplace transform operator
G	:	Solar Radiation or Irradiance
T	:	Operating temperature of the PV panel
k	:	Boltzmann's constant
n	:	Diode ideality factor
q	:	Charge of an electron
ρ	:	ρ is the reference angle of *dq* frame
ω	:	Angular frequency of the grid supply

List of Appendices

Chapter 1

1 INTRODUCTION

1.1 General

The use of renewable energy based sources for electricity generation has been on the rise globally as they represent one of the alternate and clean sources of electricity. The benefits include reduction in green-house gas emissions, energy security, strategic economic development, energy access through off-grid solutions etc. [1]. Among them, Solar Photovoltaic (PV) Systems are one of the most fastest growing renewable energy based distributed generators that are getting integrated into distribution networks worldwide [2]. The growth has been significant in Canada over the past few years by introduction of many government incentive programs such as Feed-in Tariff program, Renewable Energy Standard Offer program etc. [3]. The total installed capacity of PV system exceeds 1000 MW as of 2014 [4]. The growth of solar PV systems is expected to increase by over 3000 MW in the period from 2014 to 2040 [5].

1.2 Challenges for Grid Integration of PV systems

The increase in penetration of solar PV systems at distribution level has created a number of issues in the existing distribution systems for utilities. This is serving as a barrier for the grid integration of new PV systems in distribution networks. Some of the main issues include:

i) Voltage rise due to reverse power flow from PV systems during high PV generation and light load conditions [6].

ii) Conductor and Equipment loading due to additional generation on the distribution feeders [7].

iii) Increased switching operations of voltage regulating devices such as switched capacitor banks, tap changing transformers[7].

iv) Increase in harmonics generated by PV systems and resonant interactions of inverters with distribution systems[7].

v) Flicker in voltage due to rapid fluctuation in the generation of real power by PV systems[7].

vi) Coordination of protective devices due to increase in short circuit current contribution by PV systems during faults[8].

vii) Increase in losses due to reverse power flow from PV systems[8]

viii) Temporary Over-voltage due to increase in short-circuit current contribution by PV systems during faults[9]

ix) Transient changes in voltage and sudden loss of generation due to sudden trip of PV systems [7], [10].

The issues that are dealt with in detail in this thesis are described in the following sections.

1.2.1 Voltage flicker due to fluctuation in real power generated by PV systems

Voltage flicker is defined as the low frequency variations in voltage in distribution networks. They are caused by industrial loads such as arc furnaces, welding systems, electric boilers etc.[11] that draw fluctuating power at low frequencies. The concept of voltage flicker has now been extended to many kinds of voltage fluctuations through the use of short term flicker assessment and long term flicker assessment [7].

Voltage flicker is also caused in distribution system by rapid fluctuations of real power supplied by PV system due to cloud passing [7]. This is also one of major issues that occur in distribution networks due to high penetration of PV systems. This issue also serves as one of the barriers that limits the interconnection of PV based renewable energy power system [2].

The voltage flicker is generally estimated by using the standards developed by the International Electro Technical Commission [7, 12]. For accurate estimation of voltage flicker, long simulations in the order of minutes have to be performed. If the flicker due to PV power fluctuations is to be studied, detailed solar irradiance data has to be available for performing the studies. Flicker can also be simulated by performing an instantaneous drop of PV output from 100% to 0% if accurate solar irradiance data is not available[8].

The standard industry practice to evaluate the voltage flicker is by using GE flicker curve [8]. The flicker curve is shown in Figure 1.1.

In [8], the flicker limit for 100 % drop in irradiance is considered to be 3 % based on the assumption that this drop occurs once per hour. In Figure 1.1, 3% is the limit for borderline of visibility of flicker when the voltage dip occurs once per hour. The same limit has been adopted for the voltage flicker studies in this thesis.

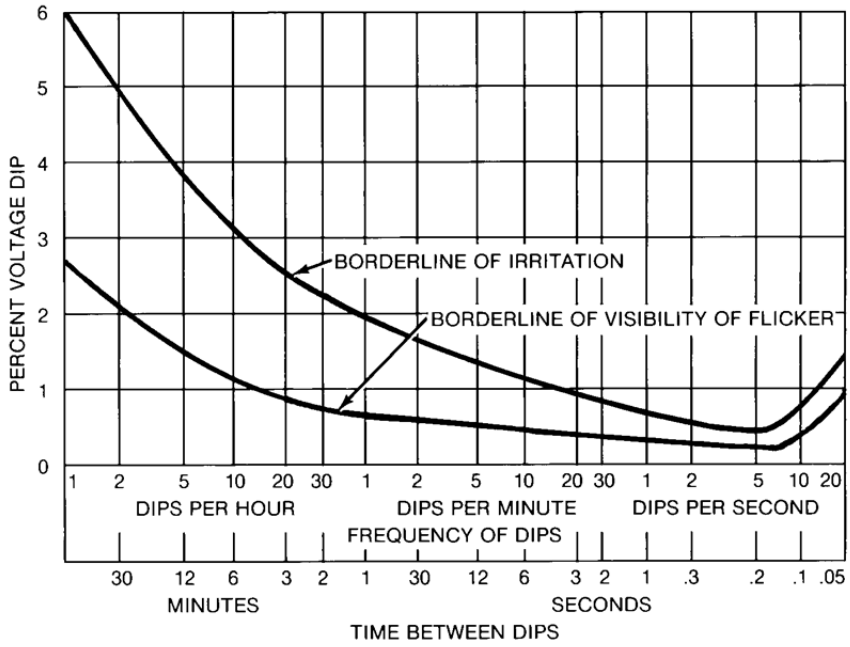

Figure 1.1 Voltage flicker curve [13] (© [1994] IEEE)

1.2.2 Voltage changes due to sudden trip of PV systems

PV systems connected to distribution network are generally required to trip within a certain period of time when the voltage at its terminals dips and stays below a certain value due to fault or any other event. The guidelines provided by IEEE standard 1547-2003 [14] are in general applicable to these PV systems. In a particular high PV penetration scenario, the sudden tripping of PV systems could lead to some of the following events:

i) Transient voltage changes or disturbances on the distribution system which might cause power quality problems such as flicker for load customers [15]

etc. These could also lead to cascading impacts on the distribution system such as tripping of other equipments etc. [8]

ii) Sudden loss of generation which could affect the stability of the grid and could lead to grid failure [16]

This issue also serves as one of the main barriers that limit the interconnection of PV systems.

1.3 Modeling and Control of Conventional PV System

The issues due to high penetration of PV systems are outlined in the previous sections. Two of the issues which are dealt with in this thesis are also described in detail. Before proceeding to understand the methods available to solve these issues, it is essential to understand the operation and modeling of a conventional PV system.

The conventional PV system refers to the PV system that is being utilized for only supply of real power generated by PV panels. It can be categorized into two types namely three phase single-stage and three phase two-stage PV systems. The scope of this thesis is limited to studies with three phase single stage PV system. The individual components and their models, overall system state space model and conventional control mode of operation are briefly explained in this section.

1.3.1 Components and their models

The components of conventional PV system include the power circuit components and control circuit components. The major power circuit components include PV panel array, PV inverter, output low pass filter and interconnection or coupling transformer [17]. The major control circuit components include phase locked loop (PLL), current controllers, dc-link voltage controller, maximum power point tracker [17]. The control of PV system is usually carried out in dq-frame [18]. The designs of various power and control circuit components have been widely discussed in the literature [17], [19], [18].

1.3.2 State Space Model of overall PV system

The state space model of a PV system is required to study its stability when it is integrated with distribution networks. Since this thesis deals with modeling studies, an

understanding of modeling of conventional PV system is required before proceeding further.

The overall state space model of PV system is nonlinear and the state variables are not decoupled from each other. Although there are many different mathematical models available for single-stage PV system, the main difference arises based on how the equations are linearized and how the state variables are decoupled. In [20], [21], robust controller based on partial feedback linearization approach for the overall state space model of PV system is proposed. In [17], [19] and [18], a control approach based on feed-forward decoupling approach is proposed. In this model, dynamics of current controllers, dc-link voltage controller and PLL are decoupled from each other by the use of feed-forward decoupling terms. An overall linearized state space model is proposed in [19] to study the interaction between PV system and distribution network.

1.3.3 Conventional mode of operation

IEEE standard 1547-2003 [14] provides guidelines for the operation of PV systems connected to distribution network. As per this standard, PV systems are not allowed to perform voltage regulation. This means that they are required to operate in unity power factor of operation. Hence, the reactive power supplied by PV system is generally regulated to zero and they supply the maximum real power generated.

1.4 Modeling and Control of Smart PV inverter

The operation and modeling of conventional PV system is described in the previous section. Now, the modeling and control of smart PV inverter is described in the following sections.

It was pointed out that increase in penetration of PV systems in distribution systems is limited due to issues pointed in section 1.2. One of the most direct approaches to solve some of these issues and increase the penetration of PV systems is by expensive grid

reinforcement measures [22]. Instead, some of these issues can be solved by using the additional capabilities of PV inverters [22], [7].

1.4.1 Smart PV inverter

The additional capabilities of PV inverters that can be used to solve some of the issues due to increase in penetration of PV systems are called “Smart Functions” and such an inverter is called smart PV inverter [23], [24]. Hence, smart PV inverter refers to PV inverter of a PV system which performs real power control (similar to a conventional PV system) and also performs some additional functions. These functions are helpful in minimising some of the expensive grid reinforcement measures and increase the penetration of PV systems in distribution networks [25], [22].

1.4.2 Control of Smart PV inverter

The control of smart PV inverter refers to the realization of required smart inverter function. The following are some of the common smart inverter functions [26]:

i) Volt/Var control: This represents the regulation of ac voltage by controlling the injection/absorption of reactive power of inverter
ii) Volt/Watt control: This represents the regulation of ac voltage by controlling the injection/absorption of active power of inverter
iii) Low/High Voltage Ride Through (LVRT/HVRT): This refers to control of PV inverter so that it stays online for a certain period of time without disconnecting during high or low voltage event caused by a system disturbance such as a fault etc.
iv) Dynamic Reactive Current Injection: This represents the regulation of ac voltage by controlling the injection/absorption of reactive current of inverter

A detailed explanation of all the smart inverter functions can be found in [26]. A brief explanation of the functions that are dealt with in this thesis is provided below.

1.4.2.1 Volt/Var Control

One of the methods available in literature for the control of voltage rise due to active power feed-in by PV systems is Volt/Var (Voltage (V) / Reactive Power (Q)) control

[24]. In this method, the ac voltage controller of each inverter is provided with a droop based Volt/Var curve as shown in Figure 1.2.

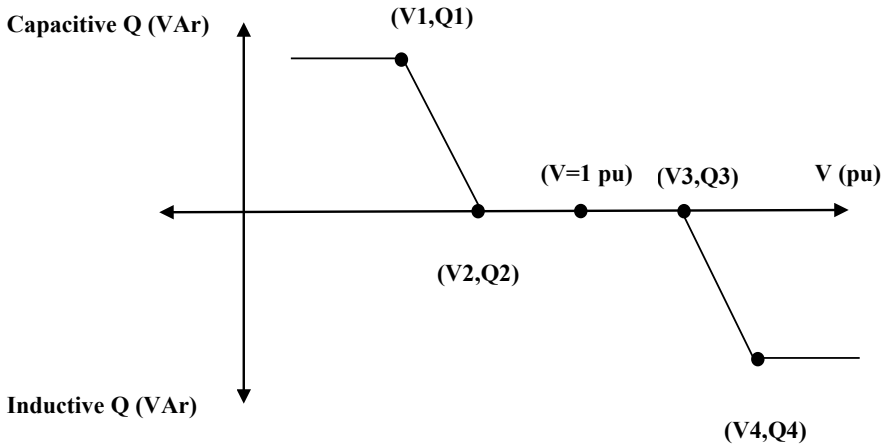

Figure 1.2 Typical Volt/Var Curve [26]

With reference to Figure 1.2, the curve has the following regions namely:

(a) Linear region with reactive power injection (capacitive) (Region between points (V1,Q1) and (V2,Q2))
(b) Linear region with reactive power absorption (inductive) (Region between points (V3,Q3) and (V4,Q4))
(c) Dead band region with zero reactive power injection / absorption (Region between points (V2,Q2) and (V3,Q3))
(d) Saturation region with constant reactive power injection (Region after (V1,Q1))
(e) Saturation region with constant reactive power absorption (Region after (V4,Q4))

The points in the Volt/Var curve can be chosen according to the distribution feeder characteristics and grid code to be followed. The curve can be configured with or without a dead band region based on the required voltage level and reactive power consumption.

The slope of linear region of the curve can be decided based on the required reactive power to mitigate the voltage rise caused by active power feed-in of PV systems.

1.4.2.2 Dynamic Reactive Current Injection

Dynamic reactive current injection is one of the methods available for PV inverters to mitigate issues related to dynamic variations in voltage such as voltage flicker, to provide voltage support during LVRT etc. It is one of the methods in which the PV system utilizes its remaining reactive power capacity (if available) to control the voltage. If required, the PV system has to curtail some of its active power to free some room for reactive power and then perform voltage control [26]. This is utilized in conjunction with other steady state reactive power controls. The characteristic of dynamic reactive current injection is shown in Figure 1.3 [26]. The voltage deviation is the error between reference and the actual value of voltage. The Reference voltage is the moving average voltage that exists over a period of time before the occurrence of voltage deviation. The slope of the curve determines the magnitude of capacitive or inductive reactive current injected for a particular voltage deviation. The dead band is the region where no reactive current is injected and is usually chosen depending on the allowable value of voltage deviation. The characteristic namely the slope of curve and dead-band region will vary depending on the application.

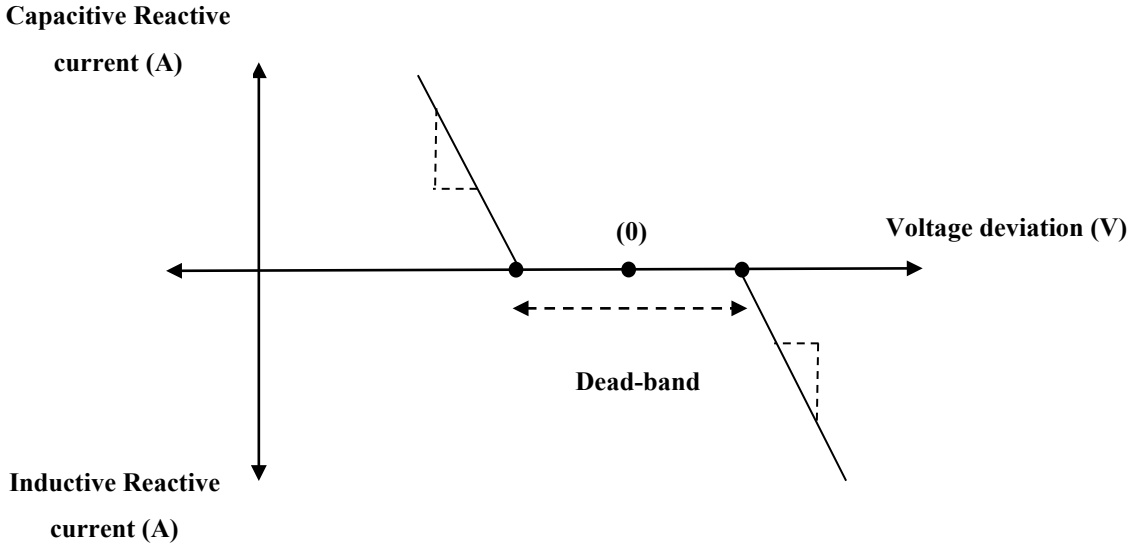

Figure 1.3 Characteristic of dynamic reactive current injection [26]

1.4.2.3 Low Voltage Ride Through (LVRT)

Low Voltage Ride Through is the capability of a PV system to stay online for a certain period of time without disconnecting during a low voltage event caused by a system disturbance such as a fault etc. This was initially the requirement for distributed generators connected to transmission systems but has now become a requirement for MV distribution systems [7]. The requirement is needed to ensure that the generators stay online during the disturbance and ready to supply power after the disturbance so that the issues due to sudden trip of PV systems can be minimized (For instance, high loss of power after the disturbance is averted [10]).

Present grid codes also require the PV systems to supply reactive power when they are performing the ride-through operation. This is required in order to stabilize the voltage level of the grid during fault and thereby prevent loss of other distributed generators etc.[27]. The reactive power injection has been defined in various grid codes by using a relation between the voltage dip during fault and the magnitude of reactive current to be injected. The characteristic defined by German grid code has been adopted in this thesis [28] as shown in Figure 1.4.

The relation between reactive current and voltage of Figure 1.4 can be implemented using dynamic reactive current injection function of smart PV inverter [12], [27].

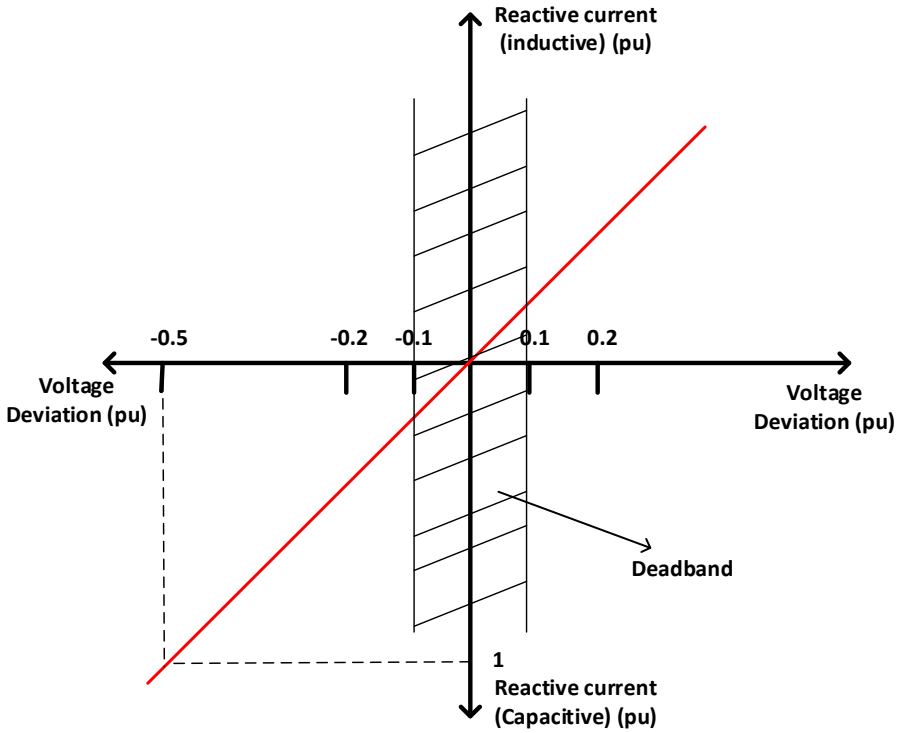

Figure 1.4 LVRT Characteristics as per German grid code [28]

1.4.3 Modelling of Smart PV Inverter

The model of a smart PV inverter incorporates the features of a conventional PV system and includes other components, depending on the smart functions to be implemented. The use of a smart PV inverter for voltage control is studied in this thesis and hence, the model with voltage control functionality is utilized for studies.

In general, a large PV power plant consists of a number PV inverters connected in parallel. A size and number of PV inverters used in a PV power plant will depend on its rating. For large power system studies, the entire PV power plant is represented by a single equivalent PV system [12]. A generic model of such a PV system with point of common coupling (PCC) voltage control capability has been proposed by WECC Renewable Energy Modeling Task Force [29], [12]. Qualitatively, it is basically an extension of the model proposed in [17] for unity power factor of operation of a conventional PV system. This represents the model of a smart PV inverter with voltage control functionality and is shown in Figure 1.5.

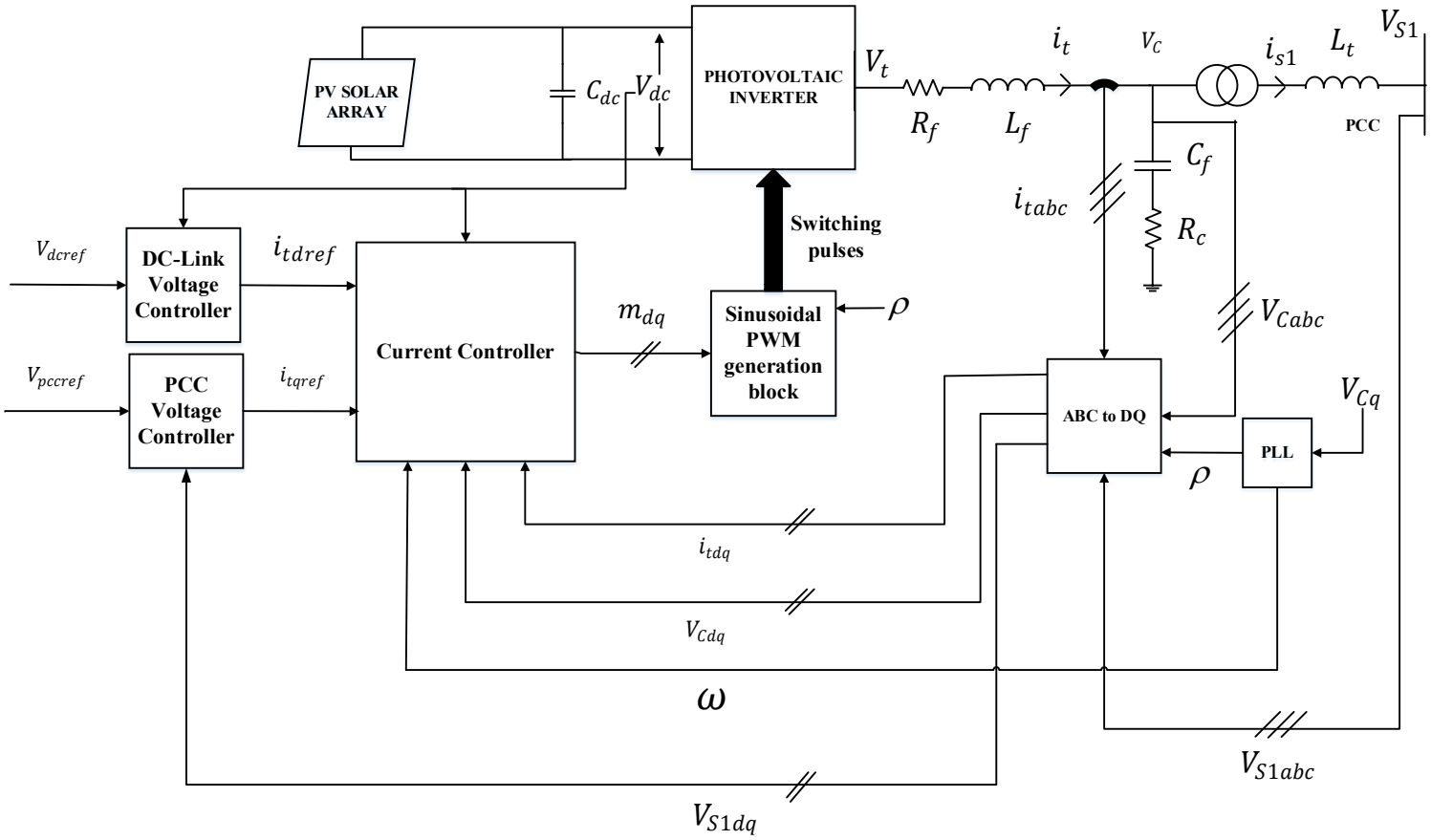

Figure 1.5 Model of a Smart PV Inverter

The quantities and variables presented in Figure 1.5 are described as follows: C_{dc} is the DC link capacitance, V_{dc} is the DC link voltage of PV system, V_t is the inverter terminal voltage, R_f is the sum of equivalent ON state resistance of power electronic component used in photovoltaic inverter and damping resistor of low pass filter, L_f is filter inductance, C_f is filter capacitance, R_c is also a damping resistor of low pass filter, i_t is the inverter output current, V_c is the voltage at the output of filter, i_{s1} is the output current of coupling transformer, V_{s1} is voltage at the output of coupling transformer (PCC voltage), L_t is the equivalent leakage inductance of coupling transformer, ρ is angle reference generated by phase locked loop (PLL) to synchronize PV system with the frequency of PCC which is represented by ω. ρ is also required for conversion of signals from *abc* to *dq* frame [18]. The signals with subscripts *abc* and *dq* represent the corresponding signals in the respective frames.

A detailed description of the functioning of different components of Figure 1.5 can be found in [18], [17] and is also presented in chapter 2. A brief description is provided in this section. The dc-link voltage controller compares the dc-link voltage V_{dc} with its reference V_{dcref} and generates the real current reference i_{tdref}. This eventually controls the real power output of PV system. The PCC voltage controller compares the PCC voltage with its reference V_{pccref} and generates the reactive current reference i_{tqref}. This eventually controls the reactive power output of PV system. The current controller (which controls inverter real current i_{td} and reactive current i_{tq}) generates the modulation index signals m_{dq} which eventually generate the sinusoidal pulse width modulation (PWM) signals required for photovoltaic inverter operation.

Having understood the overall functioning of the model of smart PV inverter, the implementation of smart inverter functions such as volt/var control and dynamic reactive current injection have to be understood.

The volt/var control of smart PV inverter is implemented using a similar control structure proposed in [30] where the PCC voltage is regulated by controlling the inverter output

reactive current. The PCC voltage control structure of volt/var control is of proportional controller type and the speed of response is determined by the response time of reactive current controller which is usually in the order of seconds. It has been pointed out in [30] that the PCC voltage is influenced by the delays in voltage after measurement due to signal processing (filtering, RMS computation etc.), communication delays etc. and this influences the stability of volt/var control.

The voltage support provided by dynamic reactive current injection during LVRT requires the measurement of voltage at the point of grid connection and injection of reactive current by PV system at the low voltage side of interconnection transformer [28]. This basically involves measuring the PCC voltage and controlling the reactive current output of PV inverter [31]. Dynamic reactive current injection can be implemented by using a proportional type PCC voltage controller [12]. In [27], it is shown that the voltage deviation is related to reactive current by a constant which can be represented by a proportional controller implementation. The response time of the current controller is low in the range of milli seconds.

1.4.4 Need for further research on Smart PV inverter modeling

DC-link voltage control loop and PCC voltage control loop are coupled in a distribution network when resistance is not negligible compared to reactance [17], [32]. The effects of this coupling on stability can be minimized by designing the PCC voltage controller bandwidth to be 2 to 10 times smaller than the dc-link voltage controller bandwidth [32]. But, the bandwidth of PCC voltage controller can be closer to the bandwidth of dc-link voltage controller for functions such as dynamic reactive current injection and this affects the coupling between the control loops. This coupling influences the stability of smart PV inverter. This issue has not been studied to the best knowledge of the author in the literature and hence, needs to be studied.

The effect of delays in voltage after measurement affects the stability of Volt/Var control [30]. These delays arise from voltage RMS computation, filtering, communication (between inverter controllers or between external controller and inverter) etc. The typical values of these delays can usually be in the range of milli seconds. These delays

potentially have an effect on the stability of dynamic reactive current injection control. This issue has not been studied to the best knowledge of the author in the literature and hence, needs to be studied.

In the smart inverter control system of Figure 1.5, grid voltage (V_c) is used as feed-forward signals to improve the performance of current controller [18]. These signals also suffer from delays after measurement. These delays in feed-forward voltage signals could affect the stability of smart PV inverter. This could also affect the interaction between dc-link voltage and PCC voltage control loops. The stability of functions such as volt/var control, dynamic reactive current injection etc. is also influenced by this interaction. These issues have not been studied to the best knowledge of the author in the literature and hence, needs to be studied.

For performing all the above indicated studies, a detailed linearized state space model of the smart PV inverter is required. The model can be used to perform eigenvalue based stability studies and the stability of smart PV inverter can be analyzed.

1.5 Control of PV solar system as STATCOM (PV-STATCOM)

This section deals operation and control of another category of device called PV-STATCOM whose function is similar to a Smart PV inverter. This can also be used to solve issues due to high penetration of PV systems.

In order to understand the operation of PV-STATCOM, an introduction to STATCOM is necessary. STATCOM (Static Synchronous Compensator) is shunt connected reactive power compensation device capable of generating / absorbing reactive power. It is usually implemented using voltage-sourced converters [33]. Some of its applications in distribution systems include dynamic voltage control, voltage flicker mitigation [33], [34] etc.

PV-STATCOM deals with the application of PV system as a dynamic reactive power compensator (as STATCOM). This is a novel patent-pending technology that has been developed in [35], [36].

1.5.1 Concept of PV-STATCOM

The PV-STATCOM operates in three modes of operation namely [37],

a) Full PV mode: The PV-STATCOM system supplies only real power and zero reactive power. This is similar to the operation of conventional PV system.

b) Partial PV-STATCOM mode: The PV-STATCOM supplies real power and utilizes the remaining available free inverter capacity for reactive power control.

c) Full STATCOM mode: The PV-STATCOM curtails its real power completely and acts as a STATCOM with full reactive power capacity.

1.5.2 Applications of PV-STATCOM

The reactive power capability of PV-STATCOM has also been used to solve some issues due to high PV penetration similar to a Smart PV inverter. In [36], it has been shown that the power transfer capability of transmission lines can be increased by using PV-STATCOM. In [38], it has been shown that the PV-STATCOM can perform voltage regulation and power factor correction in a distribution network. In [39], the application of PV-STATCOM for preventing the voltage instability of a critical induction motor load is shown. In [40], it has been shown that the PV-STATCOM can be used for mitigating temporary over-voltage.

1.5.3 Control of PV-STATCOM

The applications such as voltage regulation, temporary over-voltage mitigation etc. requires the PV-STATCOM to operate in PCC voltage control mode. For these applications, the control of PV-STATCOM is similar to a STATCOM.

The PCC voltage control structure of a STATCOM is usually a PI compensator [41], [18]. The dynamic V-I droop characteristic can be chosen depending on the application

[33]. This PI compensator based PCC control strategy has also been utilized for PV-STATCOM control in [36].

1.5.4 Need for further research on PV-STATCOM modeling

The overall model of a PV-STATCOM utilized for PCC voltage control can also be considered to be similar to a model of smart PV inverter shown in Figure 1.5. The only difference is that the PCC voltage control structure is a PI controller with a V-I droop characteristic. This also shows that functions such as volt/var control, dynamic reactive current injection can also be implemented using a PV-STATCOM.

All the issues pointed out in section 1.4.4 also need to be studied for PV-STATCOM controls. These issues need to be studied in all three modes of operation of a PV-STATCOM. For this purpose, a detailed linearized model of PV-STATCOM needs to be developed.

1.6 Scope of thesis

A number of issues which requires further research are pointed out in section 1.4.4 and section 1.5.4. This thesis deals with study of one of the issues which is interaction between dc-link voltage control loop and PCC voltage control loop due to delays in feed-forward grid voltage signals of PV inverter control system. In order to study this issue, a detailed linearized state space model of PV system with voltage control functionality is required. There are some detailed state space models for PV system with voltage control / reactive power control functionality available in literature [42], [43] and [44]. To the best knowledge of the author, there is no model available in the literature that can be used to perform studies on interaction between dc-link voltage and PCC voltage control loops due to delays in feed-forward grid voltage signals. The development of such a detailed model is one of the main contributions of this thesis. The developed model will be used to study this interaction in all three modes of operation of PV-STATCOM.

It is pointed that smart inverter functions such as volt/var control, dynamic reactive current injection can be implemented using both smart PV inverter controls (proportional type PCC voltage controller) and PV-STATCOM controls (PI type PCC voltage

controller). The interaction between dc-link voltage and PCC voltage control loops due to delays in feed-forward grid voltage signals exists for both smart PV inverter controls and PV-STATCOM controls. Hence, eigenvalue sensitivity analysis to control system parameters [45], [30] is utilized to compare the performance of both smart PV inverter and PV-STATCOM controls in the presence of this interaction.

The results of the eigenvalue analysis are further substantiated by comparing the performance of smart PV inverter controls and PV-STATCOM controls when the PV system is performing voltage control for mitigating issues due to high PV penetration such as voltage flicker and transient voltage changes due to fault.

1.7 Objectives of Thesis

The objectives of thesis are as follows:

1. To develop a detailed linearized state space model of PV-STATCOM which is capable of operating in all three modes of operation of PV-STATCOM and with which the performance of Smart PV inverter controls can be studied.

2. To perform Eigenvalue sensitivity analysis and, compare the performance of smart PV inverter controls and PV-STATCOM controls in the presence of interaction between dc-link voltage and PCC voltage control loops due to delays in feed-forward voltage signals.

3. To compare the stability of smart PV inverter function namely dynamic reactive current injection when implemented using PV-STATCOM controls and Smart PV inverter controls for the following cases:

- Voltage Control during system disturbances: For mitigating voltage flicker due to sudden change in irradiance for a single PV system and two PV systems

- Voltage Control during large system disturbances: For performing voltage support during LVRT with single PV system and two PV systems

The simulations in this thesis are carried out using MATLAB and PSCAD / EMTDC softwares. The tools of MATLAB are also used for controller design and all other studies carried out in this thesis.

1.8 Thesis Outline

Chapter 1 provides an overview of challenges due to high PV penetration faced in distribution networks with regard to grid integration of PV systems. The application of Smart PV inverter and PV-STATCOM to mitigate some of the issues is presented. The issues that need to be studied and the need for a detailed state space model of PV system with voltage control functionality for stability studies are highlighted. The scope and objectives of this thesis are developed and are stated.

Chapter 2 presents a detailed modeling of various subsystems of a Solar Photovoltaic (PV) farm operating as a PV-STATCOM which is connected to a realistic distribution feeder. The nonlinear mathematical model of the entire system is first developed and is then linearized for performing small signal stability studies. The linearized models of PV-STATCOM in different modes of operation are presented.

Chapter 3 deals with the design of various controllers of PV-STATCOM operating under Full PV, Partial PV-STATCOM and Full STATCOM modes. The various controllers are designed based on linear control techniques and Eigenvalue sensitivity analysis studies. The model of PV-STATCOM operating in all three modes is then validated by comparing the linearized and PSCAD / EMTDC model responses. Under partial PV-STATCOM operation, an interaction between dc-link voltage control loop and PCC voltage control loop is pointed out by eigenvalue and participation factor analysis studies. A comparative Eigenvalue sensitivity analysis study is carried out to understand the range of various parameters that affect the stability PCC voltage controller in the presence of this interaction.

Chapter 4 deals with the application of partial PV-STATCOM for performing voltage control during system disturbance which is a voltage flicker due to irradiance change. The performance of three types of voltage control strategies namely proportional

controller based dynamic reactive current injection, Volt/Var control and PI controller based dynamic reactive current injection are compared under the condition of worst-case scenario for the interaction between dc-link voltage control loop and PCC voltage control loop. The studies are initially performed with a single PV system performing voltage control. They are later extended to the case where there are two similar PV systems performing simultaneous voltage control to mitigate voltage flicker.

Chapter 5 deals with the application of partial PV-STATCOM and full STATCOM to perform voltage control during large system disturbance which is introduced by a three phase fault. The ability of PV system to ride-through and provide stable voltage support during the fault and to continue providing stable voltage support post fault is studied. The performance of three types of voltage control strategies namely proportional controller based dynamic reactive current injection, PI controller based dynamic reactive current injection and PV system operating in Full STATCOM mode are compared under the condition of worst-case scenario for the interaction between dc-link voltage control loop and PCC voltage control loop. The studies are initially performed with a single PV system. They are later extended to the case where there are two similar PV systems performing simultaneous voltage support during and post faults. Also, the effect of X/R ratio of distribution feeder on the effectiveness of PCC voltage control is compared when two PV systems inject only reactive power and, a combination of active and reactive powers during voltage support.

Chapter 6 concludes this thesis work and also provides recommendations for further research.

Chapter 2

2 MODELING OF PV-STATCOM

2.1 Introduction

This chapter presents a detailed modeling of various subsystems of a Solar Photovoltaic (PV) farm operating as a PV-STATCOM which is connected to a realistic distribution feeder. The nonlinear mathematical model of the entire system is first derived in space phasor domain and transformed into synchronous *dq* frame. The nonlinear model is then linearized by using Taylor series expansion method for performing small signal voltage stability studies. The linearized model of PV-STATCOM operating in different modes of operation (namely Full PV, Partial PV-STATCOM and Full-STATCOM) is then explained in detail.

2.2 Study System Description

A realistic medium voltage distribution feeder is used to represent the distribution network which is used as a study system in this thesis. The system data is adapted from an actual Hydro One distribution feeder in Ontario [40]. The data for the study system is provided in Appendix B. The distribution feeder is connected to the substation grid through a step up substation transformer. The load on the feeder is represented by a constant RL load, representing the peak load on the feeder during day time. The study system with one PV-STATCOM is shown in Figure 2.1. The modeling of this system is first carried out and then, stability studies are performed. Studies are later extended to the case where there two PV-STATCOMs as shown in Figure 2.2 in chapters 4 and 5.

With reference to Figure 2.2, it should be noted that the actual Hydro One distribution feeder contains one 8.5 MW PV system and one 9.9 MW wind power system [40]. But, the wind power system is replaced by a PV system of same rating in chapters 4 and 5 for simulation studies. This has been performed only for the sake of studies in this thesis as the scope of this thesis is restricted to studies with PV systems.

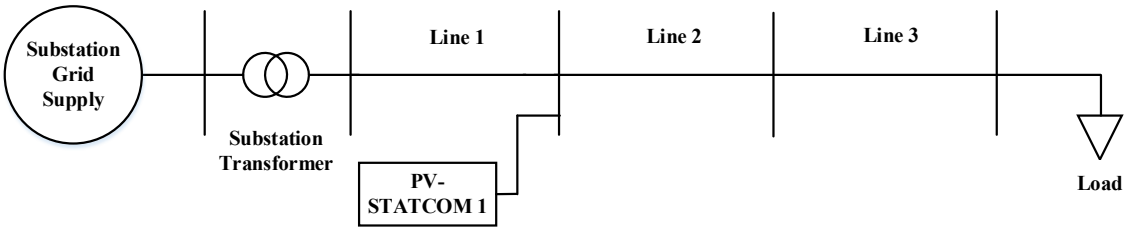

Figure 2.1 Study System with one PV-STATCOM

2.3 Distribution Network Subsystem

The distribution network subsystem consists of the substation grid supply, substation transformer, distribution line and the feeder load. This subsystem is referred to as subsystem 1 in this thesis. The modeling of each component [40] is explained in detail in the following sections.

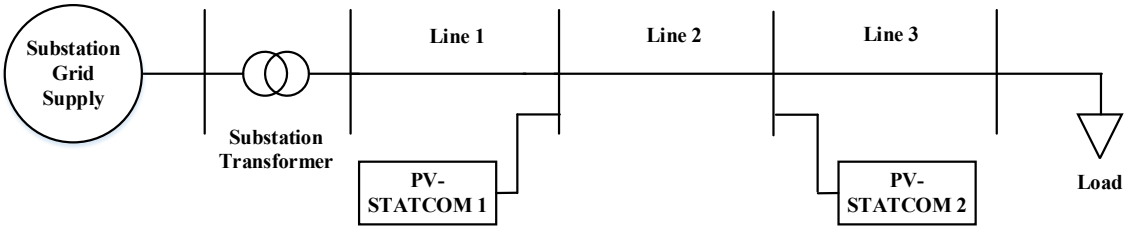

Figure 2.2 Study System with two PV-STATCOMs

2.3.1 Substation Grid Modeling

The Grid feeding the distribution line is modeled as a voltage source behind source impedance as shown in Figure 2.3. The source impedance consists of equivalent short – circuit resistance R_g and equivalent short-circuit inductance L_G. The source voltage is denoted by V_g.

2.3.2 Substation Transformer Modeling

A step down transformer is used to interconnect the grid that supplies power at a high voltage level with the distribution network at a low voltage level. The equivalent circuit of the transformer consists of series and shunt parameters. The shunt parameters, which include the shunt resistance and inductance, represent the fixed loss (eddy current and

hysteresis losses) and core flux respectively. The series parameters which include the series resistance and inductance represent the copper loss and leakage flux of the windings respectively. The shunt parameters are very high and hence, are neglected for overall power system analysis. The copper losses are negligible when compared to the network losses and hence, the series resistance is also neglected. Hence, the transformer is modelled as an ideal transformer in series with its leakage inductance L_{tm} and is shown in Figure 2.4.

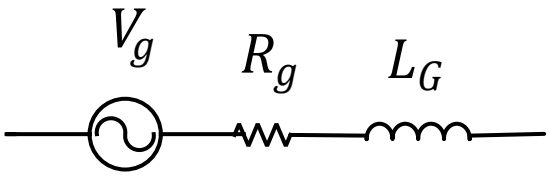

Figure 2.3 Substation Grid Model

2.3.3 Distribution Line Modeling

Electrical parameters of a distribution line are based on size of conductors and their configuration. The medium voltage distribution line is represented by a lumped equivalent π circuit model. The series parameters include the series resistance *R* and series inductance *L*. The shunt parameters include the conductance and capacitance *C*. The shunt conductance is negligible for overhead lines. The resulting equivalent π circuit model is used to represent each distribution line and is shown in Figure 2.5. The parameters are given by:

$$R = r * l \tag{2.1}$$

$$L = \frac{x_l * l}{2 * \pi * f_s} \tag{2.2}$$

$$C = \frac{l * b}{2 * \pi * f_s} \tag{2.3}$$

Where, l is the line length,

f_s is the frequency of the grid supply,

r , x_l, b is the resistance, reactance and susceptance per unit length of the distribution line respectively.

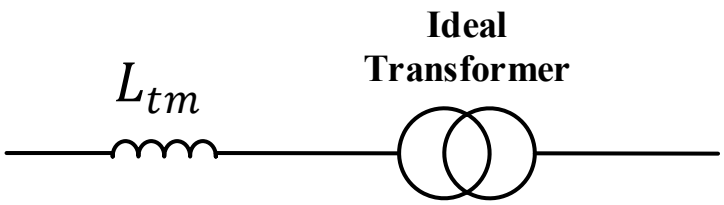

Figure 2.4 Substation Transformer Model

2.3.4 Load Modeling

The load in a distribution network consists of various types of heating, lighting and motor loads. Each load has a different performance characteristic. The equivalent characteristic of the load viewed from medium voltage side (secondary of the feeder step down transformer) will be obtained by the net effect of all loads. The net active and reactive powers of a load are affected by the system voltage and frequency from the network side [46].

In this thesis, the load is modeled as a constant impedance load as shown in Figure 2.6. The series resistance R_L and series inductance L_L represent the active power and reactive power of the load at nominal voltage respectively. The load is considered to be lumped at the receiving end of the feeder.

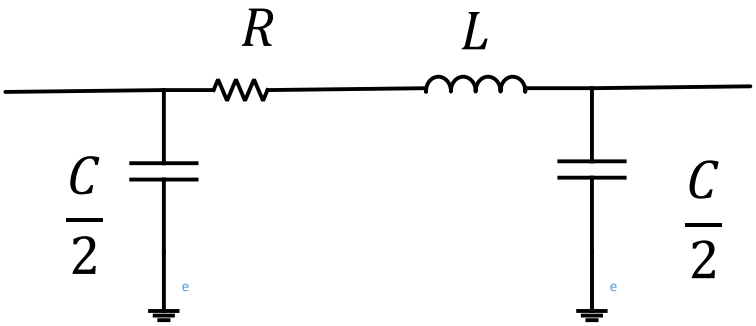

Figure 2.5 Distribution Line Model

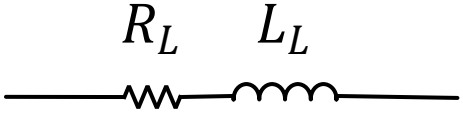

Figure 2.6 Load Model

2.3.5 State Space Model

The circuit model of the network shown in Figure 2.1 is given in Figure 2.7. The various electrical parameters are defined as follows:

R_g and L_G : Equivalent short circuit grid resistance and inductance respectively

L_{tm} : transformer leakage inductance referred to grid side

x_1 : transformer turns ratio

R_1, L_1, C_1, C_2 : Resistance, Inductance and leakage capacitance of the distribution line between buses 1 and 2 (Line 1)

R_2, L_2, C_3, C_4 : Resistance, Inductance and leakage capacitance of the distribution line between buses 2 and 3 (Line 2)

R_3, L_3, C_5, C_6 : Resistance, Inductance and leakage capacitance of the distribution line between buses 3 and 4 (Line 3)

R_L and L_L : Load resistance and inductance respectively

ω : Angular frequency of the grid supply

The various voltages and currents in space phasor domain are defined as follows:

V_g and i_g : Grid voltage and current respectively

$\widehat{V_g}$: Peak value of the grid voltage.

ω_o : Steady state angular frequency of the grid supply

V_1, V_{s1}, V_{s2} and V_L: Voltage at bus 1, 2, 3 and 4 respectively.

i_1 : Current flowing into bus 1.

i_{12} : Current flowing between bus 1 and 2 through R_1 and L_1

i_{23} : Current flowing between bus 2 and 3 through R_2 and L_2

i_{34} : Current flowing between bus 3 and 4 through R_3 and L_3

i_{s1} : Current flowing into bus 2

i_{s2} : Current flowing into bus 3 (not shown in figure) due to other renewable energy sources. It is considered to be zero for studies with one PV-STATCOM

i_L : Current flowing out of bus 4

The grid inductance and substation transformer leakage inductance can be combined and represented by an equivalent inductance L_g. Capacitances C_2 and C_3 can be combined, and represented by an equivalent capacitance C_{23}. The same applies to capacitances C_4 and C_5, and the equivalent capacitance is given by C_{45}. Hence, the circuit in Figure 2.7 can be simplified as shown in Figure 2.8.

The space phasor equations that govern the dynamics of substation grid, substation transformer, distribution line and load are as follows,

$$\frac{d\overrightarrow{i_1}}{dt} = \frac{x_1}{L_g}\overrightarrow{V_g} - \frac{x_1^2}{L_g}\overrightarrow{V_1} - \frac{R_g}{L_g}\overrightarrow{i_1} \tag{2.4}$$

$$\frac{d\overrightarrow{V_1}}{dt} = \frac{1}{C_1}\overrightarrow{i_1} - \frac{1}{C_1}\overrightarrow{i_{12}} \tag{2.5}$$

$$\frac{d\overrightarrow{i_{12}}}{dt} = \frac{1}{L_1}\overrightarrow{V_1} - \frac{1}{L_1}\overrightarrow{V_{s1}} - \frac{R_1}{L_1}\overrightarrow{i_{12}} \tag{2.6}$$

$$\frac{d\overrightarrow{V_{s1}}}{dt} = \frac{1}{C_{23}}\overrightarrow{i_{s1}} + \frac{1}{C_{23}}\overrightarrow{i_{12}} - \frac{1}{C_{23}}\overrightarrow{i_{23}} \tag{2.7}$$

$$\frac{d\overrightarrow{i_{23}}}{dt} = \frac{1}{L_2}\overrightarrow{V_{s1}} - \frac{1}{L_2}\overrightarrow{V_{s2}} - \frac{R_2}{L_2}\overrightarrow{i_{23}} \tag{2.8}$$

$$\frac{d\overrightarrow{V_{s2}}}{dt} = \frac{1}{C_{45}}\overrightarrow{i_{23}} + \frac{1}{C_{45}}\overrightarrow{i_{s2}} - \frac{1}{C_{45}}\overrightarrow{i_{34}} \tag{2.9}$$

$$\frac{d\overrightarrow{i_{34}}}{dt} = \frac{1}{L_3}\overrightarrow{V_{s2}} - \frac{1}{L_3}\overrightarrow{V_L} - \frac{R_3}{L_3}\overrightarrow{i_{34}} \tag{2.10}$$

$$\frac{d\overrightarrow{V_L}}{dt} = \frac{1}{C_6}\overrightarrow{i_{34}} - \frac{1}{C_6}\overrightarrow{i_L} \tag{2.11}$$

$$\frac{d\overrightarrow{i_L}}{dt} = -\frac{R_L}{L_L}\overrightarrow{i_L} + \frac{\overrightarrow{V_L}}{L_L} \tag{2.12}$$

The state space modeling and analysis of the entire system is performed in *dq* frame. Analysis in *dq* frame is advantageous since it involves transformation of signals and variables to equivalent DC quantities [18]. A space phasor $\overrightarrow{f}$ can be expressed in *dq* frame as [18]

$$f = (f_d + jf_q)e^{j\rho(t)} \tag{2.13}$$

Where f_d and f_q are the space phasor *dq* frame components of space phasor $\overrightarrow{f}$, $\rho(t)$ is the reference angle of *dq* frame.

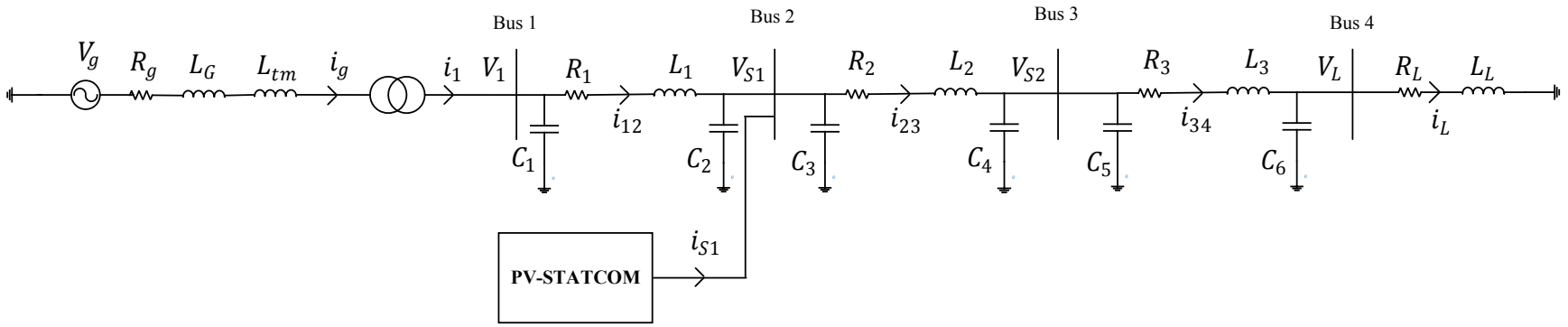

Figure 2.7 Circuit Model of the Study System

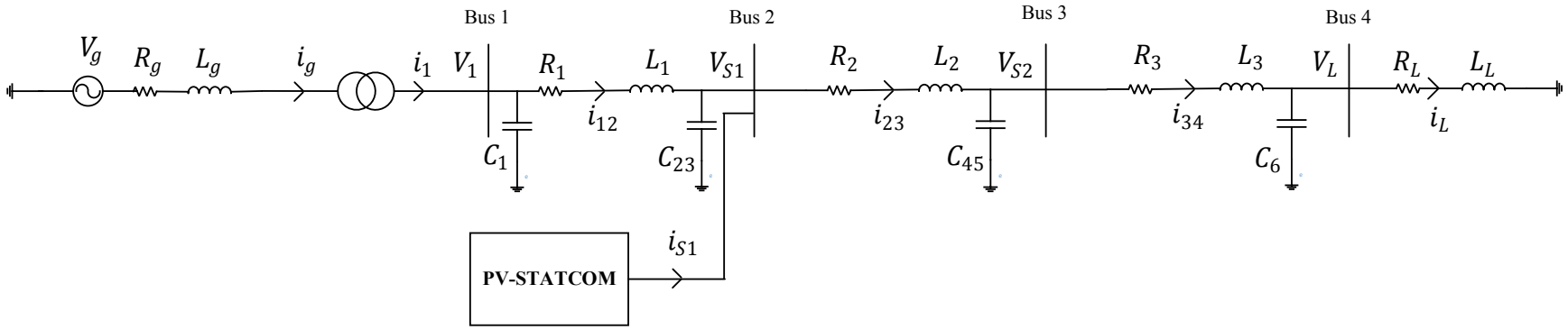

Figure 2.8 Simplified Circuit Model of the Study System

Using (2.13), the space phasor equations in (2.4) - (2.12) are expressed in *dq* frame and the equations are presented below.

$$\frac{di_{1d}}{dt} = \frac{x_1}{L_g}\widehat{V_g}\cos(\omega_o t - \frac{\pi}{2} - \rho) - \frac{x_1^2}{L_g}V_{1d} - \frac{R_g}{L_g}i_{1d} + \omega i_{1q} \tag{2.14}$$

$$\frac{di_{1q}}{dt} = \frac{x_1}{L_g}\widehat{V_g}\sin(\omega_o t - \frac{\pi}{2} - \rho) - \frac{x_1^2}{L_g}V_{1q} - \frac{R_g}{L_g}i_{1q} - \omega i_{1d} \tag{2.15}$$

$$\frac{dV_{1d}}{dt} = \frac{i_{1d}}{C_1} - \frac{i_{12d}}{C_1} + \omega V_{1q} \tag{2.16}$$

$$\frac{dV_{1q}}{dt} = \frac{i_{1q}}{C_1} - \frac{i_{12q}}{C_1} - \omega V_{1d} \tag{2.17}$$

$$\frac{di_{12d}}{dt} = \frac{V_{1d}}{L_1} - \frac{V_{s1d}}{L_1} - \frac{R_1}{L_1}i_{12d} + \omega i_{12q} \tag{2.18}$$

$$\frac{di_{12q}}{dt} = \frac{V_{1q}}{L_1} - \frac{V_{s1q}}{L_1} - \frac{R_1}{L_1}i_{12q} - \omega i_{12d} \tag{2.19}$$

$$\frac{dV_{s1d}}{dt} = \frac{i_{s1d}}{C_{23}} + \frac{i_{12d}}{C_{23}} - \frac{i_{23d}}{C_{23}} + \omega V_{s1q} \tag{2.20}$$

$$\frac{dV_{s1q}}{dt} = \frac{i_{s1q}}{C_{23}} + \frac{i_{12q}}{C_{23}} - \frac{i_{23q}}{C_{23}} - \omega V_{s1d} \tag{2.21}$$

$$\frac{di_{23d}}{dt} = \frac{V_{s1d}}{L_2} - \frac{V_{s2d}}{L_2} - \frac{R_2}{L_2}i_{23d} + \omega i_{23q} \tag{2.22}$$

$$\frac{di_{23q}}{dt} = \frac{V_{s1q}}{L_2} - \frac{V_{s2q}}{L_2} - \frac{R_2}{L_2}i_{23q} - \omega i_{23d} \tag{2.23}$$

$$\frac{dV_{s2d}}{dt} = \frac{i_{23d}}{C_{45}} + \frac{i_{s2d}}{C_{45}} - \frac{i_{34d}}{C_{45}} + \omega V_{s2q} \tag{2.24}$$

$$\frac{dV_{s2q}}{dt} = \frac{i_{23q}}{C_{45}} + \frac{i_{s2q}}{C_{45}} - \frac{i_{34q}}{C_{45}} - \omega V_{s2d} \tag{2.25}$$

$$\frac{di_{34d}}{dt} = \frac{V_{s2d}}{L_3} - \frac{V_{Ld}}{L_3} - \frac{R_3}{L_3} i_{34d} + \omega i_{34q} \tag{2.26}$$

$$\frac{di_{34q}}{dt} = \frac{V_{s2q}}{L_3} - \frac{V_{Lq}}{L_3} - \frac{R_3}{L_3} i_{34q} - \omega i_{34d} \tag{2.27}$$

$$\frac{dV_{Ld}}{dt} = \frac{i_{34d}}{C_6} - \frac{i_{Ld}}{C_6} + \omega V_{Lq} \tag{2.28}$$

$$\frac{dV_{Lq}}{dt} = \frac{i_{34q}}{C_6} - \frac{i_{Lq}}{C_6} - \omega V_{Ld} \tag{2.29}$$

$$\frac{di_{Ld}}{dt} = -\frac{R_L}{L_L} i_{Ld} + \frac{V_{Ld}}{L_L} + \omega i_{Lq} \tag{2.30}$$

$$\frac{di_{Lq}}{dt} = -\frac{R_L}{L_L} i_{Lq} + \frac{V_{Lq}}{L_L} - \omega i_{Ld} \tag{2.31}$$

Equations (2.14) - (2.31) constitute a state space model for the distribution network subsystem. The *dq* frame reference angle ρ in (2.14) and (2.15) can be generated by the phase locked loop (PLL) of the PV system and synchronized with the dq frame of PV-STATCOM.

The phase $\frac{\pi}{2}$ in (2.14) and (2.15) is required for compensating the static phase difference between the PLL angle and the grid voltage angle. It is due to the conversion from sinusoidal voltage source to cosine voltage source. The following are the state variables and inputs:

State Variables:

$i_{1d}, i_{1q}, V_{1d}, V_{1q}, i_{12d}, i_{12q}, V_{s1d}, V_{s1q}, i_{23d}, i_{23q}, V_{s2d}, V_{s1q}, i_{34d}, i_{34q}, V_{Ld}, V_{Lq}, i_{Ld}$ and i_{Lq}.

Inputs: $\widehat{V_g}, i_{s1d}, i_{s1q}, i_{s2d}, \rho$ and i_{s2q}

2.4 PV-STATCOM : PV Subsystem

The PV-STATCOM unit further consists of two subsystems namely PV subsystem and Controller Subsystem. The PV subsystem consists of photovoltaic panel array, inverter, filter and coupling transformer as shown in Figure 2.9. This subsystem is referred to as subsystem 2. The modeling of each component is explained in detail in the following sections. First, the modeling of PV subsystem is discussed in this section. The models have been adopted from [17], [18] and [47].

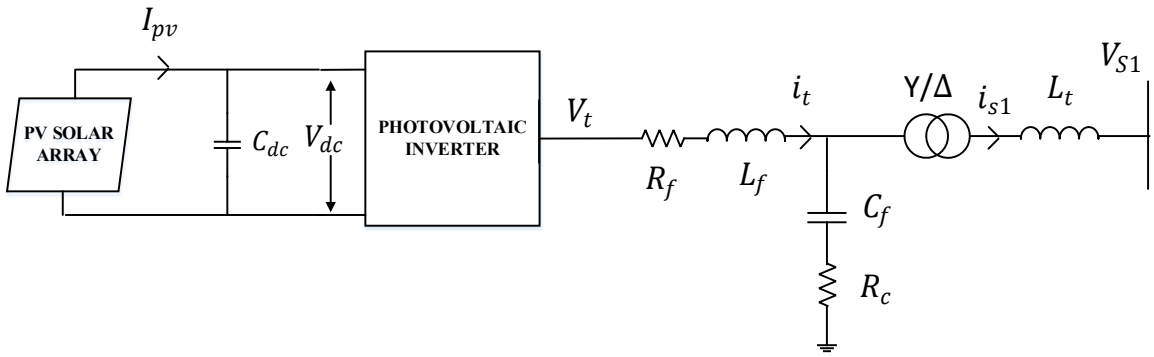

Figure 2.9 Circuit Model of PV Subsystem

2.4.1 Photovoltaic Panel Array

The Photovoltaic (PV) panel array consists of a number of PV panels in series and parallel to make up for the required capacity of PV power system. Each PV panel consists of a number of PV cells in series and parallel.

The expression for a PV Panel output current is given by [47]:

$$I_{pvpanel} = \frac{[n_s I_{SC(STC)}\{1+K_i(T-T_s)\}\{R_{sh}+R_s\} - n_p V_{oc}][e^{\frac{qV_{oc(STC)}\{1+K_v(T-T_s)\}}{nkTn_s}} - 1]G}{n_s R_{sh}[e^{\frac{qV_{oc(STC)}\{1+K_v(T-T_s)\}}{nkTn_s}} - e^{\frac{qI_{sc(STC)}\{1+K_i(T-T_s)\}R_s}{nkTn_p}}]G_{nom}}$$
$$- \frac{[n_s I_{SC(STC)}\{1+K_i(T-T_s)\{R_{sh}+R_s\} - n_p V_{oc}][e^{\frac{q(n_p V_{pvpanel}+n_s I_{pvpanel}R_s)}{nkTn_s n_p}} - 1]}{n_s R_{sh}\left[e^{\frac{qV_{oc(STC)}\{1+K_v(T-T_s)\}}{nkTn_s}} - e^{\frac{qI_{sc(STC)}\{1+K_i(T-T_s)\}R_s}{nkTn_p}}\right]}$$
$$+ \frac{Gn_p V_{oc(STC)}\{1+K_v(T-T_s)\}}{n_s R_{sh} G_{nom}}$$
$$- \frac{(n_p V_{pvpanel} + n_s I_{pvpanel} R_s)}{n_s R_{sh}} \quad (2.32)$$

Where,

$I_{pvpanel}$ is the output current of a PV panel, $I_{SC(STC)}$ is the panel short circuit current at Standard Test Conditions (STC), K_i is the temperature coefficient of PV short circuit current, T is the operating temperature of the PV panel, T_s is the standard temperature at STC, n_s is the number of cells in series per panel, n_p is the number of cells in parallel per panel, R_{sh} is the equivalent shunt resistance of each cell, R_s is the equivalent series resistance of each cell, V_{oc} is the open circuit voltage of a PV panel, q is the charge of an electron, $V_{oc(STC)}$ is the open circuit voltage of a PV panel at STC, K_v is the temperature coefficient of PV open circuit voltage, G is the solar radiation, n is the diode ideality factor, k is the Boltzmann's constant, G_{nom} is the solar radiation at STC, $V_{pvpanel}$ is the output voltage of a PV panel.

The output voltage and output current of the PV array is given by:

$$I_{pv} = I_{pvpanel} * N_p \tag{2.33}$$

$$V_{pv} = V_{pvpanel} * N_s \tag{2.34}$$

Where I_{pv} is the output current of the PV array, V_{pv} is the output voltage of the PV array, N_s is the number of panels in series, N_p is the number of panel series strings in parallel.

The expression for a PV array output current can be found by substituting (2.33) and (2.34) in (2.32). The expression for PV array output current is given by,

$$I_{pv} = a_1 G - a_2\{e^{a_3 V_{pv} + a_4 I_{pv}} - 1\} - a_5 V_{pv} \tag{2.35}$$

Where,

$$a_1 = \frac{N_p I_{phx}}{K_1 * 1000} \tag{2.36}$$

$$a_2 = \frac{N_p I_{ox}}{K_1 * 1000} \tag{2.37}$$

$$a_3 = \frac{1000 * q}{nkTn_s N_s} \tag{2.38}$$

$$a_4 = \frac{1000 * qR_s}{nkTn_p N_p} \tag{2.39}$$

$$a_5 = \frac{n_p N_p}{1000 * N_s n_s R_{sh} K_1} \tag{2.40}$$

$$K_1 = 1 + \frac{R_s}{R_{sh}} \tag{2.41}$$

$$I_{phx}$$

$$= \frac{[n_s I_{SC(STC)}\{1 + K_i(T - T_s)\}\{R_{sh} + R_s\} - n_p V_{oc}][e^{\frac{qV_{oc(STC)}\{1+K_v(T-T_s)\}}{nkTn_s}} - 1]}{n_s R_{sh}\left[e^{\frac{qV_{oc(STC)}\{1+K_v(T-T_s)\}}{nkTn_s}} - e^{\frac{qI_{sc(STC)}\{1+K_i(T-T_s)\}R_s}{nkTn_p}}\right]G_{nom}}$$

$$+ \frac{n_p V_{oc(STC)}\{1 + K_v(T - T_s)\}}{n_s R_{sh} G_{nom}} \tag{2.42}$$

$$I_{ox} = \frac{[n_s I_{SC(STC)}\{1 + K_i(T - T_s)\{R_{sh} + R_s\} - n_p V_{oc}]}{n_s R_{sh}\left[e^{\frac{qV_{oc(STC)}\{1+K_v(T-T_s)\}}{nkTn_s}} - e^{\frac{qI_{sc(STC)}\{1+K_i(T-T_s)\}R_s}{nkTn_p}}\right]} \tag{2.43}$$

2.4.2 Photovoltaic Inverter

The photovoltaic inverter used for simulation studies is a 6 pulse Voltage Sourced Converter (VSC). It consists of 6 Insulated Gate Bipolar Transistors (IGBT). The switching strategy used is Sinusoidal Pulse Width Modulation (SPWM). R_{on} is the ON state resistance of each IGBT.

The VSC is represented by its averaged model for the purpose of analytical studies [18]. The equation relating the input DC voltage and output AC voltage of the VSC is given by

$$\overrightarrow{V_t} = \frac{V_{dc}}{2}\,\overrightarrow{m} \tag{2.44}$$

Where, $\vec{V}_t$ is the output AC voltage of VSC in space phasor domain, $\overrightarrow{m}$ is the modulation index of VSC in space phasor domain, V_{dc} is the input DC voltage of VSC.

The dynamics of the DC link voltage of VSC is governed by the following equation [48], [17]:

$$C_{dc}\frac{dV_{dc}}{dt} = I_{pv} - I_{dc} \tag{2.45}$$

Where C_{dc} is the DC link capacitance of VSC and I_{dc} is the input DC current of VSC.

As mentioned in section 2.3.5, the state space analysis is carried out in *dq* frame. The input DC current is given by

$$I_{dc} = \frac{3(m_d i_{td} + m_q i_{tq})}{4} \tag{2.46}$$

Where m_d and m_q are the modulation index in *dq* frame, i_{td} and i_{tq} are the inverter output currents in *dq* frame.

2.4.3 Filter and Coupling Transformer

The output of VSC is filtered using a low pass LC filter and connected to the distribution network through a Star/Delta coupling transformer [9].

The values of filter inductance L_f and filter capacitance C_f are designed based on the following criteria:

a) The total harmonic distortion (THD) of voltage and current injected into the distribution network should be less than 5% [49].

b) The value of inductance is chosen such that the ripple of the output current is not more than 10 % to 15% [50]. This is governed by the following equation

$$L_f = \frac{V_{dc}}{8 * \Delta i L_{max} * f_s} \tag{2.47}$$

Where Δi_{tmax} is maximum output ripple current.

c) The value of capacitance should be chosen such that the reactive power consumed is not more than 5% of the rated active power [51]. This is governed by the following equation

$$C_f = \frac{x_f * P_{rated}}{3 * 2 * \pi * f_s * V_{phase}^2} \quad (2.48)$$

Where P_{rated} is the rated active power of the PV system, V_{phase} is the voltage across the filter capacitance, x_f denotes the fraction of reactive power consumed by the capacitor.

d) The resonant frequency of the LC filter should be in the range between 10 times the line frequency and one half the switching frequency of VSC.

The damping resistors R_{fL} and R_c are chosen such that there is sufficient damping of the resonant peak at the resonant frequency.

The lower limit of DC link voltage of VSC is chosen by considering the maximum voltage drop across the filter inductance when the PV-STATCOM is injecting its rated reactive power [52], [53]. This relation is governed by the following equation,

$$V_{dcmin} \geq \sqrt{6}\omega I_{rated} L_f + \sqrt{2}\, V_{LL} \quad (2.49)$$

Where V_{dcmin} is minimum DC link voltage level of VSC, I_{rated}(RMS) is the rated current of VSC, V_{LL} (RMS) is line to line voltage at the output of the filter.

It should be noted that when PV panel is connected to the input of VSC, V_{dc} becomes equal to V_{pv}.

The coupling transformer is modelled as an ideal transformer in series with its leakage inductance L_t (referred to distribution network side).

Referring to Figure 2.9, i_t is the inverter output current, V_c is the voltage at the output of filter, V_{cf} is the output across the filter capacitance, i_{s1} is the output current of the transformer, V_{s1} is voltage at the output of transformer, x is the turns ratio of the transformer, L_t is the equivalent leakage inductance of coupling transformer.

The space phasor equations that govern the dynamics of filter and coupling transformer are as follows,

$$\frac{d\overrightarrow{i_t}}{dt} = [-\frac{R_f}{L_f} - \frac{R_c}{L_f}]\overrightarrow{i_t} - \frac{\overrightarrow{V_{cf}}}{L_f} + \frac{R_c}{xL_f}\overrightarrow{i_{s1}} + \overrightarrow{V_t} \tag{2.50}$$

$$\frac{d\overrightarrow{V_{cf}}}{dt} = \frac{\overrightarrow{i_t}}{C_f} - \frac{\overrightarrow{i_{s1}}}{xC_f} \tag{2.51}$$

$$\frac{d\overrightarrow{i_{s1}}}{dt} = -\frac{R_c}{x^2L_t}\overrightarrow{i_{s1}} + \frac{\overrightarrow{V_{cf}}}{xL_t} + \frac{R_c}{xL_t}\overrightarrow{i_t} - \frac{\overrightarrow{V_{s1}}}{L_t} \tag{2.52}$$

$$\overrightarrow{V_c} = \overrightarrow{i_t}R_c + \overrightarrow{V_{cf}} - \frac{R_c}{x}\overrightarrow{i_{s1}} \tag{2.53}$$

Where,

$$R_f = R_{fL} + R_{on} \tag{2.54}$$

2.4.4 State Space Model

The state space model of the entire PV subsystem is obtained by combining (2.35), (2.44) - (2.46) and (2.50) - (2.53). All the equations are then expressed in *dq* frame using the transformation in (2.13). The nonlinear state equations are:

$$\frac{di_{td}}{dt} = \left[-\frac{R_f}{L_f} - \frac{R_c}{L_f}\right]i_{td} + \omega i_{tq} - \frac{V_{cfd}}{L_f} + \frac{R_c}{xL_f}i_{s1d} + \frac{V_{dc}m_d}{2L_f} \tag{2.55}$$

$$\frac{di_{tq}}{dt} = \left[-\frac{R_f}{L_f} - \frac{R_c}{L_f}\right]i_{tq} - \omega i_{td} - \frac{V_{cfq}}{L_f} + \frac{R_c}{xL_f}i_{s1q} + \frac{V_{dc}m_q}{2L_f} \tag{2.56}$$

$$\frac{dV_{cfd}}{dt} = \frac{i_{td}}{C_f} + \omega V_{cfq} - \frac{i_{s1d}}{xC_f} \tag{2.57}$$

$$\frac{dV_{cfq}}{dt} = \frac{i_{tq}}{C_f} - \omega V_{cfd} - \frac{i_{s1q}}{xC_f} \tag{2.58}$$

$$\frac{di_{s1d}}{dt} = \frac{R_c}{xL_t} i_{td} + \frac{V_{cfd}}{xL_t} - \frac{R_c}{x^2 L_t} i_{s1d} + \omega i_{s1q} - \frac{V_{s1d}}{L_t} \tag{2.59}$$

$$\frac{di_{s1q}}{dt} = \frac{R_c}{xL_t} i_{tq} + \frac{V_{cfq}}{xL_t} - \frac{R_c}{x^2 L_t} i_{s1q} - \omega i_{s1d} - \frac{V_{s1q}}{L_t} \tag{2.60}$$

$$\frac{dV_{dc}}{dt} = -\frac{3m_d i_{td}}{4C_{dc}} - \frac{3m_q i_{tq}}{4C_{dc}} - \frac{a_5 V_{dc}}{C_{dc}} - \frac{a_2}{C_{dc}}\{e^{a_3 V_{dc} + a_4 I_{pv}} - 1\} + \frac{a_1 G}{C_{dc}} \tag{2.61}$$

$$V_{cd} = i_{td} R_c + V_{cfd} - \frac{i_{s1d} R_c}{x} \tag{2.62}$$

$$V_{cq} = i_{tq} R_c + V_{cfq} - \frac{i_{s1q} R_c}{x} \tag{2.63}$$

$$I_{pv} = a_1 G - a_2\{e^{a_3 V_{dc} + a_4 I_{pv}} - 1\} - a_5 V_{dc} \tag{2.64}$$

Equations (2.55) - (2.64) constitute a state space model for PV subsystem. The following are the state variables, inputs and outputs:

State Variables: $i_{td}, i_{tq}, V_{cfd}, V_{cfq}, i_{s1d}, i_{s1q}$ and V_{dc}

Inputs: $G, V_{s1d}, V_{s1q}, m_d \; and \; m_q$

Outputs: V_{cd}, V_{cq} and I_{pv}

2.4.5 Assumptions made in modeling of PV Subsystem

The following are some of the major assumptions made in the modeling of PV-STATCOM:

A large PV power plant consists of a number PV inverters connected in parallel. A size and number of PV inverters used in a PV power plant will depend on its rating. There could be issues between individual inverters such as control system interactions, flow of

circulating currents etc. These issues are not considered since it is beyond the scope of this thesis. In this thesis, the entire PV power plant is represented by a single equivalent PV system [12] for the purpose of power system studies. But, the model developed is valid for any PV power plant irrespective of its power rating.

2.5 Controller Subsystem

The Controller subsystem consists of the following parts:

a. Measurement Filter
b. Phase Locked Loop (PLL)
c. Current Controller
d. DC Link Voltage Controller
e. Point of Common Coupling (PCC) Voltage Controller.

The overall block diagram of the controller subsystem is shown in Figure 2.10. The function of each control block is explained briefly in the following section:

- The VSC control system is synchronized to the grid using the PLL. This ensures that the AC signals get transformed into dq frame and the controller works directly with DC signals.
- The DC Link Voltage Controller regulates V_{dc} at its reference value V_{dcref}. The reference value can be set at the maximum power point voltage of PV array to ensure that the PV array supplies the maximum power at a particular irradiance. This controller generates the current reference i_{tdref}.
- The PCC Voltage Controller regulates V_{pcc} at its reference value V_{pccref}. This controller generates the current reference i_{tqref}.
- The current controller regulates i_{td} and i_{tq} at i_{tdref} and i_{tqref} respectively. The current controller, in turn, generates the modulation indexes m_d and m_q for the VSC PWM scheme.

This subsystem is referred to as subsystem 3 in the thesis. The modeling of each component is explained in detail in the following sections. Some of the concepts and

procedure for modeling of each component and simplification of the derived models have been adapted from [54], [55], [56] and [57].

2.5.1 Measurement Filter

The electrical point of coupling (EPC) voltages ($V_{cd}\ and\ V_{cq}$) and point of common coupling (PCC) voltages ($V_{s1d}\ and\ V_{s1q}$) are the voltage inputs to controller circuit. Due to PWM switching, these signals in *dq* frame contain some PWM switching side-band harmonics of VSC AC side signals which are modulated by 60 Hz through the *abc* to *dq* frame transformation [18]. These have to be removed using low pass filters. Also, there will be some delays present after measurement of voltage due to signal processing (filtering, RMS computation etc.), communication delays etc and this also has to be accounted for in choosing the filter time constants. In total, all these delays are accounted for using time constants τ_1, τ_2 and these filters are termed as measurement filters [30].

The dynamics of the measurement filter can be modeled by using the following state space equations,

$$\frac{dV_{cdf}}{dt} = \frac{V_{cd}}{\tau_2} - \frac{V_{cdf}}{\tau_2} \tag{2.65}$$

$$\frac{dV_{cqf}}{dt} = \frac{V_{cq}}{\tau_2} - \frac{V_{cqf}}{\tau_2} \tag{2.66}$$

$$\frac{dV_{s1df}}{dt} = \frac{V_{sd}}{\tau_1} - \frac{V_{sdf}}{\tau_1} \tag{2.67}$$

$$\frac{dV_{s1qf}}{dt} = \frac{V_{sq}}{\tau_1} - \frac{V_{sqf}}{\tau_1} \tag{2.68}$$

Where V_{cdf}, V_{cqf}, V_{s1df}, V_{s1qf} are the filtered components of V_{cd}, V_{cq}, V_{s1d}, V_{s1q} respectively

τ_1, τ_2 are the time constants of measurement filters.

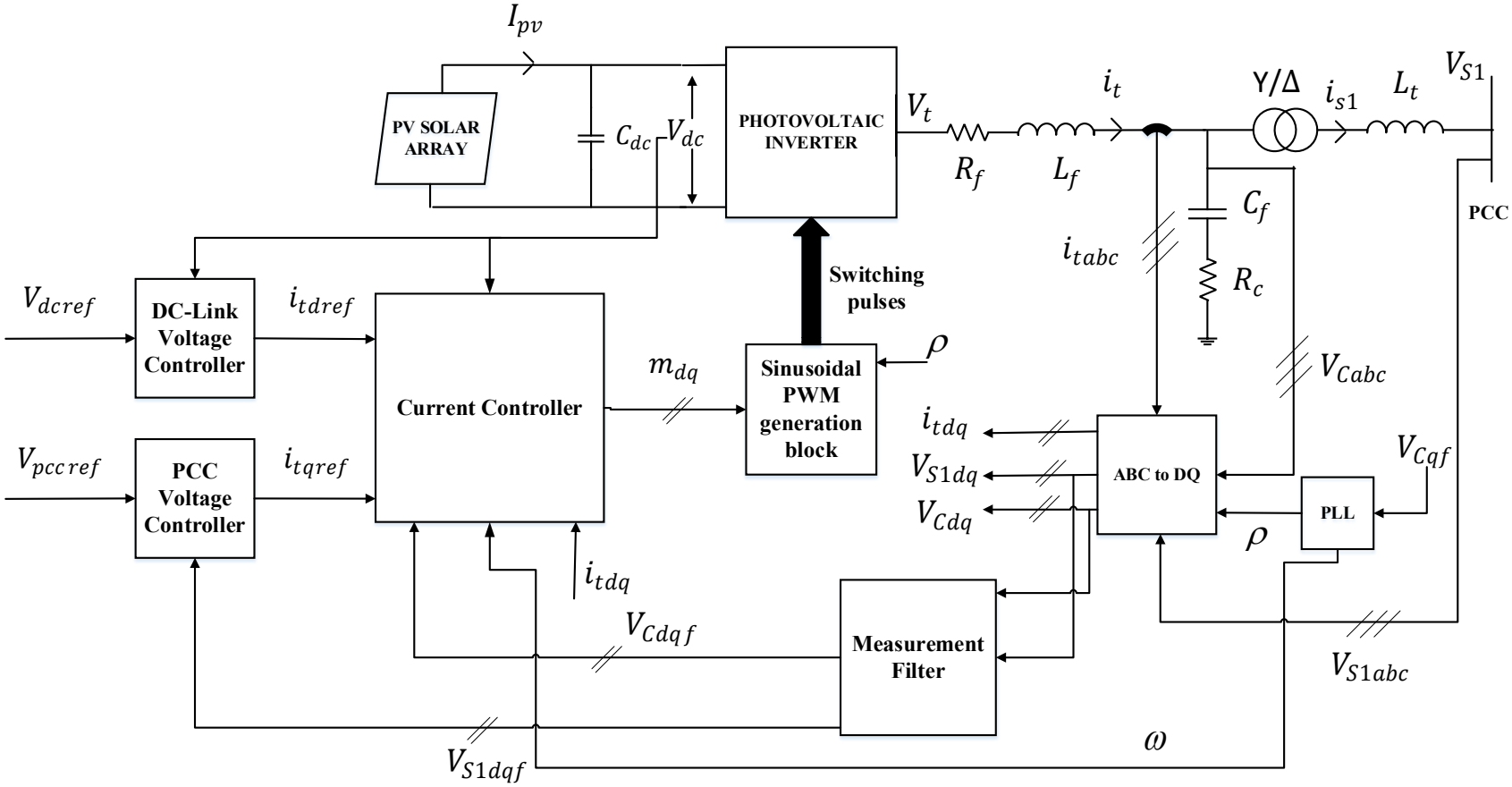

Figure 2.10 Block Diagram of Controller Subsystem

As pointed out above, the values of these time constants are chosen to model the low pass filter time constants and the additional delays. The signals V_{cd} and V_{cq} serve as feed-forward signals for the current controller in order to enhance start-up and transient responses of closed loop current controller [17]. Hence, the measurement filters of the signals V_{cd} and V_{cq} are also referred to as feed-forward filters.

2.5.2 Phase Locked Loop (PLL)

The AC voltages and currents are sinusoidally varying with time in nature at a frequency ω_o which is the steady state grid frequency. The corresponding signals in *dq* frame become DC signals when the *dq* frame rotates synchronously with a frequency ω_o [18]. This is achieved by using a PLL mechanism.

The control block diagram for PLL is shown in Figure 2.11. Voltage V_c is resolved into V_{cd} and V_{cq}. These are represented by V_{cdf} and V_{cqf} after passing through the measurement filters. V_{cqf} is processed by a compensator *H(s)* which determines ω. In steady state, V_{cqf} is forced to zero and hence, ω becomes equal to ω_o.

$$\Delta\omega(s) = H(s)V_{cqf}(s) \tag{2.69}$$

Here, $\Delta\omega$ is the change in frequency from ω_o during transients. As can be seen in Figure 2.11, a bias of ω_o is added to $\Delta\omega$ to ensure the frequency excursions are around ω_o [18]. The output is also limited by a saturation block which has ω_{min} and ω_{max} as its limits in order to limit the variations of ω. The frequency signal ω serves as an input to a voltage controlled oscillator (VCO) which is basically an integrator and this generates the angle reference ρ that is required for *abc* to *dq* (and vice versa) frame conversion.

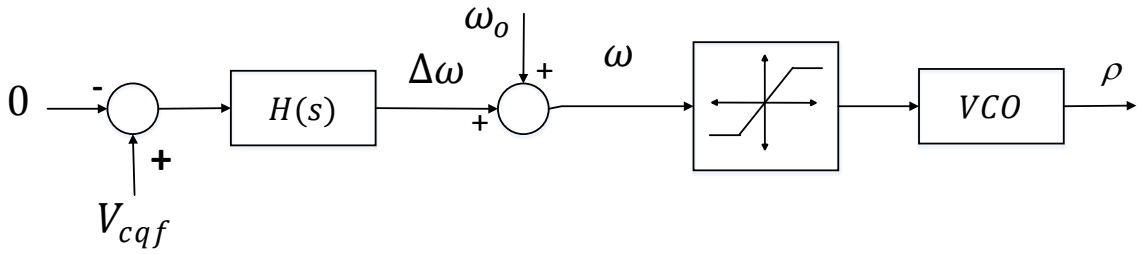

Figure 2.11 Control Block Diagram of PLL

The compensator $H(s)$ is a Proportional Integral (PI) controller and is given by,

$$H(s) = b_1 + \frac{b_2}{s} \tag{2.70}$$

Where b_1 is the proportional gain and b_2 is the integral gain. The PI controller can be designed based on the procedure outlined in [58] for a required bandwidth and phase margin.

The state variables of PLL are defined as

$$X_8(s) = \frac{b_2}{s} V_{cqf}(s) \tag{2.71}$$

$$\rho(s) = \frac{\omega(s)}{s} = \frac{\omega_o + \Delta\omega(s)}{s} \tag{2.72}$$

In time-domain, the state space model of PLL is given by,

$$\frac{dx_8}{dt} = b_2 V_{cqf}(t) \tag{2.73}$$

$$\frac{d\rho}{dt} = \omega_o + b_1 V_{cqf}(t) + x_8(t) \tag{2.74}$$

$$\omega(t) = \frac{d\rho}{dt} \tag{2.75}$$

The state variables are ρ, x_8. V_{cqf} is the input to PLL and, ρ and ω are the outputs.

The active (P_{VSC}) and reactive power (Q_{VSC}) output of VSC is given by,

$$P_{VSC} = \frac{3}{2}[V_{cd}i_{td} + V_{cq}i_{tq}] \tag{2.76}$$

$$Q_{VSC} = \frac{3}{2}[-V_{cd}i_{tq} + V_{cq}i_{td}] \tag{2.77}$$

PLL ensures that V_{cq} is zero at steady state. This makes the above equations as.

$$P_{VSC} = \frac{3}{2}[V_{cd}i_{td}] \tag{2.78}$$

$$Q_{VSC} = \frac{3}{2}[-V_{cd}i_{tq}] \tag{2.79}$$

The calculation of Q_{VSC} in the controller circuit (under steady state) is performed using the signals V_{cdf} and i_{tq}. Hence, it will be given by,

$$Q_{VSC} = \frac{3}{2}[-V_{cdf}i_{tq}] \tag{2.80}$$

This ensures that the control of VSC powers is decoupled. It can be seen that the active and reactive powers of VSC can be controlled by controlling i_{td} and i_{tq} respectively.

2.5.3 Current Controller

The objective of the current controller is to ensure i_{td} and i_{tq} tracks their references rapidly. Also, it ensures that VSC is protected against overload and faults if i_{tdref} and i_{tqref} are limited by saturation blocks [18].

The VSC AC side current dynamics are described by (2.55) - (2.56). The presence of $L_f\omega$ makes the dynamics of i_{td} and i_{tq} coupled and nonlinear [18].

In order to decouple and linearize the dynamics, the control inputs m_d and m_q are determined based on the following control laws [18]:

$$m_d = \frac{2}{V_{dc}}[u_d - L_f \omega i_{tq} + V_{cdf}] \tag{2.81}$$

$$m_q = \frac{2}{V_{dc}}[u_q + L_f \omega i_{td} + V_{cqf}] \tag{2.82}$$

Here, u_d and u_q are the new control inputs. m_d and m_q are substituted into (2.55) - (2.56) and the VSC current dynamics become,

$$L_f \frac{di_{td}}{dt} = -R_f i_{td} + u_d + V_{cdf} \tag{2.83}$$

$$L_f \frac{di_{tq}}{dt} = -R_f i_{tq} + u_q + V_{cqf} \tag{2.84}$$

Equations (2.83) and (2.84) show that the dynamics of i_{td} and i_{tq} are decoupled and linear. i_{td} and i_{tq} can be controlled by controlling u_d and u_q respectively. V_{cdf} and V_{cqf} can be considered as disturbances. The control block diagram for the current controller is shown in Figure 2.12.

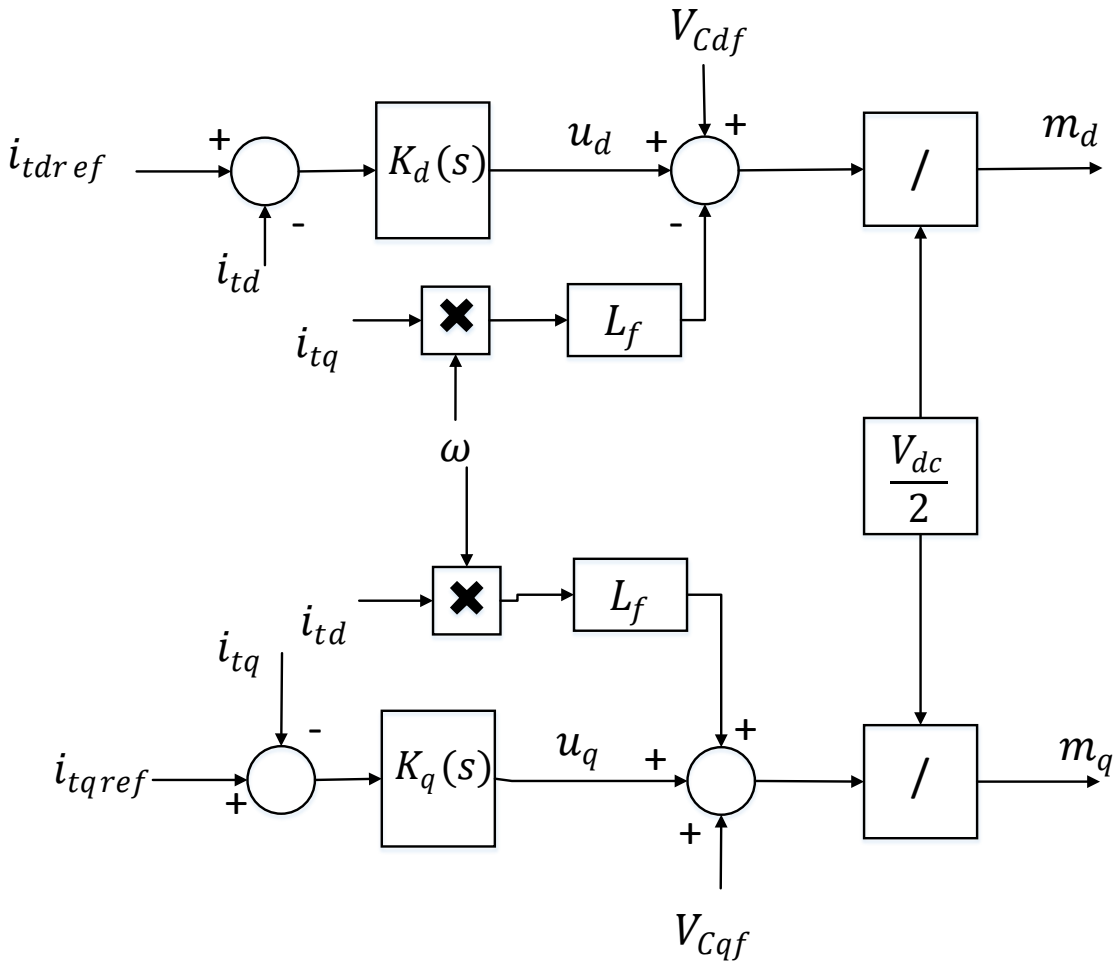

Figure 2.12 Control Block Diagram of Current Controller

It can be seen that u_d is the output of compensator $K_d(s)$ which processes the error $i_{tdref} - i_{td}$. Similarly, u_q is the output of compensator $K_q(s)$ which processes the error $i_{tqref} - i_{tq}$.

The compensators $K_d(s)$ and $K_q(s)$ are PI controllers and they are given by,

$$K_d(s) = K_{pi1} + \frac{K_{ii1}}{s} \tag{2.85}$$

$$K_q(s) = K_{pi2} + \frac{K_{ii2}}{s} \tag{2.86}$$

Where K_{pi1}, K_{pi2} are the proportional gains and K_{ii1}, K_{ii2} are the integral gains.

The values of PI controllers can be designed for a particular bandwidth and phase margin of the current controllers.

The state variables of current controller are defined as

$$X_3(s) = \frac{K_{ii1}[I_{tdref}(s) - I_{td}(s)]}{s} \tag{2.87}$$

$$X_4(s) = \frac{K_{ii2}[I_{tqref}(s) - I_{tq}(s)]}{s} \tag{2.88}$$

In time- domain, the state space model of current controller is given by,

$$\frac{dx_3}{dt} = K_{ii1}[i_{tdref} - i_{td}] \tag{2.89}$$

$$\frac{dx_4}{dt} = K_{ii2}[i_{tqref} - i_{tq}] \tag{2.90}$$

$$u_d = K_{pi1}\left[i_{tdref} - i_{td}\right] + x_3 \tag{2.91}$$

$$u_q = K_{pi2}\left[i_{tqref} - i_{tq}\right] + x_4 \tag{2.92}$$

2.5.4 DC-Link Voltage Controller

The DC-Link Voltage Controller ensures that V_{dc} is maintained at V_{dcref} so that the corresponding active power gets delivered from the PV system to the grid. This relation is governed by the following power balance equation,

$$\frac{d}{dt}\left[\frac{C_{dc}V_{dc}^2}{2}\right] \cong P_{pv} - P_{VSC} \tag{2.93}$$

As seen in (2.93), V_{dc} can be controlled by controlling P_{VSC}. As shown before, P_{VSC} can in-turn be controlled by i_{td} in steady state. Hence, it can be seen that V_{dc} can be controlled by controlling i_{td}.

The error between V_{dcref} and V_{dc} is processed by a compensator $K_V(s)$ and this generates the current reference i_{tdref} for current controller. The compensator $K_V(s)$ is PI controller in cascade with a low pass filter [19] and is given by,

$$K_V(s) = (K_{pv} + \frac{K_{iv}}{s})(\frac{1}{\tau_{Vdc}s + 1}) \tag{2.94}$$

Where K_{pv} is the proportional gain and K_{iv} is the integral gain

τ_{Vdc} is the time constant of low pass filter.

As pointed out earlier in section 2.5.1, there are PWM switching side-band harmonics of VSC AC side signals in the *dq* frame signals which are modulated by 60 Hz through the *abc* to *dq* frame conversion. These harmonics are also present in the dc-link voltage V_{dc}. Hence, the low pass filter with a time constant τ_{Vdc} is required to filter out these harmonics. The control block diagram for DC-Link voltage controller is shown in Figure 2.13.

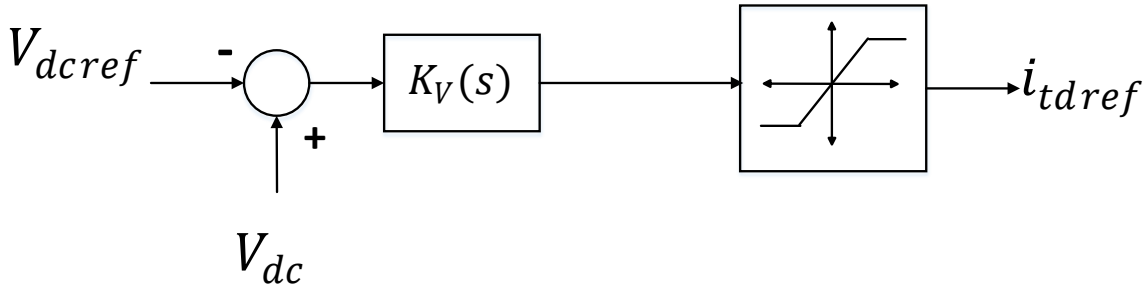

Figure 2.13 Control Block Diagram of DC-Link Voltage Controller

The DC link voltage control dynamics is described by (2.61). This can be linearized for a particular operating point and, a transfer function can be obtained between i_{td} and V_{dc}. This can be used to design the PI controller of the compensator $K_V(s)$ based on bandwidth and phase margin requirements.

The DC Link capacitance C_{dc} plays a major role in the stability of the DC-Link Voltage control loop. Reference [59] shows that the DC-Link Voltage control loop suffers from the effect of right half plane (RHP) pole if the PV array operates at a voltage less than the maximum power point voltage. The position of the pole is affected by the value of C_{dc}. A stability criteria has been established in [59] to decide the minimum value of C_{dc} relating the speed of operation (cross-over frequency) of voltage control loop $\omega_{loopVdc}$, the current and voltage at the critical operating point of the PV array. This relation is given by,

$$C_{dc} \geq \frac{I_{sc}\ of\ PV\ Array}{V_{pvmin}\omega_{loopVdc}} \tag{2.95}$$

Where V_{pvmin} is the minimum voltage of operation of PV array and I_{sc} is the short-circuit current of PV array. V_{pvmin} can be chosen to be the minimum value of dc-link voltage determined by equation (2.49). $\omega_{loopVdc}$ is generally chosen to be 2 to 10 times slower than the inner current control loop [32]. A safety factor of 25 % is included in the minimum value of C_{dc} to arrive at the final value of dc-link capacitance.

The state variables of the DC-Link Voltage Controller are defined as [54],

$$X_6(s) = \frac{-V_{dcref}(s) + V_{dc}(s)}{\tau_{Vdc}s + 1} \tag{2.96}$$

$$X_5(s) = \frac{X_6(s)}{s} \tag{2.97}$$

In time- domain, the state space model of DC-Link Voltage controller is given by,

$$\frac{dx_6}{dt} = -\frac{V_{dcref}}{\tau_{Vdc}} + \frac{V_{dc}}{\tau_{Vdc}} - \frac{x_6}{\tau_{Vdc}} \tag{2.98}$$

$$\frac{dx_5}{dt} = x_6 \tag{2.99}$$

$$i_{tdref} = K_{pv}x_6 + K_{iv}x_5 \tag{2.100}$$

2.5.5 PCC Voltage Controller

The objective of the PCC Voltage Controller is to regulate the PCC voltage V_{pcc} at its reference value V_{pccref}. In dq frame, V_{pcc} is given by,

$$V_{pcc} = \sqrt{V_{s1df}^2 + V_{s1qf}^2} \tag{2.101}$$

As pointed out earlier, the PCC voltage and dc-link voltage control loops are coupled in distribution networks where resistance is not negligible when compared to reactance. For effective control of PCC voltage, both active and reactive powers have to be controlled. But, PV systems are always operated at maximum power point for economic reasons. Hence, active power cannot be controlled as long as the PCC voltage is within the steady state voltage limits. Hence, the voltage at PCC can be regulated by controlling reactive power Q_{VSC}.

It was shown earlier that Q_{VSC} can be controlled by controlling i_{tq} in steady state. Hence, the PCC voltage can be regulated by controlling i_{tq}. The structure of the PCC voltage controller is shown in Figure 2.14. The error between V_{pccref} and V_{pcc} is processed by a compensator $K_{Vac}(s)$ and this generates the current reference i_{tqref} for current controller. The compensator $K_{Vac}(s)$ can be proportional (P) or proportional integral (PI) controller. In general, it is of the form,

$$K_{Vac}(s) = (K_{pvs} + \frac{K_{ivs}}{s}) \tag{2.102}$$

Where K_{pvs} is the proportional gain and K_{ivs} is the integral gain.

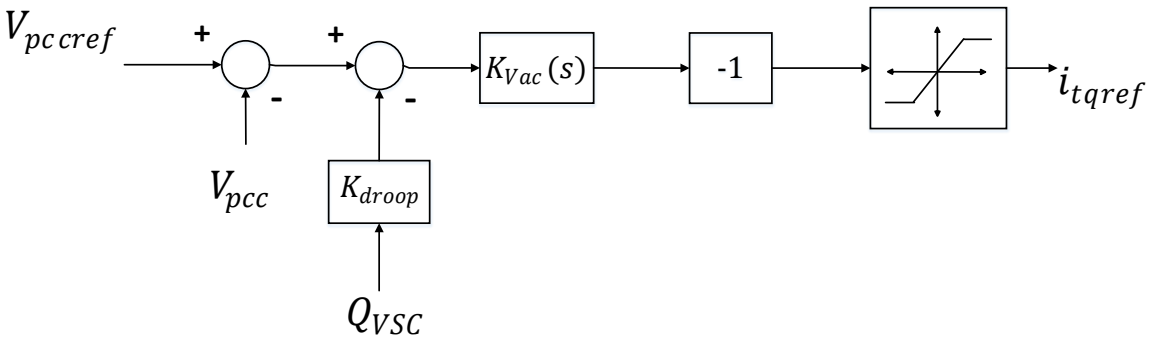

Figure 2.14 Control Block Diagram of PCC Voltage Controller

Also, the degree of voltage control will depend on droop factor K_{droop} [17]. This is important in the case of single PV system for PCC voltage reference adjustment if the voltage error is very large to prevent injection/absorption of a very large value of reactive power. For multiple PV systems, this is required for reactive power sharing [17]. As shown in Figure 2.14, Q_{VSC} is multiplied by K_{droop} which provides the necessary droop action.

The state variable of PCC voltage controller is defined as,

$$X_7(s) = (\frac{1}{s})L(V_{pccref} - \sqrt{V_{s1df}^2 + V_{s1qf}^2} - K_{droop}Q_{VSC}) \tag{2.103}$$

Where *L* represents the Laplace transform operator.

In time-domain, the state space model is,

$$\frac{dx_7}{dt} = V_{pccref} - \sqrt{V_{s1df}^2 + V_{s1qf}^2} - K_{droop}Q_{VSC} \tag{2.104}$$

$$i_{tqref} = -K_{pvs}V_{pccref} + K_{pvs}\sqrt{V_{s1df}^2 + V_{s1qf}^2} + K_{pvs}K_{droop}Q_{VSC} - K_{ivs}x_7 \tag{2.105}$$

A simplified model for designing PCC voltage controller is available in [32] and is explained in chapter 3. This model can be utilized for designing the compensator when there is no or minimum interaction with dc-link voltage control loop. Hence, the

complete linearized state space model of the distribution network, PV and controller subsystems is first derived. Eigenvalue sensitivity analysis studies are then used to choose optimal gains for the compensator $K_{Vac}(s)$ in the presence of interaction with dc –link voltage control loop. The results are later compared with the simplified model of PCC voltage controller.

2.5.6 State Space Model

The state space model of the entire controller subsystem is obtained by combining (2.65) - (2.68), (2.73) - (2.75), (2.80) - (2.82), (2.89) - (2.92), (2.98) - (2.100) and (2.104) - (2.105). All the equations are then expressed in dq frame using the transformation in (2.13).

Equations (2.62) and (2.63) are substituted in (2.65) and (2.66) to get the following:

$$\frac{dV_{cdf}}{dt} = \frac{R_c}{\tau_2} i_{td} + \frac{V_{cfd}}{\tau_2} - \frac{R_c}{x\tau_2} i_{s1d} - \frac{V_{cdf}}{\tau_2} \tag{2.106}$$

$$\frac{dV_{cqf}}{dt} = \frac{R_c}{\tau_2} i_{tq} + \frac{V_{cfq}}{\tau_2} - \frac{R_c}{x\tau_2} i_{s1q} - \frac{V_{cqf}}{\tau_2} \tag{2.107}$$

The nonlinear state space model of the Controller subsystem is:

$$\frac{dx_8}{dt} = b_2 V_{cqf}(t) \tag{2.108}$$

$$\frac{d\rho}{dt} = \omega_o + b_1 V_{cqf}(t) + x_8(t) \tag{2.109}$$

$$\frac{dV_{cdf}}{dt} = \frac{R_c}{\tau_2} i_{td} + \frac{V_{cfd}}{\tau_2} - \frac{R_c}{x\tau_2} i_{s1d} - \frac{V_{cdf}}{\tau_2} \tag{2.110}$$

$$\frac{dV_{cqf}}{dt} = \frac{R_c}{\tau_2} i_{tq} + \frac{V_{cfq}}{\tau_2} - \frac{R_c}{x\tau_2} i_{s1q} - \frac{V_{cqf}}{\tau_2} \tag{2.111}$$

$$\frac{dV_{s1df}}{dt} = \frac{V_{s1d}}{\tau_1} - \frac{V_{s1df}}{\tau_1} \tag{2.112}$$

$$\frac{dV_{s1qf}}{dt} = \frac{V_{s1q}}{\tau_1} - \frac{V_{s1qf}}{\tau_1} \tag{2.113}$$

$$\frac{dx_3}{dt} = K_{ii1}K_{pv}x_6 + K_{ii1}K_{iv}x_5 - K_{ii1}i_{td} \tag{2.114}$$

$$\frac{dx_5}{dt} = x_6 \tag{2.115}$$

$$\frac{dx_6}{dt} = -\frac{V_{dcref}}{\tau_{Vdc}} + \frac{V_{dc}}{\tau_{Vdc}} - \frac{x_6}{\tau_{Vdc}} \tag{2.116}$$

$$\begin{aligned}\frac{dx_4}{dt} = {} & -K_{ii2}K_{pvs}V_{pccref} + K_{ii2}K_{pvs}\sqrt{V_{s1df}^2 + V_{s1qf}^2} \\ & -\frac{3}{2}K_{ii2}K_{pvs}K_{droop}V_{cdf}i_{tq} - K_{ii2}K_{ivs}x_7 \\ & - K_{ii2}i_{tq}\end{aligned} \tag{2.117}$$

$$\frac{dx_7}{dt} = V_{pccref} - \sqrt{V_{s1df}^2 + V_{s1qf}^2} + \frac{3}{2}K_{droop}V_{cdf}i_{tq} \tag{2.118}$$

$$\begin{aligned}m_d = {} & \frac{2K_{pi1}K_{pv}}{V_{dc}}x_6 + \frac{2K_{pi1}K_{iv}}{V_{dc}}x_5 - \frac{2K_{pi1}i_{td}}{V_{dc}} + \frac{2x_3}{V_{dc}} \\ & - \frac{2L_f\omega i_{tq}}{V_{dc}} + \frac{2V_{cdf}}{V_{dc}}\end{aligned} \tag{2.119}$$

$$\begin{aligned}m_q = {} & -\frac{2K_{pi1}K_{pvs}}{V_{dc}}V_{pccref} + \frac{2K_{pi2}K_{pvs}}{V_{dc}}\sqrt{V_{s1df}^2 + V_{s1qf}^2} \\ & - \frac{3K_{pi2}K_{pvs}K_{droop}V_{cdf}i_{tq}}{V_{dc}} - \frac{2K_{pi2}K_{ivs}x_7}{V_{dc}} \\ & - \frac{2K_{pi2}i_{tq}}{V_{dc}} + \frac{2x_4}{V_{dc}} + \frac{2L_f\omega i_{td}}{V_{dc}} + \frac{2V_{cqf}}{V_{dc}}\end{aligned} \tag{2.120}$$

$$\omega = \omega_o + b_1V_{cqf} + x_8 \tag{2.121}$$

Equations (2.108) - (2.121) constitute a state space model for controller subsystem. The following are the state variables, inputs and outputs:

State Variables: $x_8, \rho, V_{cdf}, V_{cqf}, V_{s1df}, V_{s1qf}, x_3, x_5, x_6, x_4$ and x_7

Inputs: $V_{cfd}, V_{cfq}, i_{td}, i_{tq}, i_{s1d}, i_{s1q}, V_{dc}, \omega, V_{dcref}, V_{pccref}, V_{s1d}$ and V_{s1q}

Outputs: m_d, m_q, ρ and ω

2.5.7 Assumptions made in the modeling of Controller Subsystem

The following are some of the major assumptions made in the modeling of controller subsystem:

- Nonlinear elements such as saturation blocks are used in control system of PV-STATCOM for limiting the signals within certain values. In the derivation of nonlinear models and linearization of this model in the next section, the effects of these saturation blocks are not considered. These nonlinear elements might affect the stability of nonlinear model and affect the validity of results obtained from linearized model about the same operating point. Hence, the linearized model is valid about a particular operating point as long as the signals are within the saturation limits. Studies involving the effects of these saturation blocks on stability are beyond the scope of this thesis.

2.6 Linearization of State Space Models

This section deals with the linearization of the nonlinear state space models of distribution network subsystem and PV-STATCOM unit (PV subsystem and controller subsystem). The nonlinear model has to be linearized around an operating point to develop the linearized model. The linearized model is valid only for small perturbations of the system around the operating point. The theory for linearization has been adapted from [54], [60].

The linearized model is suitable for designing the PCC voltage controller by performing Eigenvalue studies. The model is also useful for studying the sensitivity of the

eigenvalues with respect to variation in system parameters such as X/R ratio of the distribution network and the variations in controller parameters.

The general form of nonlinear state and output equations of each subsystem is given below:

$$\dot{X} = f(X, U) \tag{2.122}$$

$$Y = h(X, U) \tag{2.123}$$

Where

$$X = [\, x_1\ x_2\ \ldots\ldots\ldots\ldots x_n]^{\mathrm{T}} \tag{2.124}$$

is a n * 1 matrix of n state variables $x_1, x_2 \ldots\ldots\ldots\ldots x_n$.

$$U = [\, u_1\ u_2\ \ldots\ldots\ldots\ldots u_p]^{\mathrm{T}} \tag{2.125}$$

is a p * 1 matrix of p input variables $u_1, u_2 \ldots\ldots\ldots\ldots u_p$.

$$Y = [\, y_1\ y_2\ \ldots\ldots\ldots\ldots y_q]^{\mathrm{T}} \tag{2.126}$$

is a q * 1 matrix of q output variables $y_1, y_2 \ldots\ldots\ldots\ldots y_q$.

$$f = [\, f_1\ f_2\ \ldots\ldots\ldots\ldots f_n]^{\mathrm{T}} \tag{2.127}$$

is a matrix of n state equations.

$$h = [\, h_1\ h_2\ \ldots\ldots\ldots\ldots h_q]^{\mathrm{T}} \tag{2.128}$$

is a matrix of q output equations.

In the same way, the state space and output equations of each subsystem can written as:

The state space and output equations of the distribution network subsystem can be represented as follows:

$$\dot{X}_1 = f_1(X_1, U_1) \tag{2.129}$$

$$Y_1 = h_1(X_1, U_1) \tag{2.130}$$

Where

$$X_1 = [\, i_{1d}\; i_{1q}\; V_{1d}\;\; V_{1q}\; i_{12d}\; i_{12q}\; V_{s1d}\; V_{s1q}\; i_{23d}\; i_{23q}\; V_{s2d}\; V_{s2q}\;\; i_{34d}\; i_{34q}\; V_{Ld}\; V_{Lq}\; i_{Ld}\; i_{Lq}]^{\mathrm{T}} \tag{2.131}$$

$$U_1 = [\rho\; \omega\;\; i_{s1d}\; i_{s1q} i_{s2d}\; i_{s2q}]^{\mathrm{T}} \tag{2.132}$$

$$Y_1 = [V_{s1d}\; V_{s1q} V_{s2d}\; V_{s2q}]^{\mathrm{T}} \tag{2.133}$$

The state space and output equations of the PV subsystem can be represented as follows:

$$\dot{X}_2 = f_2(X_2, U_2) \tag{2.134}$$

$$Y_2 = h_2(X_2, U_2) \tag{2.135}$$

Where

$$X_2 = [\, i_{td}\;\; i_{tq}\; V_{cfd}\;\; V_{cfq}\; i_{s1d}\; i_{s1q}\; V_{dc}]^{\mathrm{T}} \tag{2.136}$$

$$U_2 = [m_d\;\; m_q\; V_{s1d}\; V_{s1q}\; \omega\; G]^{\mathrm{T}} \tag{2.137}$$

$$Y_2 = [\, i_{td}\;\; i_{tq}\; V_{dc}\; V_{cd}\;\; V_{cq}]^{\mathrm{T}} \tag{2.138}$$

The state space and output equations of the Controller subsystem can be represented as follows:

$$\dot{X}_3 = f_3(X_3, U_3) \tag{2.139}$$

$$Y_3 = h_3(X_3, U_3) \tag{2.140}$$

Where

$$X_3 = [\, x_8 \; \rho \; V_{cdf} \; V_{cqf} \;\; V_{s1df} \; V_{s1qf} \; x_3 \; x_5 \; x_6 \; x_4 \; x_7]^{\mathrm{T}} \tag{2.141}$$

$$U_3 = [V_{cfd} \; V_{cfq} \; i_{td} \;\; i_{tq} \; i_{s1d} \; i_{s1q} \; V_{dc} \; \omega \; V_{dcref} \;\; V_{pccref} \; V_{s1d} \; V_{s1q}]^{\mathrm{T}} \tag{2.142}$$

$$Y_3 = \; [m_d \;\; m_q \; \rho \;\; \omega]^{\mathrm{T}} \tag{2.143}$$

In order to linearize the nonlinear equations of the form given in (2.122) and (2.123), they have to be perturbed about an operating point.

Let the operating point be such that for an input U_o, the initial state is X_o and the output is Y_o. Now, the solution of (2.122) and (2.123) about this operating point is

$$\dot{X_o} = \; f(X_o, U_o) = 0 \tag{2.144}$$

$$Y_o = h(X_o, U_o) = 0 \tag{2.145}$$

After perturbation, the state matrix, input matrix and output matrices become,

$$X = \; X_o + \tilde{X} \tag{2.146}$$

$$U = \; U_o + \tilde{U} \tag{2.147}$$

$$Y = \; Y_o + \tilde{Y} \tag{2.148}$$

Where $\tilde{X}, \tilde{U}$ and $\tilde{Y}$ represent the perturbed state variable, input variable and output variable matrices respectively.

Substituting (2.146) - (2.148) in (2.122) - (2.123),

$$\dot{X} = \; \dot{X_o} + \dot{\tilde{X}} = \; f\big(X_o + \tilde{X}, U_o + \tilde{U}\big) \tag{2.149}$$

$$\dot{Y} = \; \dot{Y_o} + \dot{\tilde{Y}} = h\big(X_o + \tilde{X}, U_o + \tilde{U}\big) \tag{2.150}$$

The perturbations are assumed to be small and hence, the equations (2.149) and (2.150) can be expanded using Taylor's series expansion. This leads to the following equations,

$$\dot{X} = \dot{X_o} + \dot{\tilde{X}} = f(X_o, U_o) + \frac{df}{dX}\tilde{X} + \frac{df}{dU}\tilde{U} + \cdots \ldots\ldots\ldots\ldots \quad (2.151)$$

$$\dot{Y} = \dot{Y_o} + \dot{Y} = h(X_o, U_o) + \frac{dh}{dX}\tilde{X} + \frac{dh}{dU}\tilde{U} + \cdots \ldots\ldots\ldots\ldots \quad (2.152)$$

In (2.151) and (2.152), the second and higher order derivatives of *f and h* can be assumed to be very small and are neglected.

By using (2.144) and (2.145) in (2.151) and (2.152), the following can be deduced,

$$\dot{\tilde{X}} = \frac{df}{dX}\tilde{X} + \frac{df}{dU}\tilde{U} \quad (2.153)$$

$$\dot{\tilde{Y}} = \frac{dh}{dX}\tilde{X} + \frac{dh}{dU}\tilde{U} \quad (2.154)$$

Equations (2.153) and (2.154) can be written in the following form as,

$$\dot{\tilde{X}} = A\tilde{X} + B\tilde{U} \quad (2.155)$$

$$\dot{\tilde{Y}} = C\tilde{X} + D\tilde{U} \quad (2.156)$$

Where

$$A = \begin{bmatrix} \frac{df_1}{dx_1} & \cdots & \frac{df_1}{dx_n} \\ \vdots & \ddots & \vdots \\ \frac{df_n}{dx_1} & \cdots & \frac{df_n}{dx_n} \end{bmatrix} \quad (2.157)$$

is a n * n system matrix

$$B = \begin{bmatrix} \frac{df_1}{du_1} & \cdots & \frac{df_1}{du_p} \\ \vdots & \ddots & \vdots \\ \frac{df_n}{du_1} & \cdots & \frac{df_n}{du_p} \end{bmatrix} \tag{2.158}$$

is a n * p control matrix

$$C = \begin{bmatrix} \frac{dh_1}{dx_1} & \cdots & \frac{dh_1}{dx_n} \\ \vdots & \ddots & \vdots \\ \frac{dh_q}{dx_1} & \cdots & \frac{dh_q}{dx_n} \end{bmatrix} \tag{2.159}$$

is a q * n output matrix

$$D = \begin{bmatrix} \frac{dh_1}{du_1} & \cdots & \frac{dh_1}{du_p} \\ \vdots & \ddots & \vdots \\ \frac{dh_q}{du_1} & \cdots & \frac{dh_q}{du_p} \end{bmatrix} \tag{2.160}$$

is a q * p feed-forward matrix

The partial derivatives in A, B, C and D are evaluated at the operating point X_o, U_o and Y_o. Equation (2.155) is the linearized state equation and (2.156) is the linearized output equation. These equations are referred to as the linearized state space model.

2.6.1 Linearized Model of Distribution Network Subsystem

The distribution network subsystem is linearized using the procedure explained in section 2.6. The linearized state and output equations of subsystem 1 are as follows:

$$\dot{\widetilde{X_1}} = A_{11}\widetilde{X_1} + B_{11}\widetilde{U_{11}} + B_{12}\widetilde{U_{12}} + B_{13}\widetilde{U_{13}} \tag{2.161}$$

$$\begin{bmatrix} \widetilde{V_{s1d}} \\ \widetilde{V_{s1q}} \end{bmatrix} = C_{311}\widetilde{X_1} \tag{2.162}$$

Where,

$$\widetilde{X_1} = [\widetilde{\iota_{1d}}\ \widetilde{\iota_{1q}}\ \widetilde{V_{1d}}\ \ \widetilde{V_{1q}}\ \widetilde{\iota_{12d}}\ \widetilde{\iota_{12q}}\ \widetilde{V_{s1d}}\ \widetilde{V_{s1q}}\ \widetilde{\iota_{23d}}\ \widetilde{\iota_{23q}}\ \widetilde{V_{s2d}}\ \widetilde{V_{s2q}}\ \ \widetilde{\iota_{34d}}\ \widetilde{\iota_{34q}}\ \widetilde{V_{Ld}}\ \widetilde{V_{Lq}}\ \widetilde{\iota_{Ld}}\ \widetilde{\iota_{Lq}}]^{\mathrm{T}} \tag{2.163}$$

is a 18 * 1 state variable matrix.

$$\widetilde{U_{11}} = \begin{bmatrix} \widetilde{\iota_{s2d}} \\ \widetilde{\iota_{s2q}} \end{bmatrix} \tag{2.164}$$

$$\widetilde{U_{12}} = \begin{bmatrix} \widetilde{\iota_{s1d}} \\ \widetilde{\iota_{s1q}} \end{bmatrix} \tag{2.165}$$

$$\widetilde{U_{13}} = \begin{bmatrix} \tilde{\rho} \\ \tilde{\omega} \end{bmatrix} \tag{2.166}$$

The matrix A_{11} is the system matrix. B_{11}, B_{12} and B_{13} are the control matrices. C_{311} is the output matrix. All these matrices are presented in Appendix A.

2.6.2 Linearized Model of PV subsystem

The PV subsystem is linearized using the procedure explained in section 2.6. The linearized state and output equations of subsystem 2 are as follows:

$$\dot{\widetilde{X_2}} = A_{22}\widetilde{X_2} + B_{21}\widetilde{U_{21}} + B_{22}\widetilde{U_{22}} + B_{231}\widetilde{U_{231}} + B_{232}\widetilde{U_{232}} \tag{2.167}$$

$$\begin{bmatrix} \widetilde{\iota_{s1d}} \\ \widetilde{\iota_{s1q}} \end{bmatrix} = C_{22}\widetilde{X_2} \tag{2.168}$$

$$\begin{bmatrix} \widetilde{V_{cfd}} \\ \widetilde{V_{cfq}} \\ \widetilde{\iota_{td}} \\ \widetilde{\iota_{tq}} \\ \widetilde{\iota_{sd}} \\ \widetilde{\iota_{sq}} \\ \widetilde{V_{dc}} \end{bmatrix} = C_{322}\widetilde{X_2} \tag{2.169}$$

Where,

$$\widetilde{X_2} = [\,\widetilde{\imath_{td}}\ \widetilde{\imath_{tq}}\ \widetilde{V_{cfd}}\ \ \widetilde{V_{cfq}}\ \widetilde{\imath_{s1d}}\ \widetilde{\imath_{s1q}}\ \widetilde{V_{dc}}\,]^{\mathrm{T}} \tag{2.170}$$

is a 7 * 1 state variable matrix.

$$\widetilde{U_{21}} = \begin{bmatrix} \widetilde{V_{s1d}} \\ \widetilde{V_{s1q}} \end{bmatrix} \tag{2.171}$$

$$\widetilde{U_{22}} = \left[\tilde{G}\right] \tag{2.172}$$

$$\widetilde{U_{231}} = \begin{bmatrix} \widetilde{m_d} \\ \widetilde{m_q} \end{bmatrix} \tag{2.173}$$

$$\widetilde{U_{232}} = [\tilde{\omega}] \tag{2.174}$$

The matrix A_{22} is the system matrix. B_{21}, B_{22}, B_{231} and B_{232} are the control matrices. C_{22} and C_{322} are the output matrices. All these matrices are presented in Appendix A.

2.6.3 Linearized Model of Controller Subsystem

The Controller subsystem is linearized using the procedure explained in section 2.6. The linearized state and output equations of subsystem 3 are as follows:

$$\dot{\widetilde{X_3}} = A_{33}\widetilde{X_3} + B_{331}\widetilde{U_{31}} + B_{332}\widetilde{U_{32}} + B_{333}\widetilde{U_{33}} + B_{33\omega}\widetilde{U_{\omega}} \tag{2.175}$$

$$\begin{bmatrix} \tilde{\rho} \\ \tilde{\omega} \end{bmatrix} = C_{13}\widetilde{X_3} \tag{2.176}$$

$$\begin{bmatrix} \widetilde{m_d} \\ \widetilde{m_q} \end{bmatrix} = C_{23m}\widetilde{X_3} + D_{231}\widetilde{U_{31}} + D_{232}\widetilde{U_{32}} + D_{233}\widetilde{U_{33}} + D_{23\omega}\widetilde{U_{\omega}} \tag{2.177}$$

$$[\tilde{\omega}] = C_{\omega}\widetilde{X_3} \tag{2.178}$$

Where,

$$\widetilde{X_3} = [\,\widetilde{x_8}\ \tilde{\rho}\ \ \widetilde{V_{cdf}}\ \widetilde{V_{cqf}}\ \ \widetilde{V_{s1df}}\ \widetilde{V_{s1qf}}\ \widetilde{x_3}\ \widetilde{x_5}\ \widetilde{x_6}\ \widetilde{x_4}\ \widetilde{x_7}\,]^{\mathrm{T}}$$

(2.179)

is a 11 * 1 state variable matrix.

$$\widetilde{U_{31}} = \begin{bmatrix} \widetilde{V_{s1d}} \\ \widetilde{V_{s1q}} \end{bmatrix} \tag{2.180}$$

$$\widetilde{U_{32}} = [\widetilde{V_{cfd}}\ \widetilde{V_{cfq}}\ \widetilde{\imath_{td}}\ \widetilde{\imath_{tq}}\ \widetilde{\imath_{s1d}}\ \widetilde{\imath_{s1q}}\ \widetilde{V_{dc}}]^{\mathrm{T}} \tag{2.181}$$

$$\widetilde{U_{33}} = \begin{bmatrix} \tilde{V}_{dcref} \\ \tilde{V}_{pccref} \end{bmatrix} \tag{2.182}$$

$$\widetilde{U_{\omega}} = [\tilde{\omega}] \tag{2.183}$$

The matrix A_{33} is the system matrix. $B_{331}, B_{332}, B_{333}$ and $B_{33\omega}$ are the control matrices. C_{13}, C_{23} and C_{ω} are the output matrices. D_{231}, D_{232}, D_{233} and $D_{23\omega}$ are the feed-forward matrices. All these matrices are presented in Appendix A.

It was pointed out in section 2.5.5 that the compensator of PCC voltage controller can be of P or PI type. If the controller is of P type, the state variable x_7 has to be eliminated from above linearized model.

The rows and columns to be removed from the matrices in (2.175), (2.176), (2.177) and (2.178) in order to eliminate the state x_7 from the system is shown boxed in black using dotted lines for the corresponding matrices and presented in Appendix A.

In order to study the effect of proportional type PCC voltage controller, the highlighted rows and columns have to be removed from the model and the order of the system reduces accordingly.

2.6.4 Linearized Model of the complete system

The linearized state space model of the complete system can be obtained by combining the linearized models of distribution network subsystem ((2.161) and (2.162)), PV

subsystem ((2.167), (2.168) and (2.169)) and controller subsystem ((2.175), (2.176), (2.177) and (2.178)).

The linearized model of the complete system is of the form,

$$\dot{\widetilde{X_{sys}}} = A_{sys}\widetilde{X_{sys}} + B_{sys}\widetilde{U_{sys}} \tag{2.184}$$

Where,

$$\widetilde{X_{sys}} = [\widetilde{X_1}\ \widetilde{X_2}\ \widetilde{X_3}]^{\mathrm{T}} \tag{2.185}$$

$$\widetilde{U_{sys}} = [\widetilde{\iota_{s2d}}\ \widetilde{\iota_{s2q}}\ \tilde{G}\ \widetilde{\tilde{V}_{dcref}}\ \widetilde{\tilde{V}_{pccref}}]^{\mathrm{T}} \tag{2.186}$$

$$A_{sys} = \begin{bmatrix} A_{11} & B_{12}C_{22} & B_{13}C_{13} \\ B_{21}C_{11} + B_{231}D_{231}C_{311} & A_{22} + B_{231}D_{232}C_{322} & B_{231}C_{23m} + B_{231}D_{23\omega}C_{\omega} + B_{232}C_{\omega} \\ B_{331}C_{311} & B_{332}C_{322} & A_{33} + B_{33\omega}C_{\omega} \end{bmatrix} \tag{2.187}$$

$$B_{sys} = \begin{bmatrix} B_{11} & 0_{18x1} & 0_{18x2} \\ 0_{7x2} & B_{22} & B_{231}D_{233} \\ 0_{mx2} & 0_{mx1} & B_{333} \end{bmatrix} \tag{2.188}$$

The order of the system matrix A_{sys} is 36 * 36 if the PCC voltage controller is of PI type and 35 * 35 if the PCC voltage controller is of P type.

Similarly, the order of B_{sys} is 36 * 5 if the PCC voltage controller is of PI type and 35 * 5 if the PCC voltage controller is of P type.

In B_{sys}, the value of m is 11 if the PCC voltage controller is of PI type and is 10 if the PCC voltage controller is of P type.

There are three modes of operation of PV-STATCOM namely:

d) Full PV mode: The PV system supplies only real power and zero reactive power.

e) Partial PV-STATCOM mode: The PV system operates in real power priority mode and supplies reactive power depending on the available free capacity for performing PCC voltage regulation.

f) Full STATCOM mode: The PV system curtails its real power completely and acts as a STATCOM with full reactive power capacity during and post faults for providing voltage support to grid.

The model developed in equation (2.184) can be used to study the dynamics of the PV system operating in all three modes. This is described as follows:

(a) For Full PV mode:

For obtaining the linearized model of PV system operating in Full PV mode, the states V_{s1df}, V_{s1qf} and the inputs V_{s1d}, V_{s1q} have to be eliminated from the controller subsystem.

The rows and columns to be removed from the matrices in (2.175), (2.176), (2.177) and (2.178) in order to eliminate the states V_{s1df}, V_{s1qf} and inputs V_{s1d}, V_{s1q} from the controller subsystem are shown highlighted in yellow for the corresponding matrices and presented in Appendix A. Also, the gain K_{pvs} has to be made zero.

The final matrices of linearized system are:

$$A_{sys} = \begin{bmatrix} A_{11} & B_{12}C_{22} & B_{13}C_{13} \\ B_{21}C_{11} & A_{22} + B_{231}D_{232}C_{322} & B_{231}C_{23m} + B_{231}D_{23\omega}C_{\omega} + B_{232}C_{\omega} \\ 0_{8x18} & B_{332}C_{322} & A_{33} + B_{33\omega}C_{\omega} \end{bmatrix} \tag{2.189}$$

$$B_{sys} = \begin{bmatrix} B_{11} & 0_{18x1} & 0_{18x2} \\ 0_{7x2} & B_{22} & B_{231}D_{233} \\ 0_{8x2} & 0_{8x1} & B_{333} \end{bmatrix} \tag{2.190}$$

The model has to be linearized about an operating point such that the PV system supplies zero reactive power.

(b) For Partial PV-STATCOM Mode:

This has already been explained and the model is the same as the model developed in equation (2.184).

(c) For Full STATCOM mode:

The model of PV-STATCOM operating in Full-STATCOM mode is similar to the model developed for Partial PV-STATCOM. The changes that have to be made in the model are that the PV array parameters namely a_1, a_2, a_3, a_4 and a_5 have to be made zero. Also, the irradiance input to the PV array namely G has to be made zero.

2.7 Simulation Platforms used for studies

The model developed in sections 2.3, 2.4 and 2.5 represent the nonlinear averaged model of the entire system. This has been developed using the nonlinear equations of system in *dq* frame. The dynamics of inverter is represented using an averaged model. The model developed in section 2.6 represent the linearized version of the nonlinear averaged model. This is valid for only small perturbations of the system around the operating point about which the model is linearized. The simulation of linearized model and nonlinear averaged model are performed using MATLAB/Simulink simulation platform.

The simulations are also performed using PSCAD/EMTDC (Power Systems Computer Aided Design - Electromagnetic Transients including DC). This is an industry standard simulation software used for electromagnetic transient simulation of power system networks [40]. For simulation in PSCAD/EMTDC, the system is model using nonlinear models available in library of PSCAD based on the nonlinear equations developed in sections 2.3, 2.4 and 2.5. The dynamics of inverter are represented using a switched model made up of insulated gate bipolar transistors (IGBTs).

The linearized model is first validated by comparing its response with the nonlinear averaged model in MATLAB. Further validation is performed by comparing the responses of linearized model and PSCAD/EMTDC models.

2.8 CONCLUSION

The detailed nonlinear state space models of distribution network, PV and Controller subsystems have been developed in *dq* frame. The need for developing the complete linearized model of entire system has been elaborated. The procedure for linearization based on Taylor series expansion of a generalized nonlinear equation has been explained in detail. This procedure has been individually applied to each subsystem and the corresponding linearized model has been developed. The developed linearized model of each subsystem has been combined to obtain the complete linearized model of the system. The various individual matrices of each subsystem have been presented in Appendix A.

Chapter 3

3 EIGENVALUE BASED SENSITIVITY ANALYSIS AND CONTROLLER DESIGN FOR PV-STATCOM

3.1 Introduction

In this chapter, the design of various controllers of PV-STATCOM operating under Full PV, Partial PV-STATCOM and Full STATCOM modes are carried out.

First, the design of PLL, current controller and DC-Link Voltage Controller for operation in Full PV mode are carried out using linear control techniques. The model of PV-STATCOM operating in Full PV mode is then validated by comparing the linearized and PSCAD model responses.

Second, Eigenvalue based sensitivity analysis studies are then used to arrive at the optimum values of PCC voltage controller gains for partial PV-STATCOM. The developed model of partial PV-STATCOM is also validated by comparing the linearized and PSCAD model responses. A comparative Eigenvalue sensitivity analysis study is carried out to understand the range of various parameters that affect the stability of PCC voltage controller.

Third, the Eigenvalue based sensitivity analysis studies are also extended to operation of PV system in Full STATCOM mode for deciding the optimum values of PCC voltage controller gains. The developed model of Full STATCOM is also validated by comparing the linearized and PSCAD model responses.

3.2 Controller Design for Partial PV-STATCOM

As explained in chapter 2, a realistic medium voltage distribution feeder data is used to represent the distribution network which is again shown in Figure 3.1. The system data is adapted from an actual Hydro One distribution feeder in Ontario. With reference to Figure 3.1, the voltage at Bus 1 is 27.6 kV. This is supplied by the 115 kV supply substation (represented by substation grid supply) through a 32 MVA, 115 kV / 27.6 kV

transformer (leakage impedance of 0.05 pu). The total length of the distribution feeder is 45 km. The length of line 1, line 2 and line 3 are 35 km, 5 km and 5 km respectively. A solar farm (PV System) of 8.5 MW is connected to bus 3 using a 10 MVA, 0.48 / 27.6 kV coupling transformer (with a leakage impedance of 0.1 pu on its own base) at 35 km from bus 1. The peak daytime load on the feeder is 4.82 MW and 2.2 MVAr. This is represented by a series RL circuit, representing the peak daytime load at nominal voltage of 27.6 kV. The distribution network, load and PV system data are provided in Table B. 1 of Appendix B.

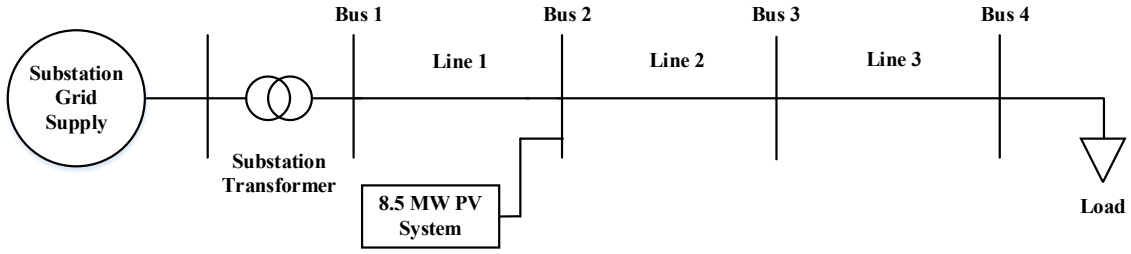

Figure 3.1 Simplified diagram of distribution network used for studies

3.2.1 Choice of operating point

Linearization of a nonlinear model requires the model to be linearized about an operating point. The operating point can be calculated by equating the linearized state and output equations to zero. In the model developed in Chapter 2, there are in total of 36 state equations. These equations are solved for a particular operating point by modeling them in MATLAB Simulink environment.

It should be noted that all the PSCAD/EMTDC waveforms shown in this thesis were obtained by passing the original signal through a noise removal filter with suitable time constant to remove PWM switching frequency harmonics and its side-band harmonics. This is to ensure that the frequency of oscillation to be studied is visible properly in all the waveforms. The noise removal filter does not affect the results in anyway.

3.2.2 Design of PLL

The function of PLL and its state space model have been explained in section 2.5.2. It has been pointed out that the choice of PI controller parameters can be found out for a particular bandwidth and phase margin requirements.

The procedure for the design of PLL has been adopted from [58]. The control block diagram for the design of PLL is shown in Figure 3.2. The first order transfer function with a time constant τ_2 represents the measurement filter dynamics. The integrator represents the dynamics of the voltage controlled oscillator (VCO), whose function is to generate the angle required for *abc* frame to *dq* frame transformation.

The loop transfer function of the PLL $l_{PLL}(s)$ is given by,

$$l_{PLL}(s) = \widehat{V_c}\left(\frac{1}{\tau_2 s + 1}\right)\left(b_1 + \frac{b_2}{s}\right)\left(\frac{1}{s}\right) \tag{3.1}$$

Where $\widehat{V_c}$ is the nominal peak voltage at the EPC.

The bandwidth and phase margin of the PLL can be adjusted by tuning gains b_1 and b_2.It is found from simulation studies in MATLAB that there is an inverse relation existing between phase margin and bandwidth of the loop transfer function of (3.1). A minimum phase margin of 45° is required to ensure the sufficient stability of closed loop systems [61]. For a phase margin of 47°, the closed loop bandwidth is 598 rad/sec. The gain crossover frequency is 360 rad/sec. The corresponding controller gains are found to be,

Table 3.1 PLL Controller parameters

Parameter	Value
b_1	1136.7
b_2	51151

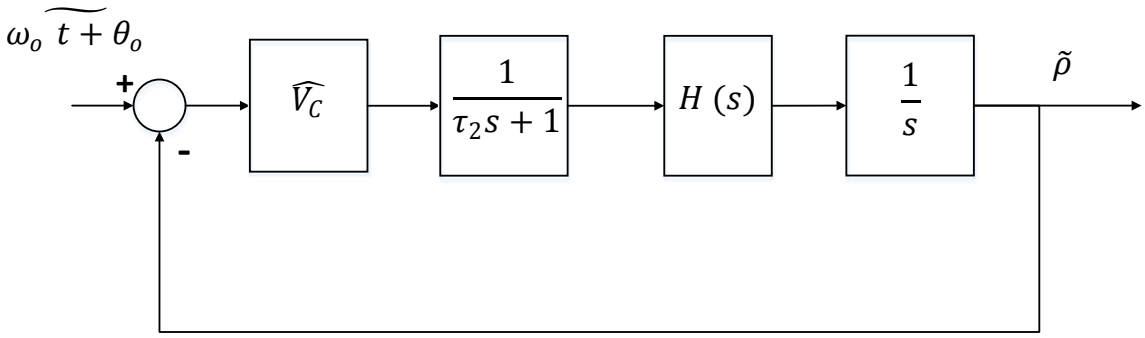

Figure 3.2 Control block diagram for design of PLL

The bode plot of (3.1) for the gains in Table 3.1 is shown in Figure 3.3.

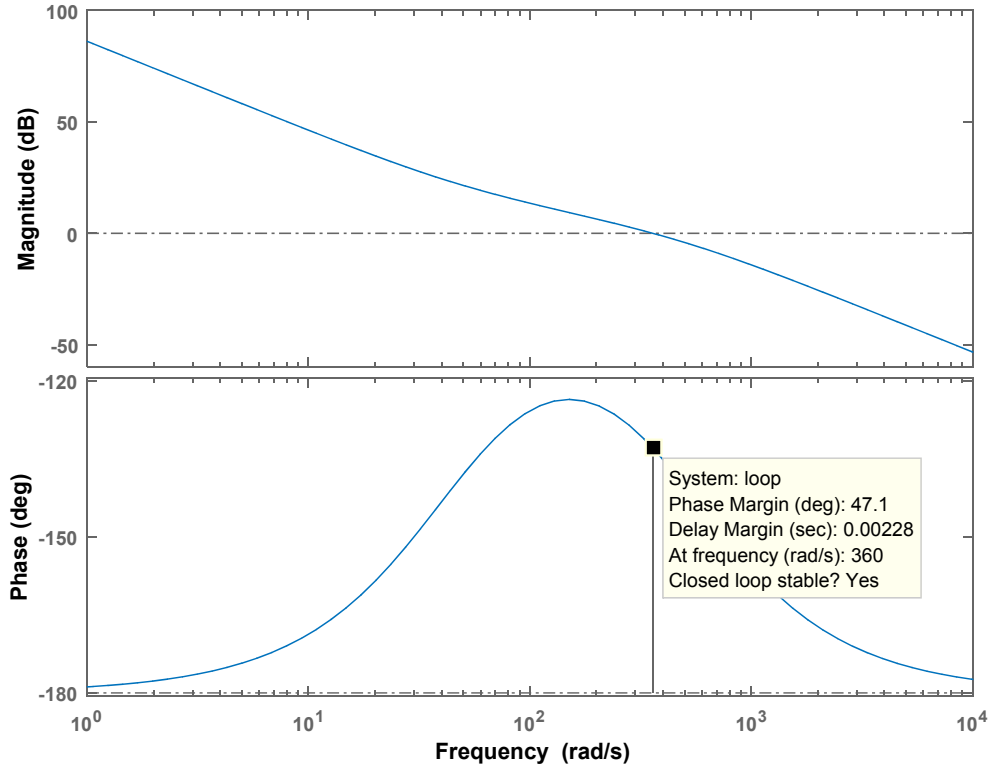

Figure 3.3 Bode Plot of PLL (for b1 = 1136.7 and b2 = 51151)

3.2.3 Design of Current Controller

The function of the current controller and its state space model have been explained in section 2.5.3. Compensators $K_d(s)$ and $K_q(s)$ are PI controllers and can be designed based on bandwidth and phase margin requirements. The control block diagram to design the compensator $K_d(s)$ is shown in Figure 3.4. The same block diagram and procedure applies to the design of $K_q(s)$.

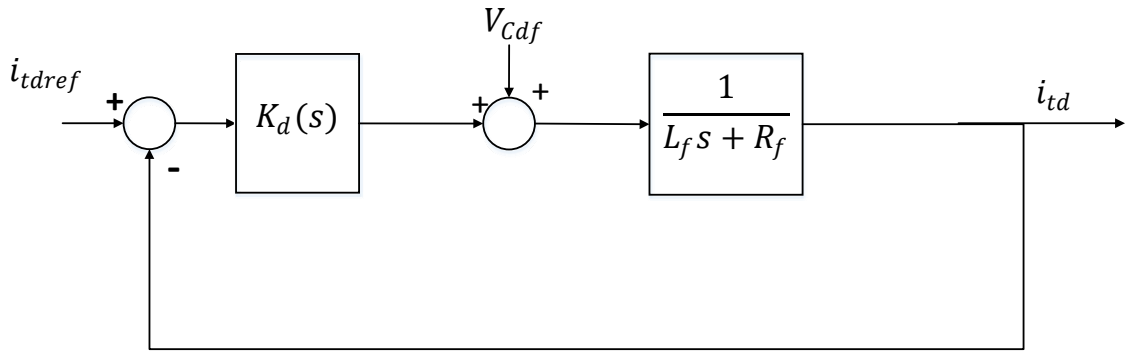

Figure 3.4 Control Block Diagram for design of current controller

Due to the delay introduced by feed-forward filter, the ac side dynamics cannot be represented only by using a RL circuit. There are some un-modeled ac side dynamics which get cancelled when the feed-forward voltage V_{cd} is perfect without any delay. But, if there is some delay, the model of ac side dynamics cannot be considered to only be a RL circuit and the method of pole zero cancellation [18] may not be the best method for current controller design. Hence, the current controller is designed with adequate phase margin so that controller remains stable even due to un-modeled system dynamics [18]. The dynamics of the feed-forward filter of V_{cd} can be considered as a disturbance and can be neglected for designing $K_d(s)$. The loop transfer function of current controller $l_I(s)$ is given by,

$$l_I(s) = (K_{pi1} + \frac{K_{ii1}}{s})(\frac{1}{L_f s + R_f}) \tag{3.2}$$

The closed transfer function of the current controller $C_I(s)$ is given by,

$$C_I(s) = \frac{\frac{K_{pi1}}{L_f}s + \frac{K_{ii1}}{L_f}}{s^2 + s\left(\frac{R_f + K_{pi1}}{L_f}\right) + \frac{K_{ii1}}{L_f}} \tag{3.3}$$

The current controller is designed based on the following specifications:

a) Bandwidth
b) Phase margin

The bandwidth of the current controller is usually chosen to be at least 10 to 20 times lower than the switching frequency of inverter [62]. The switching frequency of the inverter is chosen to be 5940 Hz (or 37303.2 rad/sec). For a phase margin of approximately 60°, the PI controller parameters are tuned such that the bandwidth of current controller is 1910 rad/sec (approximately 20 times lower than the switching frequency). The gain crossover frequency is 1380 rad/sec. The controller gains are given in Table 3.2.

Table 3.2 Current Controller Parameters

Parameter	Value
K_{pi1} (and K_{pi2})	0.034672
K_{ii1} (and K_{ii2})	31.52

The bode plot is shown in Figure 3.5. The response of the control block diagram (linearized model) of current controller and PSCAD / EMTDC model to a step of 2.5 kA is shown in Figure 3.6. A comparison between the responses are shown in Table 3.3. It can be seen that the peak time and settling time of both the models are very close to each other. This validates the designed current controller gains.

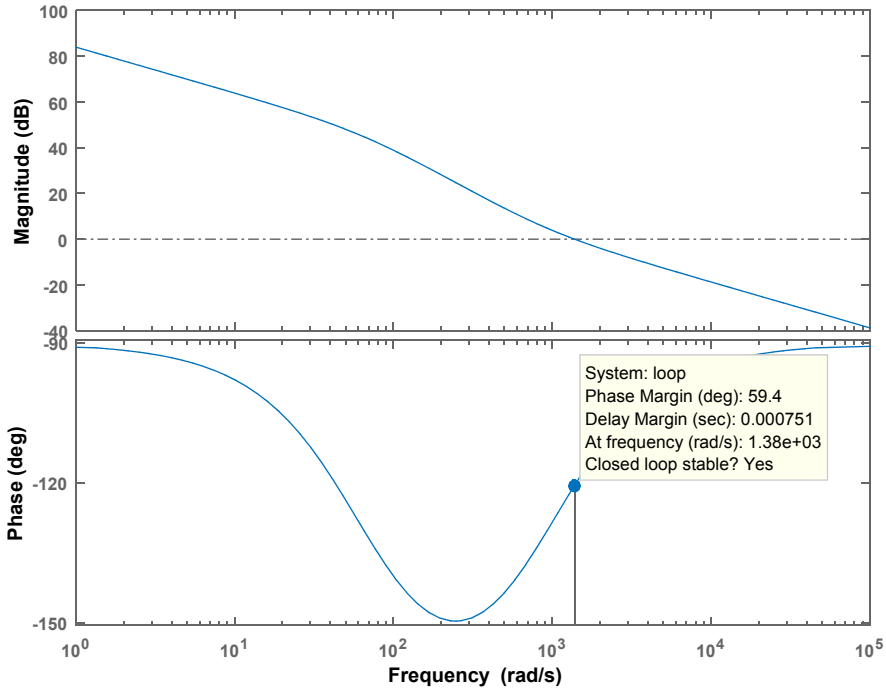

Figure 3.5 Bode Plot of Current Controller (for Kp = 0.0347 and Ki = 31.52)

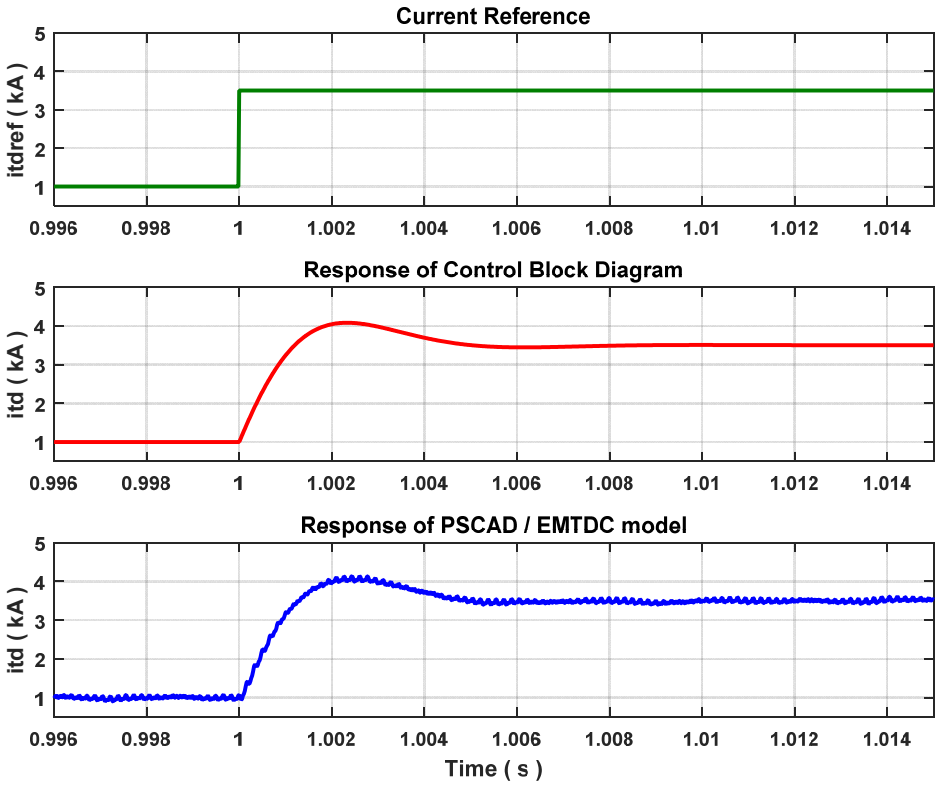

Figure 3.6 Step Response of Current Controller

Table 3.3 Comparison between current controller responses

Parameter	Time of first peak (Peak Time) (ms)	Settling Time (5 % error of steady state) (ms)
Control Block Diagram	2.3	4.1
PSCAD / EMTDC Model	2.6 (approximately)	4.2 (approximately)

3.2.4 Design of DC-Link Voltage Controller

The function of the DC-Link Voltage controller and its state space model have been explained in section 2.5.4. The PI controller of the compensator $K_V(s)$ can be designed based on bandwidth and phase margin requirements. The control block diagram (simplified model) to design the controller is shown in Figure 3.7.

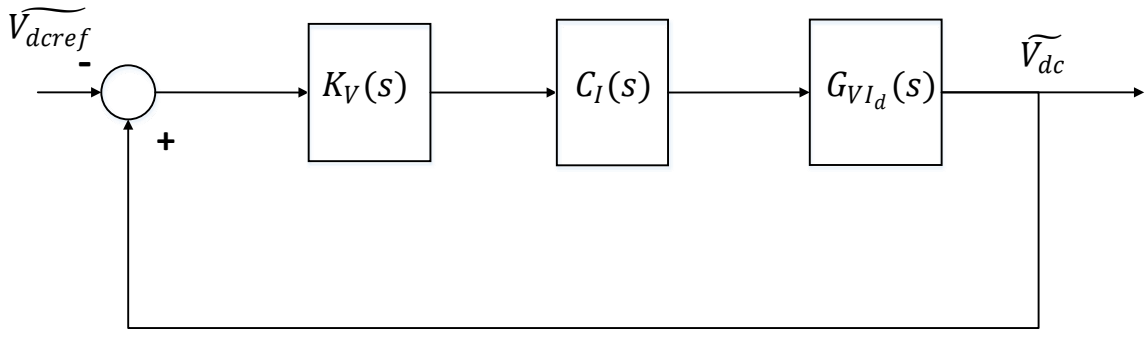

Figure 3.7 Control Block Diagram to design DC-link voltage controller (simplified model)

The value of V_{dcref} depends on the maximum power point voltage for a given irradiance of the PV array. The value of this voltage has been calculated for the maximum irradiance of 1 kW/m^2 and is found to be 1.0255 kV. The PV panel data given in Appendix B pertains to LDK-230P-20 [47]. It can be understood from the IV curve of this panel [63] that the maximum power point voltage is relatively less sensitive to irradiance. Hence, it is assumed that it remains fairly constant with change in irradiance.

The transfer function between i_{td} and V_{dc} is $G_{VI_d}(s)$, and it can be obtained by linearizing equation (2.61). The effect of i_{tq} and m_q on the dynamics of V_{dc} is very small and have been neglected for simplicity. $G_{VI_d}(s)$ is given by,

$$G_{VI_d}(s) = \frac{x_{Vdc2}}{s - x_{Vdc1}} \tag{3.4}$$

Where,

$$x_{Vdc1} = \frac{(-a_2 a_3 e^{a_3 V_{dco} + a_4 I_{pvo}}) - \left(a_2 a_4 e^{a_3 V_{dco} + a_4 I_{pvo}} * I_{pvvo}\right) - a_5}{C_{dc}} \tag{3.5}$$

$$x_{Vdc2} = \frac{(-3 * m_{do})}{4C_{dc}} \tag{3.6}$$

The steady state values can be found for a particular operating by equating (2.61) and (2.93) to zero. The data for one such operating point is provided in Table B. 2 of Appendix B.

The loop transfer function of the control block diagram in Figure 3.7 without considering the PI controller of $K_V(s)$ is,

$$l_v(s) = \left(\frac{1}{\tau_{Vdc} s + 1}\right) C_I(s) G_{VI_d}(s) \tag{3.7}$$

Equation (3.7) represents the loop gain of the uncompensated system. The bode plot of the uncompensated system is shown in Figure 3.8.

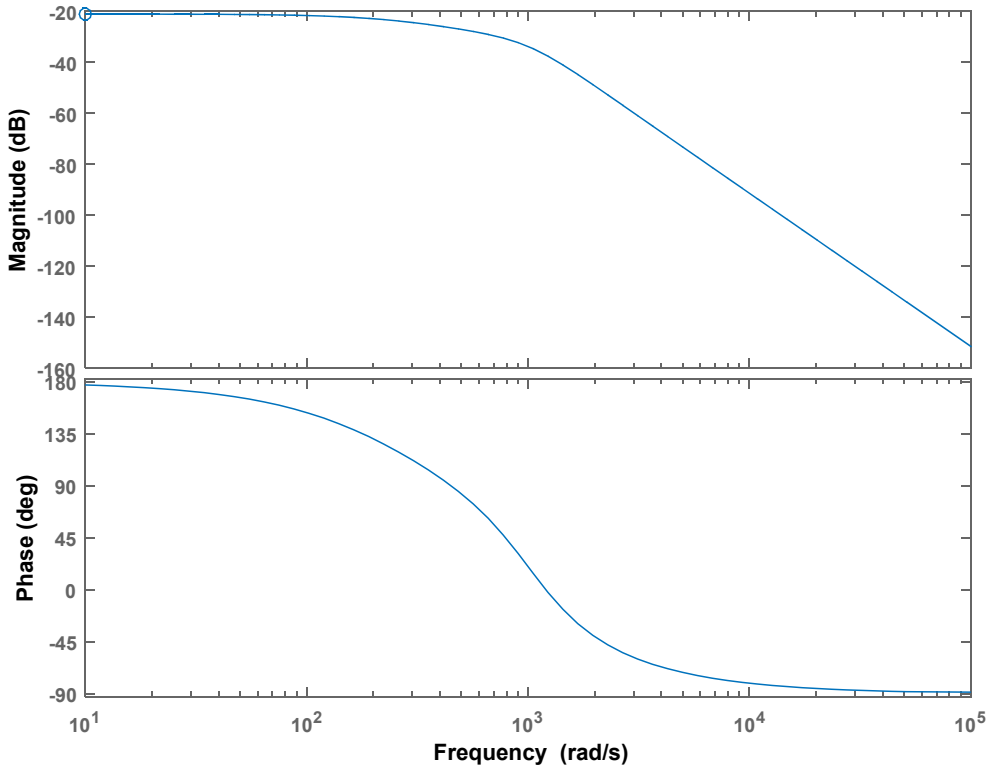

Figure 3.8 Bode plot of uncompensated system of DC-Link Voltage Controller

It is evident in Figure 3.8 that the system suffers steady state error although it has infinite phase margin. This can be solved by designing the PI controller for a particular bandwidth and phase margin. The cross-over frequency $\omega_{loopVdc}$ of the DC-link voltage controller is chosen to be 3 times slower than that of the current controller. For a cross over frequency of 1380 rad/sec for the current controller, $\omega_{loopVdc}$ will be 460 rad/sec. The PI values are tuned such that a phase margin of 60° is available at $\omega_{loopVdc}$. The values of PI gains are given in Table 3.4.

Table 3.4 DC-Link Voltage Controller Parameters

Parameter	Value
K_{pv}	19.0492
K_{iv}	4762.3

The bode plot of the compensated system is shown in Figure 3.9.

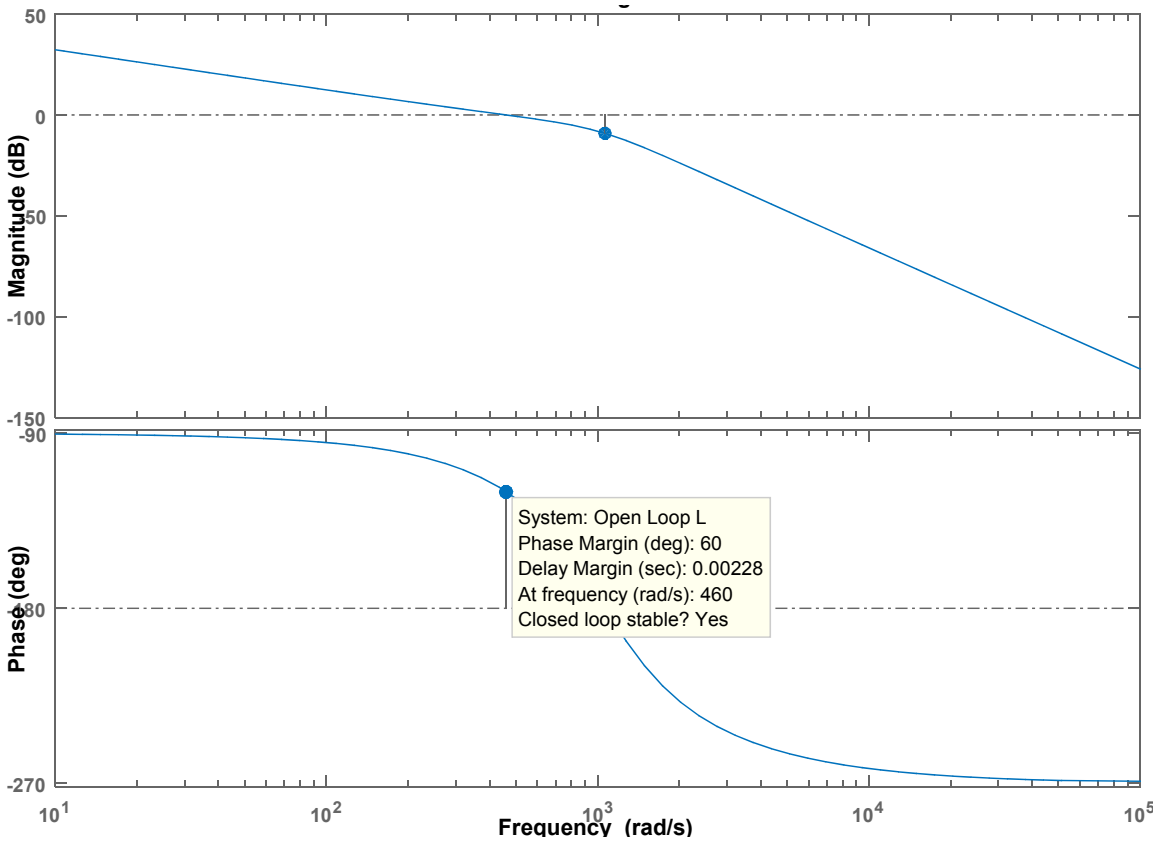

Figure 3.9 Bode plot of compensated system of DC-Link Voltage Controller

The response of the control block diagram (simplified model) of DC-Link Voltage controller and PSCAD / EMTDC model to a step of 10% of V_{dcref} is shown in Figure 3.10. The settling time of PSCAD / EMTDC model is around 6.5 ms whereas the settling time of linearized model is around 5.8 ms for 1% error margin. This shows that the responses of both the models are close to each other. But, the transient response of PSCAD / EMTDC model is more damped when compared with the transient response of simplified model. The reason for this discrepancy can be explained as follows:

The transfer function of (3.4) was obtained by linearizing equation (2.61). Equation (2.61) consists of the dynamics of inverter and PV array. With regard to simplified dc-link voltage controller model, the dynamics of inverter is represented by the term $-\frac{3m_d i_{td}}{4C_{dc}}$ and dynamics of PV array is represented by the term $-\frac{a_5 V_{dc}}{C_{dc}}$ –

$\frac{a_2\{e^{a_3 V_{dc}+a_4 I_{pv}}-1\}}{C_{dc}}$. It is due to high degree of nonlinearity of the term representing PV array dynamics that the transient responses exhibit differences. But, the controller designed with a phase margin of 60° remains stable even when subjected to large signal disturbances as it can be understood from studies in the next chapters.

For operation of PV system in Full STATCOM mode, the simplified model of dc-link voltage controller will be represented only by the inverter dynamics. In this case, the transient response of simplified model and PSCAD / EMTDC models matches closely. This will be shown later in this chapter while validating Full STATCOM model which will confirm the difference in response of Figure 3.10 is only due to nonlinearity of PV array.

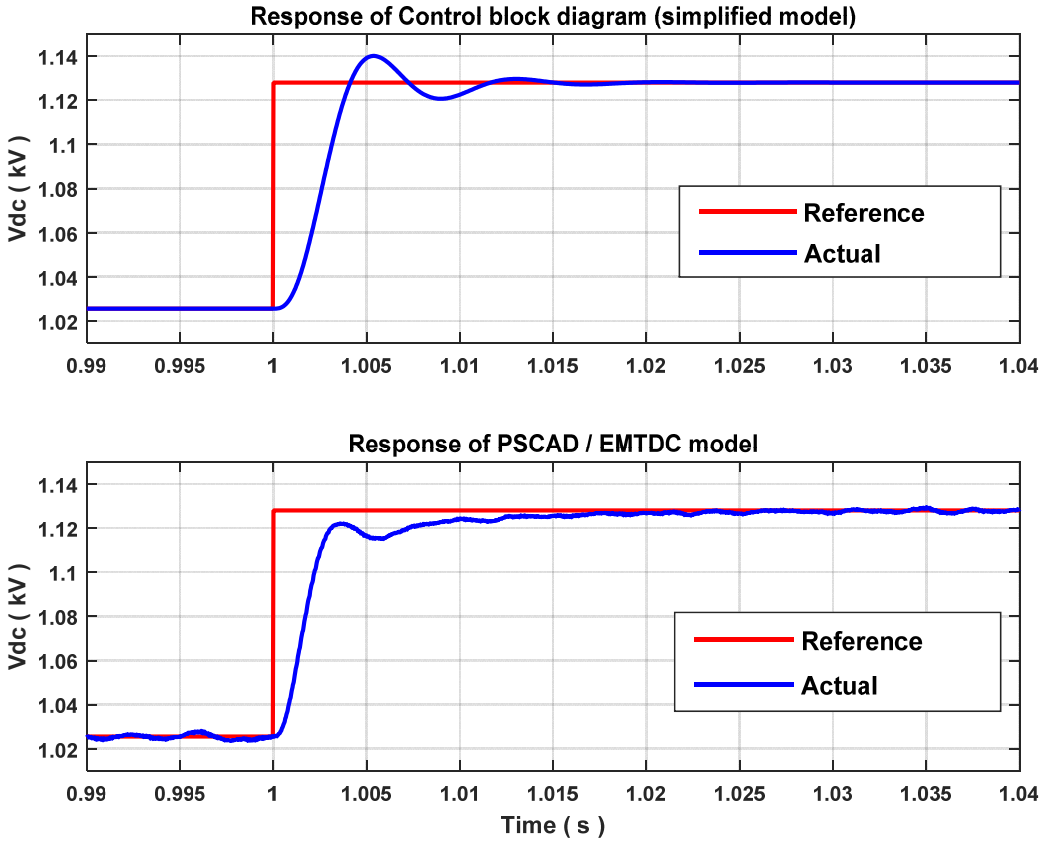

Figure 3.10 Step Response of DC-link Voltage Controller (for G = 0.85 kW/m^2)

3.2.5 Validation of linearized model operating in Full PV mode

The linearized model of PV system operating in Full PV mode has been developed in section 2.6.4. The controller subsystem consists of the measurement filter, PLL, current controllers and DC-link voltage controller. It does not include the dynamics of PCC voltage controller. The measurement filter time constants τ_1 and τ_2 are initially chosen as 2 ms to represent delays. They are chosen such that the bandwidths of measurement filters are in the range of bandwidths of current controllers and dc-link voltage controller. This presents a scenario where there could exist an interaction between these controllers and measurement filters since their bandwidths are closer. Further analysis will be performed in this chapter where the time constants would be varied to study its effect on PV system stability.

All the controllers have been designed except the PCC voltage controller. The model can be linearized about an operating point and its performance can be validated by performing step-response studies.

The model is linearized about three operating points such that G=0.95 kW/m^2, 0.5 kW/m^2 and 0.25 kW/m^2. At each operating point, a step response of 0.05 kW/m^2 is applied to the irradiance input and, the responses of dc-link voltage V_{dc} and active power P_{VSC} are compared for the linearized and PSCAD / EMTDC models for validating the linearized model.

Figure 3.11, Figure 3.12 and Figure 3.13 shows the responses of dc-link voltage V_{dc} and active power P_{VSC} to a step change in irradiance from 0.95 kW/m^2 to 1 kW/m^2, 0.5 kW/m^2 to 0.55 kW/m^2 and 0.25 kW/m^2 to 0.3 kW/m^2 respectively. It can be seen that the response of both linearized and PSCAD/EMTDC models match closely in both transient and steady state for all the cases. This validates the developed model for the operation of PV system in Full PV mode.

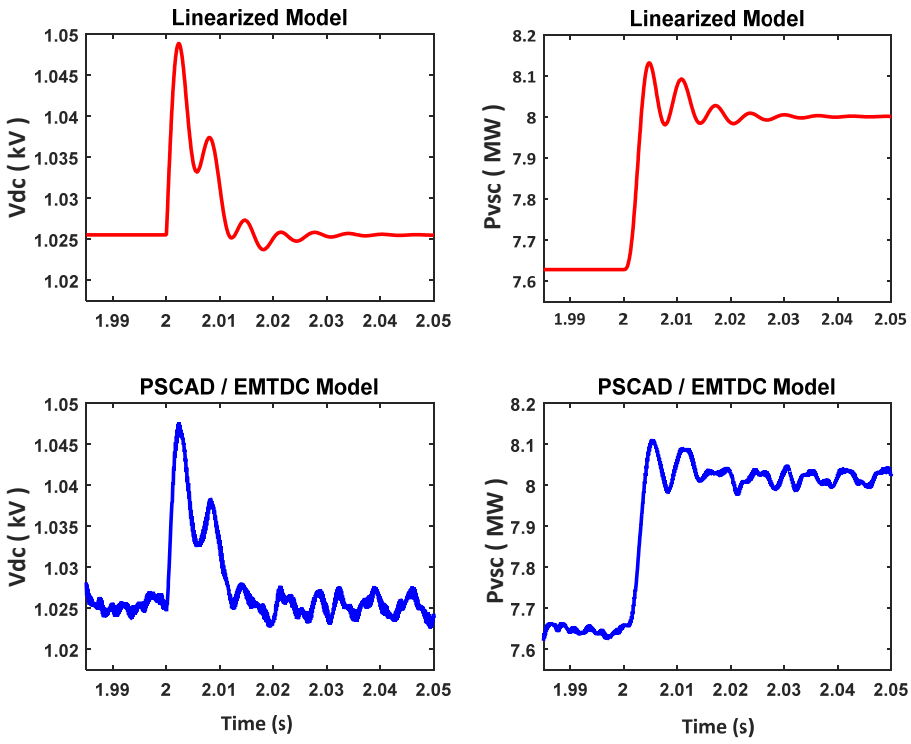

Figure 3.11 Response of V_{dc} and P_{VSC} for a step change in G = 0.95 to 1 kW/m^2

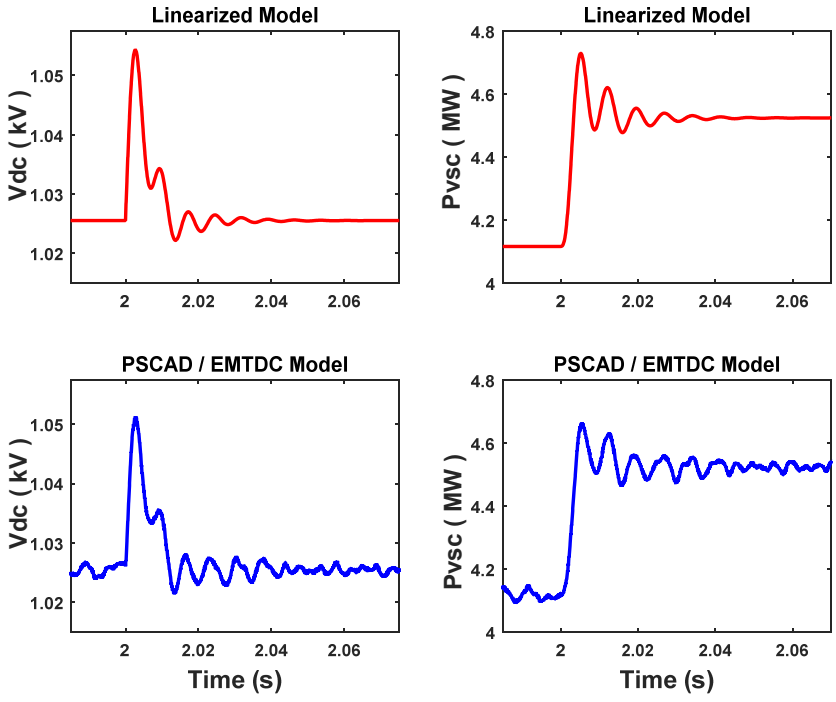

Figure 3.12 Response of V_{dc} and P_{VSC} for a step change in G = 0.5 to 0.55 kW/m^2

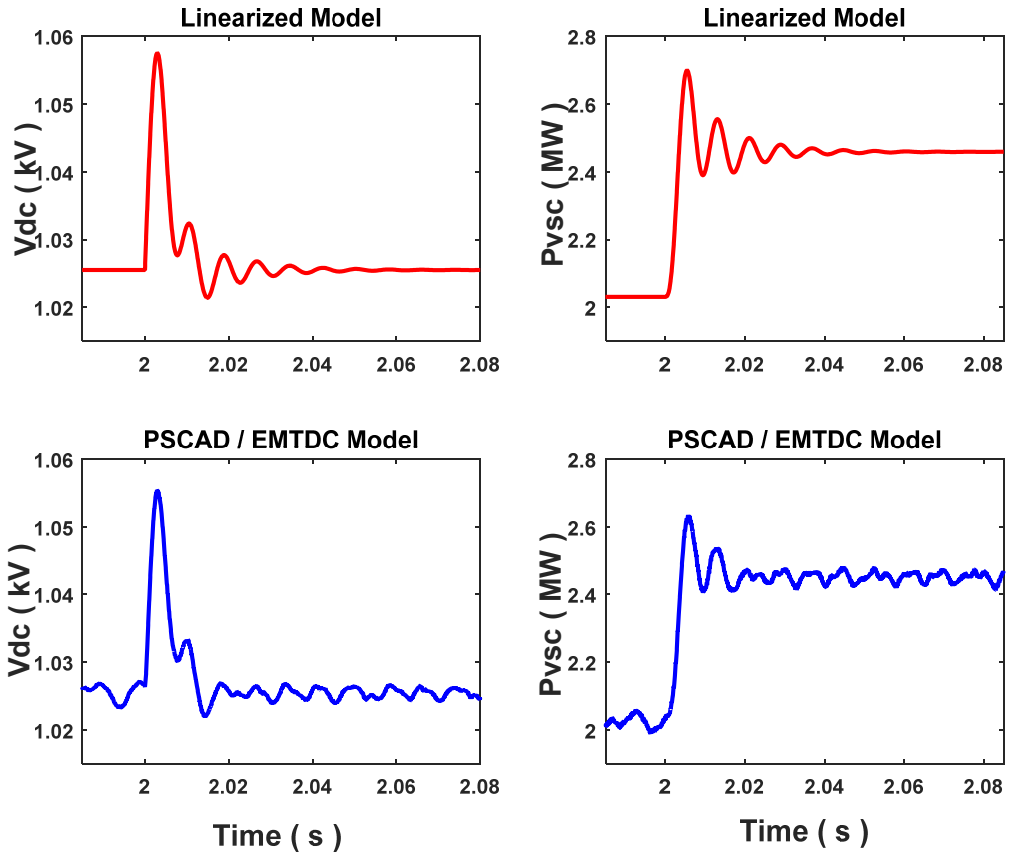

Figure 3.13 Response of V_{dc} and P_{VSC} for a step change in G = 0.25 to 0.3 kW/m^2

3.2.6 Design of PCC Voltage Controller

The function of the PCC Voltage controller and its state space model has been explained in section 2.5.5. It was pointed out that the controller can be of P or PI type. The state space model developed in section 2.6.4 is used for designing the PCC voltage controller.

The design of P type PCC voltage controller is first discussed and its disadvantages are shown. The design of PI type PCC voltage controller is discussed later and its advantages over the P type controller are shown.

3.2.6.1 Proportional Controller

The proportional controller represents the implementation of Volt/Var control and dynamic reactive current injection with a Smart PV inverter. Both these functions were explained in chapter 1. Both functions eventually involve injection of reactive current

based on an error between a reference voltage and actual voltage. The only main difference is that the speed of operation of reactive current controller is much faster for dynamic reactive current injection when compared to Volt/Var control. Initially, it is assumed that both functions are implemented with a fast reactive current controller so that a common platform for performing studies is established. This ensures that any proportional gain calculated for Volt/Var control is equally valid for dynamic reactive current injection and vice versa.

In order to calculate the slope of Volt/Var control curve, an equation has been developed in [30] which relates the active power rating of PV system and the maximum allowed power factor at PCC. This is given by,

$$K_1 = \frac{P_N \tan \varphi_{max}}{\Delta V_{droop}} \tag{3.8}$$

Where,

P_N is the nominal active power rating of the PV system

φ_{max} is the maximum displacement angle to which the PV inverter can operate

ΔV_{droop} is the voltage range of the volt/var curve and is given by [64],

$$\Delta V_{droop} = V_d - V_{th} \tag{3.9}$$

Where,

V_d is the maximum voltage allowed at the PCC. This depends on the grid code. In this thesis, the maximum value of V_d is chosen as 1.06 pu (per unit) which is the maximum steady state voltage limit as per Hydro One Distributed Generation (DG) Technical Interconnection Requirements [9].

V_{th} is the voltage threshold beyond which the PV system should start absorbing reactive power to mitigate voltage rise. This depends on whether the Volt/Var curve contains a dead band region or not.

φ_{max} can be calculated based on the maximum power factor allowed at the PCC. In this thesis, Hydro One DG interconnection requirements are followed [9] which limits the power factor between 0.95 leading and 0.95 lagging. Hence, the initial value of power factor is chosen as 0.95 to determine the limit for the magnitude of reactive power absorption/injection.

In this thesis, it is assumed that there is no dead band in the volt/var curve. This is because stability problems occur only in the linear region and this is of interest for study in this thesis. Also, the reference voltage of PCC voltage controller (determined by V_{th} for the volt/var curve) is chosen as 1 pu although the maximum steady state voltage limit allowed is 1.06 pu. This is because maintaining voltage at 1 pu ensures the availability of sufficient steady state over-voltage margin and in-turn increases the hosting capacity of distribution feeders for connecting additional distribution generators [22]. Also, this represents a symmetrical linear curve for the entire range of Volt/Var operation. The calculation of pu voltage is shown in Appendix B.

The proportional gain K_{pvs} represents the relation between the error in PCC voltage from the reference which is 1 pu and inverter reactive current i_{tq}. Hence, it has the unit kA/kV. K_1 represents the relation between error in PCC voltage from the reference and reactive power. It has a unit of MVAr/kV, where ΔV_{droop} is in kV. A relation can be established between K_1 and K_{pvs} as given below,

$$K_{pvs} = \frac{2K_1}{3V_{cdo}} \tag{3.10}$$

The various parameters in equations (3.8) and (3.10) have been calculated, and provided in Table B. 3 of Appendix B. The value of K_1 is 2.122 and K_{pvs} is 3.609 for $V_d =$ 1.06 pu. This is considered as an initial value for the proportional gain. The discussion

provided for the stability of proportional controller is applicable to both volt/var control and the dynamic reactive current injection.

Stability studies are carried out with the model developed in chapter 2 using the proportional controller defined in equation (3.10). The operating point is chosen for the PV system operating with an irradiance of 0.85 kW/m^2 such that $P_{VSC} = 6.88\ MW$. This ensures that there is sufficient free capacity in inverter where it can inject / absorb a maximum of 4.99 MVAr reactive power and perform PCC voltage control. The nonlinear state equations are solved using MATLAB/Simulink to obtain the steady state values at the chosen operating point data and the model is linearized about this point.

Eigenvalue studies are carried out using the state space model of (2.184) in MATLAB. There are a total of 35 Eigenvalues obtained for this model. Out of these, only the dominant eigenvalues that are strongly influenced by the PCC voltage controller parameters are shown below.

Table 3.5 Dominant Eigenvalue for K_{pvs} = 3.609 and G = 0.85 kW/m^2

Eigenvalues	Damping Ratio (in %)	Natural Frequency (rad/s)
-29.702 $\pm$ j 1032	2.88	1030

Participation Factor analysis is used to find out the states that participate in this eigenvalue. It is define as the product of left and right eigenvectors of an eigenvalue. The participation factor of a state variable $\tilde{x_i}$ in an eigenvalue λ_p can be found by [54] [65],

$$p_{ip} = v_p^i u_p^i \tag{3.11}$$

Where v_p^i and u_p^i represent the *i* th elements of the vector of v_p and u_p. v_p and u_p are the left and right eigenvectors of A_{sys} respectively. The participation factor p_{ip} is a complex number and hence, only the magnitude of the complex number is used for studies.

The eigenvectors and participation factors are computed in MATLAB by utilizing the program available in [65]. The participation factors of all 35 state variables are computed but only those that have a significant participation in the eigenvalue are studied. State variables with participation factors smaller than 0.01 are ignored in this case. The participation factors of dominant states are shown in Table 3.6.

Table 3.6 Participation Factors in -29.702 ± j 1032 (K_{pvs} = 3.609 and G = 0.85)

State Variables	Participation Factor	State Variables	Participation Factor
$\widetilde{\iota_{12d}}$	0.0775	$\widetilde{V_{cdf}}$	0.0782
$\widetilde{\iota_{12q}}$	0.0279	$\widetilde{V_{cqf}}$	0.0421
$\widetilde{\iota_{Ld}}$	0.0231	$\widetilde{V_{s1df}}$	0.0969
$\widetilde{\iota_{td}}$	0.133	$\widetilde{V_{s1qf}}$	0.0122
$\widetilde{\iota_{tq}}$	0.079	$\widetilde{x_3}$	0.249
$\widetilde{\iota_{s1d}}$	0.0301	$\widetilde{x_5}$	0.0464
$\widetilde{\iota_{s1q}}$	0.0223	$\widetilde{x_6}$	0.1429
$\widetilde{V_{dc}}$	0.196	$\widetilde{x_4}$	0.0938
$\tilde{\rho}$	0.022		

From participation factor analysis, it can be understood that the major states that participate in the eigenvalue are $\widetilde{x_3}$, $\widetilde{V_{dc}}$, $\widetilde{x_6}$ and $\widetilde{\iota_{td}}$. These states pertain to the DC-link voltage control loop. Also, the other states namely $\widetilde{x_4}$, $\widetilde{\iota_{tq}}$ (PCC voltage control loop), $\widetilde{\iota_{12d}}$ (distribution feeder current) and $\widetilde{\mathrm{V_{cdf}}}$, $\widetilde{\mathrm{V_{s1df}}}$ (measurement filters) also have significant participation in the eigenvalue. This shows that there is an interaction between the DC-Link Voltage control loop, PCC voltage control loop and the distribution feeder current $\widetilde{\iota_{12d}}$. The interaction is further influenced by the filter time constants namely τ_1

and τ_2. But, it will be shown later than the participation of PCC voltage control loop states will increase as the value of K_{pvs} increases.

The presence of the eigenvalue -29.702 $\pm$ j 1032 in the system and the interaction can be confirmed by applying a step response to PCC voltage of the linearized, nonlinear averaged and PSCAD / EMTDC models, and comparing the responses of PCC voltage and DC-Link voltage. The response of nonlinear averaged model is shown only for this case for comprehensive comparison of models and is not shown later in this thesis.

At the operating point about which the system is linearized, V_{pccref} is 1.0098 pu. The PCC voltage controller regulates the PCC voltage at 1.0113 pu. The steady state error is due to the controller being proportional in nature. A step of -2.5 % is applied to the PCC voltage controller. The PCC voltage response of linearized model, nonlinear averaged model and PSCAD/EMTDC model are shown in Figure 3.14. The comparison between the damped frequency of the dominant eigenvalue and the damped frequency of the different model responses is shown in Table 3.7.

Table 3.7 Comparison between damped frequencies (K_{pvs} = 3.609, G = 0.85)

Parameter	**Damped frequency (rad/s)**	**Settling time (ms) (for 5 % of steady state value)**
Dominant Eigenvalue -29.702 $\pm$ j 1032	1032 (164.33 Hz)	
Linearized Model	1031.4 (164.23 Hz)	47
Nonlinear Averaged Model	1052.9 (167.65 Hz)	132
PSCAD / EMTDC Model	1049.3 (167.08 Hz)	77

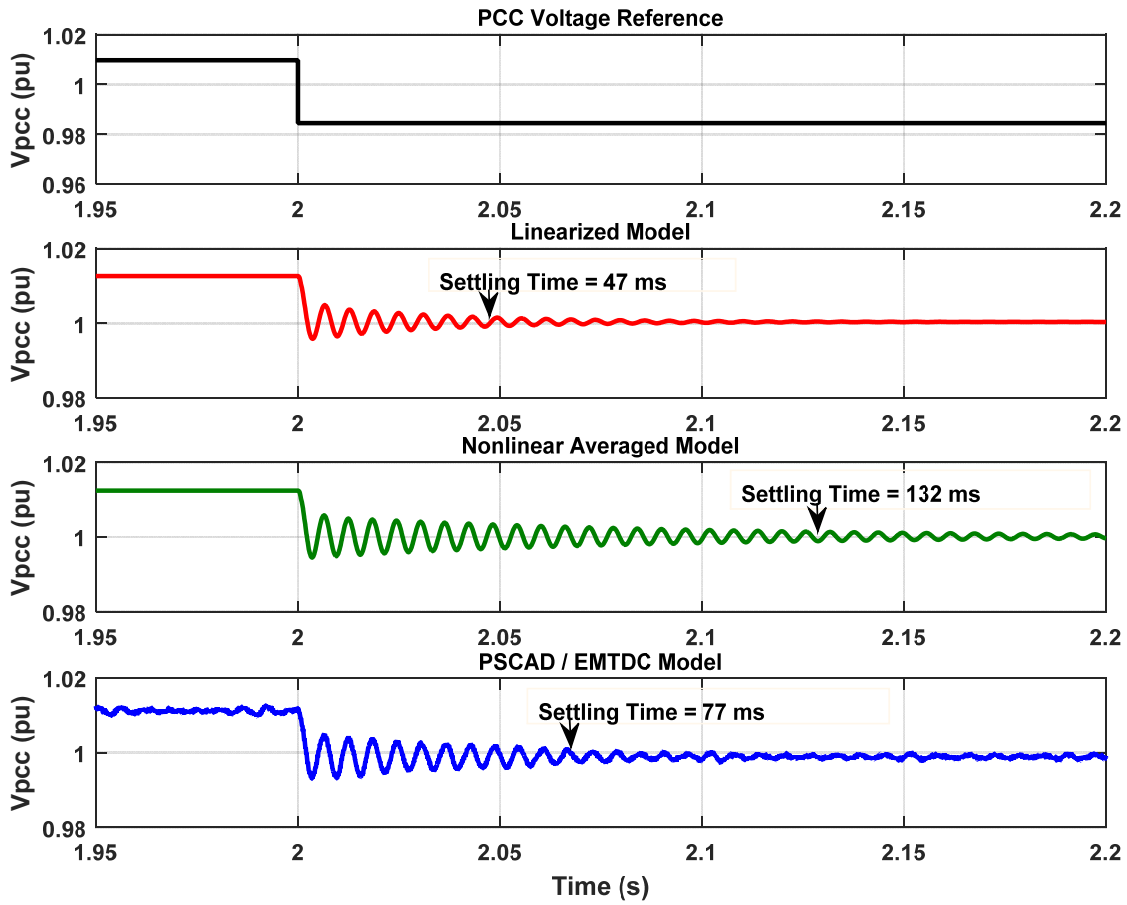

Figure 3.14 Step Response of PCC Voltage (For K_{pvs} = 3.609, G = 0.85)

From Table 3.7, it can be seen that the damped frequencies of different models are very close to each other. This confirms the presence of the eigenvalue -29.702 $\pm$ j 1032 in the system.

The response of DC-Link voltage of linearized model, nonlinear averaged model and PSCAD/EMTDC are shown in Figure 3.15. It can be seen that the transient response of both the models exhibit oscillations which are due to the presence of eigenvalue -29.702 $\pm$ j 1032 in the system.

It is clear from Figure 3.14 and Figure 3.15 that the interaction exists between the DC-link voltage control loop, PCC voltage control loop, distribution feeder current i_{12d}, and the output of measurement filters V_{cdf} and V_{s1df} as shown earlier by participation factor analysis.

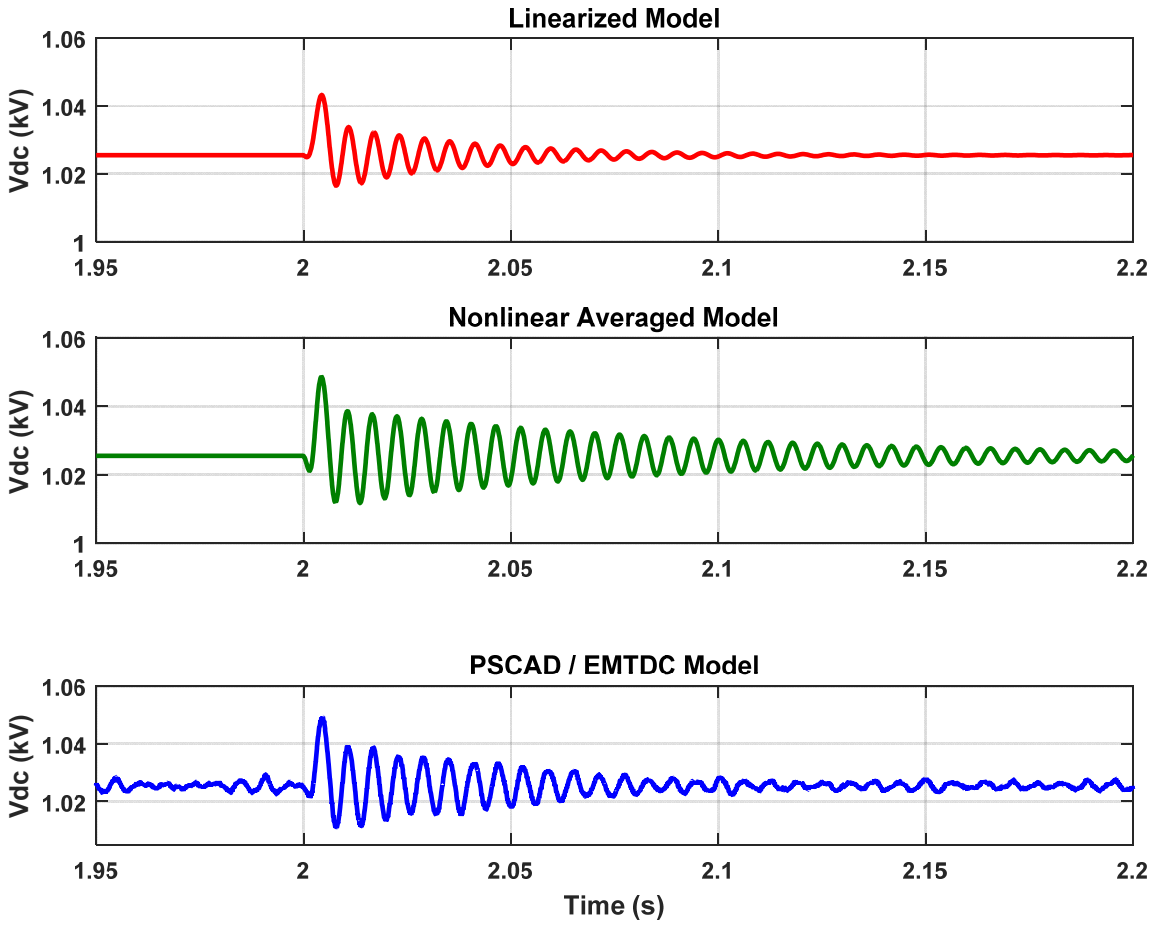

Figure 3.15 DC-Link Voltage Response to a step change in PCC voltage (for K_{pvs} = 3.609, G = 0.85)

In Figure 3.14 and Figure 3.15, there are differences in the damping of oscillations in the PCC voltage and DC-link voltage responses of the models. The responses of the linearized model are more damped when compared with the responses of nonlinear averaged and PSCAD / EMTDC models. This can be attributed to the degree of nonlinearity of the model. Also, the responses of PSCAD / EMTDC models are more damped when compared with the responses of nonlinear averaged model. This is due to the presence of parasitic resistances in the models of components such as IGBT, Diode etc. in PSCAD / EMTDC.

It can clearly be seen from Figure 3.14 and Figure 3.15 that the presence of the eigenvalue -29.702 $\pm$ j 1032 renders the response of the system to be poorly damped and

it could become oscillatory for large disturbances. Hence, the system with this eigenvalue is not desirable and its sensitivity to controller parameters has to be studied.

The interaction between dc-link voltage control loop, PCC voltage control loop, distribution feeder current i_{12d}, and the output of measurement filters can be understood as follows:

The excess active power generated by the PV system (power available after load consumption) flows towards the substation grid and this active power affects the PCC voltage. When the PV system performs PCC voltage control, it exchanges reactive power with the substation grid. In steady-state, the relation between PCC voltage, active power and reactive power of the PV system is given by [22]:

$$V_{s1}(V_{pcc}) = \frac{(P_1R_1) + (\pm Q_1X_1)}{V_1} + j\frac{(P_1X_1) - (\pm Q_1R_1)}{V_1} + V_1 \qquad (3.12)$$

Where P_1 and Q_1 are net powers flowing towards the substation grid.

P_1 and Q_1 are dependent on P_{VSC} and Q_{VSC} respectively. In steady state, P_{VSC} is controlled by i_{td} which is determined by the DC-link voltage control loop and Q_{VSC} is controlled by i_{tq} which is determined by the PCC voltage control loop. Equation (3.12) shows the coupling between the P_{VSC} and Q_{VSC}. When Q_{VSC} is increased / decreased to change PCC voltage, P_{VSC} gets affected. In order to maintain P_{VSC} constant (under maximum power point operation by PV system), the dc-link voltage control loop changes i_{td} according to the change in PCC voltage. This proves that there exists a coupling between DC-link voltage and PCC voltage control loops.

Changes in V_{s1} also affect V_c. Voltages V_{cd} and V_{cq} have been used as feed-forward signals to improve the transient performance of current controllers. These feed-forward signals also help in minimizing the interactions between the DC-link voltage and PCC voltage controllers in transient. Signal V_{cq} is also the input to PLL which outputs signal ω to decouple i_{td} and i_{tq} control loops. When there are delays (due to measurement system, communication etc.) in obtaining signals $\mathrm{V_{cd}}$ and $\mathrm{V_{cq}}$, they influence the transient

coupling between dc-link and PCC voltage control loops. If such an interaction exists, delays in PCC voltage controller (determined by τ_1) also influences the interaction. This is the reason for the interaction observed between DC-link voltage control loop, PCC voltage control loop, distribution feeder current i_{12d} and measurement filters of V_{cdf} and V_{s1df}. This is depicted using a simple diagram as shown in Figure 3.16.

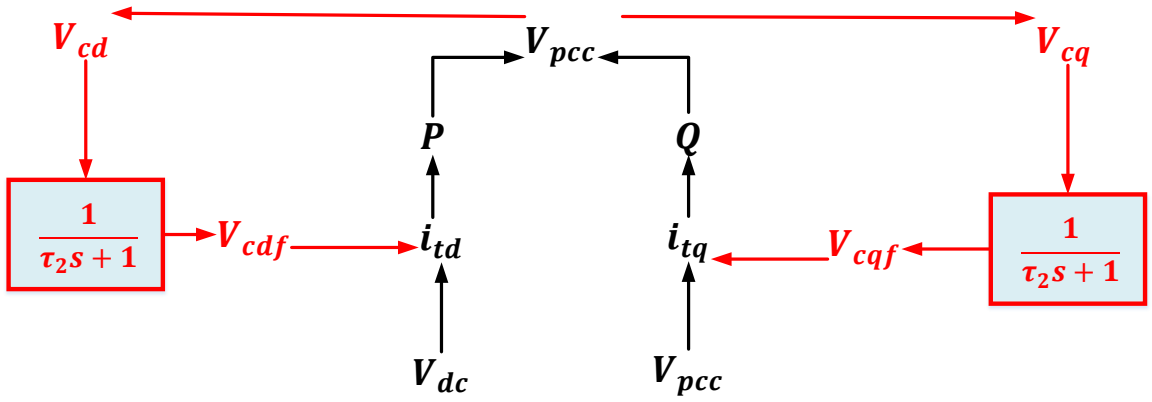

Figure 3.16 Depiction of interaction between PCC voltage control loop, dc-link voltage control loop and delays of feed-forward filters

The interaction described above has also been reported in [32] and [17]. In [17], it has been reported that the PCC voltage controller is affected by the injected real power since the PCC voltage depends on both the injected active and reactive powers in distribution networks where resistance is not negligible. In [32], it has been reported that the DC-Link Voltage controller and PCC voltage controller are dynamically coupled in distribution networks where the value of X/R ratio is very small. It can also be seen that the interaction is influenced by distribution feeder current i_{12d} whose dynamics are dependent on X/R ratio of distribution feeder (2.18) as reported in [17], [32].

The eigenvalue that represents the interaction is sensitive to the following controller parameters:

a) K_{pv},K_{iv},τ_{Vdc},K_{pi1}, K_{ii1} : These parameters pertain to the dc-link voltage control loop. They mainly influence the states $\widetilde{i_{td}}$, $\widetilde{V_{dc}}$, $\widetilde{x_3}$ and $\widetilde{x_6}$. These parameters have been chosen based on particular phase margin and bandwidth requirements. These

parameters can be changed and the sensitivity of above reported eigenvalue can be studied. This is avoided for the following reasons:

- This might reduce the bandwidth of dc-link voltage controller. A faster dc-link voltage controller is a primary requirement for proper supply of active and reactive powers by PV system.
- The focus is on studying the sensitivity of this eigenvalue to PCC voltage controller gains and establish guidelines for minimizing the interaction. This would ensure that the dc-link voltage controller designed using the simplified model is valid.

b) τ_1 and τ_2: The participation of V_{cdf} and V_{s1df} implies that the stability of this eigenvalue is affected by the measurement filter time constants τ_1 and τ_2. The values will be changed and its sensitivity to the dominant eigenvalue will be studied later in this chapter.

c) K_{pvs},K_{pi2}, K_{ii2} : These parameters pertain to the PCC voltage control loop. They mainly influence the states $\widetilde{\imath_{tq}}$, $\widetilde{x_4}$. K_{pvs} represents the proportional gain. Parameters K_{pi2} and K_{ii2} determine the bandwidth of q-axis current controller. These values will be changed and its sensitivity to the dominant eigenvalue will be studied later in this chapter.

The sensitivity of this eigenvalue to proportional gain is studied in this section. K_{pvs} is varied from 3.609 to 6.75 and the movement (sensitivity) of the dominant eigenvalue of the system is plotted in Figure 3.17. It can be seen that the dominant eigenvalue moves towards the right half of S-plane. For $K_{pvs} = 6.25$, the dominant eigenvalue is 0.99 $\pm$ j 1096.4 and this represents an unstable eigenvalue.

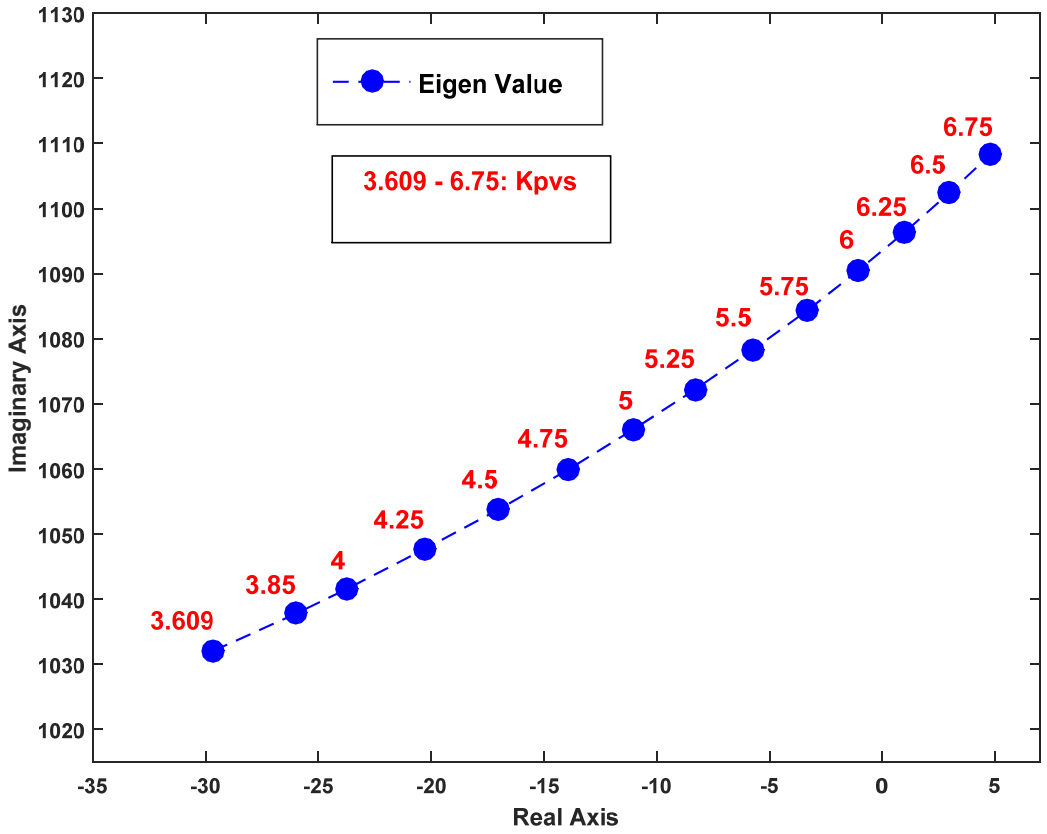

Figure 3.17 Sensitivity of dominant eigenvalue to variation in K_{pvs} (for G=0.85)

The existence of the unstable eigenvalue for $K_{pvs} = 6.25$ in the system can be confirmed by observing the step response in PCC voltage of PSCAD / EMTDC model. A step of -2.5% is applied to the PCC voltage controller at a time of 1 second and the response is shown in Figure 3.18. It can be seen that the PCC voltage begins to oscillate and it keeps growing leading to an unstable response. The damped frequency of the oscillation is found to be 175.4 Hz (1101.5 rad/s) which confirms the presence of the eigenvalue 0.99 $\pm$ j 1096.4.

It can be seen that when the proportional gain increases beyond a certain value (represented by increase in K_{pvs}), the system becomes unstable. This imposes limitations on the application of volt/var curve or dynamic reactive current injection to perform effective and fast voltage control. These limitations can be overcome by the use of a PI controller for PCC voltage control.

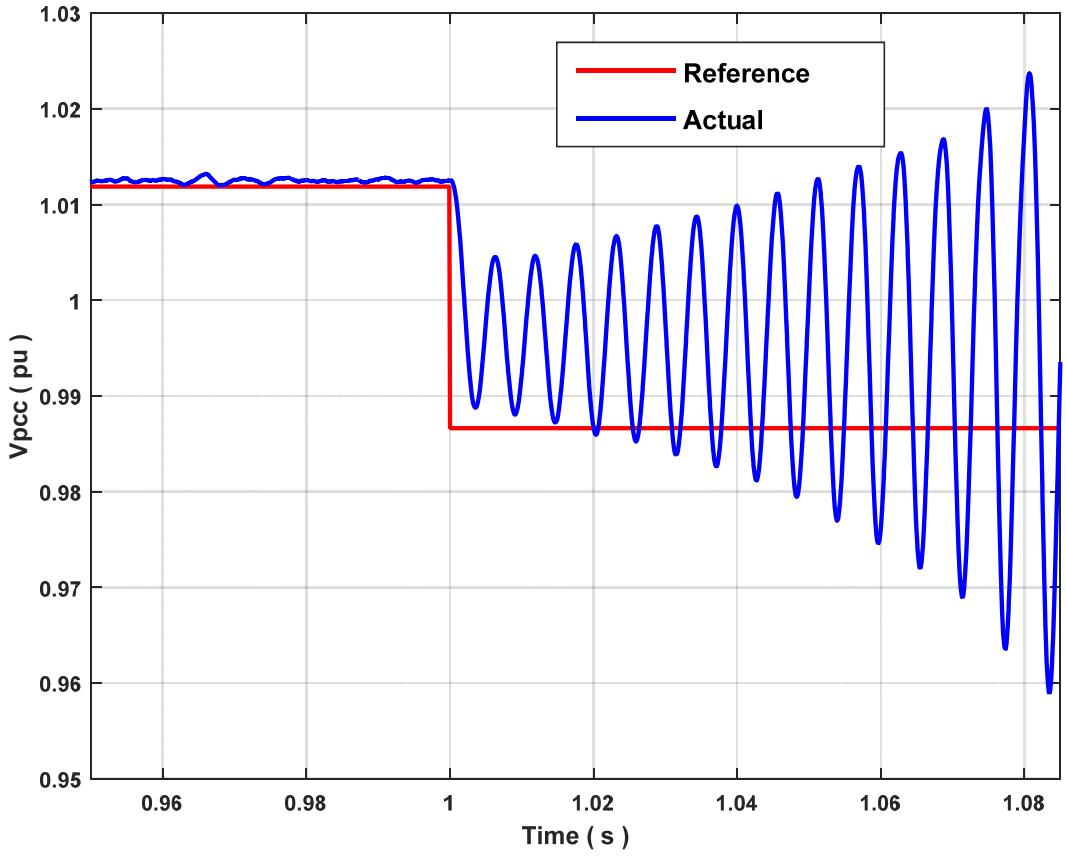

Figure 3.18 Step Response of PCC Voltage in PSCAD / EMTDC Model

(For K_{pvs} = 6.25, G = 0.85)

3.2.6.2 Proportional Integral Controller

The PI controller represents the control structure of a PV-STATCOM. The PI controller has two adjustable control parameters namely K_{pvs} and K_{ivs}. The value of K_{droop} is considered to be zero throughout this chapter. The design of these two parameters will be carried out based on sensitivity studies using the state space model developed in section 2.6.4.

The nonlinear system is linearized about the same operating point utilized for the design of proportional controller where the PV system is operating with an irradiance of 0.85 kW/m^2 such that $P_{VSC} = 6.88\,MW$. Eigenvalue sensitivity analysis is performed using the linearized model for variation in K_{pvs} and K_{ivs}.

At first, K_{ivs} is fixed at 1 and the value of K_{pvs} is varied from 0.1 to 6. For $K_{pvs} = 0.1$, the dominant eigenvalues of the system that are strongly related to PCC voltage controller gains are given in Table 3.8.

Table 3.8 Dominant Eigenvalues for K_{pvs} = 0.1, K_{ivs}= 1 and G = 0.85 kW/m^2

Eigenvalues	Damping Ratio (in %)	Natural Frequency (rad/s)
-114.54 $\pm$ j 960.96	11.8	968 (154.14 Hz)
-0.2556	--	--

The sensitivity of these two eigenvalues to variation in K_{pvs} from 0.1 to 6 is studied. The sensitivity of the eigenvalue -114.54 $\pm$ j 960.96 to variation in K_{pvs} is shown in Figure 3.19. It can be seen that the eigenvalue is very sensitive to K_{pvs} and it moves towards the right half of S-plane as K_{pvs} increases. For K_{pvs} = 6 and K_{ivs}= 1, the eigenvalue is at 3.5285 $\pm$ j 1098.3. This represents an unstable eigenvalue.

The sensitivity of the eigenvalue -0.2556 to variation in K_{pvs} is shown in Figure 3.20. It can be seen that the eigenvalue is less sensitive to K_{pvs} but it moves towards the right half of S-plane as K_{pvs} increases. For K_{pvs} = 6 and K_{ivs}= 1, the eigenvalue is at -0.1019.

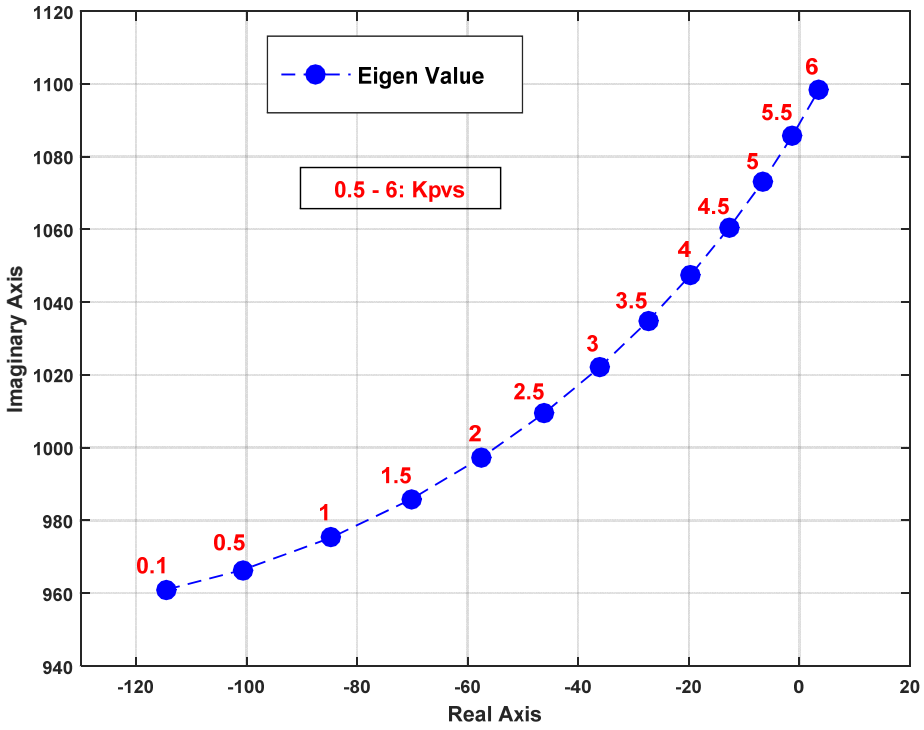

Figure 3.19 Sensitivity of eigenvalue -114.54 ± j 960.96 to variation in K_{pvs} (for K_{ivs}= 1 and G = 0.85 kW/m^2)

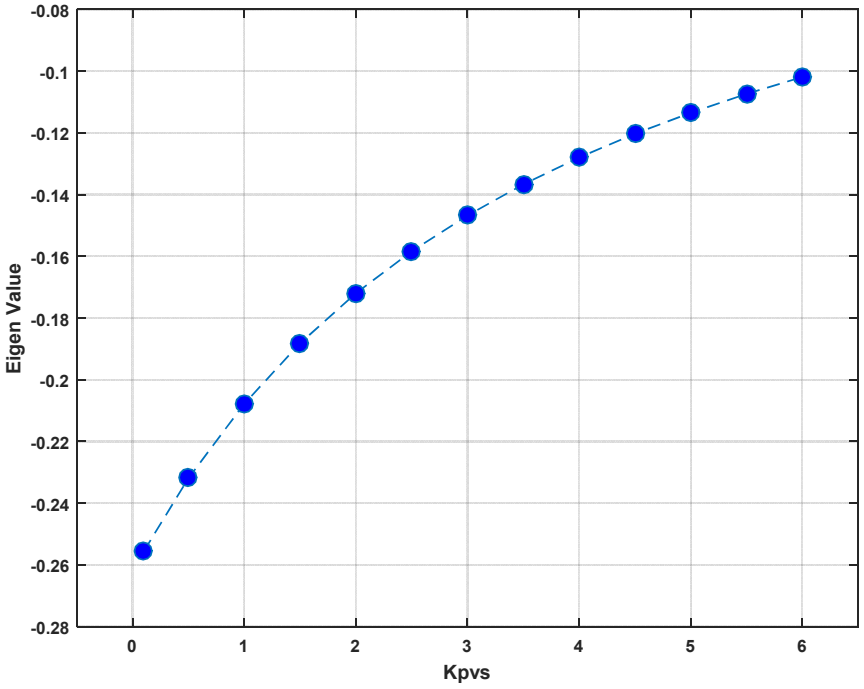

Figure 3.20 Sensitivity of eigenvalue -0.2556 to variation in K_{pvs} (for K_{ivs}= 1 and G = 0.85 kW/m^2)

Participation factor analysis is performed to identify the states that participate in the eigenvalues 3.5285 ± j 1098.3 and -0.1019. The participation factors of states that have a significant participation in both the eigenvalues are shown in Table 3.9.

Table 3.9 Participation Factors in dominant eigenvalues (K_{pvs} = 6, K_{ivs}= 1 and G = 0.85)

State Variables	Participation Factor		State Variables	Participation Factor	
	For Eigenvalue 3.5285 ± j 1098.3	For Eigenvalue -0.1019		For Eigenvalue 3.5285 ± j 1098.3	For Eigenvalue -0.1019
$\widetilde{\imath_{12d}}$	0.0832	0	$\widetilde{V_{cdf}}$	0.0711	0
$\widetilde{\imath_{12q}}$	0.0340	0	$\widetilde{V_{cqf}}$	0.0496	0
$\widetilde{\imath_{Ld}}$	0.0278	0	$\widetilde{V_{s1df}}$	0.141	0
$\widetilde{\imath_{Lq}}$	0.0103	0	$\widetilde{V_{s1qf}}$	0.0233	0
$\widetilde{\imath_{td}}$	0.124	0	$\widetilde{x_3}$	0.206	0
$\widetilde{\imath_{tq}}$	0.108	0	$\widetilde{x_5}$	0.0347	0
$\widetilde{\imath_{s1d}}$	0.0263	0	$\widetilde{x_6}$	0.115	0
$\widetilde{\imath_{s1q}}$	0.0295	0	$\widetilde{x_4}$	0.117	0
$\widetilde{V_{dc}}$	0.156	0	$\widetilde{x_7}$	0	1.00
$\tilde{\rho}$	0.0241	0			

It can be seen from Table 3.9 that for the eigenvalue 3.5285 ± j 1098.3, the states that relatively have a dominant participation are $\widetilde{\imath_{td}}$, $\widetilde{V_{dc}}$, $\widetilde{x_3}$, $\widetilde{x_6}$ (DC-link voltage control loop), $\widetilde{\imath_{tq}}$, $\widetilde{x_4}$ (PCC voltage control loop), $\widetilde{\imath_{12d}}$ (distribution feeder current) and $\widetilde{V_{cdf}}$, $\widetilde{V_{s1df}}$ (measurement filters). This shows that there is an interaction between the

DC-Link Voltage control loop, PCC voltage control loop, the distribution feeder current $\widetilde{\iota_{12d}}$ and the measurement filters which was earlier observed during the design of proportional type PCC voltage controller. For the eigenvalue -0.1019, the only state that has a significant participation is $\widetilde{x_7}$ which pertains to the PCC voltage controller.

From the above participation factor analysis, it can be concluded that increase in proportional gain of the PI controller will only render the system unstable due to increased interaction between DC-Link Voltage control loop, PCC voltage control loop, the distribution feeder current $\widetilde{\iota_{12d}}$ and the measurement filters.

Second, K_{pvs} is fixed at 0.5 and the value of K_{ivs} is varied from 1 to 600. For $K_{ivs} = 50$, the dominant eigenvalues of the system that are strongly related to PCC voltage controller gains are given in Table 3.10.

Table 3.10 Dominant Eigenvalues for K_{pvs} = 0.5, K_{ivs}= 50 and G = 0.85 kW/m^2

Eigenvalues	Damping Ratio (in %)	Natural Frequency (rad/s)
-100.14 $\pm$ j 964.63	10.3	970 (154.45 Hz)
-11.82	--	--

The sensitivity of these two eigenvalues to variation in K_{ivs} from 50 to 600 is studied. The sensitivity of the eigenvalue -100.14 $\pm$ j 964.63 to variation in K_{ivs} is shown in Figure 3.21. It can be seen that the eigenvalue is less sensitive to K_{ivs} but it moves towards the right half of S-plane as K_{ivs} increases. For K_{pvs} = 0.5 and K_{ivs}= 600, the eigenvalue is at -92.46 $\pm$ j 942.17.

The sensitivity of the eigenvalue -11.82 to variation in K_{ivs} is shown in Figure 3.22. It can be seen that the eigenvalue is very sensitive to K_{ivs} and it moves towards the left half

of S-plane as K_{ivs} increases which indicates the system becomes more stable. For K_{pvs} = 0.5 and K_{ivs}= 600, the eigenvalue is at -210.50.

Participation factor analysis is performed to identify the states that participate in the eigenvalues -92.46 ± j 942.17 and -210.50. The participation factors of states that have a significant participation in both the eigenvalues are shown in Table 3.11.

It can be seen from Table 3.11 that for the eigenvalue -92.46± j 942.17, the states that relatively have a dominant participation are $\widetilde{\iota_{td}}$, $\widetilde{V_{dc}}$, $\widetilde{x_3}$, $\widetilde{x_6}$ (DC-link voltage control loop), $\widetilde{x_4}$ (PCC voltage controller), $\widetilde{\iota_{12d}}$ (distribution feeder current) and $\widetilde{V_{cdf}}$ (measurement filter). This again represents interaction between the DC-Link Voltage control loop, PCC voltage control loop, the distribution feeder current $\widetilde{\iota_{12d}}$ and the measurement filter.

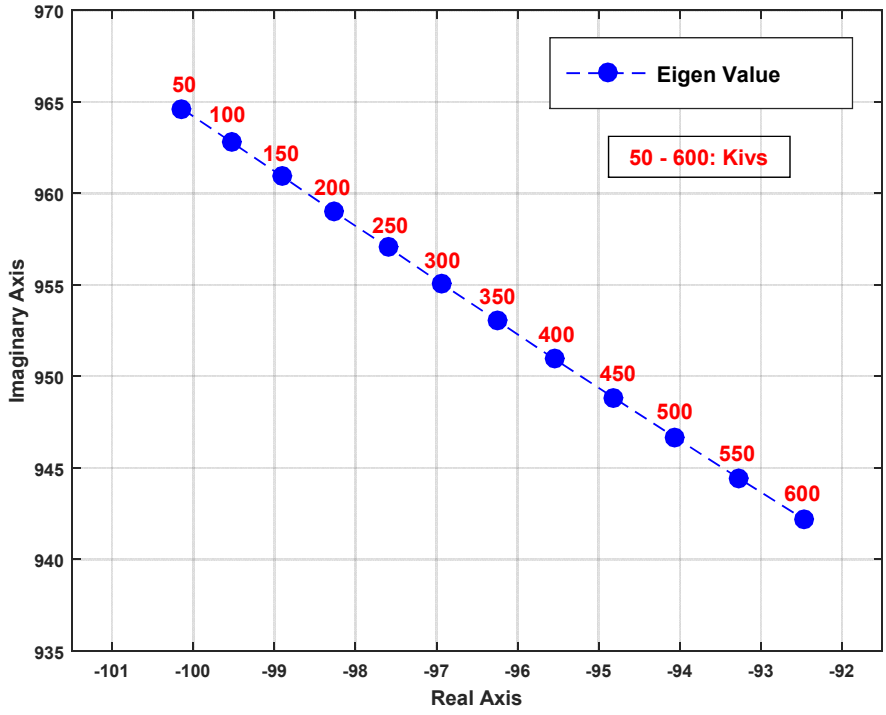

Figure 3.21 Sensitivity of eigenvalue -100.14 ± j 964.63 to variation in K_{ivs} (for K_{pvs}= 0.5 and G = 0.85 kW/m^2)

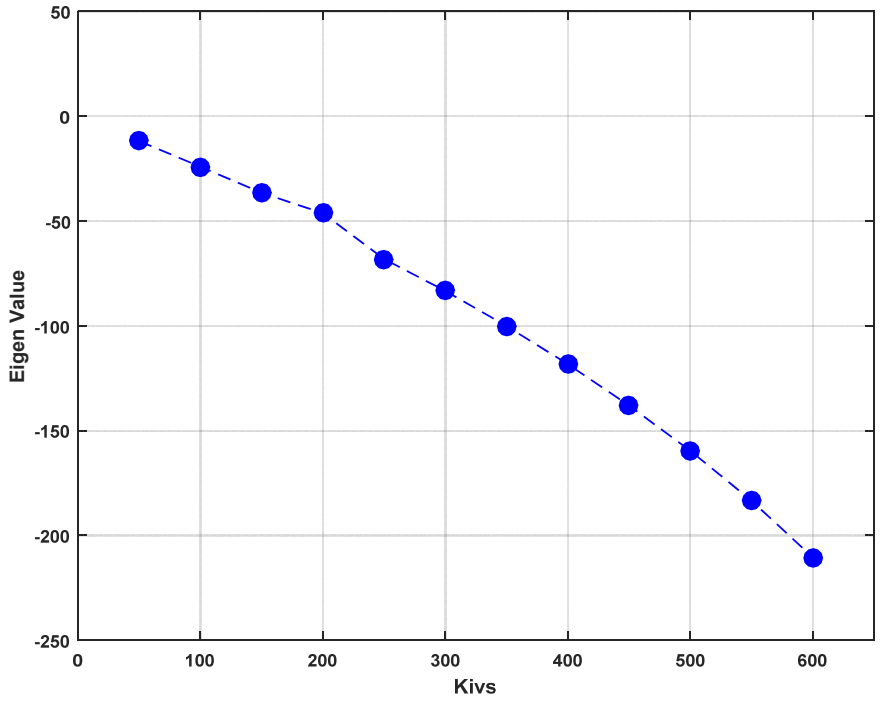

Figure 3.22 Sensitivity of eigenvalue -11.82 to variation in K_{ivs} (for K_{pvs}= 0.5 and G = 0.85 kW/m^2)

Table 3.11 Participation Factors in dominant eigenvalues (K_{pvs} = 0.5, K_{ivs}= 600 and G = 0.85)

State Variables	Participation Factor		State Variables	Participation Factor	
	For Eigenvalue -92.46 ± j 942.17	For Eigenvalue -210.50		For Eigenvalue -92.46 ± j 942.17	For Eigenvalue -210.50
$\widetilde{\iota_{1d}}$	0.0081	0.011	$\tilde{\rho}$	0.022	0.0068
$\widetilde{\iota_{12d}}$	0.096	0.139	$\widetilde{V_{cdf}}$	0.101	0.0327
$\widetilde{\iota_{12q}}$	0.022	0.101	$\widetilde{V_{cqf}}$	0.040	0.0180
$\widetilde{\iota_{Ld}}$	0.015	0.0097	$\widetilde{V_{s1df}}$	0.033	0.984
$\widetilde{\iota_{Lq}}$	0.010	0.0421	$\widetilde{V_{s1qf}}$	0.0025	0.022

$\widetilde{\imath_{td}}$	0.204	0.0014	$\widetilde{x_3}$	0.400	0.022
$\widetilde{\imath_{tq}}$	0.053	0.0715	$\widetilde{x_5}$	0.093	0.153
$\widetilde{\imath_{s1d}}$	0.0527	0.0011	$\widetilde{x_6}$	0.258	0.0064
$\widetilde{\imath_{s1q}}$	0.0161	0.0846	$\widetilde{x_4}$	0.075	0.067
$\widetilde{V_{dc}}$	0.357	0.0233	$\widetilde{x_7}$	0.031	1.677

For the eigenvalue -210.50, the state that has a dominant participation is $\widetilde{x_7}$ (PCC voltage controller). The other states that have a significant participation are $\widetilde{x_5}$ (DC-link voltage control loop), $\widetilde{\imath_{12d}}$, $\widetilde{\imath_{12q}}$ (distribution feeder currents) and $\widetilde{V_{s1df}}$ (measurement filter). This eigenvalue is strongly coupled to PCC voltage controller and is also affected to a very smaller extent by the dynamics of DC-link voltage control loop, distribution feeder currents and measurement filter.

From the above eigenvalue and participation factor analysis, it can be concluded that the increase in integral gain of the PI controller has very less effect on the eigenvalue that is affected by the interaction between DC-Link Voltage control loop, PCC voltage control loop, the distribution feeder current and the measurement filter. This shows that the speed and accuracy of voltage control action can be improved by using relatively larger values (when compared with proportional controller gain) of integral gain of the PI controller without any stability issues.

The optimal gains of PI controller are chosen as K_{pvs} = 0.5 and K_{ivs}= 400. This ensures that the dominant (most critical) eigenvalue -95.55 $\pm$ j 950.96 has a damping ratio of 10 % [30]. This along with the presence of other dominant eigenvalue -118.28 will make the system sufficiently damped. The step response of the system is now plotted to study the time response characteristics of the system.

At the operating point about which the system is linearized, V_{pccref} is 1.009 pu. The PCC voltage controller regulates the PCC voltage at this reference value. A step of -2.5 % is

applied to the PCC voltage controller. The PCC voltage response of linearized model, and PSCAD/EMTDC model are shown in Figure 3.23.

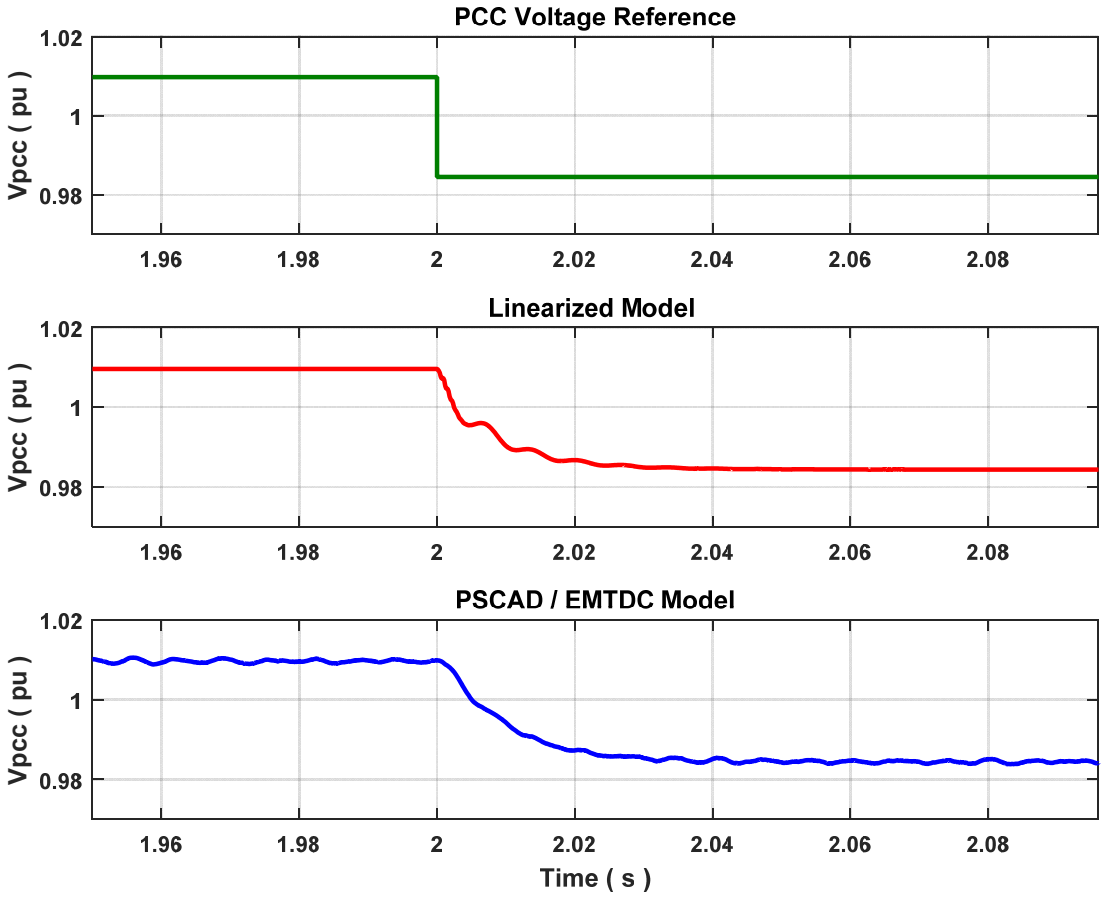

Figure 3.23 Step Response of PCC Voltage (For K_{pvs} = 0.5, K_{ivs}= 400 and G = 0.85)

From Figure 3.23, it can be seen that the response of PCC voltage is well damped without any overshoot. The response of the linearized model and PSCAD / EMTDC model shows the presence of minor damped oscillations. The comparison between the frequency of damped oscillations and the settling time is shown in Table 3.12. Due to the nonlinearity of the PSCAD / EMTDC model, the oscillations are more damped and the frequency of oscillation is somewhat different when compared to that of the linearized model. The settling times of the models are fairly close to each other. All these confirm that the linearized model and PSCAD / EMTDC model responses are close to each other.

Table 3.12 Comparison between damped frequencies and settling times (For K_{pvs} = 0.5, K_{ivs}= 400 and G = 0.85)

Parameter	Damped frequency (rad/s)	Settling time (ms) (for 1 % error margin)
Dominant Eigenvalue -95.55 ± j 950.96	950.96 (151.42 Hz)	
Linearized Model	956.33 (152.28 Hz)	8
PSCAD / EMTDC Model	927.87 (147.75 Hz)	10.2

Hence, it can be seen that fast and accurate voltage control can be achieved without any instability issues by utilizing a properly tuned PI controller over a proportional controller.

In the next sections, comparative studies between proportional and PI controllers are carried out. Before proceeding to those studies, the common factors for comparison between proportional and PI controllers have to be pointed out. They are as follows:

- The q-axis current controller bandwidth is the same for both controllers

- For proportional controller, the initial gain is chosen as 3.609 which is based on the calculation of required reactive current (or reactive power) to keep voltage deviations within certain limits. The formula used for calculation of this gain does not consider the effect of other control system and power system parameters on the stability of proportional controller. This stability has been evaluated using the developed model. The gain is then increased to the largest value possible till instability occurs. Larger gains are required to get minimum possible voltage deviation within fastest time possible. The chosen gain of proportional controller is 6.25 and this is used for comparison with PI controller. Although the system is unstable for this value of gain, the effect of measurement filter constants on the

stability of proportional controller is studied to determine whether the system becomes stable or more unstable for this value of gain.

- For PI controller, the optimal gains are chosen as K_{pvs} = 0.5 and K_{ivs}= 400. The system is stable for this set of gains. A value of 400 can be considered as a relatively higher value of integral gain. The effects of measurement filter constants on PI controller for this set of gains are studied to determine whether the system becomes unstable.

3.2.7 Study of eigenvalue sensitivity to τ_1 and τ_2

A comparison between the participation factors of major states that participate in the dominant eigenvalues pertaining to the interaction for K_{pvs} = 6.25 and K_{pvs} = 0.5, K_{ivs}= 400 is shown in Table 3.13. The participation of states that pertain to PCC voltage control loop are shown highlighted in Table 3.13. A clear reduction in the participation factors of these states can be seen for a PI controller over the proportional controller. This proves the use of integral control action (in PI controller) makes the PCC voltage controller states less susceptible to the interaction.

Table 3.13 Participation Factors Comparison for proportional and PI controller

State Variables	Participation Factors	
	For proportional controller (K_{pvs} = 6.25) (Eigenvalue 0.99 ± j 1096.4)	**For PI controller (K_{pvs} = 0.5, K_{ivs}= 400) (Eigenvalue -95.544 ± j 950.96)**
$\widetilde{\iota_{12d}}$	0.0834	0.0916
$\widetilde{\iota_{12q}}$	0.0352	0.0166
$\widetilde{V_{s1d}}$	0.0016	0.00092

$\widetilde{V_{s1q}}$	0.0011	0.00043
$\widetilde{\iota_{td}}$	0.125	0.204
$\widetilde{\iota_{tq}}$	0.111	0.0391
$\widetilde{V_{cf1d}}$	0.0022	0.0014
$\widetilde{V_{cf1q}}$	0.0016	0.00071
$\widetilde{\iota_{s1d}}$	0.026	0.052
$\widetilde{\iota_{s1q}}$	0.030	0.011
$\widetilde{V_{dc}}$	0.149	0.339
$\tilde{\rho}$	0.0247	0.018
$\widetilde{V_{cdf}}$	0.0727	0.0971
$\widetilde{V_{cqf}}$	0.0494	0.0328
$\widetilde{V_{s1df}}$	0.1419	0.0248
$\widetilde{V_{s1qf}}$	0.0242	0.00167
$\widetilde{x_3}$	0.2077	0.3895
$\widetilde{x_5}$	0.0331	0.0881
$\widetilde{x_6}$	0.1101	0.247
$\widetilde{x_4}$	0.118	0.057
$\widetilde{x_7}$	not applicable	0.018

From the Table 3.13, it can also be seen that the participation of states of measurement filters $\widetilde{V_{cdf}}$ and $\widetilde{V_{cqf}}$ are almost similar. The sensitivity of the eigenvalues of both proportional and PI controller to τ_2 is studied. Only the sensitivity of these eigenvalues are studied since they are the dominant eigenvalues that represent the interaction and maximum sensitivity to change in parameters. τ_2 is varied from 0.4 ms to 2.5 ms. The movement of the eigenvalues for the proportional controller and PI controller are shown in Figure 3.24 and Figure 3.25.

From Figure 3.24 and Figure 3.25, it is clear that for τ_2 = 0.75 ms, proportional controller renders the system more unstable (dominant eigenvalue at 33.42 $\pm$ j 1271.2) when compared to PI controller which ensures that the system is stable (dominant eigenvalue at -75.7 $\pm$ j 1060.9). This shows that although the participation of feed-forward filter states are same for both controllers, the PI controller is less susceptible to interaction even for a time constant of τ_2 = 0.75 ms for which the proportional controller becomes more unstable.

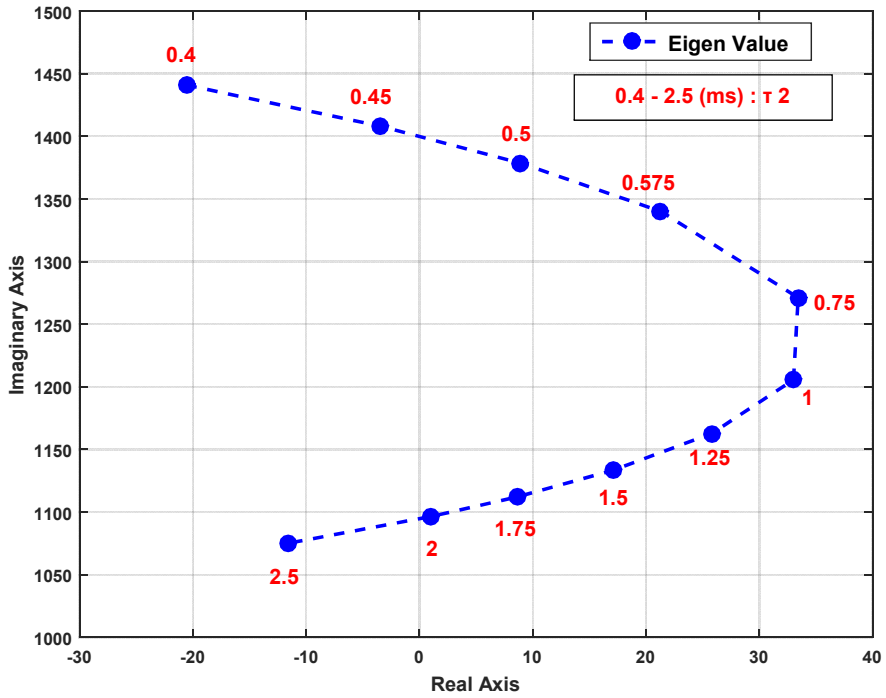

Figure 3.24 Sensitivity of eigenvalue 0.99 $\pm$ j 1096.4 to variation in τ_2 (for K_{pvs}= 6.25 and τ_1= 2 ms)

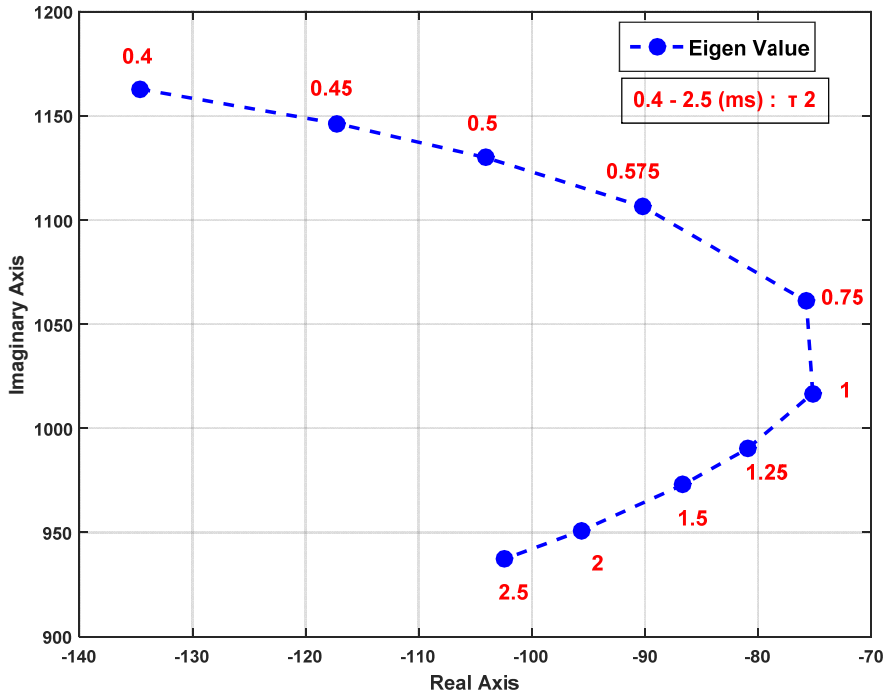

Figure 3.25 Sensitivity of eigenvalue -95.544 ± j 950.96 to variation in τ_2 (for K_{pvs} = 0.5, K_{ivs}= 400 and τ_1= 2 ms)

It can also be seen that when the value of τ_2 is 0.75 ms (which is close to the designed gain crossover frequencies of current controllers which is 1380 rad/sec), the interaction is at its maximum. The purpose of using the feed-forward signals is to try and nullify the impact of transient disturbances in the EPC voltage on the current controllers. If there are delays in feed-forward signals, the current controllers start responding to the EPC voltage disturbances. If the delays are such that the speed of operation of feed-forward filters are in the range of speed of operation of current controllers, both the current controllers and feed-forward filters respond simultaneously to EPC voltage disturbances. This leads to a transient interaction between the current controllers which eventually lead to interaction between dc-link voltage and PCC voltage control loops. Hence, τ_2 = 0.75 ms can be considered as the worst case scenario for interaction.

Now, τ_2 is fixed at 0.75 ms and τ_1 is varied from 0.25 ms to 6 ms and the sensitivity of dominant eigenvalues are studied. The movement of the eigenvalues for the proportional controller and PI controller is shown in Figure 3.26 and Figure 3.27 respectively.

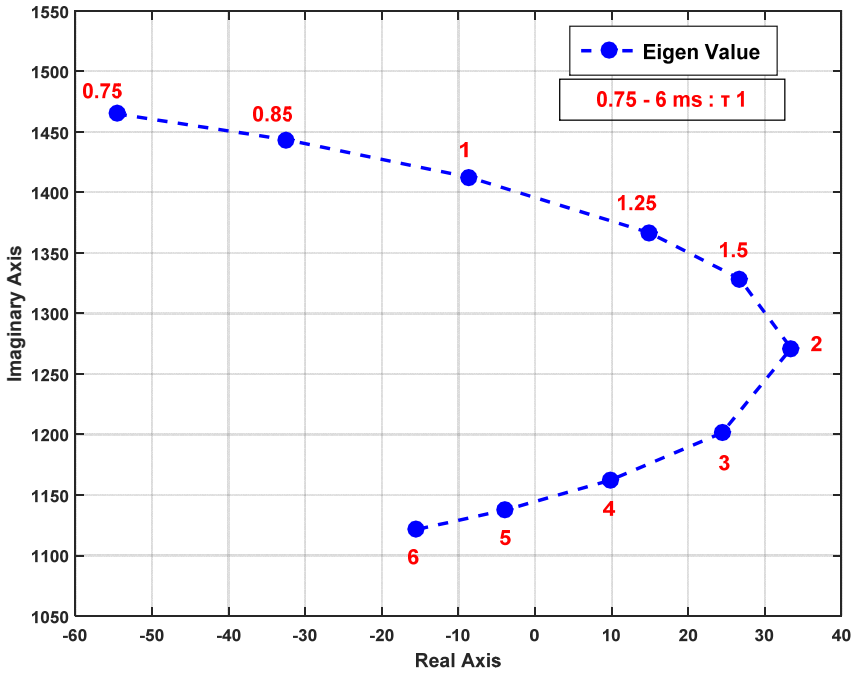

Figure 3.26 Sensitivity of eigenvalue 33.42 ± j 1271.2 to variation in τ_1 (for K_{pvs}= 6.25 and τ_2= 0.75 ms)

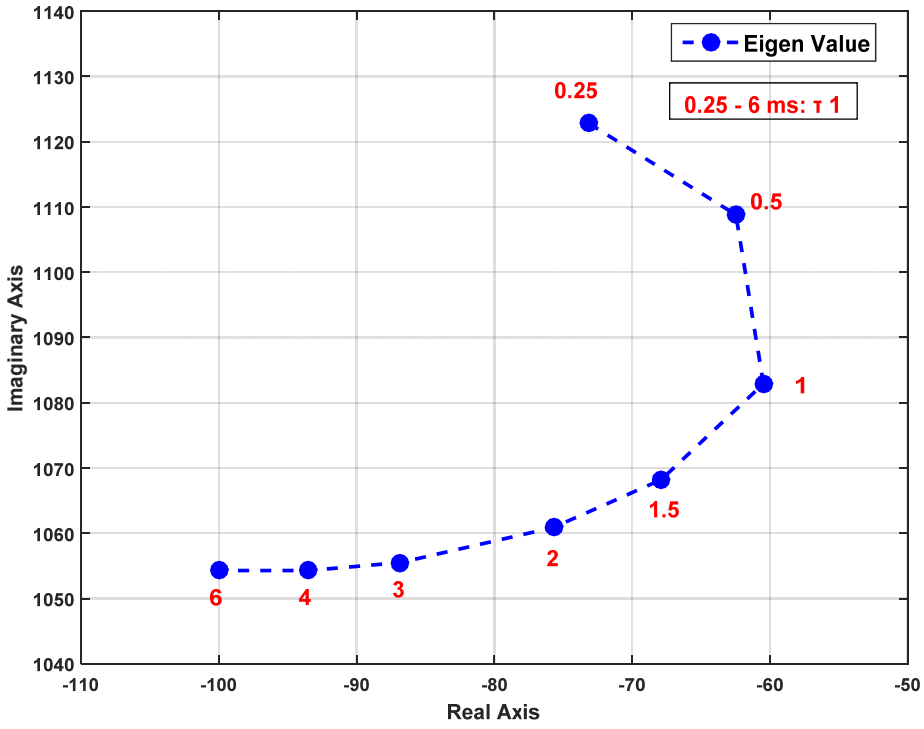

Figure 3.27 Sensitivity of eigenvalue -75.7 ± j 1060.9 to variation in τ_1 (for K_{pvs} = 0.5, K_{ivs}= 400 and τ_2= 0.75 ms)

From Figure 3.26 and Figure 3.27, it can be seen that the interaction is more when the value of τ_1 is in the range of 1 to 2 ms. There is an instability for the case of proportional controller when τ_1 is 2 ms.

It was shown in Table 3.13 that the participation of q-axis current controller in the interaction is less when a PI controller is used. This phenomenon can be understood from considering the state equation of q-axis current controller which is given by (2.117). The participation of the state x_4 is influenced by parameters $\mathrm{K_{pvs}}$, $\mathrm{K_{ivs}}$ and τ_1. From the analysis in section 3.2.6, Figure 3.26 and Figure 3.27, it is clear that the participation of state x_4 in the interaction increases as $\mathrm{K_{pvs}}$ increases and τ_1 is in a particular range. For the same range of τ_1, the participation of state x_4 is less when $\mathrm{K_{ivs}}$ increases (for a small value of $\mathrm{K_{pvs}}$).

A better understanding of the influence of the parameters $\mathrm{K_{pvs}}$, $\mathrm{K_{ivs}}$ and τ_1 on the stability of the system can be obtained by considering the transfer function i_{tqref} to $\mathrm{V_{pcc}}$ about this operating point. Here, the effect of other inputs on $\mathrm{V_{pcc}}$ and the effect of i_{tqref} on other inputs are neglected for simplicity. This assumption is valid as long the PV system operates close to considered operating point and there is no change in other controller dynamics or the power system. The transfer function is of order 33 and is shown in Appendix B.

The simplified model of PCC voltage controller when considering the above transfer function is as shown in Figure 3.28. The transfer function from i_{tqref} to $\mathrm{V_{pcc}}$ is of order 33 and hence, Nyquist plot is used to calculate the relative stability margins since the transfer function has multiple crossover frequencies [66].

The Nyquist plots for the open loop transfer function and loop transfer function with the filter (without the controller) are shown in Figure 3.29. It can be seen that the addition of the filter of time constant of 2 ms causes additional phase lag and reduces the phase margin of the system. The loop transfer function has a gain margin of 11.9 dB at the phase crossover frequency of 1190 rad/sec.

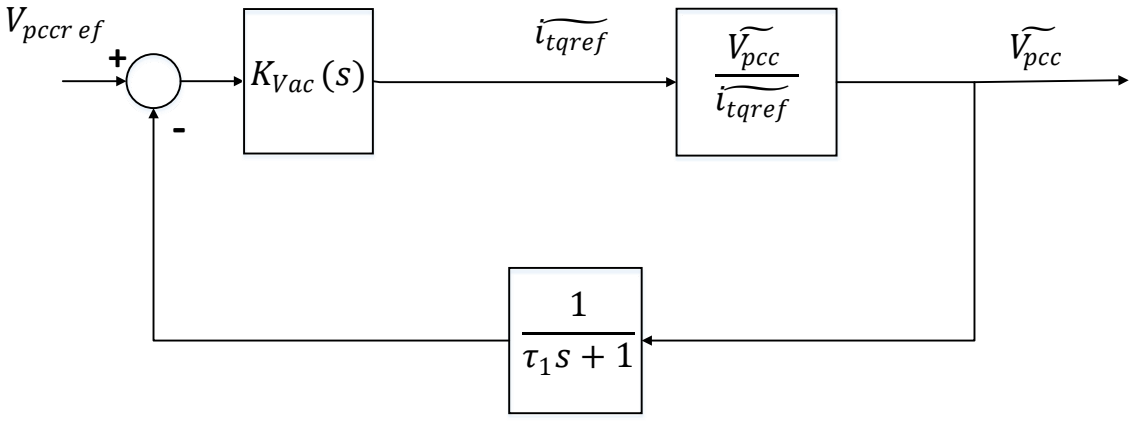

Figure 3.28 Simplified model of PCC voltage controller when considering transfer function approach

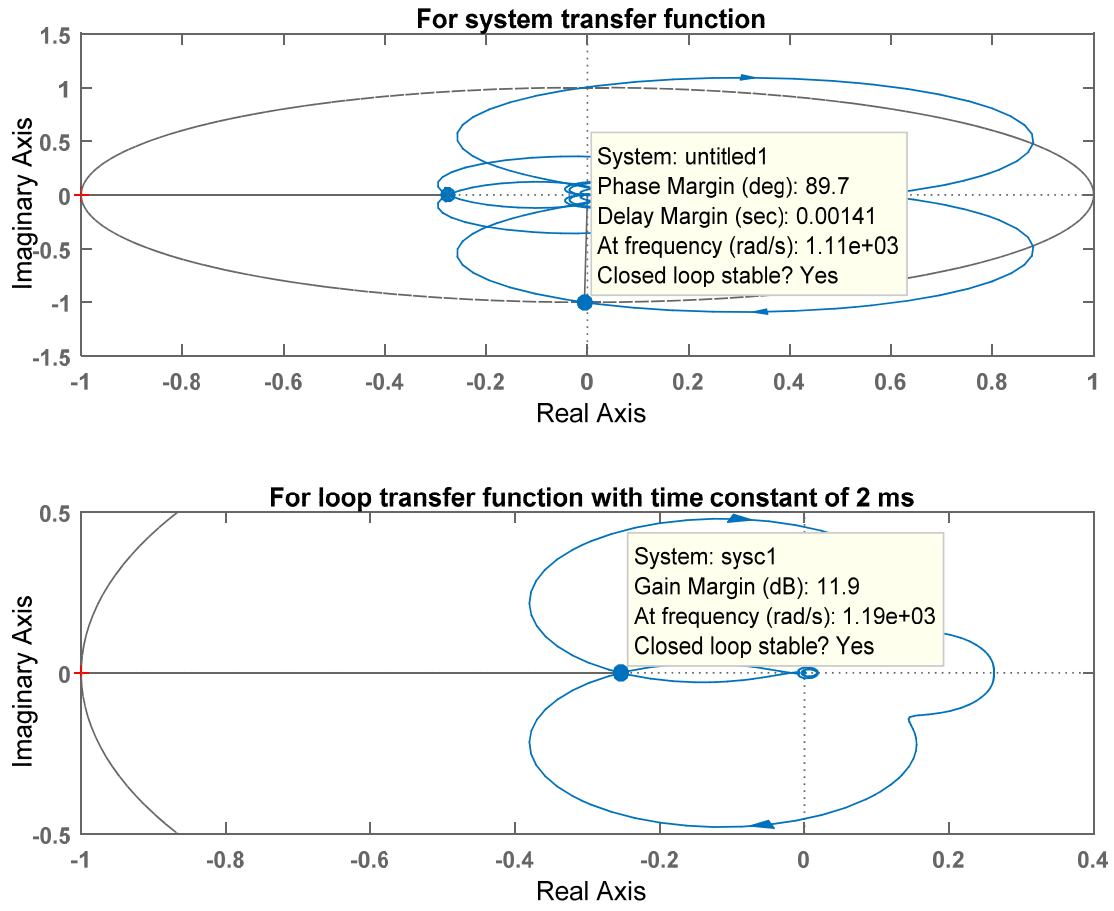

Figure 3.29 Nyquist plot comparison between system and loop transfer functions

Now, the effect of adding a proportional controller with a gain of K_{pvs} = 6.25 and a PI controller with gains of K_{pvs} = 0.5 and K_{ivs} = 400 on the system are shown in Figure 3.30. From Figure 3.30, it is clear that increase in proportional gain decreases the gain margin and render the system to be unstable. But, addition of an integral controller provides voltage control without affecting the gain margin much. This is the reason as to why increase in proportional gain moved the eigenvalue due to interaction towards the right half of the S-plane.

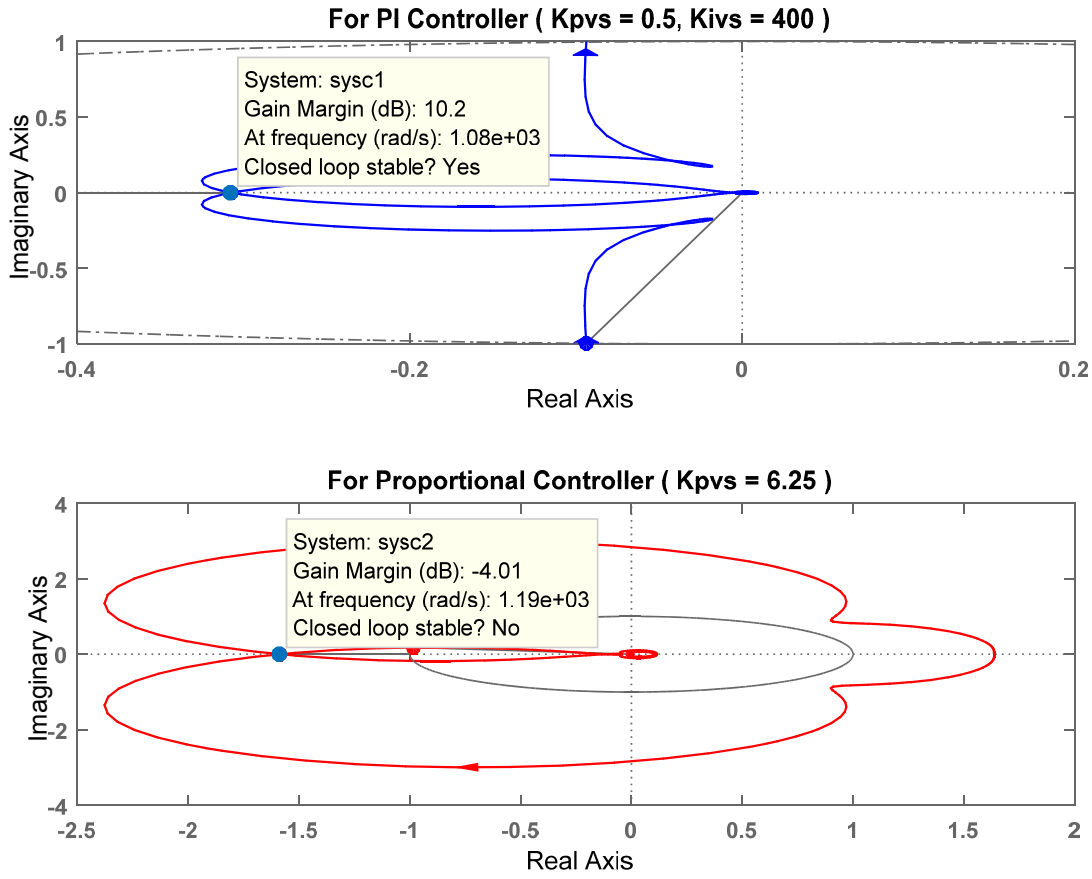

Figure 3.30 Nyquist Plot comparison for proportional and PI controllers

From the studies conducted in this section, it can be concluded that the value of feed-forward filter time constant should be lesser and farer from the gain crossover frequencies of the current controllers to ensure that there is minimum interaction between the current controllers and to ensure the effectiveness of feed-forward. This will

eventually lead to minimum interaction between dc-link voltage control loop and PCC voltage control loop. A criterion to decouple the feed-forward filter dynamics from the current controller dynamics can be adopted from [32] which states that the difference in speed between two loops should be at least 2 to 10 times. Once this criteria is satisfied, the value of τ_1 has very little impact on the interaction. It only influences the stability of PCC voltage control loop.

3.2.8 Study of eigenvalue sensitivity to current controller bandwidth

It was shown in section 3.2.7 the participation of current controller state x_4 is influenced by parameters K_{pvs}, K_{ivs} and τ_1. From equation (2.117), it is clear that the stability is also influenced by parameters K_{pi2} and K_{ii2} which determine the gain crossover frequency and hence, the bandwidth of q-axis current controller. In this section, it will be shown that if the gain crossover frequency of q-axis current controller changes, the instability can be prevented. This is because the speed of operation of q-axis current controller will be different from that of d-axis current controller and the feed-forward filters and hence, the interaction can be minimized.

The sensitivity of dominant eigenvalue 33.42 $\pm$ j 1271.2 (for K_{pvs}= 6.25, τ_2= 0.75 ms and τ_1= 2 ms) to variation in the gain crossover frequency of q-axis current controller is shown in Figure 3.31. The sensitivity of dominant eigenvalue for PI controller case is not shown here since there are no issues with stability.

From Figure 3.31, it can be seen that the eigenvalue that represents interaction moves towards the left half of S-plane as the speed of current controller increases or decreases. This, once again, clearly proves that the interaction occurs when the time constant of feed-forward filters are in the range of speed of operation of current controllers. Hence, one of the ways to minimize this interaction is to operate the q-axis current controller atleast 2 to 10 times slower than the d-axis current controller when the time constant of feed-forward filters cannot be guaranteed and they exhibit changes due to nonlinearity or any other delay. Operation of q-axis current controller at a speed greater than the d-axis current controller may not be an optimal solution since the dc-link voltage controller has

to be faster than the PCC voltage controller for effective supply of reactive power by the PV inverter.

Such constraints are not there when a PI controller is utilized for PCC voltage control. A PI controller can provide a stable control operation even in the presence of interaction without compromising on the bandwidth of q-axis current controller.

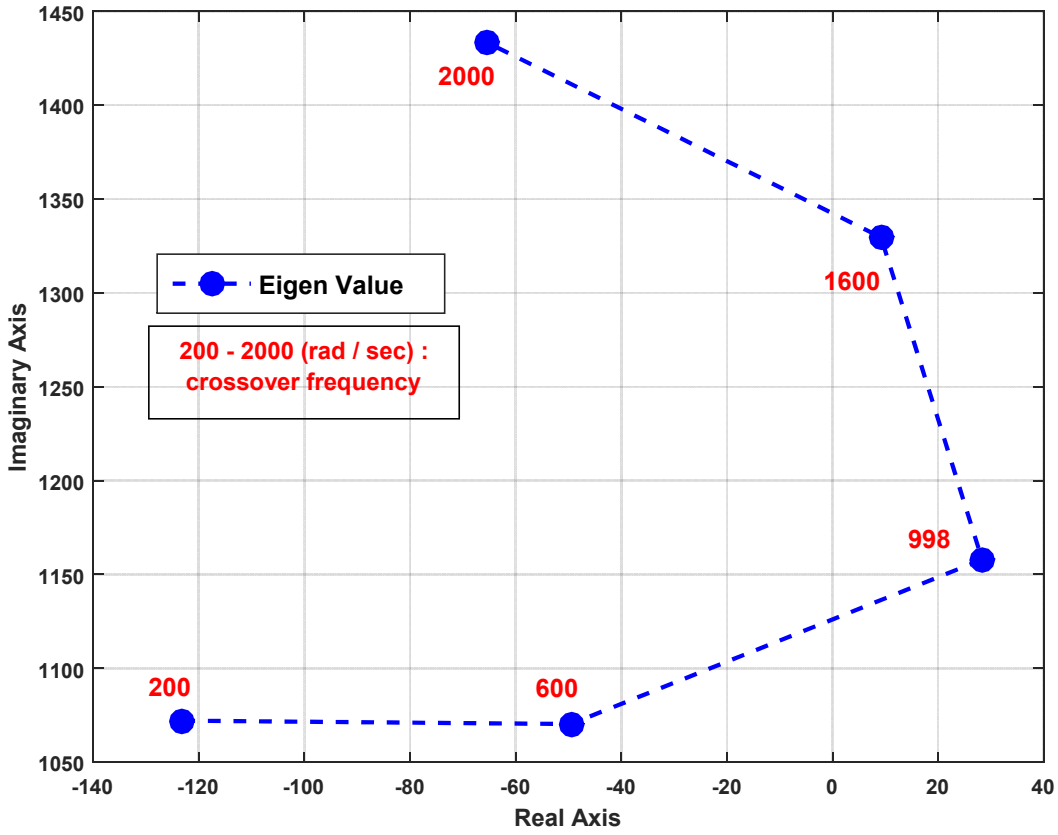

Figure 3.31 Sensitivity of eigenvalue 33.42 ± j 1271.2 to variation in q-axis current controller crossover frequency (for K_{pvs}= 6.25, τ_2= 0.75 ms and τ_1= 2 ms)

3.2.9 Comparison of results with simplified model of PCC voltage controller

PCC voltage controller is generally designed based on a simplified model which ignores the dynamics of dc-link voltage controller and PLL [17], [32]. The model has been adopted from [32] and is shown in Figure 3.32. The dynamics of filter capacitor and transformer are neglected in the derivation of this model.

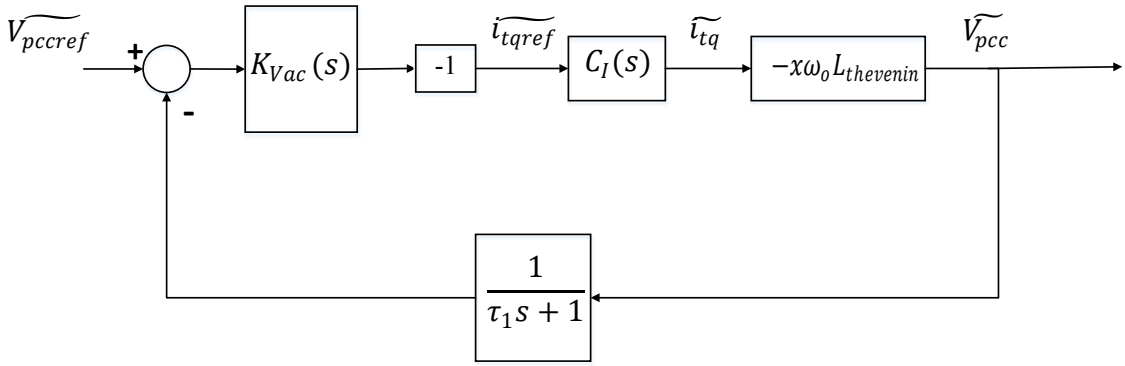

Figure 3.32 Simplified model of PCC voltage controller

The step response of -2.5 % for both proportional (K_{pvs}= 3.609) and PI controllers (K_{pvs} = 0.5, K_{ivs}= 400) are shown in Figure 3.33. The eigenvalues of the closed loop system and the settling time for 1% error margin are shown in Table 3.14.

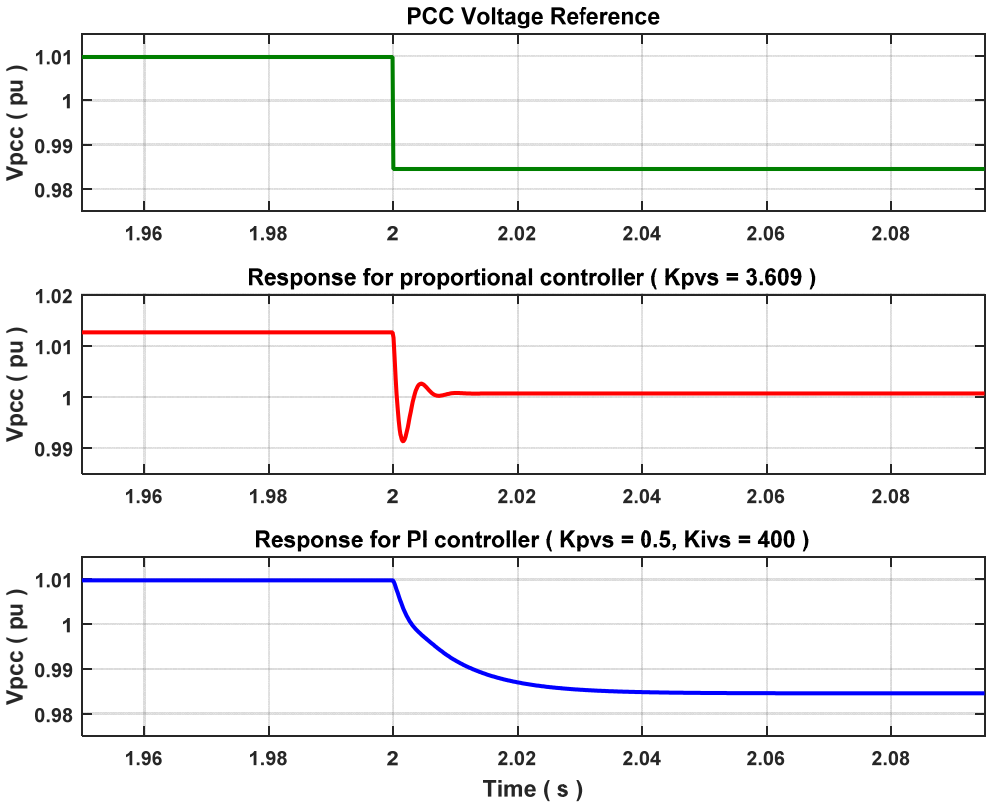

Figure 3.33 Step Response of simplified PCC voltage controller model (for q-axis current controller crossover frequency of 1380 rad/sec)

Table 3.14 Simplified PCC voltage controller model - comparison

Parameter	Closed loop poles	Closed loop zeros	Settling time (ms) (for 1 % error margin)
Proportional Controller	-731, -495 ± j 1260	-909, -500	--
PI controller	-573 ± j 833, - 468, -110	-909, -800, -500	7.3

By comparing the results of linearized model, PSCAD / EMTDC model and simplified PCC voltage controller model (Table 3.7, Table 3.12 and Table 3.14), it can be seen that the simplified PCC voltage controller model does not show the eigenvalue that occurs due to interaction between dc-link voltage control loop, PCC voltage control loop, distribution feeder current and measurement filters. For PI controller, the settling time and one of the dominant poles –110 are very much closer to those of the linearized model. For proportional controller, the results exhibit major deviation due to strong interaction between the control loops.

This model can be utilized when the speed of q-axis current controller is atleast 2 to 10 times slower than the speed of the d-axis current controller. This is required to approximately decouple the current controllers and, thereby decouple the dc-link and PCC voltage control loops. The feed-forward voltage filter time constants are fixed at the same value of 0.75 ms. In order to validate the simplified model, the q-axis current controller is designed to operate with a gain crossover frequency of 200 rad/sec. For PCC voltage controller, the gains are similar to the gains utilized for Figure 3.33. A step of -5% is applied to the PCC voltage controller.

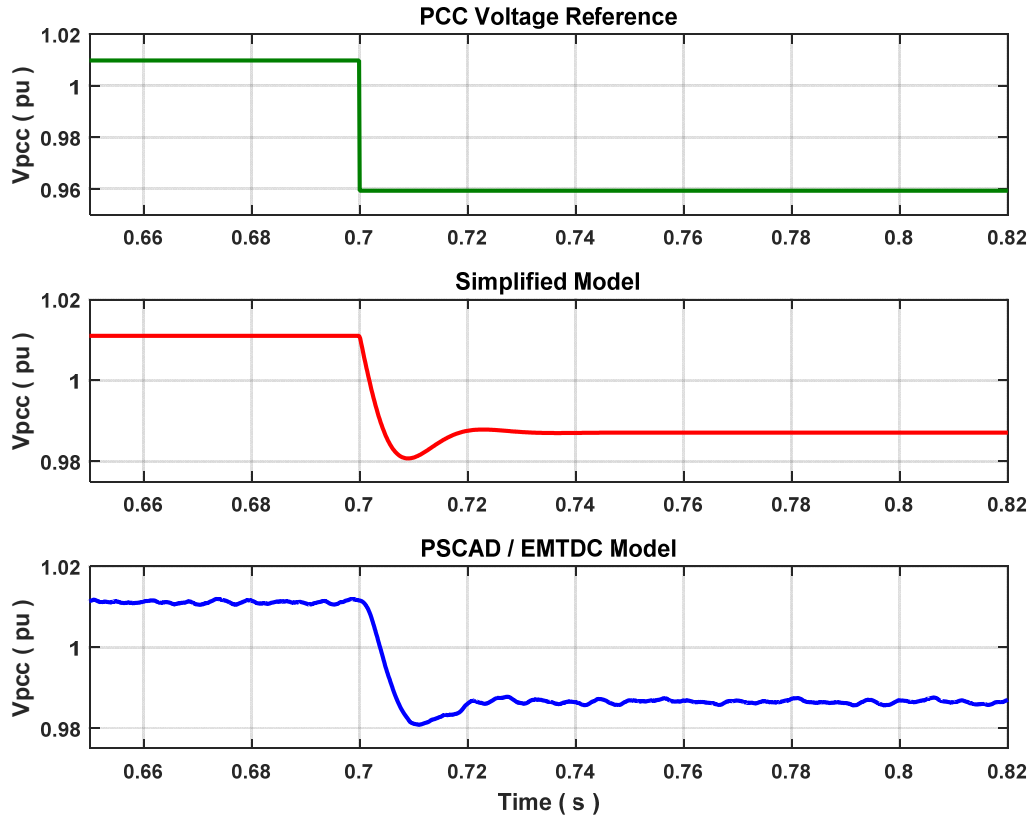

Figure 3.34 Comparison between Simplified and PSCAD / EMTDC models – for Proportional controller (K_{pvs}= 3.609)

Table 3.15 Comparison between models – Proportional Controller

Proportional Controller	
Closed Loop Poles: -401, -152 ± j 227 **Closed Loop Zeros:** -500, -227	
Parameter	**Settling Time (1 % of corresponding steady state) (ms)**
Simplified Model	2.4
PSCAD / EMTDC Model	4.6

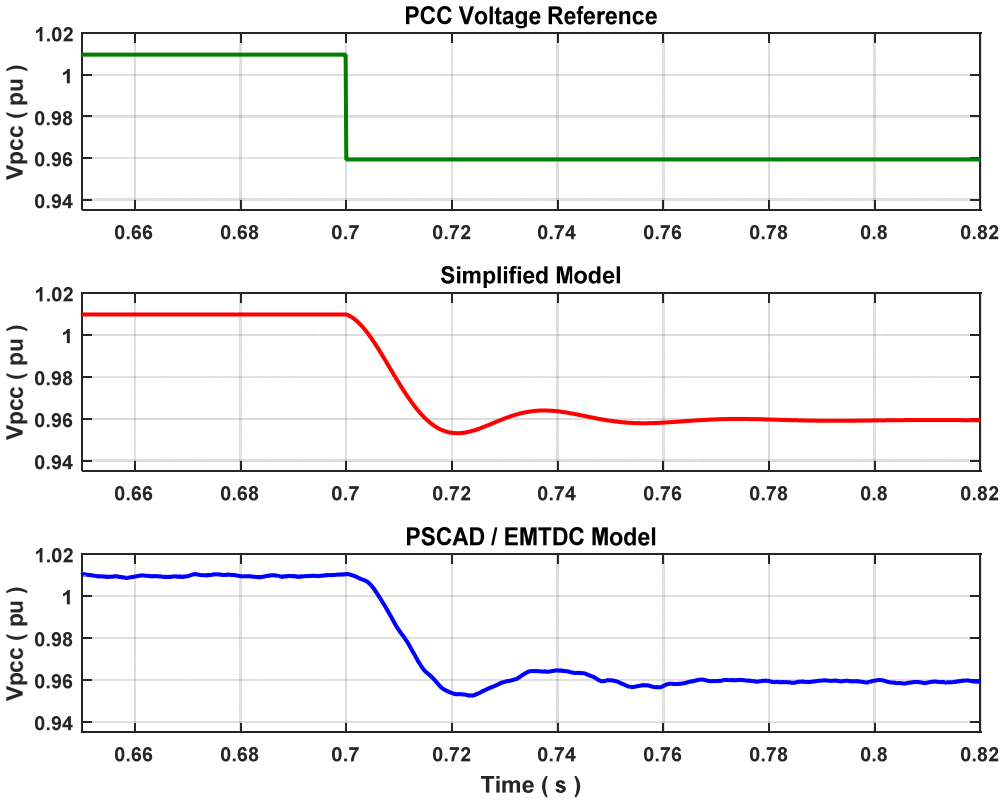

Figure 3.35 Comparison between Simplified and PSCAD / EMTDC models – for PI controller (K_{pvs}= 0.5, K_{ivs}= 400)

Table 3.16 Comparison between models – PI Controller

PI Controller		
Parameter	**Damped frequency (rad/s)**	**Settling Time (1 % error of steady state) (ms)**
Closed Loop Poles and Zeros	Poles : -508, -94.8 , -51.7 ± j 174 Zeros: -800, -500, -227	
Simplified Model	177.45 (28.25 Hz)	12.2
PSCAD / EMTDC Model	182.12 (29 Hz)	13.7

From Figure 3.34, Figure 3.35, Table 3.15 and Table 3.16, it can be seen that the simplified model matches closely with the PSCAD / EMTDC model for both proportional and PI controller cases.

3.2.10 Effect of change in operating point on the interaction

The interaction between dc-link voltage control loop and PCC voltage control loop that caused instability in the case of a proportional type PCC voltage controller was studied about an operating point where G = 0.85. In this section, the movement of the dominant eigenvalue that represents the interaction for three more operating points namely G = 0.6, G = 0.4 and G = 0.2 will be shown. In each case, the dc-link voltage controller is re-designed so that it meets the same performance criteria.

Figure 3.36 and Figure 3.37 show the sensitivity of the eigenvalue due to interaction to change in irradiance for both proportional and PI controller cases respectively. The time constants are kept at τ_2= 0.75 ms and τ_1= 2 ms to represent the case for maximum interaction. For proportional controller, the gain is kept at 3.609 for all operating points. For PI controller, the gains are kept at K_{pvs} = 0.5 and K_{ivs} = 400 for all operating points. The reference voltage is maintained at 1 pu for all the cases. From Figure 3.36 and Figure 3.37, it can clearly be seen that the eigenvalue that represents interaction exists for all irradiance but moves towards the left half of S-plane as the value of irradiance (hence, active power) decreases in cases of both the controllers. But, the interaction is always more in the case of the proportional controller. This, once again, shows the PI controller exhibits better performance over proportional controller at all operating points.

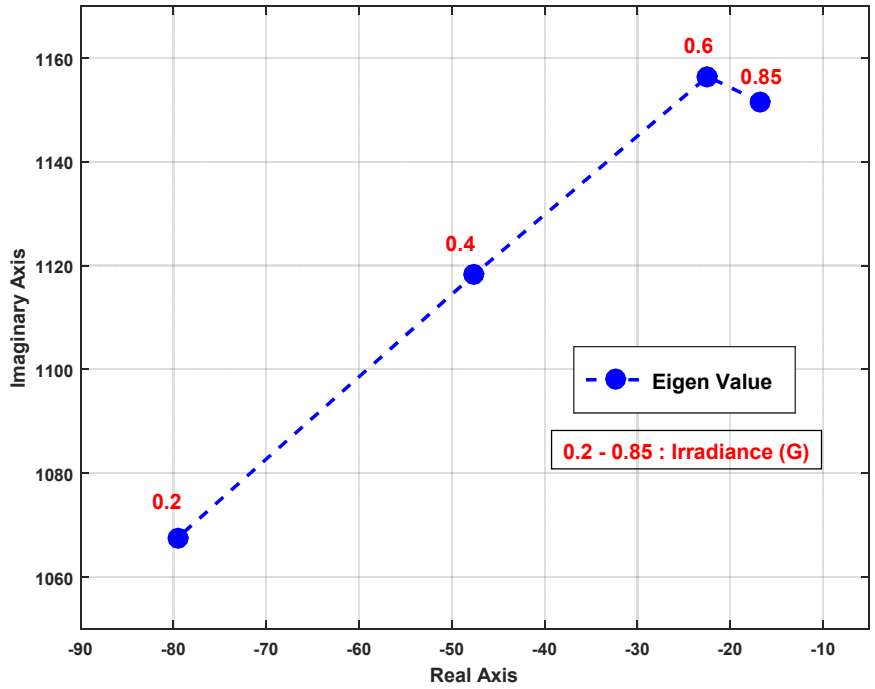

Figure 3.36 Sensitivity of eigenvalue due to interaction to irradiance of PV system (for K_{pvs} = 3.609, τ_2= 0.75 ms and τ_1= 2 ms)

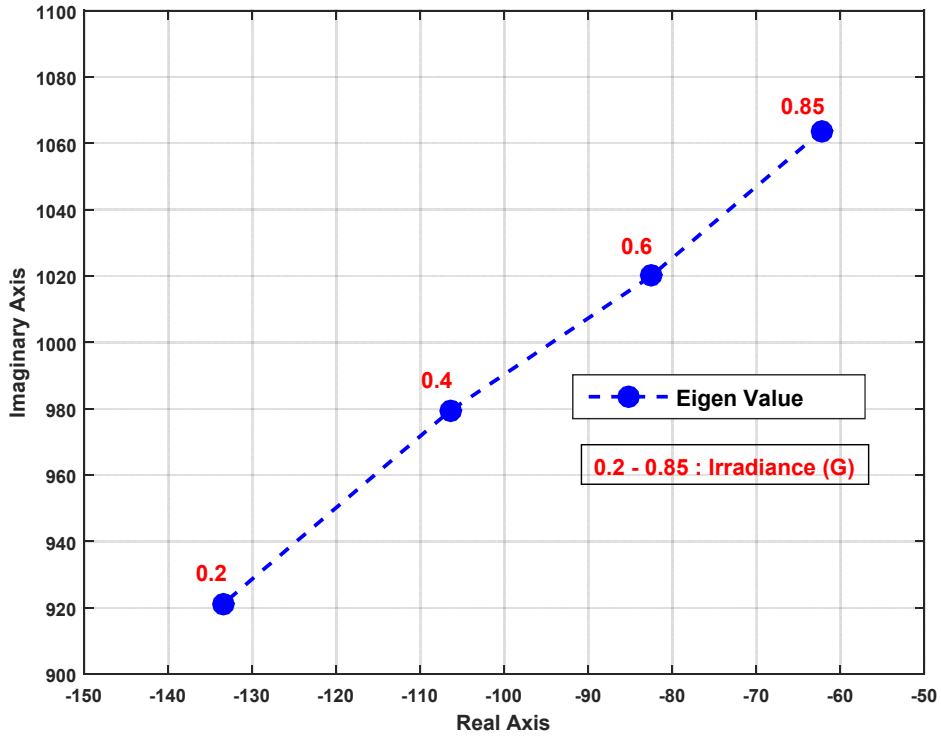

Figure 3.37 Sensitivity of eigenvalue due to interaction to irradiance of PV system (for K_{pvs} = 0.5, K_{ivs} = 400, τ_2= 0.75 ms and τ_1= 2 ms)

3.3 Validation of PV-STATCOM model operating in Full STATCOM mode

The PV system operates in Full STATCOM mode by curtailing its real power partially (or) completely and acts as a STATCOM with reactive power capacity during and post faults for providing voltage support to grid. The model developed for Full STATCOM mode operation has been explained in section 2.6.4. The purpose of this section is to validate the model by observing the step responses of linearized and PSCAD / EMTDC models.

The parameters of the various controller subsystem components namely PLL and current controller which are designed for the operation of PV-STATCOM in partial and full PV modes are also used for Full STATCOM mode operation.

The dc-link voltage controller has to be re-designed here for operation in Full STATCOM mode. The same performance criteria of a speed of 460 rad/sec (3 times slower than d-axis current controller) and a phase margin of 60 degrees are considered. The control structure of dc-link voltage controller is similar to Figure 3.7 and the transfer function relating d-axis current and dc-link voltage is given by (3.4). The pole x_{Vdc2} which is due to PV array dynamics is zero since the power from PV system is zero under Full STATCOM mode operation. The parameter x_{Vdc1} is determined from the value of modulation index (given in Appendix B) when the STATCOM regulates its dc-link voltage at reference value which is 1.0255 kV here but exchanges zero reactive power with the grid.

The compensator $K_V(s)$ is an integral controller in cascade with a lead filter. The procedure for designing the compensator is adopted from [18]. Although the low pass filter with time constant τ_{Vdc} has been removed, the design of $K_V(s)$ operating at 460 rad/sec ensures that the harmonics are filtered out of the control loop.

The compensator $K_V(s)$ is given by,

$$K_V(s) = \frac{(K_{iv})}{s}\left(\frac{n_o(s+z_o)}{s+p_o}\right) \tag{3.13}$$

Where,

K_{iv} is the integral gain

n_o is the gain of lead filter

z_o and p_o are the zero and pole of lead filter respectively.

The parameters of $K_V(s)$ are provided in Table B. 4 of Appendix B.

The step response of the dc-link voltage controller of the control block diagram of Figure 3.7 and PSCAD / EMTDC model are shown in Figure 3.38.

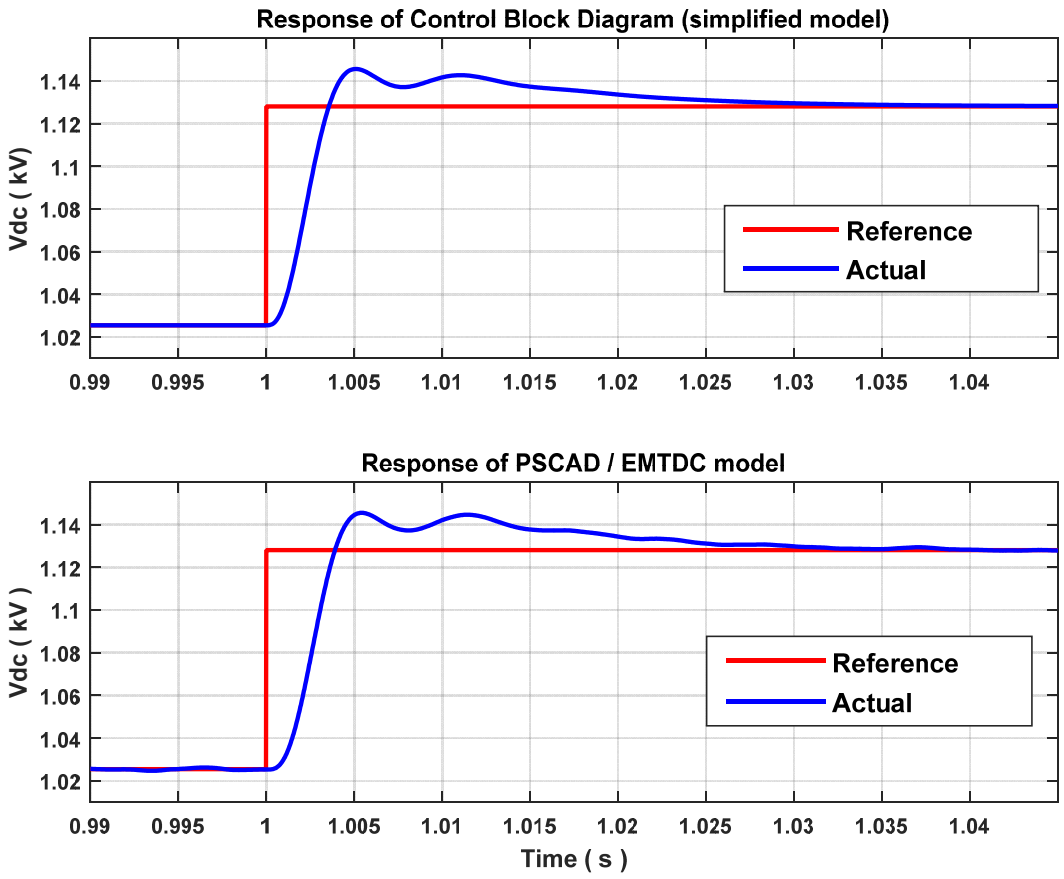

Figure 3.38 Step Response of DC-link voltage controller (for Full STATCOM mode)

Table 3.17 Comparison between step responses of dc-link voltage controller (Full STATCOM mode)

Parameter	Damped Frequency (rad/sec)	Settling time (for 1% steady state error) (ms)
Control Block Diagram	1052.7 (167.62 Hz)	13.7
PSCAD / EMTDC model	1051.96 (167.50 Hz)	14.1

A comparison between the step responses is shown in Table 3.17. It can be seen that the damped frequency and settling time of both the responses are very close to each other, thus validating the controller design.

This also further substantiates the reason for discrepancy which was observed during the design of dc-link voltage controller for partial PV-STATCOM mode operation. With reference to equation (2.61) , the model of dc-link voltage controller for Full STATCOM mode of operation is represented only by the term $-\frac{3m_d i_{td}}{4C_{dc}}$ which represents inverter dynamics. The term $-\frac{a_5 V_{dc}}{C_{dc}} - \frac{a_2}{C_{dc}}\{e^{a_3 V_{dc}+a_4 I_{pv}} - 1\}$ is not present since PV array does not supply any power and hence, its nonlinearity does not affect the dc-link voltage controller performance.

The PCC voltage controller is considered to be only of PI type for Full STATCOM operation. The sensitivity of PI controller gains will be studied in order to choose the optimal gains.

The validation of the linearized model for Full-STATCOM involves comparing the step responses of DC-link voltage controller and PCC voltage controller with the corresponding step responses of PSCAD / EMTDC model.

The PV-STATCOM operating in Full STATCOM mode is linearized about an operating point such that it is regulating its DC-link voltage at its reference value and regulating the PCC voltage at 1 pu. The operating point data are obtained by solving the nonlinear

system equations using MATLAB/Simulink. The feed-forward filter time constant is fixed at 0.75 ms and the PCC voltage measurement filter constant is fixed at 2 ms.

Eigenvalue analysis is performed using the linearized model developed in section 2.6.4. At first, the integral gain is fixed at 1 and the proportional gain is varied from 0.5 to 6. The most sensitive (and dominant) eigenvalues are at -134.05 $\pm$ j908.82 and -0.2166 for proportional gain at 0.5. The sensitivity of these eigenvalues to variation in proportional gain are shown in Figure 3.39 and Figure 3.40. It can be seen that the -134.05 $\pm$ j908.82 is very sensitive to K_{pvs} and it goes towards right half of S-plane as K_{pvs} goes beyond 5. For K_{pvs} = 6, the eigenvalue is at 18.31 $\pm$ j969.8. The eigenvalue -0.2166 is less sensitive to K_{pvs} but it also goes towards the right half of S-plane. From participation factor analysis, it is confirmed that the unstable eigenvalue represents the interaction between dc-link voltage control loop, PCC voltage control loop, measurement filters and distribution feeder current i_{12d}. The other eigenvalue -0.2166 is strongly coupled to the PCC voltage controller state x_7.

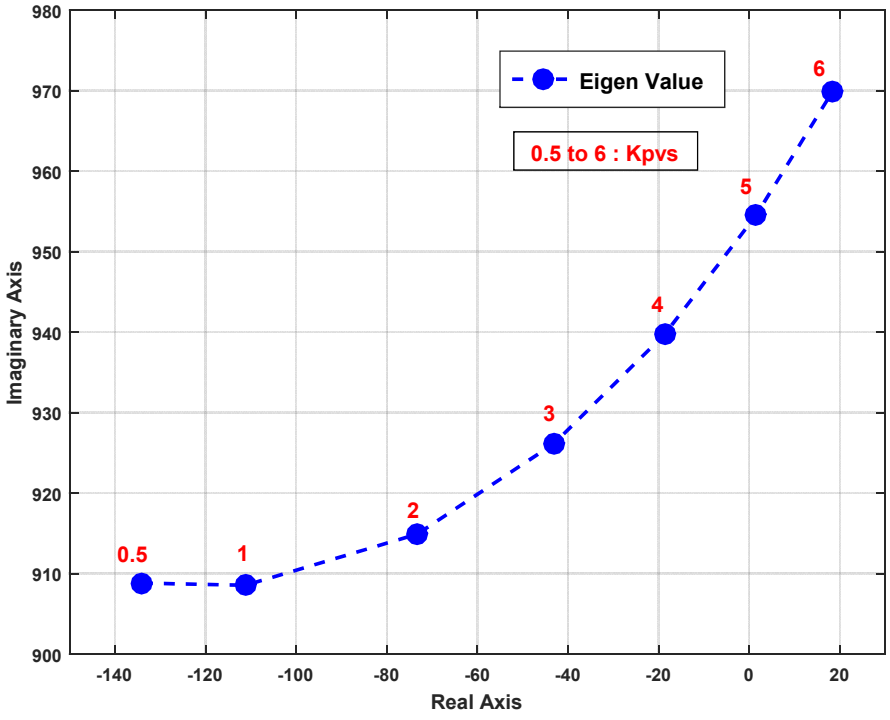

Figure 3.39 Sensitivity of eigenvalue -134.05 $\pm$ j 908.82 to variation in K_{pvs} (for K_{ivs}= 1)

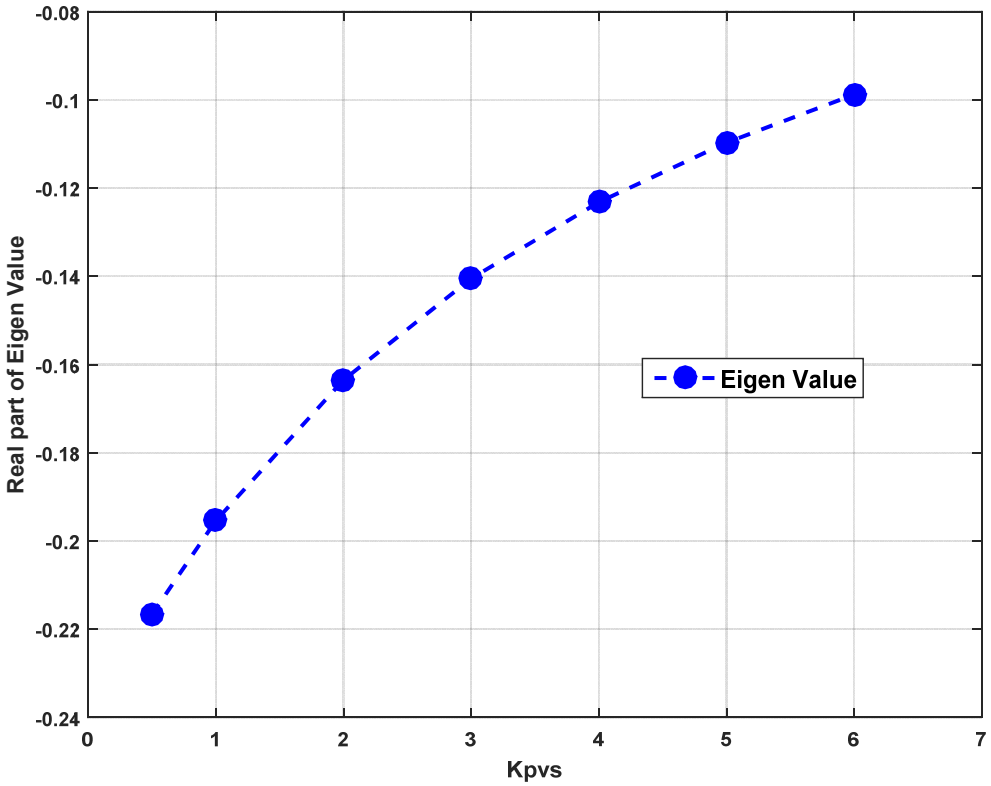

Figure 3.40 Sensitivity of eigenvalue -0.2166 to variation in K_{pvs} (for K_{ivs}= 1)

Now, the proportional gain is fixed at 0.5 and the integral gain is varied from 1 to 600 to study the sensitivity of eigenvalues, as shown in Figure 3.41 and Figure 3.42. It can be seen that the -134.05 $\pm$ j908.82 (which represents the interaction) is less sensitive to K_{ivs} but moves towards left half of S-plane. The other eigenvalue -0.2166 (which is strongly coupled to PCC voltage controller) is very sensitive to K_{ivs} and also moves towards left half of S-plane. Hence, it can be concluded that increasing K_{pvs} will only render the system unstable. But, increasing K_{ivs} (after fixing K_{pvs} at a low value) will make the system more stable. The characteristics exhibited by the eigenvalues are very much similar to those of partial PV-STATCOM. Hence, the best gains of PI controller are fixed at K_{pvs} = 0.5 and K_{ivs} = 400 to ensure that the eigenvalue which represents the interaction (most critical eigenvalue) has a damping ratio of more than 10 %.

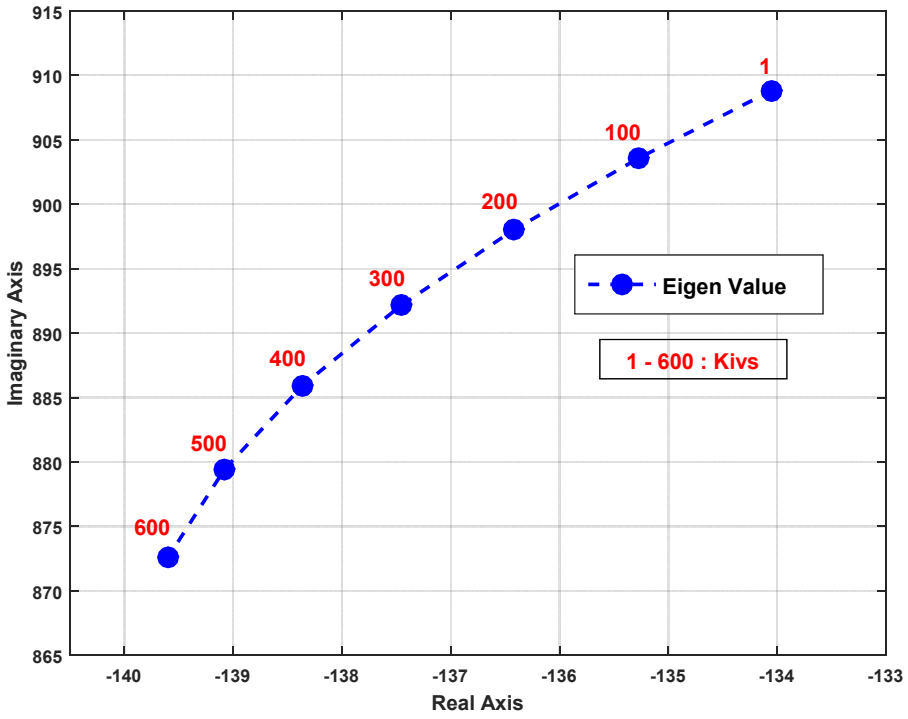

Figure 3.41 Sensitivity of eigenvalue -134.05 ± j 908.82 to variation in K_{ivs} (for K_{pvs}= 0.5)

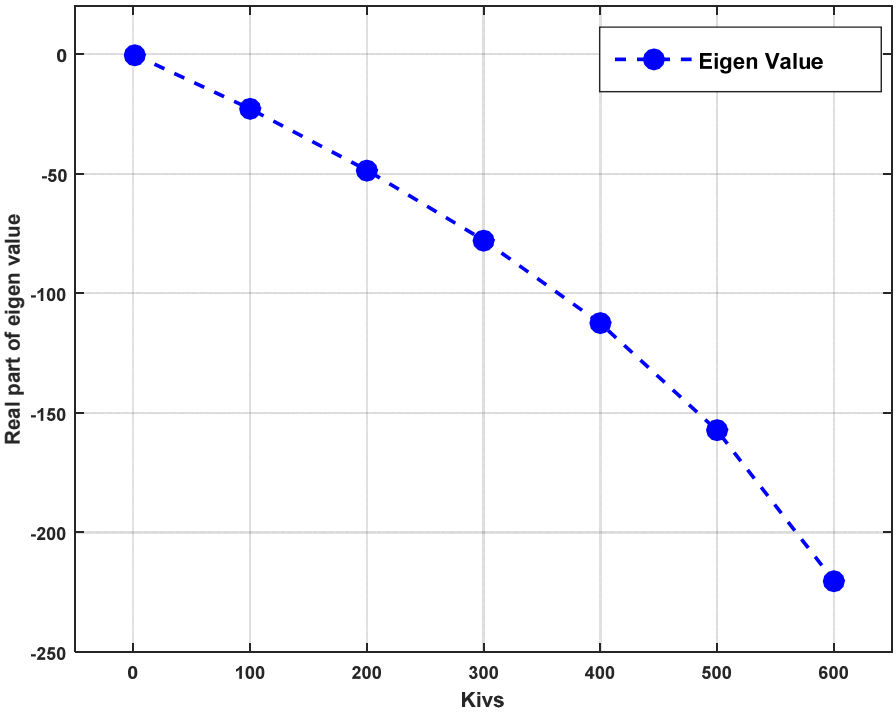

Figure 3.42 Sensitivity of eigenvalue -0.2166 to variation in K_{ivs} (for K_{pvs}= 0.5)

A step of 10 % is provided to dc-link voltage controller at a time of 1 second and the responses of linearized and PSCAD / EMTDC models are compared as shown in Figure 3.43

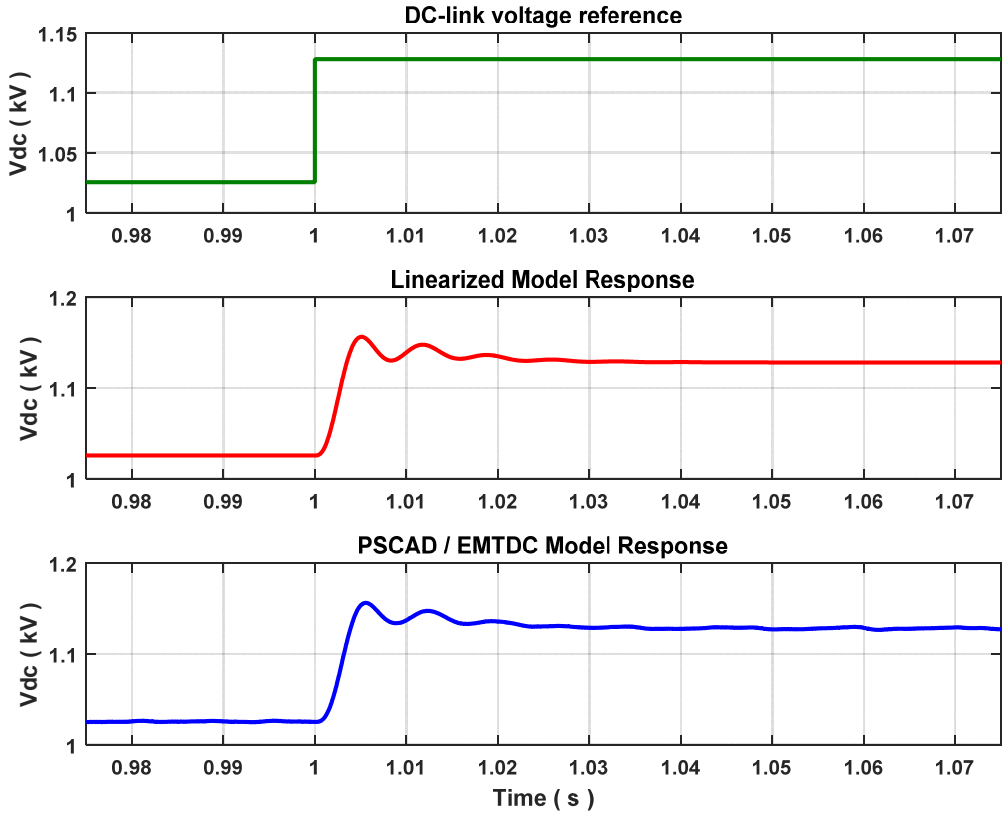

Figure 3.43 Full STATCOM – DC link voltage step response

A comparison between the step responses of the linearized model and PSCAD / EMTDC model is made in Table 3.18.

Table 3.18 Comparison between DC-link voltage step responses

Parameter	Damped Frequency (rad / s)	Settling Time for 1 % error margin (ms)
Linearized Model	945.36 (150.53 Hz)	13.8
PSCAD / EMTDC Model	935.092 (148.9 Hz)	14.6

It can be seen from Table 3.18 that the damped frequency and settling time of both the responses are very close to each other, thus validating the dc-link voltage control of the model.

Now, a step of -2.5 % is provided to the PCC voltage controller at a time of 1 second. The step response of PCC voltage of linearized model and PSCAD / EMTDC model is shown in Figure 3.44.

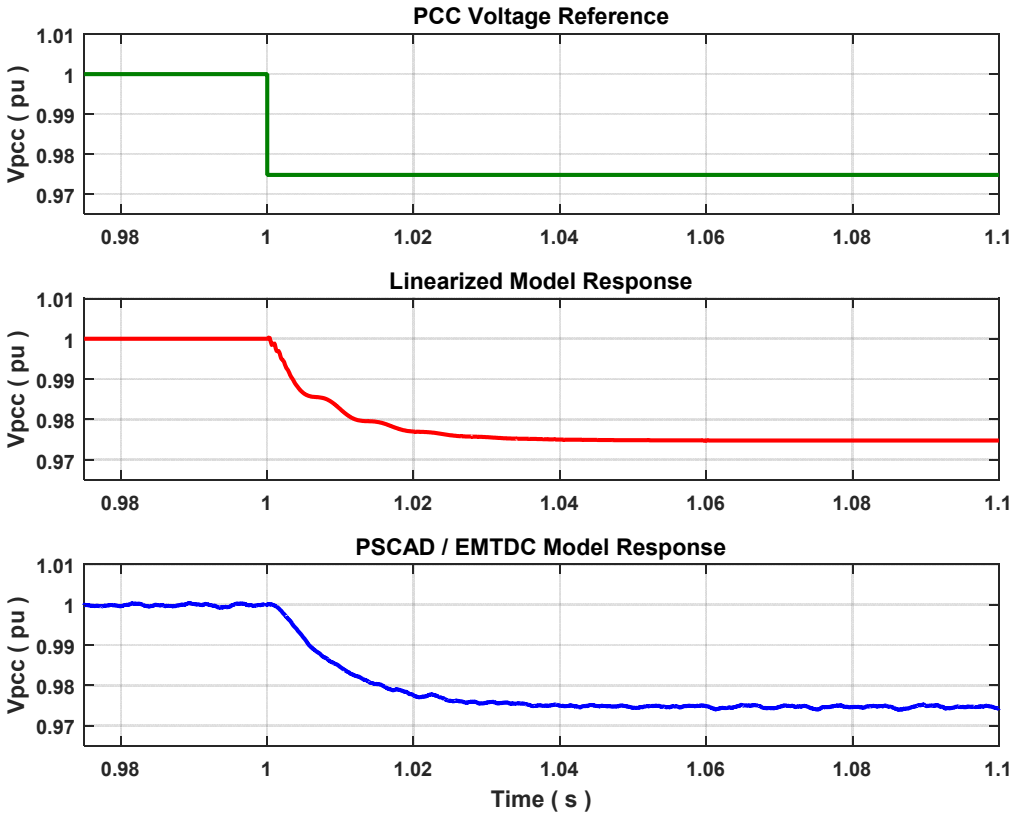

Figure 3.44 Full STATCOM – PCC voltage step response

A comparison between the step responses of the linearized model and PSCAD / EMTDC model is made in Table 3.19. It can be seen that the settling time of both the responses are very close to each other, thus validating the PCC voltage control of the model.

Table 3.19 Comparison between PCC voltage step responses

Parameter	Settling Time for 1% error margin (ms)
Linearized Model	8.7
PSCAD / EMTDC Model	10

From these studies, it is clear that the performance of the developed linearized model of Full-STATCOM is very close to that of the PSCAD / EMTDC model. Hence, this model can be utilized for controller design and stability analysis of PV-STATCOM operating in Full-STATCOM mode.

Also, the interaction between dc-link voltage control loop and PCC voltage control loop due to feed-forward filters exists in the case of Full STATCOM operation. The guidelines established for minimizing the interaction for partial PV-STATCOM operation is equally applicable for Full STATCOM operation.

3.4 Conclusion

The controllers for PV-STATCOM operating in the three modes namely Full PV, Partial PV-STATCOM and Full STATCOM have been designed. The linearized model for each mode of operation is validated by comparing the linearized and PSCAD / EMTDC model responses.

For partial PV-STATCOM, the Eigenvalue sensitivity analysis studies are used to compare the performance of both proportional and PI controllers when there exists an interaction between dc-link voltage and PCC voltage control loops. It has been proved comprehensively that the performance of PI controller is better than the performance of proportional controller for fast voltage control. Eigenvalue sensitivity analysis is also extended for Full-STATCOM operation to show the existence of this interaction and to decide the optimum values of PCC voltage controller gains.

Chapter 4

4 VOLTAGE CONTROL DURING SYSTEM DISTURBANCES

4.1 Introduction

This chapter deals with the application of partial PV-STATCOM for performing voltage control during system disturbances. Voltage flicker in the PCC voltage due to a 100% change in irradiance of PV system is considered as a system disturbance. The ability of partial PV-STATCOM to perform stable voltage control in order keep the change in PCC voltage within limits is studied.

From the studies in chapter 3, the feed-forward filter time constants are fixed at 0.75 ms so that interaction between dc-link voltage control loop and PCC voltage control loop is at a maximum. Under such circumstances, the performance of three types of voltage control strategies namely proportional controller based dynamic reactive current injection, Volt/Var control and PI controller based dynamic reactive current injection are compared.

The studies are initially performed with a single PV system performing voltage control. They are later extended to the case where there are two similar PV systems performing simultaneous voltage control to mitigate voltage flicker.

4.2 Application of dynamic reactive current for voltage flicker mitigation

It is mentioned in Chapter 1 that voltage flicker can be simulated by performing an instantaneous drop of PV output from 100% to 0% if accurate solar irradiance data is not available. The limit for voltage flicker is considered to be 3 % based on the assumption that this drop occurs once per hour.

It is also mentioned in Chapter 1 that dynamic reactive current injection can be used for voltage flicker mitigation. It can be implemented by using a proportional type AC voltage controller. The controller structure for making such an implementation is shown in Figure

4.1. The dead-band is not shown in the Figure 4.1. The injection of reactive current starts when the voltage error goes outside the dead-band (limit of 3%). The current injection should be continued for a certain time after the voltage error comes within the dead-band [26].

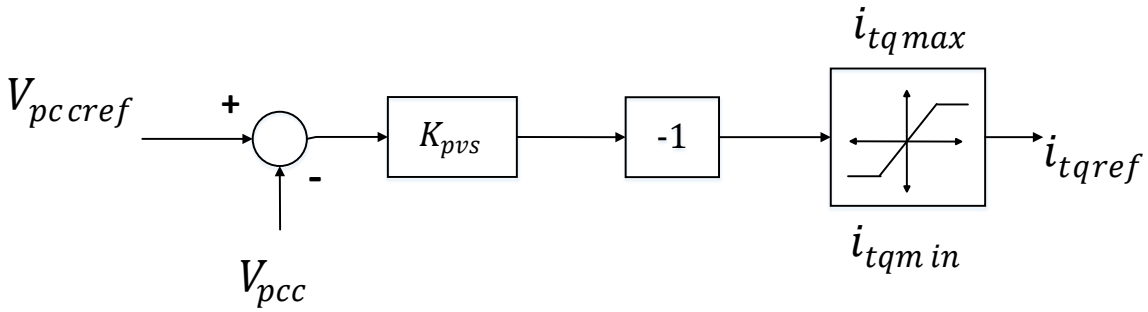

Figure 4.1 Proportional controller structure for dynamic reactive current injection

From the studies made in chapter 3, it is evident that proportional type PCC voltage controller results in poorly damped response for certain values of voltage measurement filter time constants. It has also been shown that PI type PCC voltage controller results in a fast and highly damped response for the same values of voltage measurement filter constants. In this case, the dynamic reactive current injection can also be implemented using a PI type PCC voltage controller. The controller structure for making such an implementation is shown in Figure 4.2.

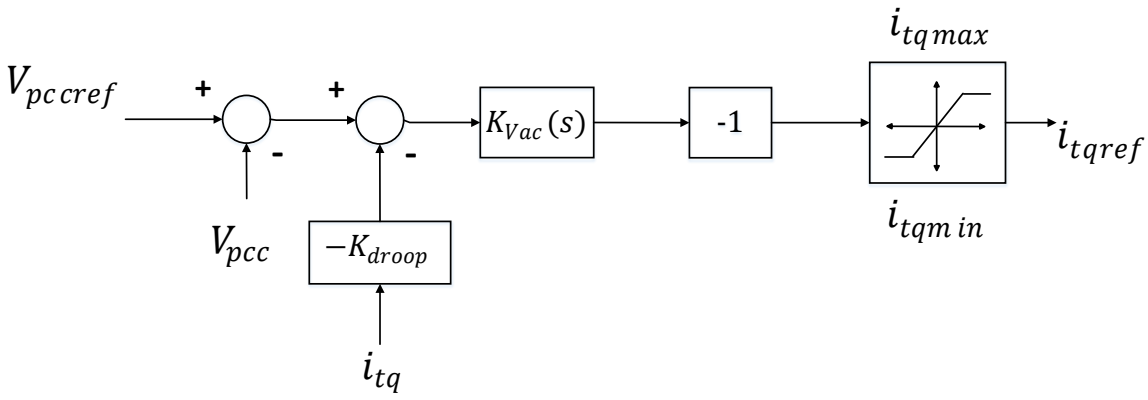

Figure 4.2 PI controller structure for dynamic reactive current injection (PI controller based droop)

For PI controller, the droop action (K_{droop}) is introduced in chapter 2 through the use of Q_{VSC} and this is applicable for steady state voltage control. For dynamic reactive current injection, the droop action (K_{droop}) is achieved using reactive current i_{tq}. The compensator $K_{Vac}(s)$ is a PI controller. The droop factor K_{droop} is the inverse of the slope of curve for dynamic reactive current injection. The negative sign is used to compensate for the convention used for reactive current controller. Once the voltage drops due to a flicker, the PCC voltage controller should respond as fast as possible to keep the voltage within a limit of 3%.

By eigenvalue analysis studies, it was shown in Chapter 3 that the interaction between dc-link voltage control loop, PCC voltage control loop and distribution feeder current i_{12d} is at a maximum when the feed-forward filter time constant is at 0.75 ms and the PCC voltage measurement filter constant is at 2 ms. This can be considered as the worst case scenario for the interaction when the bandwidths of two current controllers are the same. These time constants are used throughout this chapter for all the simulations. Also, for PI controller, an anti-integral windup scheme is utilized in order to prevent integral controller windup effect (if it occurs) on the output. The scheme for this has adopted from [67]. Integral windup effect refers to the accumulation of error by integral controller which could lead to increase in overshoot of the PCC voltage. This occurs due to saturation of the reactive current reference signal.

The objective of performing these studies in this chapter is to show effect of this interaction on the stability of PCC voltage control while performing voltage flicker mitigation. This kind of study has not been performed so far in the literature to the best knowledge of the author. This is also one of the major contributions of this thesis.

4.3 Voltage control methods

In this section, the ability of PV systems to mitigate voltage flicker and remain stable is being studied. First, studies will be performed using a single PV system and then, the interaction between two PV systems when both are trying to mitigate voltage flicker will

be studied. The voltage flicker is simulated by applying a step change in irradiance of the PV system from 0.85 kW/m^2 to 0 kW/m^2. In each case, the controllers of the PV system will be designed for the particular operating point using the models developed in Chapter 3 for Partial PV-STATCOM mode of operation. The ability of the controllers to remain stable during the disturbance and post disturbance will be studied.

For the voltage flicker studies, the performance of three kinds of control strategies will be compared as follows:

i) The first strategy is dynamic reactive current injection, implemented using a proportional type PCC voltage controller. The response time of voltage control for voltage flicker mitigation can be fast [7] in the range of few milliseconds. This is achieved by designing the q-axis current controller with a closed loop settling time of 6.6 ms (for 2% error margin) (gain crossover frequency of 1380 rad/sec).

ii) The second strategy is dynamic reactive current injection, implemented using a PI type PCC voltage controller. Similar to (i), the current controller is designed with a closed loop settling time of 6.6 ms (for 2% error margin) (gain crossover frequency of 1380 rad/sec).

iii) The third strategy is Volt/Var control presented in chapter 1 and chapter 3. This is not intended to be used for voltage flicker mitigation but for mitigating steady state voltage rise caused by PV systems. But, its ability to mitigate to voltage flicker is studied in this thesis. The response time of volt/var control is determined by the response time of inner q-axis current controller loop [30] and is usually large (in the range of seconds). In this thesis, this strategy is also considered to be represented by the same dynamic reactive current injection characteristic which is utilized for the other two control strategies. This is valid since each volt/var control curve can be represented by an equivalent dynamic reactive current characteristic curve under certain

assumptions. This is done for direct comparison with other two control strategies. It can be implemented by the control structure of Figure 4.1 and the q-axis current controller is designed to operate with a closed loop settling time of 1.52 seconds (for 2% error margin) (gain crossover frequency at 2.5 rad/sec). The current controller gains are designed as $K_{pi2} = 0$ and $K_{ii2} = 0.0049978$.

4.4 Flicker due to irradiance change in one PV system

The simplified diagram of the circuit utilized for the simulation of voltage flicker is shown in Figure 4.3. The 8.5 MW PV system is operating at an irradiance of 0.85 kW/m^2 so that there is some free reactive power capacity available for voltage control. The PCC reference voltage (moving average voltage) is set at 1.0124 pu since it is the average value of voltage that exists at this operating point. A step change in irradiance from 0.85 kW/m^2 to 0 kW/m^2 is introduced at a time of 2.5 seconds (simulation time - t) for 200 milli seconds. Its effect on the PCC voltage without voltage control action (with zero reactive current injection by PV system) is shown in Figure 4.4. The voltage drops to 0.970 pu from the original value of 1.0124 pu which is outside the 3 % voltage deviation limit (0.982 pu). This shows that the PCC voltage control action is required.

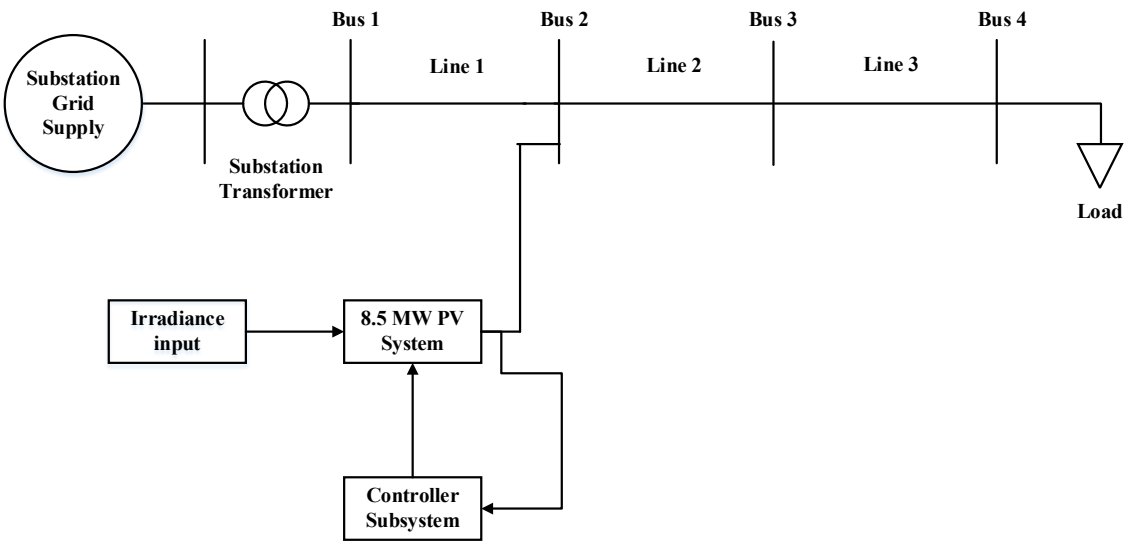

Figure 4.3 Simplified diagram of the circuit utilized for the simulation of voltage flicker due to irradiance change

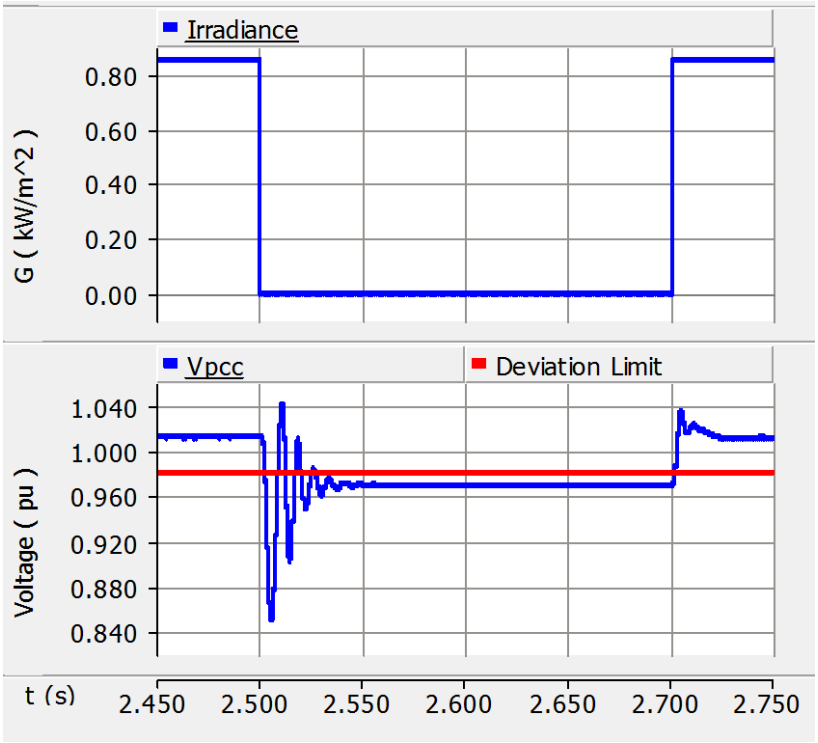

Figure 4.4 Voltage change at PCC due to irradiance change from 0.85 kW/m^2 to 0 kW/m^2

4.4.1 Dynamic reactive current injection with proportional controller

The ability of proportional controller based dynamic reactive current injection to mitigate voltage flicker is studied in this section. It is found that a proportional gain of 2 is sufficient to keep the voltage within a limit of 3%. The responses of PCC voltage controller and q-axis current are shown in Figure 4.5.

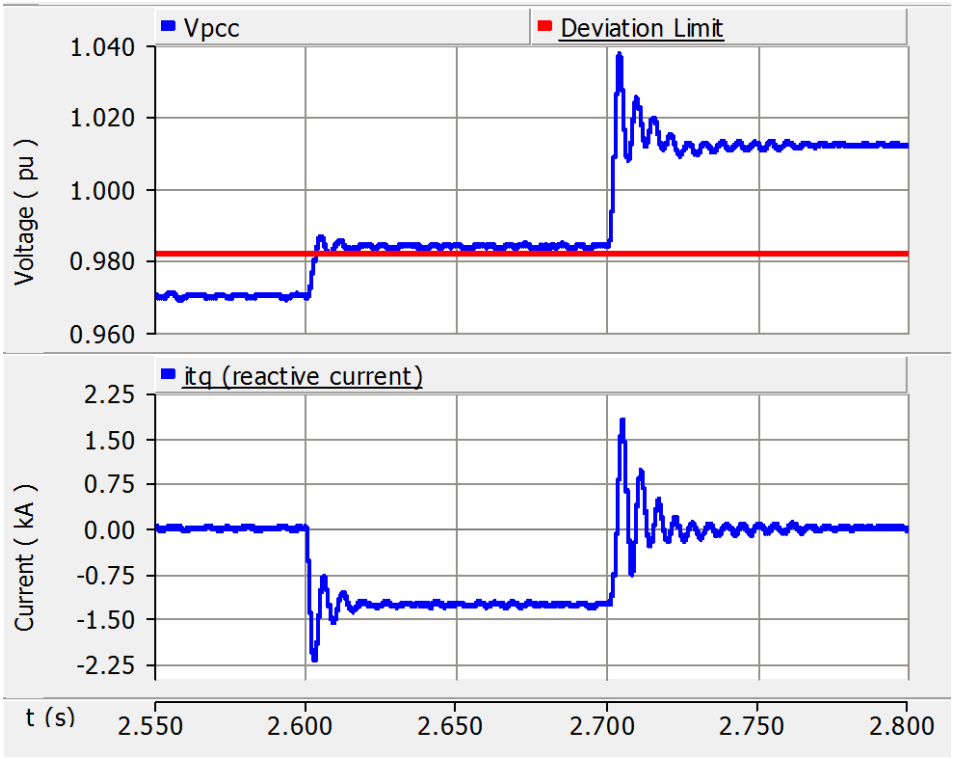

Figure 4.5 Response of proportional type PCC voltage controller (for K_{pvs} = 2)

The voltage controller is turned on at 2.6 seconds in order to given time for the system transient (due to irradiance change) to settle. This is done to study the stability of PCC voltage controller without any interference from the system dynamics although the voltage controller can be turned on at the instant of irradiance change. The voltage is regulated at 0.9843 pu which is within 3% by supplying a capacitive reactive current of 1.27 kA.

Now, the proportional gain is increased to 5 to regulate the voltage at a higher value and the response is shown in Figure 4.6. It can be seen that the voltage is regulated at 0.992

pu which is well within 3%. But, at 2.7 seconds when the irradiance returns back to 0.85 kW/m^2, the PCC voltage response becomes unstable with a damped frequency of 193.86 Hz (1217.44 rad/sec). By using the linearized model, it is found that an eigenvalue of 12.544+/-j 1226.4 is present at this operating point. The imaginary part of the eigenvalue matches closely with the frequency of oscillation of PCC voltage. By participation factor analysis, it is confirmed that this eigenvalue is due to the interaction between dc-link voltage control loop, PCC voltage control loop, distribution feeder current i_{12d} and measurement filters which was reported in chapter 3. By eigenvalue sensitivity analysis, it has been found that proportional controller cannot be used beyond a gain of 4 to prevent the system from going into instability.

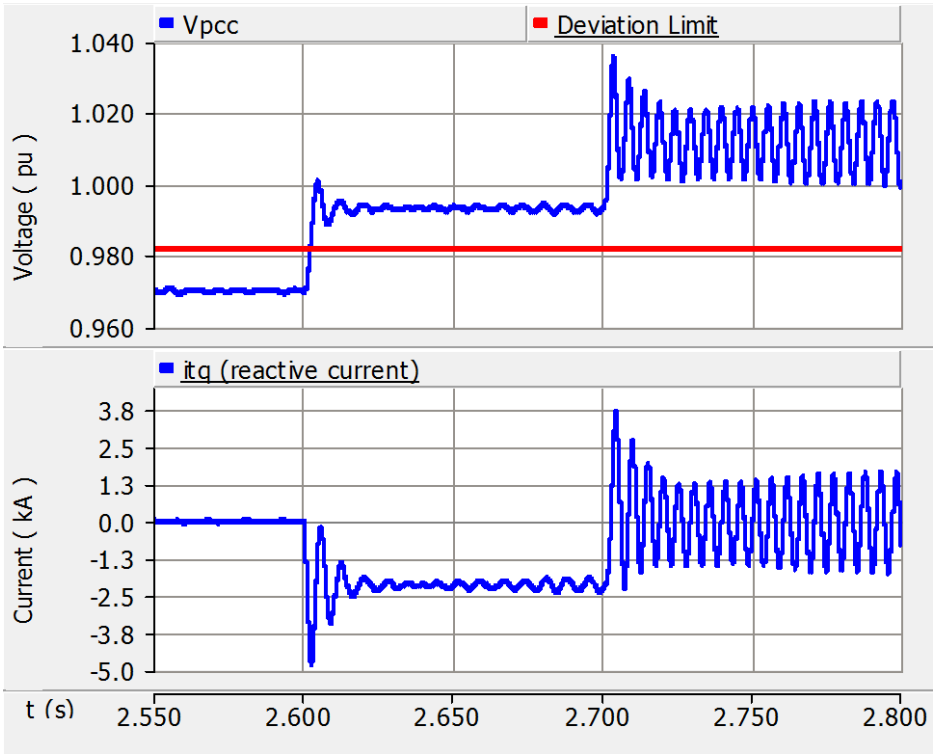

Figure 4.6 Response of proportional type PCC voltage controller (for K_{pvs} = 5)

4.4.2 Dynamic reactive current injection with PI controller

The ability of PI controller based dynamic reactive current injection to mitigate voltage flicker is studied in this section. The PI controller gains are chosen as K_{pvs} = 0.5 and K_{ivs} = 400 based on stability studies performed in chapter 3. The droop K_{droop} is chosen as

0.5 which is inverse of proportional gain 2 (slope of dynamic reactive current injection curve). The responses of PCC voltage and q-axis current are shown in Figure 4.7.

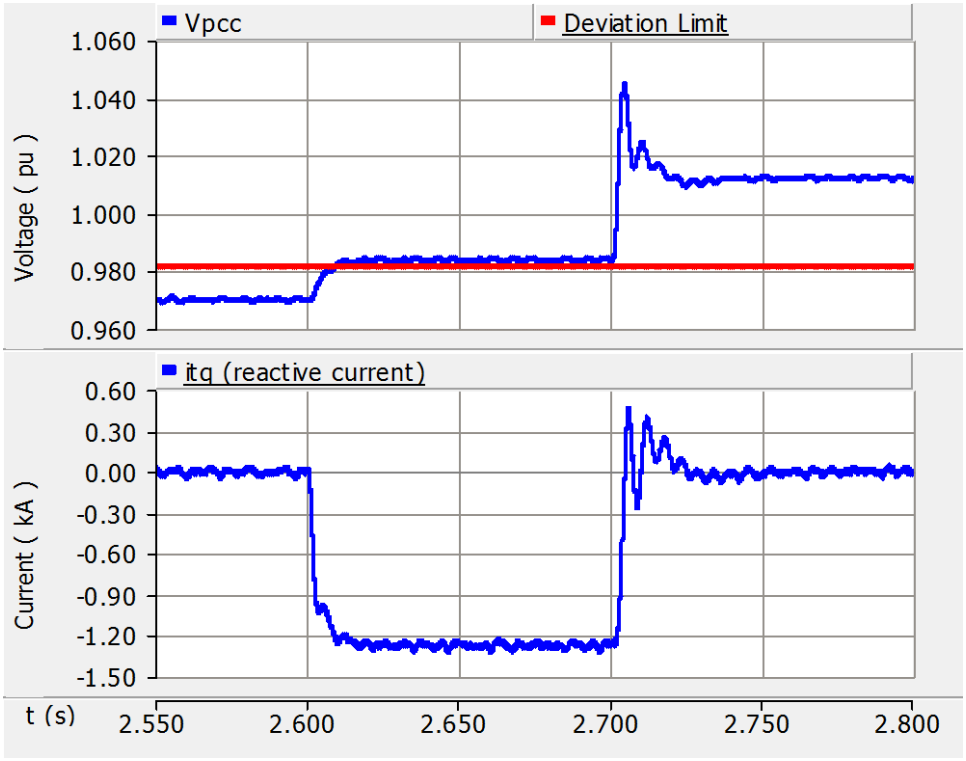

Figure 4.7 Response of PI type PCC voltage controller (K_{pvs} = 0.5, K_{ivs}= 400, $K_{droop} = 0.5$)

The voltage controller is turned on at 2.6 seconds in order to given time for the system transient (due to irradiance change) to settle. The voltage is regulated at 0.9843 pu which is within 3% by supplying a capacitive reactive current of 1.27 kA. By comparing Figure 4.5 and Figure 4.7, it can be seen that the steady state responses of proportional controller and PI controller during the period of irradiance change are similar. This shows that a particular slope of dynamic reactive current injection can be implemented using both proportional and PI type PCC voltage controllers.

Now, the response of PI controller with a droop of 0.2 (equivalent to proportional controller with a gain of 5) is shown in Figure 4.8. The voltage is regulated at 0.993 pu which is well within 3% during irradiance change and at 1.024 pu when the irradiance returns back to 0.85 kW/m^2 without any stability issues.

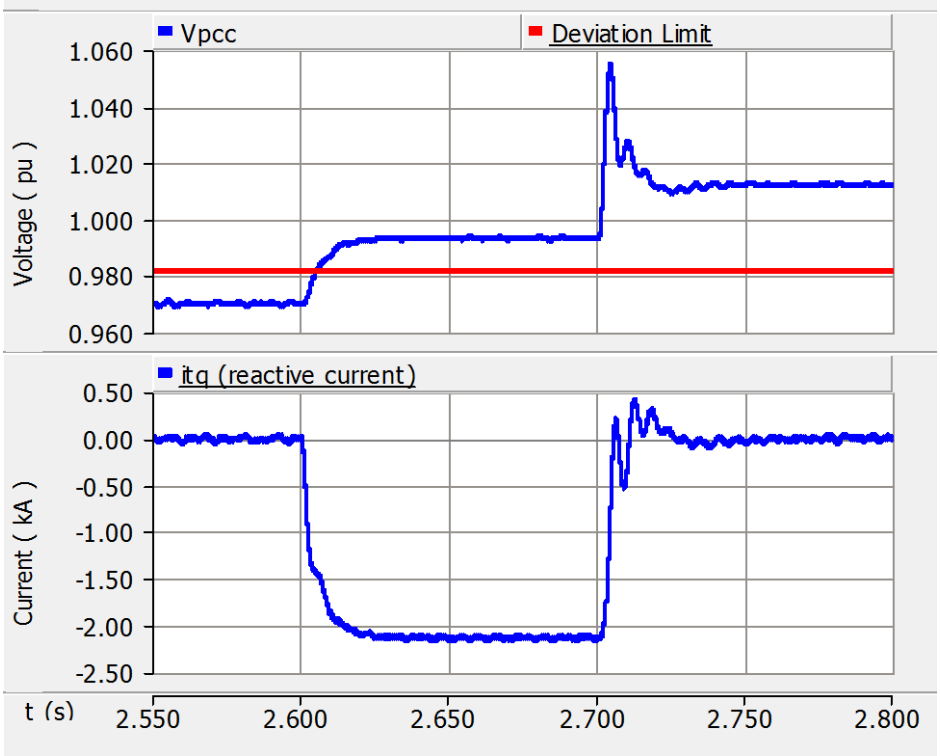

Figure 4.8 Response of PI type PCC voltage controller (K_{pvs} = 0.5, K_{ivs}= 400, $K_{droop} = 0.2$)

4.4.3 Volt/Var Control with Proportional Controller

The ability of proportional controller based volt/var control to mitigate voltage flicker is studied in this section. The proportional controller gain is initially chosen as 2 and the response of PCC voltage and q-axis current are shown in Figure 4.9. It can be seen that due to irradiance change at 2.5 seconds, the reactive current deviates from its reference value of zero to a positive value and this causes the PCC voltage to drop further to 0.966 pu (shown from time of 2.55 to 2.6 seconds) before the voltage controller is turned on at 2.6 seconds. This is because of the slow nature of q-axis current controller. After the controller is turned on at 2.6 seconds, it is unable to regulate the voltage within the allowed deviation limit of 3 %.

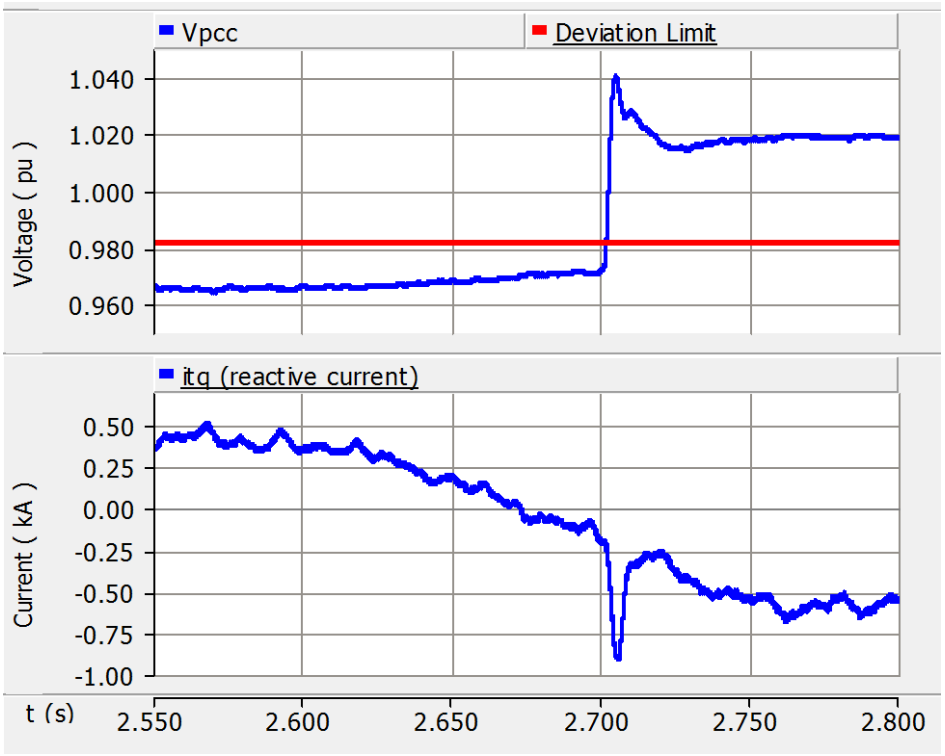

Figure 4.9 Response of proportional type Volt/Var control (for K_{pvs} = 2)

Now, the proportional gain is increased to 5 and the response is shown in Figure 4.10. In spite of increasing the proportional gain to 5, the controller is able to regulate the voltage at a maximum of 0.9785 pu but still it is not within the allowed deviation limit of 3%. The reason due to which the controller is unable to regulate the voltage within 3% for proportional gains of 2 and 5 is again due to the slow nature of q- axis current controller which has a closed loop response time of 1.52 seconds. But, there are no stability issues once the irradiance returns back to its original value.

4.4.4 Comparison between the three types of controllers

A comparative study is performed between the three kinds of control strategies utilized for mitigating the voltage flicker due to irradiance change. The considered factors are the ability to regulate voltage within limits during irradiance change and to perform without any stability issue during and post irradiance change.

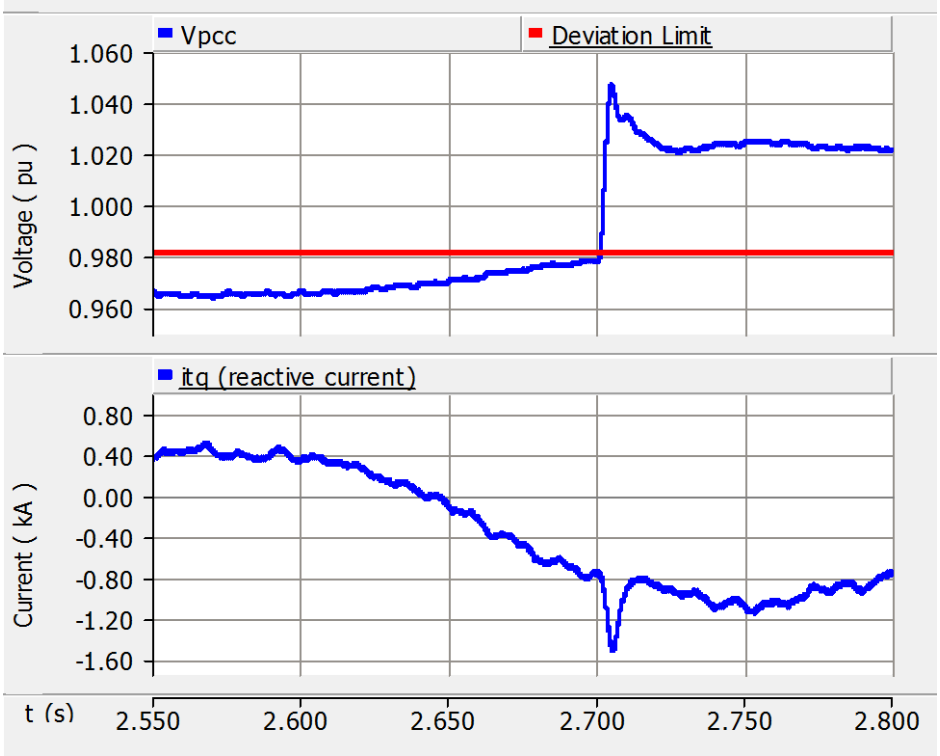

Figure 4.10 Response of proportional type Volt/Var control (for K_{pvs} = 5)

First, the comparison is made between proportional controller and PI controller based dynamic reactive current injection. Both controllers are able to regulate PCC voltage within limit during irradiance change. For a slope of 5, the proportional controller shows unstable response once the irradiance gets back to 0.85 kW/m^2 whereas the PI controller exhibits a stable response. This shows that the performance of PI controller based dynamic reactive current injection is not affected by interaction between dc-link voltage loops, PCC voltage control loops, distribution feeder current i_{12d} and measurement filters.

Second, the comparison is made between PI controller based dynamic reactive current injection and proportional controller based volt/var control. During irradiance change, the volt/var control is not able to regulate the PCC voltage within a limit of 3%. But post irradiance change, it does not exhibit any instability issue and results in a stable response. Although the slow q-axis current controller is disadvantageous when it comes to voltage flicker mitigation, it results in a stable response due to less interaction with d-axis current

controller (difference in current controller gain crossover frequency is more than 10 times) in presence of feed-forward filter constant of 0.75 ms.

All these clearly show the superiority in performance of PI controller based dynamic reactive current injection over the other two control strategies.

4.5 Flicker due to irradiance change in two PV systems

This section deals with the stability studies when there are two PV systems performing voltage control. The simplified diagram of the circuit utilized for the study with two PV systems is shown in Figure 4.11. A 9.9 MW PV system is connected at bus 3 which is 5 km away from the 8.5 MW PV system.

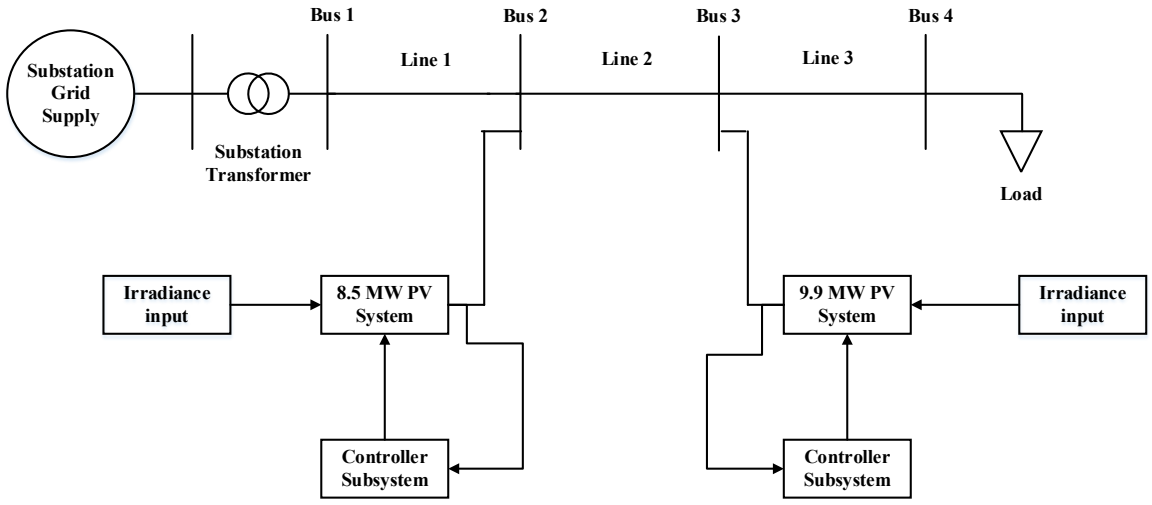

Figure 4.11 Simplified diagram of the circuit utilized for the simulation of voltage flicker due to irradiance change with two PV systems

The design of the 9.9 MW PV system is explained as follows:

(i) The photovoltaic panel array is designed using the same PV panel (LDK-230P-20) which was utilized for designing 8.5 MW PV system. The parameters N_s and N_p are chosen so as to achieve a dc-link voltage level of 1.172 kV and PV array capacity of 9.9 MW. The minimum value of dc-link capacitance is decided using (2.95). The MPPT

voltage at maximum irradiance is 1.172 kV and this is assumed to be constant for all values of irradiance. All these parameters are provided in Table C. 1 of Appendix C.

(ii) The 9.9 MW PV system is connected to the PCC using a 12 MVA, 0.48 / 27.6 kV coupling transformer with a leakage impedance of 0.1 pu (on its own base).

(iii) The bandwidth of PLL, current controllers and dc-link voltage controllers are similar to values utilized for the design of controllers of 8.5 MW PV system. Hence, the controller parameters of PLL and current controllers are the same as the ones utilized for 8.5 MW PV system controllers. The dc-link voltage controller is designed for each operating point using the model developed in section 3.2.4. The PCC voltage controller parameters will be designed in a coordinated manner (by hit and trail method) in the following sections.

(iv) The feed-forward filter time constant is chosen as 0.75 ms and the PCC voltage measurement filter constant is chosen as 2 ms to represent the worst case scenario for the control system interaction similar to 8.5 MW PV system.

(v) All other parameters are similar to those utilized for the design of 8.5 MW system.

The interaction between two PV systems occurs through power transfer between the two buses in the distribution network [42]. Both the PV systems are designed to have the same control system parameters as this represents the worst case scenario where both PV systems respond in a similar way to any system disturbance. This has been pointed out in [30] that the oscillation risk between two PV systems is less when the control system settings are different as they respond differently to any disturbance. The objective of this section is to show how two PV systems interact with each other when each PV system is already having stability issues due to interaction between its controllers. The interaction is studied by introducing irradiance change of 100 % in both the PV systems at the same time.

With reference to Figure 4.11, the PCC voltage (at bus 2) of 8.5 MW PV system is V_{pcc1} and the reactive current output of its inverter is i_{tq1}. The PCC voltage (at bus 3) of 9.9 MW PV system is V_{pcc2} and the reactive current output of its inverter is i_{tq2}.

Initially, both the PV systems are operating with an irradiance of 0.85 kW/m^2. A step change from 0.85 kW/m^2 to 0 kW/m^2 in the irradiance of both the PV systems is introduced at a time of 2.5 seconds for 200 milli seconds. The PCC voltage responses of both PV systems are shown in Figure 4.12. V_{pcc1} drops to 0.968 pu which is 6.7 % from the original value of 1.038 pu and it is outside the allowed 3% limit. V_{pcc2} drops to 0.957 pu which is 7.4 % from the original value of 1.034 pu and it is also outside the allowed 3% limit. This shows the PCC voltage control action is required.

4.5.1 Dynamic reactive current injection with PI controller

Both the PV systems are designed to perform dynamic reactive current injection using PI controller to mitigate voltage flicker at its corresponding PCC voltage. The droop factors of both PV systems (K_{droop}) are set to zero for first tuning the optimum values of PI controller gains.

Initially, the PI controller gains are chosen as K_{pvs} = 0.5 and K_{ivs}= 400 for both the PV systems (similar to the gains used for a single PV system). But, it is found that this results in an unstable PCC voltage response when either of the PV system performs voltage control individually with zero reactive current supplied by the other. The PI gains of both the PV systems were changed simultaneously and it is found stable PCC voltage responses can be obtained for gains of K_{pvs} = 0 and K_{ivs}= 200 when both perform voltage control simultaneously. These are chosen as the optimum gains for both PV systems.

Then, the slopes of dynamic reactive current injection characteristic (inverse of K_{droop}) of both PV systems are increased simultaneously from a value of 0.5 in order to keep both the PCC voltages within 3%. The reason to increase them simultaneously is that the

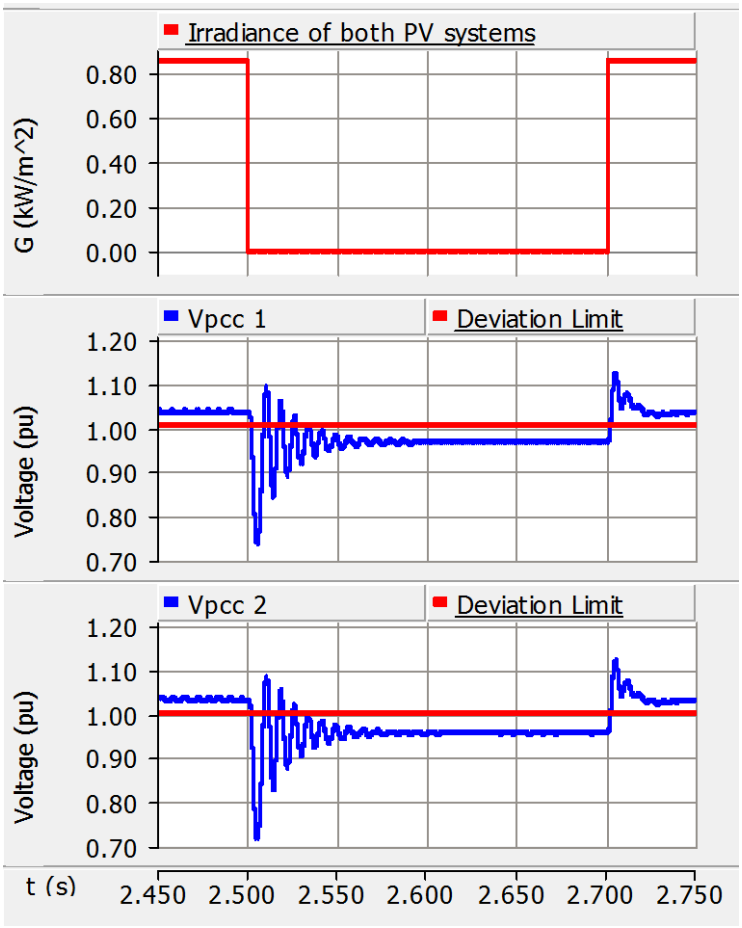

Figure 4.12 Voltage change at PCC of both PV systems due to irradiance change from 0.85 kW/m^2 to 0 kW/m^2

reactive current supplied by either PV system affects both the PCC voltages. It is found that a slope of 3 for 8.5 MW PV system and a slope of 3.5 for 9.9 MW system is sufficient to keep both PCC voltages within 3%. To study the voltage control action, the voltage controllers are turned on at 2.6 seconds (simulation time) and the response of both PCC voltages during the duration of irradiance change are shown in Figure 4.13. It can be seen that the V_{pcc1} is regulated at 1.012 pu and V_{pcc2} 1.004 pu which are within the 3% limit. The capacitive reactive currents supplied are i_{tq1} of 1.73 kA and i_{tq2} of 2.29 kA.

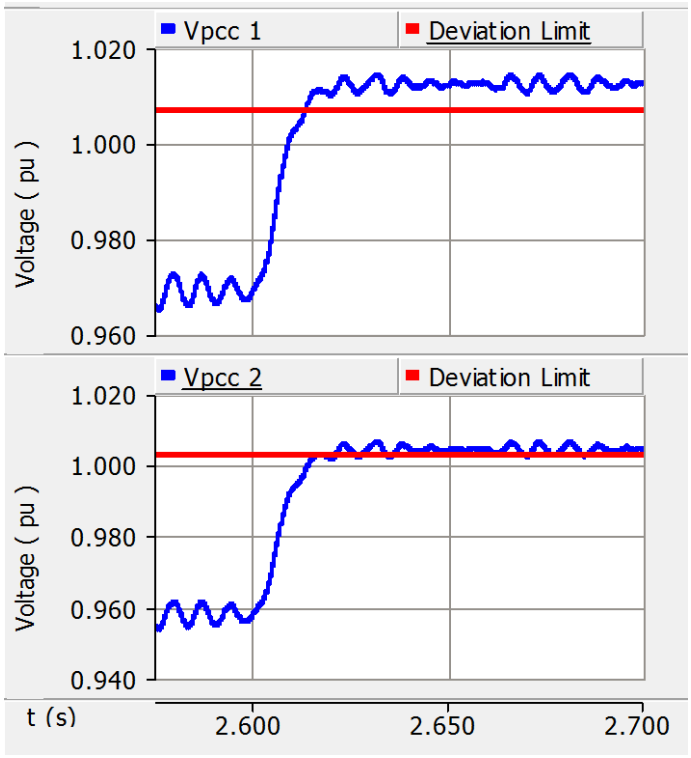

Figure 4.13 Response of PI type dynamic reactive current injection of both PV systems (for mitigating flicker due to irradiance change)

The response of PCC voltages after the irradiance returns to back to original value is shown in Figure 4.14. It can be seen that the voltages return back to their original values without any stability issues. The initial overvoltage which is more than 1.1 pu is due to rapid rise of active power supplied by the PV systems but it is still within the temporary overvoltage limit of 1.3 pu [9].

4.5.2 Dynamic reactive current injection with proportional controller

Now, the ability of both PV systems to mitigate voltage flicker using dynamic reactive current injection based proportional controller is studied. The same slopes of 3 for 8.5 MW PV system and a slope of 3.5 for 9.9 MW system utilized for PI controller implementation are chosen as respective proportional controller gains for direct comparison of responses.

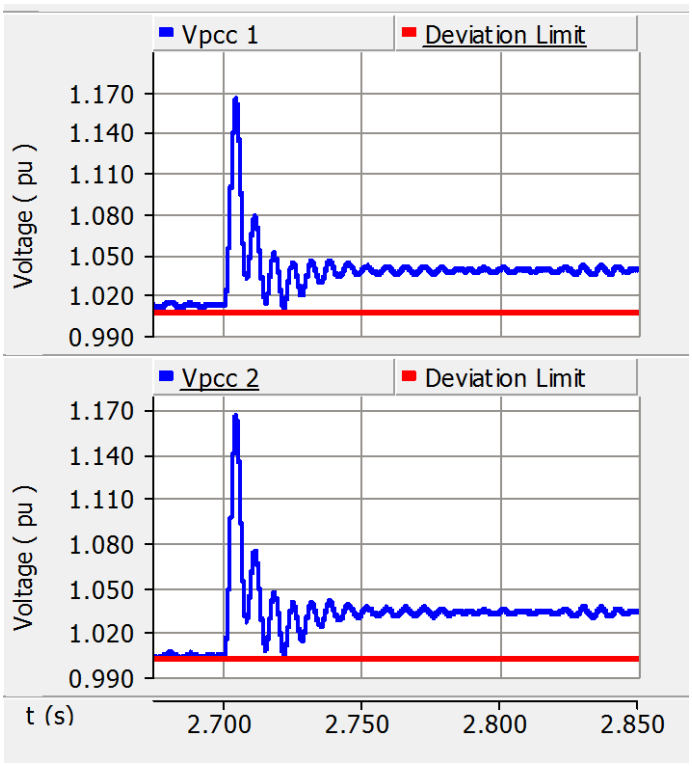

Figure 4.14 Response of PI type dynamic reactive current injection of both PV systems (post irradiance change)

The PCC voltage responses after the turn-on of voltage controllers at 2.6 seconds and during the duration of irradiance change are shown in Figure 4.15. It can be seen that the responses become oscillatory due to which modulation index saturates and hence, a pattern of non-sinusoidal oscillations result. This continues into the period when the irradiance returns back to the original value after 2.7 seconds as shown in Figure 4.16.

4.5.3 Volt/Var Control with proportional controller

Now, the ability of both PV systems to mitigate voltage flicker using volt/var control based proportional controller is studied. The proportional controller gains are chosen as 3 and 3.5 similar to proportional controller based dynamic reactive current injection. The q-axis current controllers of both the PV systems are designed to operate with a closed loop settling time of 1.52 seconds (for 2% error margin).

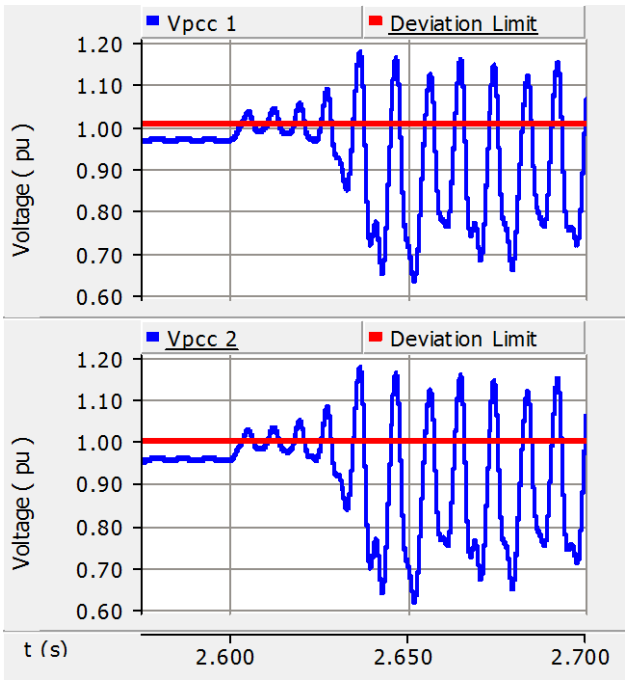

Figure 4.15 Response of proportional type dynamic reactive current injection of both PV systems (for mitigating flicker due to irradiance change)

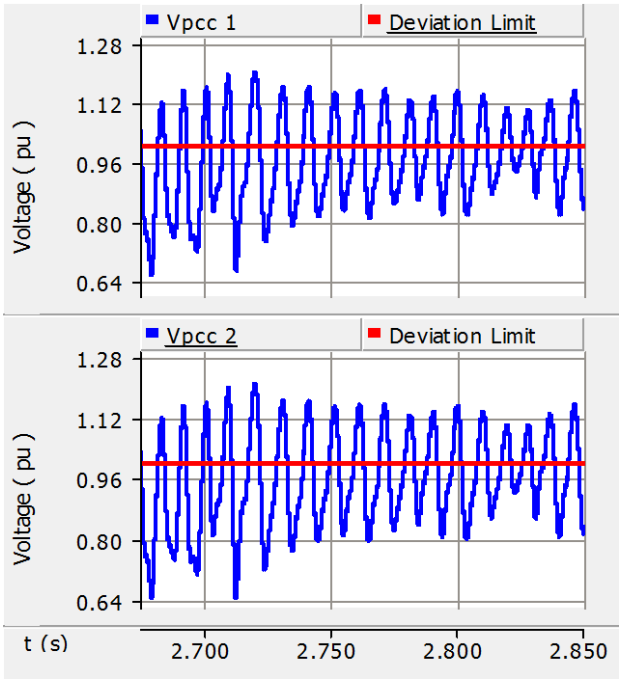

Figure 4.16 Response of proportional type dynamic reactive current injection of both PV systems (post irradiance change)

Figure 4.17 shows the responses of q-axis (reactive) currents of both the PV systems after the irradiance change. It can be seen that the irradiance change causes the current controller of both the PV systems to deviate from its reference value of zero and it is unable to regulate them back to zero (due to being slow by design). The response of PCC voltages during irradiance change are shown in Figure 4.18. The PCC voltage V_{pcc1} drops further to around 0.96 pu and V_{pcc2} drops further to around 0.949 pu before the PCC voltage controllers are turned on at 2.6 seconds.

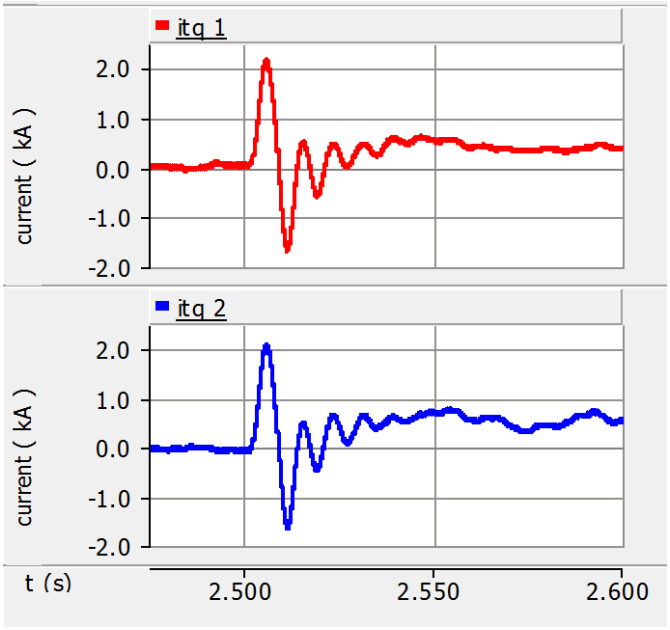

Figure 4.17 Reactive current deviations from reference due to irradiance change

Once the controllers are turned on at 2.6 seconds, it can be seen that the volt/var based proportional controllers are not able to regulate the voltage within the 3% limit due to the slowness of q-axis current controllers. But, there is no stability issue once the irradiance returns back to original value after 2.7 seconds as shown in Figure 4.19. Similar to the case of dynamic reactive current injection with PI controller, there is an initial overvoltage above 1.1 pu which is due to rapid rise of active power from PV systems. This is within the temporary overvoltage limit of 1.3 pu.

4.5.4 Comparison between the three types of controllers

A comparative study is performed between the three kinds of control strategies utilized for mitigating the voltage flicker with two PV systems due to irradiance change. The considered factors are the ability to regulate voltage within limits during irradiance change and to perform without any stability issue during and post irradiance change.

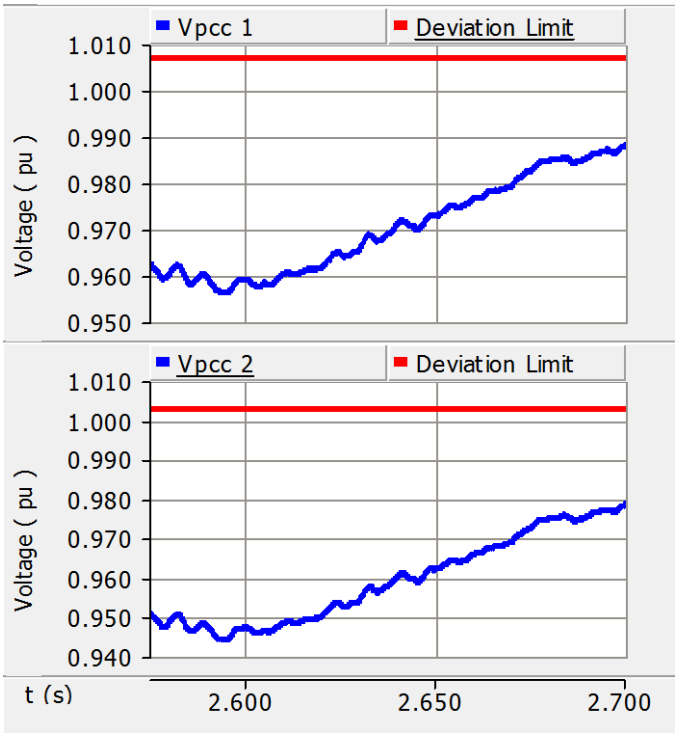

Figure 4.18 Response of proportional type Volt/Var controller of both PV systems (for mitigating flicker due to irradiance change)

First, the comparison is made between proportional controller and PI controller based dynamic reactive current injection. The proportional controller based implementation becomes unstable for gains as low as 0.5 when both the PV systems perform voltage control simultaneously. The reason for the instability is understood to be interaction between the controllers of two PV systems (which is influenced by feed-forward filter time constants of each PV system) as they respond similarly to the change in their respective PCC voltages. As pointed out in section 4.5.1, the same issue exists in the case of PI controllers but the integral controller gains were fine-tuned simultaneously to obtain a stable response. In the case of proportional controllers, a stable response can be

obtained by decreasing the speed of operation of q-axis current controllers (in the presence of feed-forward filter time constants at 0.75 ms) of one or both PV systems. This shows that PI controller based dynamic reactive current injection can result in an effective and stable PCC voltage control response even in the presence of interaction between the PV systems without compromising on the bandwidth of q-axis current controllers.

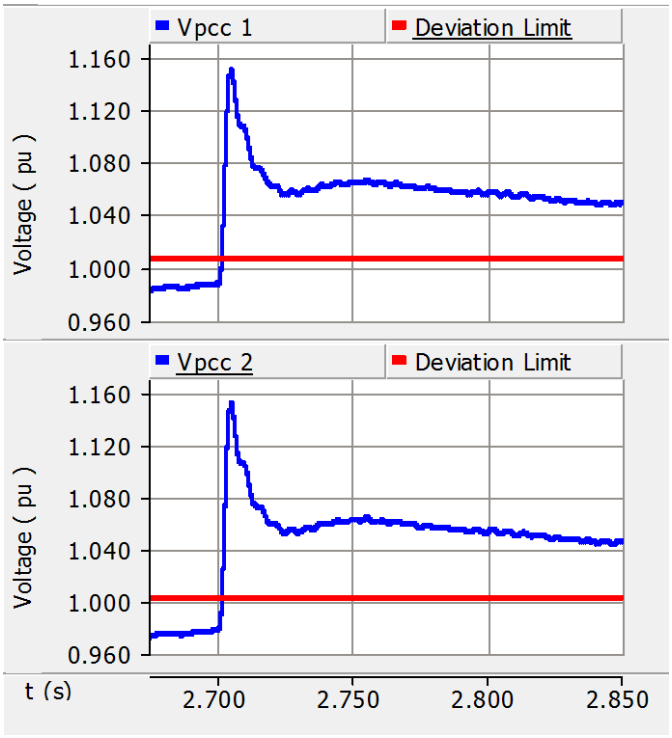

Figure 4.19 Response of proportional type Volt/Var controller of both PV systems (post irradiance change)

Second, the comparison is made between PI controller based dynamic reactive current injection and proportional controller based volt/var control. The volt/var control is a slow control and hence, it is not able to regulate the PCC voltage within the limits of 3% during irradiance change. But, it does not exhibit any instability issue during and after irradiance change, resulting in a stable response. The reason is that the bandwidth of q-axis current controllers are very small when compared with that of d-axis current controllers bandwidth (difference in current controller gain crossover frequency is more than 10 times) in presence of feed-forward filters. This proves that the volt/var based

control strategy is not suitable for applications that require relatively faster reactive current injection.

All these clearly show the superiority in performance of PI controller based dynamic reactive current injection over the other two control strategies.

4.6 Conclusion

This chapter deals with application of partial PV-STATCOM for performing voltage control to mitigate flicker in PCC voltage introduced by 100% change in irradiance. The PV system is made to perform PCC voltage control with feed-forward voltage filter time constants at 0.75 ms so that the interaction between dc-link voltage control loop and PCC-voltage control loop is at a maximum. Under this condition, the stability of proportional and PI controller based dynamic reactive current injections, and Volt/Var controls are compared.

Studies are first performed with single PV system. For higher values of slopes of dynamic reactive current injection characteristic, the PI controller exhibits a stable response when the irradiance returns back to its nominal value whereas the proportional controller exhibits instability. Also, the proportional controller based volt/var control is found to be a slow control and is not effective is regulating the voltage within 3% during irradiance change.

Studies are also performed with two similar PV systems performing simultaneous voltage control to mitigate voltage flicker at their respective PCCs. The PI controller based dynamic reactive current injection can ensure a stable simultaneous voltage control by both PV systems without compromising on the bandwidth of q-axis current controllers, which is not possible with proportional controller. Also, the volt/var control by both PV systems is not effective in regulating their respective PCC voltages within the allowed limits of 3%.

Thus, it can be concluded that PI controller based dynamic reactive current injection strategy ensures a stable response even in the presence of interactions between dc-link voltage and PCC voltage control loops of single PV system or between two PV systems.

Chapter 5

5 VOLTAGE CONTROL DURING LARGE SYSTEM DISTURBANCES

5.1 Introduction

This chapter deals with the application of partial PV-STATCOM and full STATCOM to perform voltage control during large system disturbances. A three phase fault at the load end is used to simulate a large disturbance for the system. The ability of PV system to ride-through and provide stable voltage support during the fault, and to continue providing stable voltage support post fault are studied.

The PV system (or PV systems) is made to perform PCC voltage control with feed-forward voltage filter time constants at 0.75 ms so that the interaction between dc-link voltage control loop and PCC-voltage control loop is at a maximum. Under such circumstances, the performance of three types of voltage control strategies namely proportional controller based dynamic reactive current injection, PI controller based dynamic reactive current injection and PV system operating in Full STATCOM mode are compared.

The studies are initially performed with a single PV system. They are later extended to the case where there are two similar PV systems performing simultaneous voltage support during and post faults. Finally, the effect of X/R ratio on the effectiveness of PCC voltage control is compared when two PV systems inject only reactive power and, a combination of active and reactive powers during voltage support.

5.2 Application of dynamic reactive current injection for voltage support during LVRT operation

It is mentioned in Chapter 1 that dynamic reactive current injection is one of the methods available to provide voltage support during Low Voltage Ride Through operation. The effectiveness of reactive current injection on voltage depends of X/R ratio of the distribution network. For lower X/R ratio, voltage is more sensitive to active power than reactive power [68].

For dynamic reactive current injection, the proportional controller implementation is shown in Figure 4.1 and it can be represented using the equation,

$$i_{tqref} = -K_{pvs}(V_{pccref} - V_{pcc}) \tag{5.1}$$

As shown in chapter 4, this can also be implemented using a PI controller implementation as shown in Figure 4.2 and it can be represented using the equations,

$$i_{tqref} = -K_{pvs}V_{pccref} + K_{pvs}V_{pcc} - K_{pvs}K_{droop}i_{tq} - K_{ivs}x_7 \tag{5.2}$$

$$\frac{dx_7}{dt} = V_{pccref} - V_{pcc} - K_{droop}i_{tq} \tag{5.3}$$

These equations were already introduced in chapter 2. The only difference is that the droop in voltage is achieved by using reactive current i_{tq} instead of reactive power Q_{VSC} as explained in chapter 4. Similar to chapter 4, it will be shown in this chapter that PI controller based implementation gives a stable performance in presence of feed-forward filter time constants when compared to proportional controller based implementation.

5.3 Control of Active power during and post fault

In single-stage three phase photovoltaic power systems, the active power is controlled by regulating of voltage of the dc-link capacitor during normal operation in order to extract the maximum power from the PV array. This means that only the free capacity of inverter available after real power injection (or real current) can be used for reactive power (or reactive current) injection. This mode of operation is referred to as P-priority [12]. Here, the maximum active current is limited by the rating of the inverter and the maximum reactive current limits are calculated based on the active current injection by inverter.

When the PV system is performing reactive current injection during a ride-through operation caused by a voltage drop due to a fault, it has to inject an appropriate reactive current for the particular voltage drop. Post fault, the reactive current injection has to be continued for a certain period of time depending on the grid code (500 ms as per German grid code) to be followed. This is possible only when sufficient reactive current capacity is available. Hence, the PV inverter has to operate in a mode termed as “Q-priority” [12].

Here, the maximum reactive current is limited by the rating of the inverter and the maximum active current limits are calculated based on the reactive current injection by inverter.

When operating in Q-priority, the active power injected has to be curtailed in order to make room for reactive current injection. During a fault, the voltage of dc-link capacitor V_{dc} will increase momentarily due to sudden drop in active power P_{VSC} supplied by the PV system (due to drop in ac voltage V_{pcc} (and V_c)) for the same power output by PV array P_{pv}. Due to the same, the power output from the PV array will automatically decrease. If the inverter operates in Q-priority, the active current cannot be controlled effectively to regulate the dc-link voltage and hence, the dc-link voltage will continue to stay at a value which is higher than the maximum power point voltage of PV array.

Post fault, the active power supplied by PV system will increase due to increase in voltage V_c and settle at a new value depending on the active current injected during fault. The active power should be ramped up towards the nominal value very slowly which depends on the grid code followed (As per German grid code, the ramp-up rate should be at least 20 % of rated power per second). The dc-link voltage will automatically start decreasing towards the maximum power point voltage immediately after fault and hence, this will lead to rapid increase in power output of PV system which is not permitted. In [69], it has been mentioned that the dc-link voltage reference can be regulated at a higher value to limit the power from PV array during fault. A relation has been established between the ac voltage and the operating voltage of PV array to decide the new value of dc-link voltage reference in [69]. This concept of controlling the dc-link voltage reference has been adopted in this thesis.

The dc-link voltage reference is increased by the same amount as the actual dc-link voltage and maintained constant (using a sample and hold circuit) at the new value after a certain period of time after the fault is detected. The new dc-link voltage reference (V_{dcrefn}) is given by,

$$V_{dcrefn} = (V_{dcref} + (V_d - V_{dcref})) \tag{5.4}$$

This is achieved by measuring the actual dc-link voltage. The reference value is held constant at the new higher value after a period of 25 ms once the fault is detected. This time is chosen based on the assumption that the duration of fault is at least 2 cycles of power system frequency (60 Hz). A value of 25 ms (which is within 2 cycles of 60 Hz) is chosen based on the following requirements:

i) Sufficient time is available for dc-link voltage to increase due to fault, settle at a new higher value and remain fairly constant. The value of dc-link voltage at this instant can be considered to be the new value of dc-link voltage reference.
ii) Once the dc-link voltage reaches the new higher value, the new dc-link voltage reference has to be maintained constant. This is to ensure that the reference does not change further (decrease after the fault is cleared) in order to ensure a constant supply of power from PV array and prevent rapid ramp-up of power.

In practice, there are some delays involved in the detection of fault by the controller circuit of PV inverter but these are not considered in this thesis. This, along with other factors such as delays due to measurement of dc-link voltage etc., might affect the dynamics of dc-link voltage during a fault and the performance of the above control strategy. All these will eventually affect the output of dc-link voltage controller which is active current reference i_{tdref} but no stability issues can occur. This is due to the operation of inverter in Q-priority during a fault in which the active current reference is limited by the injected reactive current.

By changing the dc-link voltage reference to a new higher value, the following objectives are achieved:

i) During fault, the dc-link voltage error is close to zero and the change in active current reference is very small. This ensures that the active current reference remains fairly constant at the value before fault and it is affected only by its saturation limits which are dependent on injected reactive current. The active

power injected by PV system will change depending on the ac voltage level due to fault.

ii) Post fault, the active power supplied by PV system will increase depending on the ac voltage level for a particular value of active current. The active power from PV array can be maintained fairly close to the value that existed during fault. It can then be ramped-up slowly towards the nominal value by ramping down the dc-link voltage reference towards the maximum power point voltage. Also, a stable operating point can be obtained immediately after the fault for the entire system so that the reactive current support can be continued for a certain period of time (as per grid code).

This method of controlling the active power during and post fault by increasing the dc-link voltage reference by the same amount as actual dc-link voltage is also one of the contributions of this thesis. This particular type of control is not available in the literature to the best knowledge of author.

5.4 Objective of simulation studies

The purpose of simulation studies is to evaluate and compare the performance of voltage support provided by PV system during ride-through operation for the following types of control strategies:

i) Voltage support provided by proportional controller based dynamic reactive current injection

ii) Voltage support provided by PI controller based dynamic reactive current injection

iii) Voltage support provided by Full STATCOM where the PV system curtails its active power and supplies full reactive power

These studies will be performed with single PV system and two PV systems. In each of the above three cases, the objective is to study the interaction between dc-link voltage control loop and PCC voltage control loop in the presence of feed-forward filter time constants during and post faults. For this purpose, the feed-forward filter time constants

are fixed at 0.75 ms and PCC voltage measurement filter constant is fixed at 2 ms for all studies in this chapter which represent the worst case scenario for the interaction.

5.5 Voltage support using single PV system

The simplified version of the circuit utilized for fault simulation studies is shown in Figure 5.1. The 8.5 MW PV system is connected at bus 2. A three phase to ground resistive fault is introduced at the load end (bus 4). Three phase fault is used since the PV system controllers are designed to operate only on balanced distribution network. The load resistance is chosen as 25 Ω to ensure that the voltage levels on distribution feeder stays in the range from 0.6 to 0.8 pu without any reactive current support. As per German grid code reactive current injection requirements, voltages in this range will require injection of significant reactive power and active power (remaining capacity). This will be helpful for performing the following categories of studies:

i) Interaction between dc-link voltage control loop and PCC voltage control loop during and post fault
ii) Impact of X/R ratio of distribution feeder on the effectiveness of voltage support provided by using reactive power and active power.

Also, faults with equivalent resistances in the range of 8 to 16 Ohms [70] and 90 to 200 Ohms [71] have been reported in MV distribution systems which justifies the usage of a value of 25 Ohm.

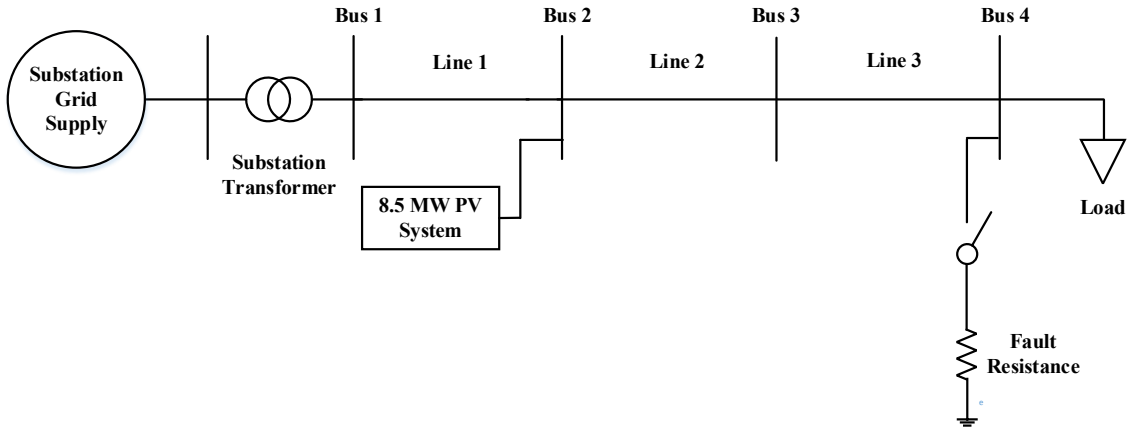

Figure 5.1 Simplified diagram of the circuit utilized for the simulation of fault

The PV array of the 8.5 MW PV system is designed using the parameters of the PV panel FS 272 [72], [73]. The PV array parameters, the maximum power point dc-link voltage and dc-link capacitance are provided in Table D. 1 of Appendix D. First, the ability of the PV system to ride-through (supplying only active power and zero reactive power) during a fault and continue supplying active power post fault is studied. The dc-link voltage controller parameters used are those designed for the operation of PV system in Full STATCOM mode since this can be considered as the worst-case operating point. If the controller is stable in the worst-case operating point (zero active power injection), it remains stable at all other operating points when active power varies from zero to maximum value [18].

The PV system is operating with maximum irradiance of 1 kW/m^2 and supplying maximum power. The fault is introduced at a time of 0.5 seconds for a period of 100 ms (6 cycles of 60 Hz). The responses of dc-link voltage, PV current and active current are shown in Figure 5.2. Before fault, the dc-link voltage is maintained at a value of 1.0656 kV (MPP voltage) with a PV current I_{pv} of 7.98 kA and active current i_{td} of 13.42 kA. Due to fault, the dc-link voltage rises to 1.262 kV and the dc-link voltage reference is also increased to same value. This ensures that I_{pv} reduces to 5.13 kA and i_{td} remains constant at 13.42 kA. Post fault, the dc-link voltage is continued to be regulated at 1.262 kV which ensures that I_{pv} remains close to 5.13 kA. The current i_{td} decreases to 10.42 kA due to increase in PCC voltage.

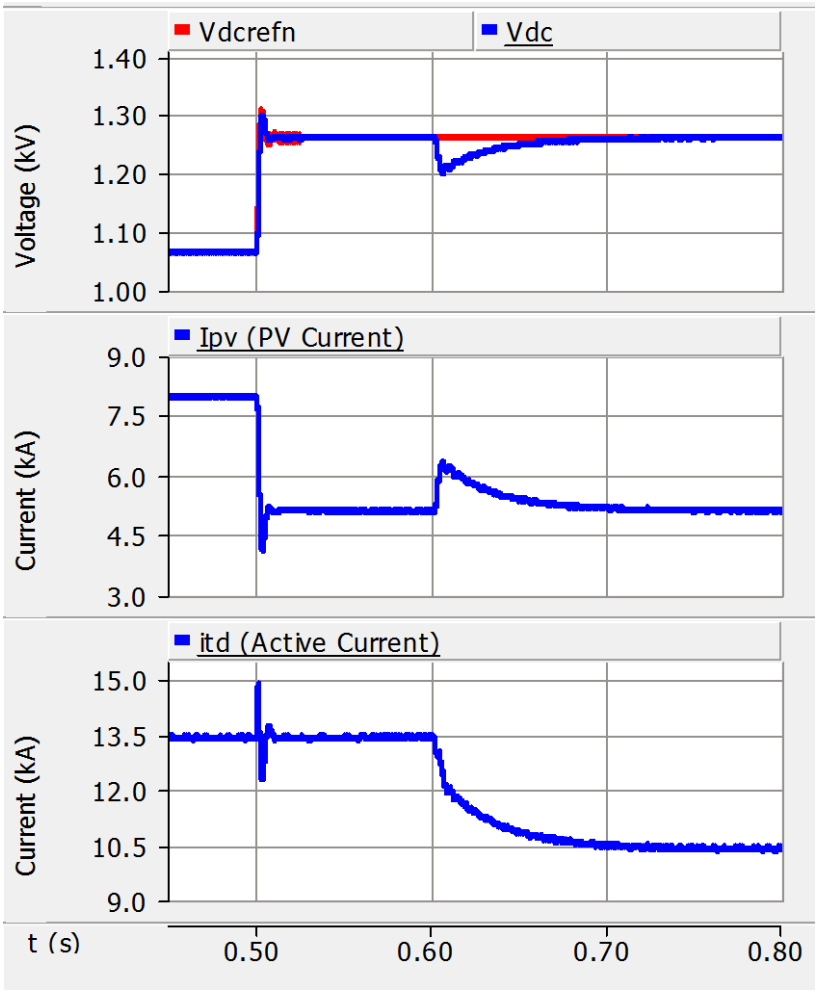

Figure 5.2 Response of dc voltage, PV and active currents during and post fault

The response of active power, reactive power and PCC voltage are shown in Figure 5.3. It can be seen that the PCC voltage falls from 1.015 pu to 0.76 pu during fault and returns back to 1.01 pu post fault. The active power reduces from 7.98 MW to 5.98 MW during fault and increases close to 6.18 MW post fault. The reactive power remains zero throughout the simulation. This clearly shows that the PV system performs ride-through operation during fault and continues to supply almost the same active power post fault. The benefit of increasing the dc-link voltage reference is clearly visible as the active power does not exhibit any rapid increase post fault. The active power can then be ramped-up slowly by controlling the dc-link voltage reference.

As pointed out earlier, the other advantage of utilizing this control strategy is that a stable operating point can be obtained immediately after the fault for the entire system which may not be possible by switching to active current control during and after fault.

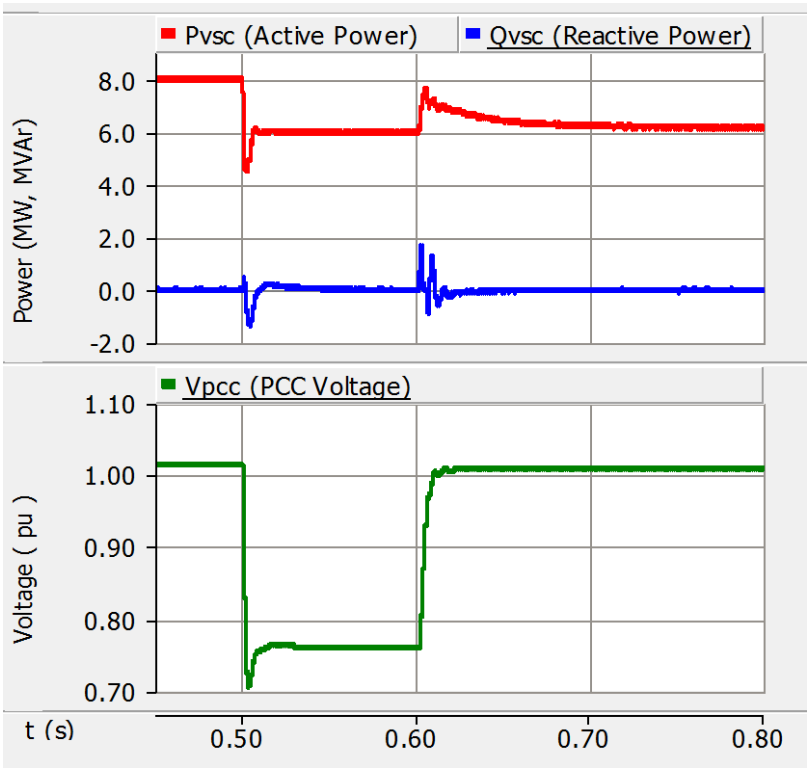

Figure 5.3 Response of active and reactive powers, and PCC voltage during and post fault

5.5.1 Voltage support using proportional controller based dynamic reactive current injection

First, the voltage support provided by proportional controller based dynamic reactive current injection is studied. As per the German grid code, a minimum of 2% reactive current injection per percent voltage drop below 0.9 pu is required. The proportional gain is calculated as per this requirement and it is found to be 1.282 (for 2% reactive current injection per percent of voltage drop). The calculation of this value is provided in Appendix D. The response of PCC voltage (V_{pcc}) , inverter reactive current (i_{tq}), the active power supplied by inverter (P_{VSC}) and reactive power supplied by inverter (Q_{VSC}) are shown in Figure 5.4.

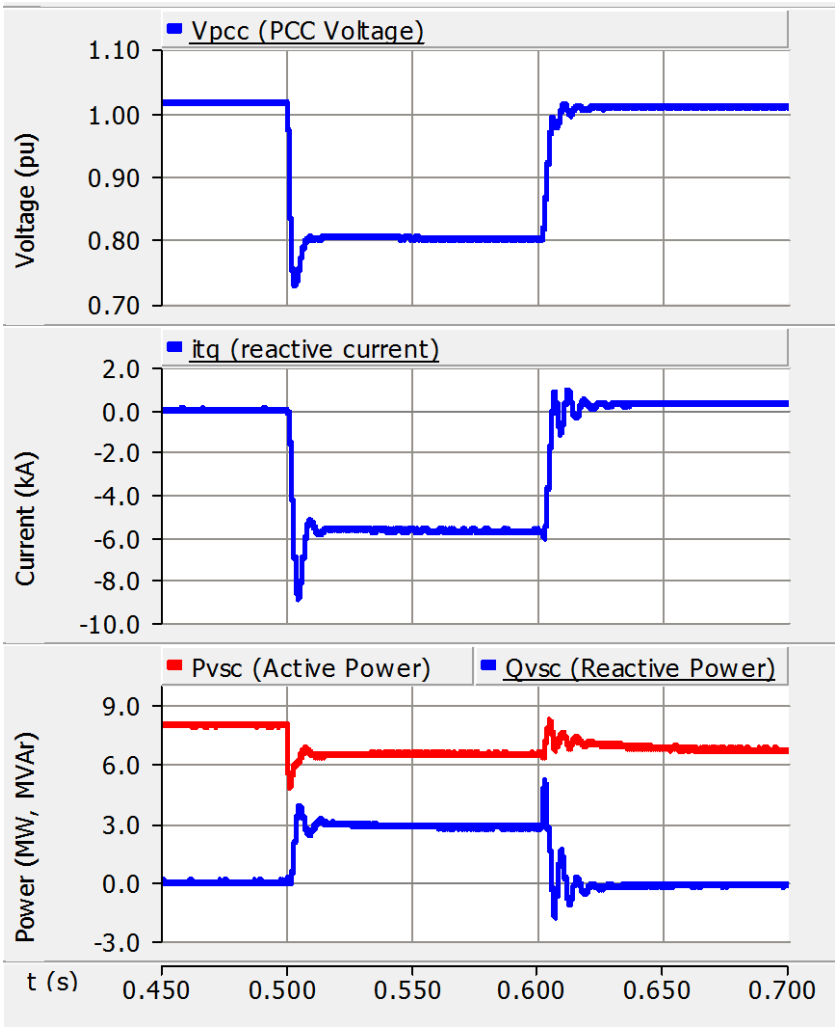

Figure 5.4 Response of proportional controller (for 2% reactive current injection)

The PCC voltage controller is turned on at 0.5 seconds at which the fault is also applied. It can be seen that the V_{pcc} is regulated at 0.80 pu during fault by supplying a capacitive reactive current of 5.7 kA. The active power drops to 6.47 MW and the reactive power supplied is 2.82 MVAr. The voltage support has been provided within 20 ms from the application of fault which is one of the requirements of German grid code. Post fault (after 0.6 seconds), V_{pcc} increases to 1.008 pu and the reactive current injection is continued (as per the German grid code) to provide an inductive reactive current of 0.26 kA. The active power increases to around 6.68 MW and the reactive power absorbed is close to 0.15 MVAr. The response of dc-link voltage and active current are conceptually

similar to the responses exhibited during ride-through operation with zero reactive power injection.

Now, the proportional gain is increased to 2.565 in order to inject 4% of reactive current per percent of voltage drop below 0.9 pu. The response of PCC voltage, inverter reactive current, the active power and reactive power supplied by inverter are shown in Figure 5.5. Due to the increase in the reactive current injection from 2% to 4%, the PCC voltage is now regulated at 0.82 pu and the capacitive reactive current injected is at 10.36 kA. The reactive power injection increases to 5.36 MVAr and the active power injection drops to 5.19 MW during fault. This shows that the PCC voltage can be regulated at higher values by increasing the reactive current injection per percent voltage drop.

5.5.2 Voltage support using PI controller based dynamic reactive current injection

Second, the voltage support provided by PI controller based dynamic reactive current injection is studied. The PI controller gains are chosen as $K_{pvs} = 0.5$ and $K_{ivs} = 400$ based on sensitivity studies carried out in chapter 3 both for operation of PV system in partial PV-STATCOM and Full STATCOM modes of operation. The droop K_{droop} is set at 0.78 to represent a reactive current injection of 2% per percent of voltage drop. As pointed out in chapter 4, K_{droop} is the inverse of corresponding proportional gain of PV system for the case studied. The fault is applied at 0.5 seconds for 100 ms and the PCC voltage controller is turned on at 0.5 seconds. The response of PCC voltage, inverter reactive current, the active power and reactive power supplied by inverter are shown in Figure 5.6.

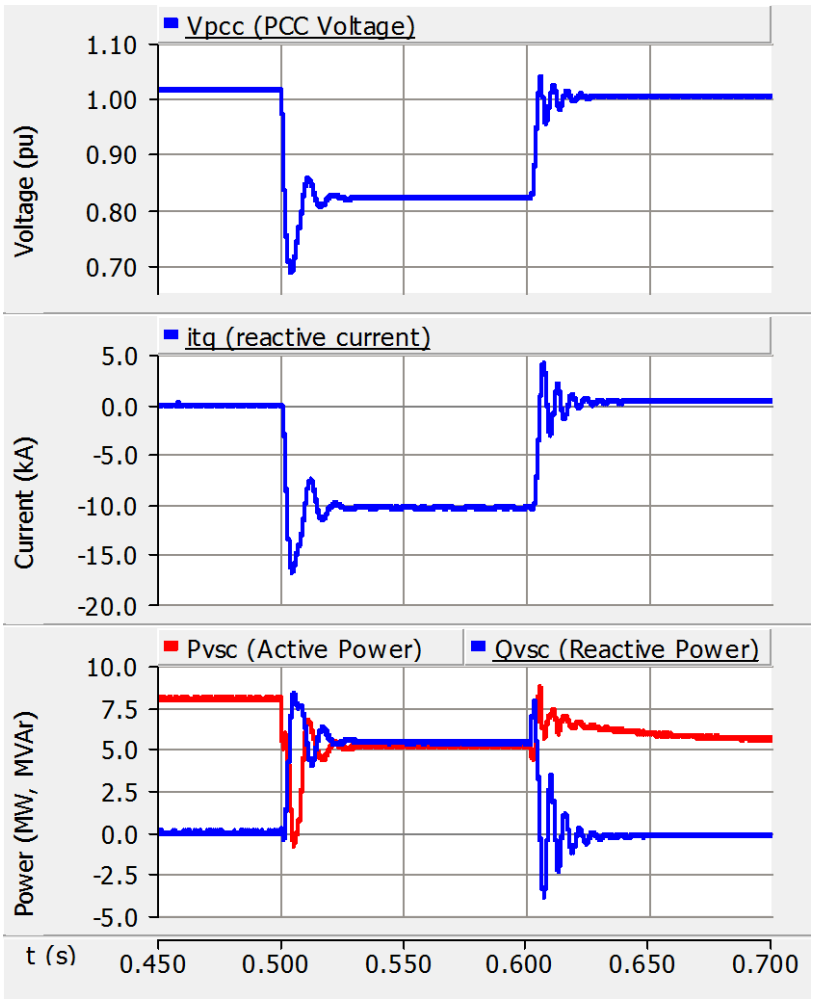

Figure 5.5 Response of proportional controller (for 4% reactive current injection)

During fault, the PCC voltage is regulated at 0.80 pu by supplying a capacitive reactive current of close to 5.69 kA. The active and reactive powers supplied during fault are 6.48 MW and 2.78 MVAr. The voltage support is also provided within 20 ms from the application of fault. Post fault, the PCC voltage increases to 1.008 pu and the reactive current injection is continued to provide an inductive reactive current of 0.258 kA. The active power supplied rises close to 6.67 MW and the reactive power absorbed is close to 0.15 MVAr. This clearly shows that the steady state responses of PI controller based dynamic reactive current injection is very close to that of the proportional controller during and post fault.

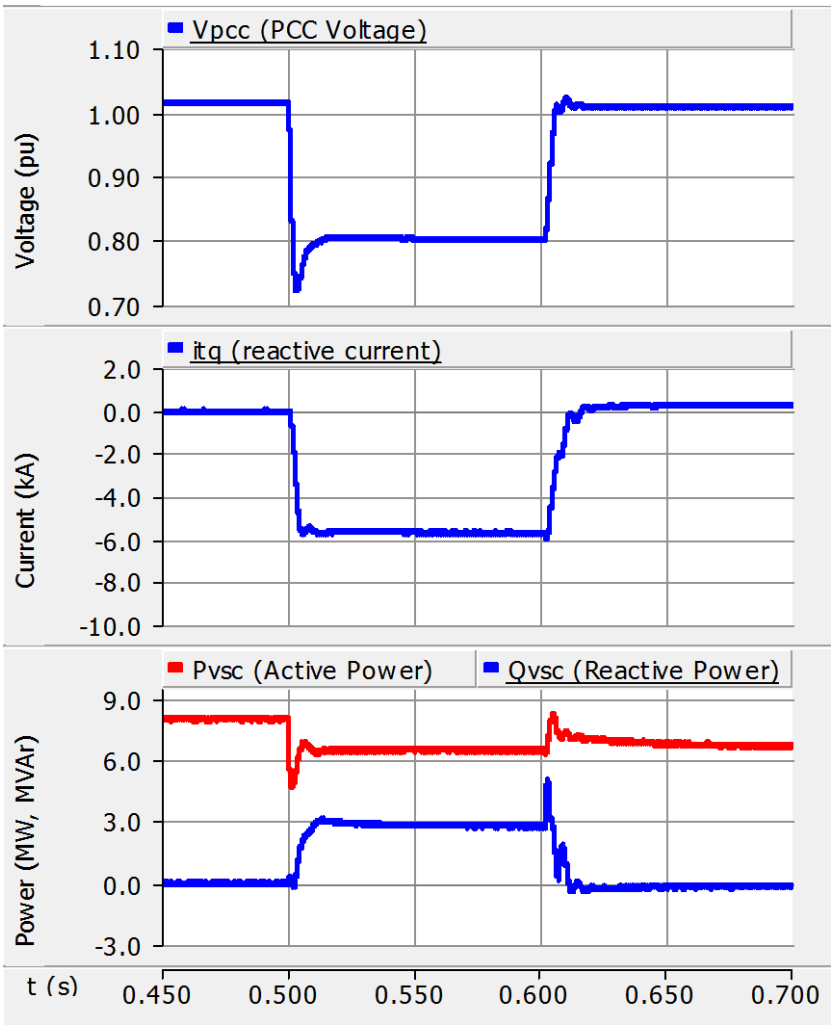

Figure 5.6 Response of PI controller (for 2% reactive current injection)

Now, the droop K_{droop} is set at 0.389 to represent a reactive current injection of 4% per percent of voltage drop. The response of PCC voltage, inverter reactive current, the active power and reactive power supplied by inverter are shown in Figure 5.7. It can be seen that the PCC voltage is now regulated at 0.82 pu by supplying a capacitive reactive current of 10.39 kA. The reactive power increases to 5.39 MVAr and the active power drops close to 5.19 MW during fault. This, once again, shows that the steady state response of PI controller matches with that of proportional controller for 4% reactive current injection per percent voltage drop.

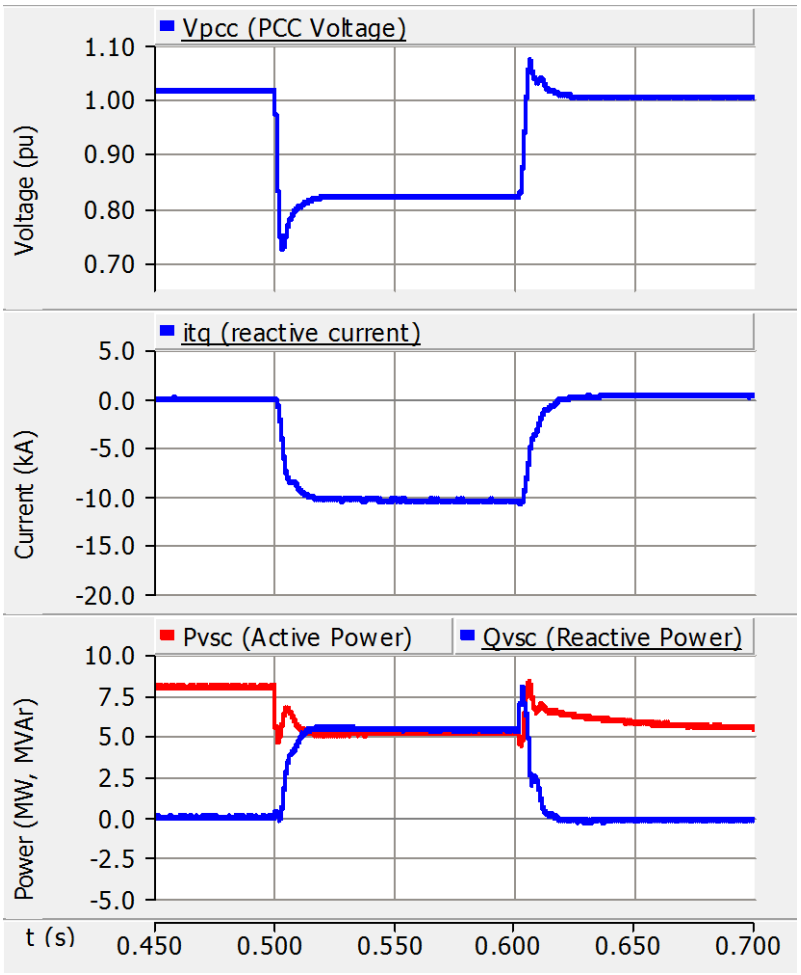

Figure 5.7 Response of PI controller (for 4% reactive current injection)

5.5.3 Voltage support using Full STATCOM

Third, the voltage support achieved using Full STATCOM operation of PV system is studied. For operation in Full STATCOM mode, the 8.5 MW PV system has to curtail all its real power in order to supply complete reactive power. In order to curtail its real power completely, the dc-link voltage is regulated at the open circuit voltage of the 8.5 MW PV array so that the power from PV array goes towards zero. To ensure that the dc-link voltage is properly regulated at the open circuit voltage, the PV system has to operate in P-priority instead of Q-priority during and post fault. This ensures that the real power is curtailed completely without any stability issue and the entire capacity is available for reactive power support during fault.

It is found that the dc-link voltage controller exhibits relatively slower response in regulating the dc-link voltage at the open circuit voltage. It takes around 135 ms for the voltage to reach within 1% of steady state value of 1.4192 kV from maximum power point voltage of 1.0656 kV. In chapter 3, it was pointed out that the dc-link voltage controller is designed to operate with a bandwidth of 460 rad/sec (settling time of 14.1 ms for 10 % step) for STATCOM (without considering the dynamics of PV array). Due to the presence of nonlinearities exhibited by PV array, the controller exhibits a slower response. The controller design can be changed to obtain a faster response. But, the design is not changed as the objective is to make a direct comparison with the responses obtained for voltage support using proportional and PI controller based dynamic reactive current injection. In order to study the effect of only reactive power injection (with close to zero active power injection) on the PCC voltage, the duration of fault is increased from 100 ms to 200 ms. This is done to provide extra time for the dc-link voltage controller to regulate the voltage at open circuit voltage so that active power from PV array is close to zero. It is understood that a 200 ms fault may not occur practically but it is introduced for the sake of comparative studies.

For the PCC voltage controller, the PI controller gains are chosen as $K_{pvs} = 0.5$ and $K_{ivs} = 400$ based on studies in chapter 3. The droop K_{droop} is usually chosen in the range of 1 % to 10 % [33]. A droop of 1 % means that 100% reactive current injection is required for 1% percent drop in voltage below 1 pu. The droop K_{droop} is initially chosen as 2 % for which the value is calculated using the relation provided in appendix D and it is found to be 0.0312. The fault is introduced at 0.5 seconds for a duration of 200 ms. The application of step of 0.3536 kV to regulate the dc-link voltage at open circuit voltage and the turn-on of PCC voltage controller are performed at 0.5 seconds. The response of PCC voltage, reactive current, active and reactive power supplied by inverter are shown in Figure 5.8. The PCC voltage is regulated close to 0.78 pu by supplying full capacitive reactive current of 14.41 kA at a time of about 0.68 s. At the same time, the active power supplied is close to zero and the reactive power supplied is around 7.36 MVAr. It is clear that the PV system curtails its active power completely and acts as a Full STATCOM during fault. Post fault, the PCC voltage is regulated close to 0.996 pu

by supplying a capacitive reactive current of 2.33 kA. The reactive power supplied is close to 1.36 MVAr and active power supplied is close to zero.

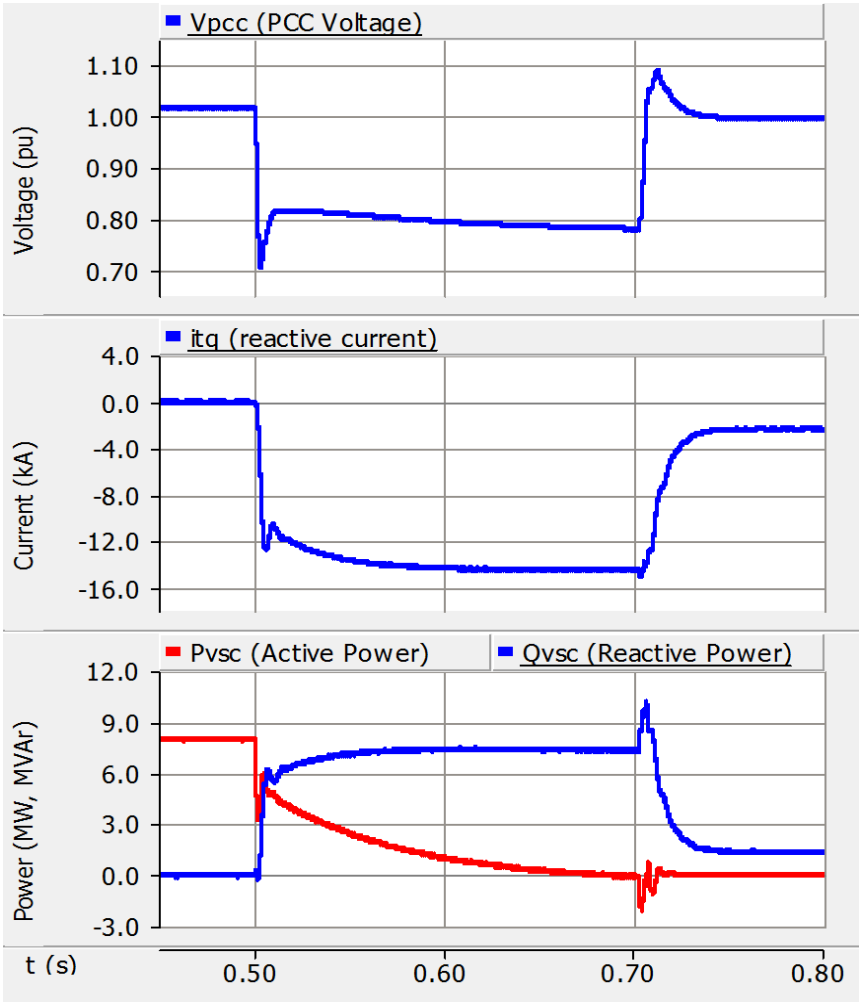

Figure 5.8 Response of Full STATCOM (for 2% droop)

The studies were also performed for droops of 5% and 10% but it was found that there is no significant difference in these responses when compared with the response for a droop of 2%. In both the cases, the PCC voltage is regulated at 0.78 pu by supplying the maximum capacitive reactive current.

5.5.4 Comparison between the voltage support provided by three control strategies

A comparative study is performed between the three types of voltage support strategies utilized for ride-through operation of the PV system during a fault. The following are the considered factors for comparison:

i) PCC voltage level during fault

ii) Transient response of PCC voltage and reactive current during and post fault

First, the comparison is made between proportional controller and PI controller based dynamic reactive current injection strategies. The steady state responses of both types of controllers are similar during and post faults for both 2% and 4% reactive current injections per percent voltage drop. For proportional controller, the transient oscillations in the responses of PCC voltage and reactive current increase (during and post fault) as the value of proportional gain increases. It was shown in chapter 3 that the interaction between DC-link voltage control loop and PCC voltage control loop increases as the value of proportional gain increases.

From the PCC voltage response of Figure 5.5, the damped natural frequency is found to be approximately 178.02 Hz (1117.96 rad/sec) (measured after a time of 0.62 seconds to ensure modulation index values are within +/-1). Such oscillations also exist in the response of reactive current. The system is linearized about the operating point that exists (post fault for Figure 5.5) using the model developed in chapter 3 for partial PV-STATCOM. By eigenvalue analysis, it is found that one of the eigenvalues is at -152.79+/-j 1132.7. The damped frequency of this eigenvalue is close to the damped frequency of the PCC voltage response. By participation factor analysis, it is found that the dominant states that participate in this eigenvalue pertain to dc-link voltage control loop (x_3), PCC-voltage control loop (x_4), and measurement filters (V_{cqf}, V_{s1df}). It shows that for the proportional controller, this interaction influences the performance of partial PV-STATCOM while performing voltage support during LVRT operations. For higher values of proportional gain, the oscillations could increase and could lead towards instability. Also, it will be shown later that this interaction leads to instability when two

PV systems are simultaneously performing voltage support with proportional controller based dynamic reactive current injection.

This is not the case with PI controller based dynamic reactive current injection. For the case of 4% reactive current injection (Figure 5.7), the transient response of PCC voltage and reactive current does not exhibit any significant damped oscillations which are an advantage of this control strategy over proportional controller. Also, the advantage of PI controller based dynamic reactive current injection will clearly be shown later in this chapter when two PV systems are simultaneously performing voltage support.

Second, the comparison is made between the responses obtained for PI controller based dynamic reactive current injection and Full STATCOM. Total reactive current injection using Full STATCOM regulates the PCC voltage to only 0.78 pu during fault. The PI controller based dynamic reactive current injection strategy is able to regulate the voltage at 0.80 pu (for 2% reactive current injection) and 0.82 pu (for 4% reactive current injection) during fault due to significant active power injections. This shows the effectiveness of reactive power control on voltage is dependent on X/R ratio of the distribution feeder. For X/R ratio of 2.47 (for the considered distribution feeder), only reactive power injection is less effective when compared to injecting a combination of active and reactive powers. But, as the X/R ratio increases, reactive power will have more effect on voltage which will be shown later in this chapter.

5.6 Voltage Support using Two PV systems

This section deals with voltage support provided by reactive current injection using two PV systems. The simplified diagram of the circuit utilized for the study with two PV systems is shown in Figure 5.9. A 9.9 MW PV system is connected at bus 3 which is 5 km away from the 8.5 MW PV system, similar to the studies performed in chapter 4. A three phase to ground fault is applied at load end using a resistance of 25 Ohm.

The PV array of 9.9 MW PV system is designed using the parameters of FS 272 PV panel. The PV array parameters, the maximum power point dc-link voltage and dc-link capacitance are provided in Table D. 1 of Appendix D.

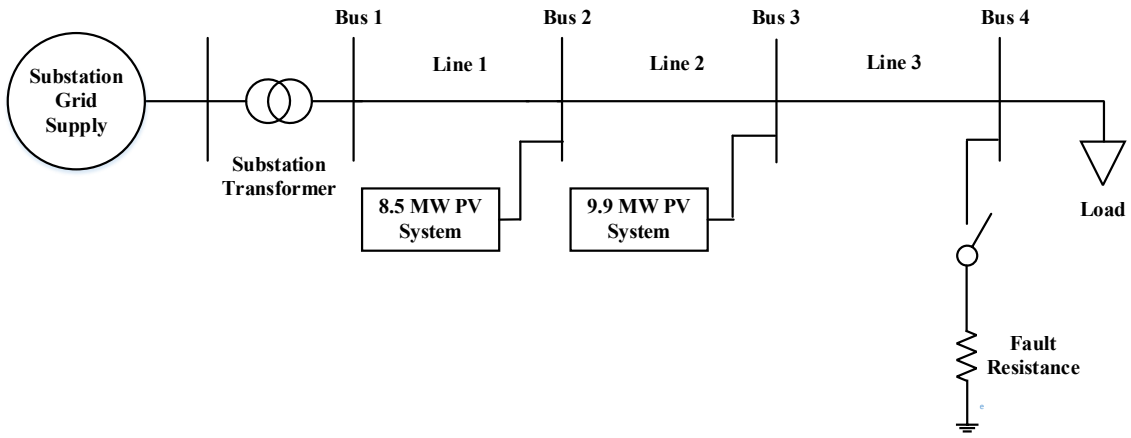

Figure 5.9 Simplified diagram of the circuit utilized for the simulation of fault with two PV systems

The dc-link voltage controller parameters for the 9.9 MW PV system are similar to those utilized for 8.5 MW PV system. Similar to section 4.5, both the PV systems are designed to have the same control system parameters (current controllers, PLL, dc-link voltage controller etc.) as this represents the worst case scenario where both PV systems respond in a similar way to any system disturbance. The PCC voltage (at bus 2) of 8.5 MW PV system is V_{pcc1}, the reactive current output of its inverter is i_{tq1}, the active and reactive power supplied by its inverter are P_{VSC1} and Q_{VSC1}. The PCC voltage (at bus 3) of 9.9 MW PV system is V_{pcc2}, the reactive current output of its inverter is i_{tq2}, the active and reactive power supplied by its inverter are P_{VSC2} and Q_{VSC2}.

Both the PV systems are operating with maximum irradiance of 1 kW/m^2 and supplying maximum active power. The fault is introduced at a time of 0.5 seconds for a period of 100 ms (6 cycles of 60 Hz). The ride-through operation performed by both PV systems (with zero reactive current injection) is shown in Figure 5.10. V_{pcc1} and V_{pcc2} drop to 0.834 pu and 0.8 pu respectively. P_{VSC1} and P_{VSC2} are 6.46 MW and 7.2 MW respectively. Both PV systems continue to maintain the active currents close to value that existed before the application of fault as the respective dc-link voltage errors are maintained close to zero. Post faults, P_{VSC1} and P_{VSC2} are 6.67 MW and 7.48 MW respectively which are close to the powers supplied during fault. This shows the change in dc-link voltage reference of both PV systems ensure that they ride-through the fault by

supplying active power and a stable operating point is reached for both PV systems post fault.

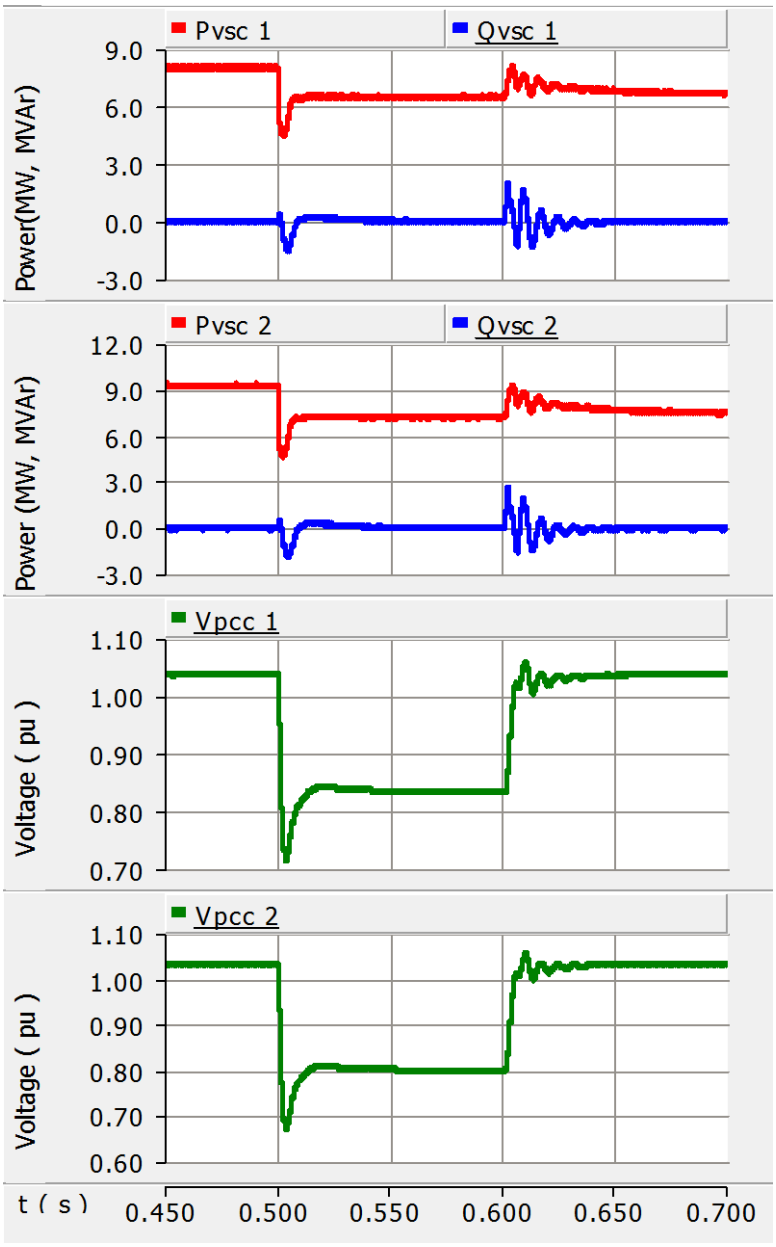

Figure 5.10 Ride-through operation by both PV systems (with zero reactive current injection) during and post fault

5.6.1 Voltage support using proportional controller based dynamic reactive current injection

First, the voltage support provided by proportional controller based dynamic reactive current injection (by both PV systems) is studied. Both the PV systems are designed to inject a minimum of 2% reactive current injection per percent voltage drop below 0.9 pu. The proportional gains are calculated as 1.282 for 8.5 MW PV system and 1.494 for 9.9 MW PV system. The PCC voltage controllers are turned on at 0.5 seconds. The voltage support provided by both PV systems is shown in Figure 5.11. It can be seen that V_{pcc1} and V_{pcc2} are regulated at 0.892 pu and 0.862 pu respectively by supplying capacitive reactive currents of i_{tq1} = 3.1 kA and i_{tq2} = 4.6 kA. P_{VSC1} and P_{VSC2} are 7.03 MW and 7.92 MW respectively during fault. The reactive powers supplied namely Q_{VSC1} and Q_{VSC2} are 1.66 MVAr and 2.39 MVAr respectively during fault. Post fault, the transient response of PCC voltages exhibit damped oscillations of 163.37 Hz (1025.96 rad/sec) which take approximately 140 ms (at 0.74 s) to get completely damped. These oscillations are due to interaction between the controllers of two PV systems (which is influenced by feed-forward filter time constants of each PV system) as they respond similarly to the change in their respective PCC voltages.

Now, both the PV systems are designed to inject 3% reactive current injection per percent voltage drop below 0.9 pu. The proportional gains are calculated as 1.926 for 8.5 MW PV system and 2.23 for 9.9 MW PV system. The voltage support provided by both PV systems is shown in Figure 5.12. Due to increase in reactive current injections, the PCC voltages are now regulated at 0.908 pu (V_{pcc1}) and 0.88 pu (V_{pcc2}) by injecting capacitive reactive currents are at 3.96 kA (i_{tq1}) and 6.02 kA (i_{tq2}). Post fault, the PCC voltage responses exhibit instability as they become oscillatory initially due to which modulation index saturates and hence, a pattern of non-sinusoidal oscillations result.

5.6.2 Voltage support using PI controller based dynamic reactive current injection

Second, the voltage support provided by PI controller based dynamic reactive current injection (by both PV systems) is studied. The PI controller gains are chosen as $K_{pvs} =$

0.5 and $K_{ivs} = 400$ for each PV system. The droop K_{droop} is set at 0.78 for 8.5 MW PV system and 0.66 for 9.9 MW PV system to represent reactive current injection of 2% per percent of voltage drop.

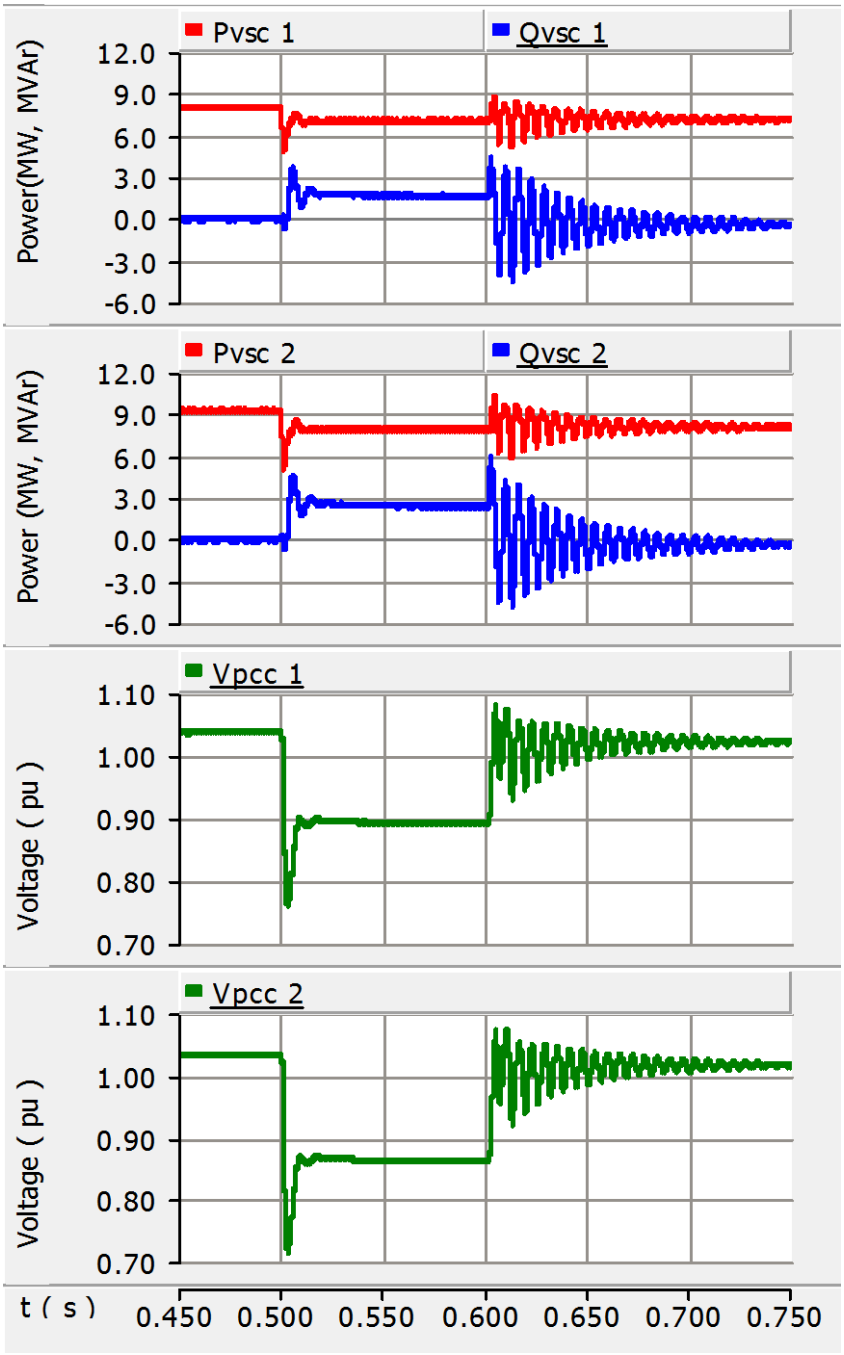

Figure 5.11 Response of proportional controller for 2% reactive current injection by both PV systems

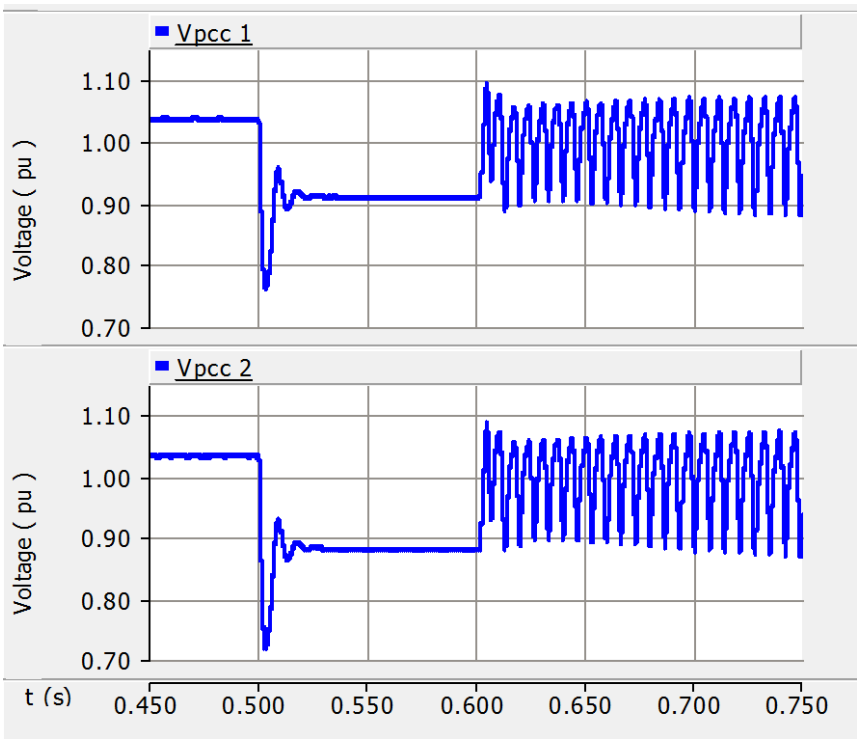

Figure 5.12 Response of proportional controller for 3% reactive current injection by both PV systems

The fault is applied at 0.5 seconds for 100 ms and the PCC voltage controllers are turned on at 0.5 seconds. The voltage support provided by both PV systems is shown in Figure 5.13. The PCC voltages V_{pcc1} and V_{pcc2} are regulated at 0.892 pu and 0.862 pu respectively by supplying capacitive reactive currents of i_{tq1} = 3.1 kA and i_{tq2} = 4.62 kA. P_{VSC1} and P_{VSC2} are 7.02 MW and 7.91 MW respectively during fault. The reactive powers supplied namely Q_{VSC1} and Q_{VSC2} are 1.64 MVAr and 2.43 MVAr respectively during fault. Post fault, the transient response of PCC voltages exhibit damped oscillations of 162.04 Hz (1017.6 rad/sec) which take approximately 75 ms (at 0.675 s) to get completely damped.

Now, both the PV systems are designed to inject 3% reactive current per percent voltage drop below 0.9 pu. The droops are calculated as 0.519 and 0.448 for the 8.5 MW and 9.9 MW PV systems respectively. The voltage support provided by both PV systems is shown in Figure 5.14. The PCC voltages are now regulated at 0.908 pu (V_{pcc1}) and 0.88 pu (V_{pcc2}) by injecting capacitive reactive currents of 3.96 kA (i_{tq1}) and 6.02 kA (i_{tq2}).

Post fault, there are damped oscillations of frequency 160.02 Hz (1004.92 rad/sec) which get damped out completely in approximately 100 ms (at 0.7 sec).

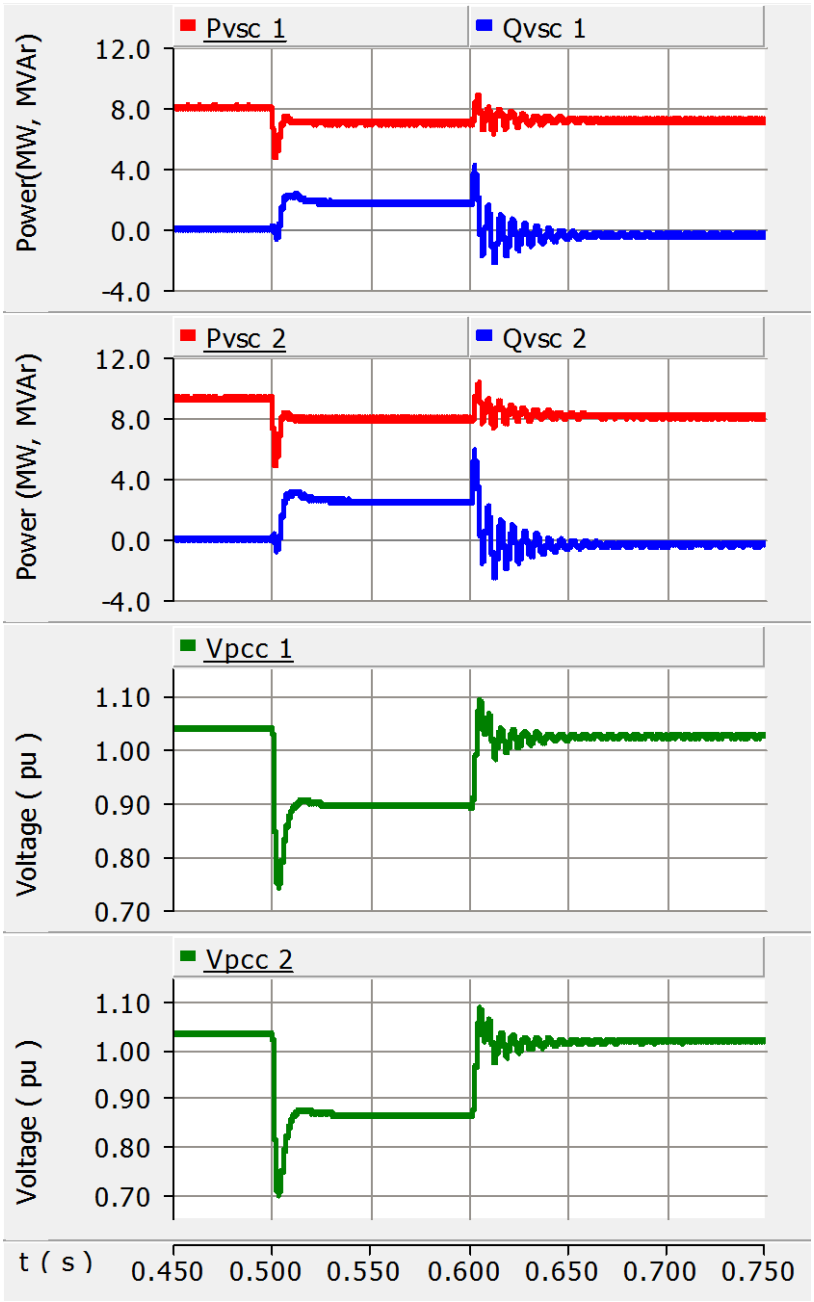

Figure 5.13 Response of PI controller for 2% reactive current injection by both PV systems

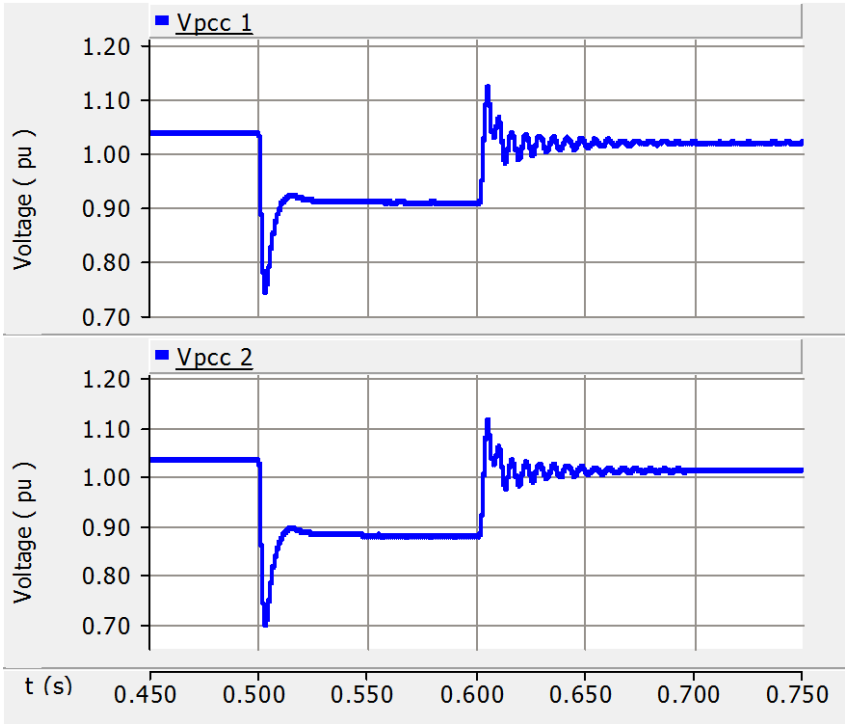

Figure 5.14 Response of PI controller for 3% reactive current injection by both PV systems

5.6.3 Voltage support using Full STATCOM

Third, the voltage support provided by two Full STATCOMs is studied. Both the PV systems operate in P-priority to curtail their real power completely. The dc-link voltage controllers of both PV systems exhibit slow responses in regulating their respective dc-link voltages at open circuit voltage of PV array. Similar to the reasons pointed out in section 5.5.3, the fault is simulated for a duration of 200 ms. The PI controller gains are chosen as $K_{pvs} = 0.5$ and $K_{ivs} = 400$ for both the PV systems. The droops are set at 2% for both the PV systems initially and are calculated to be 0.0312 and 0.0268 for 8.5 MW and 9.9 MW PV system respectively. The voltage support provided by the Full STATCOMs is shown in Figure 5.15. The fault is applied at 0.5 s. Step responses to regulate the dc-link voltage at respective open circuit voltages and turn-on of PCC voltage controllers are performed at 0.5 s. It can be seen from the responses that the active powers are regulated to zero. The PCC voltages V_{pcc1} and V_{pcc2} are regulated at 0.835 pu and 0.817 pu respectively by supplying full capacitive reactive currents of i_{tq1}

= 14.45 kA and i_{tq2} = 16.84 kA. The reactive powers supplied Q_{VSC1} and Q_{VSC2} are 7.8 MVAr and 8.89 MVAr respectively during fault.

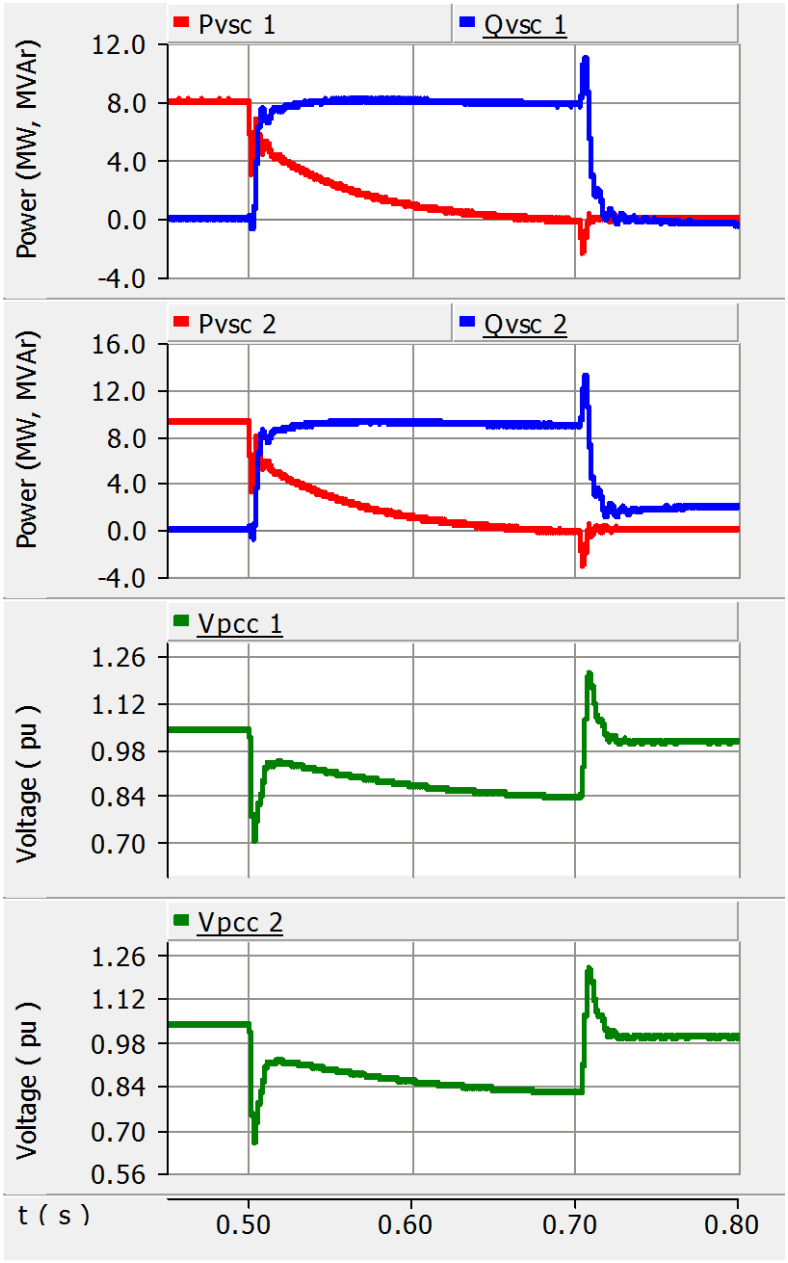

Figure 5.15 Response of two PV systems operating in Full STATCOM mode (for 2% droop)

The studies were also performed for droops of 5% and 10% for both PV systems but it is found that there is no significant difference in these responses when compared with the

response for a droop of 2%. In both cases, the PCC voltages V_{pcc1} and V_{pcc2} are regulated at 0.835 pu and 0.817 pu by supplying the maximum capacitive reactive currents.

5.6.4 Comparison between the voltage support provided by three control strategies

A comparative study is performed between the three types of voltage support strategies utilized for ride-through operation of both PV systems during a fault. The following factors are considered for comparison:

i) PCC voltage level during fault
ii) Transient response of PCC voltage and reactive current during and post fault

First, the comparison is made between proportional controller and PI controller based dynamic reactive current injection strategies. The steady state responses of both types of controllers are almost similar during faults for both 2% and 3% reactive current injections per percent voltage drop.

Post fault, the proportional controller response exhibits damped oscillations of frequency 163.37 Hz for 2% reactive current injection which take 140 ms to get completely damped. With a PI controller, the oscillations of similar frequency exist but they get damped in around 75 ms. For 3% reactive current injection, proportional controller results in a unstable response whereas PI controller results in a stable response. This shows the clear advantage of PI controller based dynamic reactive current injection which can result in an effective and stable PCC voltage control response even in the presence of interaction between the PV systems.

Second, the comparison is made between the responses obtained for PI controller based dynamic reactive current injection and Full STATCOM. The inferences are similar to those mentioned in the case of comparative studies of control strategies with single PV system. For an X/R ratio of 2.47, full reactive power injection by both PV systems operating in Full STATCOM mode is less effective in PCC voltage control during fault when compared to injecting a combination of active and reactive powers. For higher X/R

ratios, full reactive power injections have more effect as will be shown in the next section.

5.7 Effect of X/R ratio of distribution feeder on PCC voltage control

It was mentioned earlier that the effectiveness of full reactive power injection on PCC voltage control is dependent on the X/R ratio of distribution feeder. In this section, the X/R ratio is changed to values such as 2.47, 5, 7.5 and 10 to represent a range of distribution feeders with different characteristics. For changing X/R ratio, the resistance and reactance per unit length of the distribution line are changed while maintaining the impedance per unit length constant (for maintaining the same conductor ampacity).

For each X/R ratio, the PCC voltage levels reached during fault are compared for the following cases:

i) Two PV systems providing voltage support with PI controller based dynamic reactive injection (2% reactive current injection per percent voltage drop)
ii) Two PV systems providing voltage support by operating in Full STATCOM mode (with 2% droop each)

The values of PCC voltages, reactive current, active power and reactive powers supplied by each PV system for different X/R ratio are summarized in Table 5.1. The following inferences can be made:

i) For voltage support using LVRT with 2% reactive current injection: As the value of X/R ratio increases, the reactive current (and hence, the reactive power) supplied by each PV system decreases which leads to increase in active power injected. The PCC voltage levels during fault (without reactive current injection) are also dependent on X/R ratio and active power injected during fault. For instance, the PCC voltages V_{pcc1} and V_{pcc2} are at 0.848 pu and 0.824 pu for X/R ratio of 10 which are higher when compared to the PCC voltage levels for X/R ratio of 2.47.

Table 5.1 Effectiveness of X/R ratio on PCC voltage control

		LVRT with 2% reactive current injection per percent voltage drop		Full STATCOM	
X/R ratio	**Parameter**	**8.5 MW PV system**	**9.9 MW PV system**	**8.5 MW PV system**	**9.9 MW PV system**
2.47	V_{pcc} (pu)	**0.892**	**0.862**	**0.835**	**0.817**
	P_{VSC} (MW)	7.02	7.91	-0.164	-0.187
	Q_{VSC} (MVAr)	1.64	2.43	7.8	8.89
	i_{tq} (kA)	-3.1	-4.62	-14.45	-16.84
5	V_{pcc} (pu)	**0.901**	**0.878**	**0.885**	**0.878**
	P_{VSC} (MW)	7.43	8.4	-0.146	-0.212
	Q_{VSC} (MVAr)	1.525	2.18	8.22	9.47
	i_{tq} (kA)	-2.83	-4.11	-14.45	-16.84
7.5	V_{pcc} (pu)	**0.905**	**0.885**	**0.906**	**0.903**
	P_{VSC} (MW)	7.61	8.62	-0.138	-0.223
	Q_{VSC} (MVAr)	1.47	2.07	8.42	9.77
	i_{tq} (kA)	-2.71	-3.86	-14.45	-16.84

10	V_{pcc} (pu)	**0.907**	**0.88**	**0.916**	**0.916**
	P_{VSC} (MW)	7.68	8.67	-0.138	-0.246
	Q_{VSC} (MVAr)	1.45	2.01	8.47	9.88
	i_{tq} (kA)	-2.66	-3.78	-14.44	-16.84

Hence, for a particular characteristic of dynamic reactive current injection, the magnitude of reactive current injected depends on PCC voltage level (with zero reactive current) which is in-turn dependent on X/R ratio. Eventually, the magnitude of reactive current injected determines the net increase in PCC voltage levels.

ii) **For Full STATCOM operation**: Irrespective of X/R ratio, both the PV systems inject full reactive current (hence, reactive power) by curtailing their real powers to zero. The increase in PCC voltage is determined by the X/R ratio. As X/R ratio increases, the PCC voltage levels increase as it is more sensitive to injected reactive powers.

These studies show that the application of Full STATCOMs for PCC voltage control during fault becomes more effective as the value of X/R ratio of the distribution feeder increases.

5.8 Conclusion

In this chapter, the ability of PV-STATCOM to ride-through, and provide stable voltage support during and post a three phase fault is studied. The PV system (or PV systems) is made to perform PCC voltage support with feed-forward voltage filter time constants at 0.75 ms so that the interaction between dc-link voltage control loop and PCC-voltage control loop is at a maximum. Under this condition, the stability of proportional controller based dynamic reactive current injection, PI controller based dynamic reactive current injection and PV system operating in Full STATCOM mode is compared.

Studies are first performed with single PV system. For higher values of slopes of dynamic reactive current injection characteristic, the PI controller exhibits a better damped response when compared to proportional controller.

Studies are also performed with two similar PV systems providing simultaneous voltage support during and post fault. The proportional controller based dynamic reactive current injection results in oscillatory PCC voltage responses post fault and this goes towards instability as the slope of dynamic reactive current injection characteristic increases. The PI controller results in a relatively better damped and stable response for all values of considered slopes.

The studies with PV systems operating in Full STATCOM mode (with single and two PV systems) for voltage support revealed that X/R ratio plays a crucial role in the effectiveness of voltage control. As the value of X/R ratio increases, complete reactive power injection becomes more effective.

Chapter 6

6 CONCLUSIONS AND FUTURE WORK

6.1 General

There are many challenges involved in the grid integration of PV systems which are created by high penetration of PV systems. Smart PV inverters have been shown capable of mitigating some of the issues and increase the penetration level of PV systems in distribution networks. The smart inverter functions such as Volt/Var control, dynamic reactive current injection and low voltage ride through are some of the functions for voltage control purposes. It has been shown in this thesis these functions can also be implemented using PV-STATCOM controls.

Further, a particular control system interaction issue that is capable of causing instability when there is PCC voltage control action has been pointed out using the developed detailed state space model of PV-STATCOM. It has been shown by Eigenvalue sensitivity analysis studies that PI type PCC voltage controller (PV-STATCOM controls) can remain stable even in the presence of this issue whereas proportional type PCC voltage controller (Smart Inverter controls) cannot remain stable.

The performance of PI and proportional type PCC voltage controllers in the presence of control system interaction is studied while performing voltage control during system disturbances. Disturbance due to irradiance change and a three phase fault are studied. Dynamic reactive current injection is considered as the smart PV inverter function for which both proportional and PI controllers are designed. It has been shown that PI controller based dynamic reactive current injection is more stable than proportional controller based dynamic reactive current injection while performing voltage control during disturbances.

The studies are initially performed with a single PV system and are later extended to the case where there are two PV systems.

6.2 PV-STATCOM Modeling

The nonlinear modeling of PV-STATCOM unit connected to a distribution network is carried out in chapter 2. The distribution network subsystem includes substation grid, substation transformer, distribution line and load. The PV-STATCOM unit consists of PV and Controller subsystems. The PV subsystem includes PV panel array, PV inverter, filter and coupling transformer. The control subsystem includes the PLL, current controllers, dc-link voltage controller and PCC voltage controller. The model for each subsystem has been developed in *dq* frame.

The need for developing the complete linearized model of entire system which is to study the interaction between dc-link voltage control loop and PCC voltage control loop has been explained. The procedure for linearization which is based on Taylor series expansion has been individually applied to each subsystem and the corresponding linearized model has been developed. Finally, the linearized model of the overall system has been developed by combining the linearized models of each subsystem. The linearized model in each mode of operation of PV-STATCOM namely full PV, partial PV-STATCOM and Full STATCOM modes is presented.

The model and results obtained for the PV-STATCOM are valid for a PV system of any rating.

6.3 Controller Design for PV-STATCOM

In chapter 3, the controller design for PV-STATCOM is carried out. The individual controllers of PV-STATCOM namely PLL, current controllers and dc-link voltage controller are designed based on linear control techniques. The model of PV-STATCOM operating in Full PV mode is first validated by comparing the dc-link voltage and active power outputs of linearized and PSCAD / EMTDC model responses for a step change in irradiance at three different operating points.

For partial PV-STATCOM, the stability of proportional controller based PCC voltage controller is studied using the Eigenvalue sensitivity analysis. An interaction between dc-link voltage control loop and PCC voltage control loop due to delays in the measurement

filters of EPC feed-forward signals is pointed out. The performance of both proportional and PI controllers have been compared in the presence of the interaction. For both the controllers, the sensitivity of critical eigenvalue to measurement filter time constants, PCC voltage controller gains and reactive current controller bandwidth are studied. Based on these studies, it has been proved that proportional controller exhibits instability for higher gains which can be mitigated by slowing down the reactive current controller in the presence of interaction. The PI controller results in a stable response even in the presence of interaction without compromising on the bandwidth of reactive current controller. The partial PV-STATCOM linearized model has been validated by applying a step in PCC voltage and, comparing the responses of linearized and PSCAD / EMTDC models for both cases of proportional and PI controller.

For Full STATCOM mode, the dc-link voltage controller is re-designed with the same performance characteristics as Full PV mode. Eigenvalue sensitivity analysis is then used to decide the optimum values of PI type PCC voltage controller gains in the presence of interaction between dc-link voltage control loop and PCC voltage control loop. The linearized model of Full STATCOM is then validated for both a step change in dc-link voltage and PCC voltage by making comparisons with PSCAD / EMTDC model.

6.4 Voltage control to mitigate voltage flicker

The application of partial PV-STATCOM for performing voltage control to mitigate flicker in PCC voltage introduced by 100% change in irradiance is studied in chapter 4. The PV system is made to perform PCC voltage control with feed-forward voltage filter time constants at 0.75 ms so that the interaction between dc-link voltage control loop and PCC-voltage control loop is at a maximum. Under this condition, the stability of proportional and PI controller based dynamic reactive current injections, and Volt/Var controls are compared.

Studies are performed with single PV system and two PV systems performing simultaneous voltage control. For studies with single PV system, higher values of slopes of dynamic reactive current injection characteristic can be implemented with a PI controller over proportional controller without any stability issues. For studies with two

PV systems, PI controller based dynamic reactive current injection can ensure a stable simultaneous voltage control without compromising on the bandwidth of q-axis current controllers, which is not possible with proportional controller. The volt/var control is found to be a slow control which is not effective in regulating the PCC voltages within the allowed limits of 3% in studies with single and two PV systems.

6.5 Voltage support during LVRT

In chapter 5, the ability of PV-STATCOM to ride-through, and provide stable voltage support during and post a three phase fault is studied. The PV system is made to perform PCC voltage support with feed-forward voltage filter time constants at 0.75 ms so that the interaction between dc-link voltage control loop and PCC-voltage control loop is at a maximum. Under this condition, the stability of proportional controller based dynamic reactive current injection, PI controller based dynamic reactive current injection and PV system operating in Full STATCOM mode is compared.

Studies are performed with single PV system and two PV systems. For studies with single PV system, the PI controller exhibits a better damped response when compared to proportional controller for higher values of slopes of dynamic reactive current injection. For studies with two PV systems, PI controller results in a relatively better damped and stable response post fault whereas proportional controller results in instability for higher values of slopes of dynamic reactive current injection.

Studies with PV systems operating in Full STATCOM mode (with single and two PV systems) for voltage support showed that complete reactive power injection becomes more effective as the value of X/R ratio of distribution feeder increases.

6.6 Thesis Contributions

The following are the major contributions of this thesis:

1) A detailed linearized state space model of a PV system with PCC voltage control functionality (PV-STATCOM) has been developed. Model can be used for

performing stability studies in all three modes of operation namely Full PV, partial PV-STATCOM and Full STATCOM. ***Such a detailed model with all these features is not available in the literature to the best knowledge of author.***

2) The developed model has been used to identify the interaction between dc-link voltage control loop and PCC voltage control loop, influenced by grid voltage feed-forward filters. The performance of proportional and PI type PCC voltage controllers has been evaluated in the presence of the interaction. ***This kind of analysis is not available in the literature to the best knowledge of the author.***

3) The dynamic reactive current injection function is implemented using PI controller with droop. Its superiority in performance over proportional controller based dynamic reactive current injection is brought out while performing voltage control during system disturbances such as irradiance change and faults. ***These kinds of comparative studies are not available in the literature to the best knowledge of author.***

Papers to be published from this thesis (tentative details which are subject to change):

[1] R. K. Varma and Sridhar.BS, "Smart PV Inverter Voltage Control Strategies", Paper under preparation to be submitted to *IEEE Transactions on Sustainable Energy*.

6.7 Future Work

Some of the work that can be carried out as part of future research is provided below:

- The model developed for one PV-STATCOM can be extended and a detailed model with two PV-STATCOMs can be developed. The model can be used for coordinated controller design between two PV-STATCOMs.

- The model developed for the PV-STATCOM is valid for a PV system irrespective of its rating. In practice, a large PV power plant consists of multiple PV inverters in parallel. A detailed model can be developed for a large PV power plant that

includes the models for each individual inverter. This could be used to study the interactions between individual inverters etc.

- A detailed model for a two stage PV-STATCOM can be developed. The control system interaction issues can be studied using the detailed model.

- Voltage flicker studies were conducted by introducing a 100% step change in irradiance. This can be extended by performing the studies with high resolution location based solar irradiance data.

- A detailed model of single stage and two stage PV-STATCOMs for operation under unbalanced conditions can be developed. The control system interaction issues can be studied using the detailed model. This is beneficial for applications such as unbalanced load compensation and operation under asymmetrical faults.

References or Bibliography

[1] I. E. Agency. *About renewable energy* [Online]. Available: http://www.iea.org/topics/renewables/

[2] F. Katiraei and J. R. Aguero, "Solar PV Integration Challenges," *IEEE Power and Energy Magazine,* vol. 9, pp. 62-71, 2011.

[3] Y. Poissant, L. Dignard-Bailey, and P. Luukkonen, "Photovoltaic Technology Status and Prospects: Canadian Annual Report 2013," Natural Resources Canada and Canadian Solar Industries Association,CETC number: 2014-039, July 2014.

[4] N. R. Canada. (2016, March 14). *About Renewable Energy* [Online]. Available: http://www.nrcan.gc.ca/energy/renewable-electricity/7295

[5] N. E. Board. (2016, January 24). *Fact Sheet - Canada's Energy Future 2016: Energy Supply and Demand Projections to 2040 - Electricity Highlights* [Online]. Available: https://www.neb-one.gc.ca/nrg/ntgrtd/ftr/2016/fslctrct-eng.html

[6] R. Tonkoski, L. A. C. Lopes, and T. H. M. El-Fouly, "Coordinated Active Power Curtailment of Grid Connected PV Inverters for Overvoltage Prevention," *IEEE Transactions on Sustainable Energy,* vol. 2, pp. 139-147, 2011.

[7] C. Schauder, "Advanced Inverter Technology for High Penetration Levels of PV Generation in Distribution Systems,",NREL Subcontract Report : NREL/SR-5D00-60737, 2014.

[8] E. Stewart, J. MacPherson, S. Vasilic, D. Nakafuji, and T. Aukai, "Analysis of High-Penetration Levels of Photovoltaics into the Distribution Grid on Oahu, Hawaii - Detailed Analysis of HECO Feeder WF1 ",NREL Subcontract Report: NREL/SR-5500-54494, 2013.

[9] "Distributed generation technical interconnection requirements: interconnections at voltages 50 kV and below," Hydro One Networks Inc., DT-10-015 REV. 3, March 2013.

[10] J. E.-G. Carrasco, J. M. Tena, D. Ugena, J. Alonso-Martinez, D. Santos-Martin, and S. Arnaltes, "Testing Low Voltage Ride Through capabilities of solar inverters," *Electric Power Systems Research,* vol. 96, pp. 111-118, 3// 2013.

[11] J. J. Gutierrez, J. Ruiz, A. Lazkano, and L. A. Leturiondo, "Measurement of Voltage Flicker: Application to Grid-connected Wind Turbines," in *Advances in Measurement Systems*, ed: InTech 2010.

[12] E. Muljadi, M. Singh, and V. Gevorgian, "User Guide for PV Dynamic Model Simulation Written on PSCAD Platform,", NRELTechnical Report: NREL/TP-5D00-62053, 2014.

[13] "IEEE Recommended Practice for Electric Power Distribution for Industrial Plants," *IEEE Std 141-1993,* pp. 1-768, 1994.

[14] "IEEE Standard for Interconnecting Distributed Resources with Electric Power Systems," *IEEE Std 1547-2003,* pp. 1-28, 2003.

[15] Y. Yang, P. Enjeti, F. Blaabjerg, and H. Wang, "Suggested grid code modifications to ensure wide-scale adoption of photovoltaic energy in distributed power generation systems," in *2013 IEEE Industry Applications Society Annual Meeting*, 2013, pp. 1-8.

[16] J. Berdner. (2014 July, 11). *Inverter Ride through Functions* [Online]. Available: http://www.iso-

ne.com/committees/comm_wkgrps/prtcpnts_comm/pac/mtrls/2014/jul112014/inverter_manufacturers_perspective.pdf

[17] A. Yazdani, A. R. D. Fazio, H. Ghoddami, M. Russo, M. Kazerani, J. Jatskevich, *et al.*, "Modeling Guidelines and a Benchmark for Power System Simulation Studies of Three-Phase Single-Stage Photovoltaic Systems," *IEEE Transactions on Power Delivery,* vol. 26, pp. 1247-1264, 2011.

[18] A. Yazdani and R. Iravani, *Voltage-Sourced Converters in Power Systems : Modeling, Control, and Applications*. Hoboken, NJ: Wiley, 2010.

[19] A. Yazdani and P. P. Dash, "A Control Methodology and Characterization of Dynamics for a Photovoltaic (PV) System Interfaced With a Distribution Network," *IEEE Transactions on Power Delivery,* vol. 24, pp. 1538-1551, 2009.

[20] M. A. Mahmud, M. J. Hossain, H. R. Pota, and N. K. Roy, "Robust Nonlinear Controller Design for Three-Phase Grid-Connected Photovoltaic Systems Under Structured Uncertainties," *IEEE Transactions on Power Delivery,* vol. 29, pp. 1221-1230, 2014.

[21] M. A. Mahmud, H. R. Pota, M. J. Hossain, and N. K. Roy, "Robust Partial Feedback Linearizing Stabilization Scheme for Three-Phase Grid-Connected Photovoltaic Systems," *IEEE Journal of Photovoltaics,* vol. 4, pp. 423-431, 2014.

[22] T. Stetz, F. Marten, and M. Braun, "Improved Low Voltage Grid-Integration of Photovoltaic Systems in Germany," *IEEE Transactions on Sustainable Energy,* vol. 4, pp. 534-542, 2013.

[23] T. Fawzy, D. Premm, B. Bletterie, and A. Goršek, "Active contribution of PV inverters to voltage control – from a smart grid vision to full-scale implementation," *e & i Elektrotechnik und Informationstechnik,* vol. 128, pp. 110-115, 2011.

[24] J. W. Smith, W. Sunderman, R. Dugan, and B. Seal, "Smart inverter volt/var control functions for high penetration of PV on distribution systems," in *2011 IEEE/PES Power Systems Conference and Exposition (PSCE)* 2011, pp. 1-6.

[25] T. V. Loon, T. V. Van, A. Woyte, F. Truyens, B. Bletterie, J. Reekers, *et al.*, "Increasing photovoltaics grid penetration in urban areas through active distribution systems: First large scale demonstration," in *2010 Third International Conference on Infrastructure Systems and Services: Next Generation Infrastructure Systems for Eco-Cities (INFRA)*, 2010, pp. 1-4.

[26] "Common Functions for Smart Inverters, Version 3," EPRI, Palo Alto, CA, 3002002233, 2013.

[27] Y. Yang, H. Wang, and F. Blaabjerg, "Reactive Power Injection Strategies for Single-Phase Photovoltaic Systems Considering Grid Requirements," *IEEE Transactions on Industry Applications,* vol. 50, pp. 4065-4076, 2014.

[28] "Grid Code High and Extra High Voltage," *E.ON Netz GmbH,* April 2006.

[29] "Model User Guide for Generic Renewable Energy System Models," EPRI, Palo Alto, CA, 3002006525, 2015.

[30] F. Andren, B. Bletterie, S. Kadam, P. Kotsampopoulos, and C. Bucher, "On the Stability of Local Voltage Control in Distribution Networks With a High Penetration of Inverter-Based Generation," *IEEE Transactions on Industrial Electronics,* vol. 62, pp. 2519-2529, 2015.

[31] A. Camacho, M. Castilla, J. Miret, J. C. Vasquez, and E. Alarcon-Gallo, "Flexible Voltage Support Control for Three-Phase Distributed Generation Inverters Under Grid Fault," *IEEE Transactions on Industrial Electronics,* vol. 60, pp. 1429-1441, 2013.

[32] B. K. Perera, P. Ciufo, and S. Perera, "Point of common coupling (PCC) voltage control of a grid-connected solar photovoltaic (PV) system," in *IECON 2013 - 39th Annual Conference of the IEEE Industrial Electronics Society*, 2013, pp. 7475-7480.

[33] R. M. Mathur and R. K. Varma, *Thyristor-Based FACTS Controllers for Electrical Transmission Systems*. New York, NY: Wiley-IEEE Press, 2002.

[34] M. Castilla, J. Miret, A. Camacho, J. Matas, and L. G. d. Vicuna, "Voltage Support Control Strategies for Static Synchronous Compensators Under Unbalanced Voltage Sags," *IEEE Transactions on Industrial Electronics,* vol. 61, pp. 808-820, 2014.

[35] R. K. Varma, S. A. Rahman, A. C. Mahendra, R. Seethapathy, and T. Vanderheide, "Novel nighttime application of PV solar farms as STATCOM (PV-STATCOM)," in *2012 IEEE Power and Energy Society General Meeting*, 2012, pp. 1-8.

[36] R. K. Varma, S. A. Rahman, and T. Vanderheide, "New Control of PV Solar Farm as STATCOM (PV-STATCOM) for Increasing Grid Power Transmission Limits During Night and Day," *IEEE Transactions on Power Delivery,* vol. 30, pp. 755-763, 2015.

[37] E. M. Siavashi, "Smart PV Inverter Control for Distribution Systems," Ph.D. dissertation, Electrical and Computer Engineering, The University of Western Ontario, London, ON, Canada, 2015.

[38] R. K. Varma, B. Das, I. Axente, and T. Vanderheide, "Optimal 24-hr utilization of a PV solar system as STATCOM (PV-STATCOM) in a distribution network," in *2011 IEEE Power and Energy Society General Meeting*, 2011, pp. 1-8.

[39] R. K. Varma, S. A. Rahman, V. Sharma, and T. Vanderheide, "Novel control of a PV solar system as STATCOM (PV-STATCOM) for preventing instability of induction motor load," in *2012 25th IEEE Canadian Conference on Electrical & Computer Engineering (CCECE)*, 2012, pp. 1-5.

[40] M. AC, "Novel Control of PV Solar and Wind Farm Inverters as STATCOM for Increasing Connectivity of Distributed Generators," M.E.Sc. thesis, Electrical and Computer Engineering, The University of Western Ontario, London, ON, Canada, 2013.

[41] M. Saeedifard, R. Iravani, and J. Pou, "Control and DC-capacitor voltage balancing of a space vector-modulated five-level STATCOM," *IET Power Electronics,* vol. 2, pp. 203-215, 2009.

[42] M. J. Hossain, M. A. Mahmud, H. R. Pota, and N. Mithulananthan, "Design of Non-Interacting Controllers for PV Systems in Distribution Networks," *IEEE Transactions on Power Systems,* vol. 29, pp. 2763-2774, 2014.

[43] S. Liu, P. X. Liu, and X. Wang, "Stochastic Small-Signal Stability Analysis of Grid-Connected Photovoltaic Systems," *IEEE Transactions on Industrial Electronics,* vol. 63, pp. 1027-1038, 2016.

[44] F. Delfino, G. B. Denegri, M. Invernizzi, and R. Procopio, "Feedback linearisation oriented approach to Q-V control of grid connected photovoltaic units," *IET Renewable Power Generation,* vol. 6, pp. 324-339, 2012.
[45] M. A. Kashem and G. Ledwich, "Multiple Distributed Generators for Distribution Feeder Voltage Support," *IEEE Transactions on Energy Conversion,* vol. 20, pp. 676-684, 2005.
[46] P. Kundur, *Power System Stability and Control*: McGraw-Hill, 1993.
[47] S. A. Rahman, R. K. Varma, and T. Vanderheide, "Generalised model of a photovoltaic panel," *IET Renewable Power Generation,* vol. 8, pp. 217-229, 2014.
[48] Y. Yang, M. Kazerani, and V. H. Quintana, "Modeling, control and implementation of three-phase PWM converters," *IEEE Transactions on Power Electronics,* vol. 18, pp. 857-864, 2003.
[49] "IEEE Recommended Practices and Requirements for Harmonic Control in Electrical Power Systems," *IEEE Std 519-1992,* pp. 1-112, 1993.
[50] S. R. Nandurkar and M. Rajeev, "Design and Simulation of three phase Inverter for grid connected Photovoltic systems," in *Proceedings of Third Biennial National Conference NCNTE*, 2012.
[51] B. Liu and B. M. Song, "Modeling and analysis of an LCL filter for grid-connected inverters in wind power generation systems," in *2011 IEEE Power and Energy Society General Meeting*, 2011, pp. 1-6.
[52] N. Mohan, T. M. Undeland, and W. P. Robbins, *Power Electronics: Converters, Applications, and Design*, 3rd Edition ed.: John Wiley & Sons, Inc., 2003.
[53] M. Kazerani, "ECE 663: Energy Processing Lecture Notes," University of Waterloo, Waterloo, ON, Canada, 2014.
[54] P. P. Dash, "Design Methodology and Stability Analysis for a PhotoVoltaic (PV) Plant Interfaced with a Distribution Network," M.E.Sc. thesis, Electrical and Computer Engineering, The University of Western Ontario, London, ON, Canada, 2008.
[55] N. Kroutikova, C. a. Hernandez-Aramburo, and T. C. Green, "State-space model of grid-connected inverters under current control mode," *IET Electric Power Applications,* vol. 1, pp. 329-338, 2007.
[56] S. Podrucky, "Small Signal Modeling of Resonant Controlled VSC Systems," M.A.Sc. thesis, Computer and Electrical Engineering, University of Toronto, Toronto, Canada, 2009.
[57] A. Kashyap, "Small-signal Stability Analysis and Power System Stabilizer Design for Grid-Connected Photovoltaic Generation System," M.A.Sc. thesis, Electrical and Computer Engineering, Carleton University, Ottawa, Ontario, 2014.
[58] C. Se-Kyo, "A phase tracking system for three phase utility interface inverters," *IEEE Transactions on Power Electronics,* vol. 15, pp. 431-438, 2000.
[59] T. Messo, J. Jokipii, J. Puukko, and T. Suntio, "Determining the Value of DC-Link Capacitance to Ensure Stable Operation of a Three-Phase Photovoltaic Inverter," *IEEE Transactions on Power Electronics,* vol. 29, pp. 665-673, 2014.
[60] C.-T. Chen, *Linear System Theory and Design*. New York, NY: Oxford University Press, 1999.
[61] *Phase margin* [Online]. Available: https://en.wikipedia.org/wiki/Phase_margin

[62] C. Bajracharya, M. Molinas, J. A. Suul, and T. M. Undeland, "Understanding of tuning techniques of converter controllers for VSC-HVDC " in *Nordic Workshop on Power and Industrial Electronics* 2008.

[63] L.D.K.Solar. (February 2012). *LDK-230P-235P-20 Solar Module Datasheet* [Online]. Available: http://www.ldksolar.com/uploadfiles/down/LDK_230P_235P_20_Ontario_DCC_EN_V1_12_120229.pdf

[64] A. Samadi, E. Shayesteh, R. Eriksson, B. Rawn, and L. Söder, "Multi-objective coordinated droop-based voltage regulation in distribution grids with PV systems," *Renewable Energy,* vol. 71, pp. 315-323, 11// 2014.

[65] I. S. University. *Participation Factors* [Online]. Available: http://home.eng.iastate.edu/~jdm/ee554/Participation_factors.pdf

[66] J. Hahn, T. Edison, and T. F. Edgar. *A Note On Stability Analysis Using Bode Plots* [Online]. Available: http://www.engr.uky.edu/~aseeched/SummerSchool/2007/session_handouts/new_approaches/Process%20Control/Frequency%20Domain/A%20Note%20on%20Stability%20Analysis%20Using%20Bode%20Plots%20(2).pdf

[67] A. Samadi, M. Ghandhari, and L. Söder, "Reactive Power Dynamic Assessment of a PV System in a Distribution Grid," *Energy Procedia,* vol. 20, pp. 98-107, // 2012.

[68] R. Tonkoski and L. A. C. Lopes, "Voltage Regulation in Radial Distribution Feeders with High Penetration of Photovoltaic," in *Energy 2030 Conference, 2008. ENERGY 2008. IEEE*, 2008, pp. 1-7.

[69] Z. Yajing, M. Liang, and T. Q. Zheng, "Application of feedback linearization strategy in voltage fault ride-through for photovoltaic inverters," in *IECON 2011 - 37th Annual Conference on IEEE Industrial Electronics Society*, 2011, pp. 4666-4671.

[70] Correa-Tapasco.E, Mora-Flórez.J, and Pérez-Londoño.S, "Generalised strategy for implementing the minimum fault reactance based fault location algorithm in real power distribution systems," *Ingeniería e Investigación,* vol. 31, pp. 71-75, October 2011.

[71] D. Hou, "Comparing Fault Resistance Coverage of Different Distribution System Grounding Methods " in *37th Annual Western Protective Relay Conference*, 2010.

[72] S. A. Rahman, "Novel Controls of Photovoltaic (PV) Solar Farms," Ph.D. dissertation, Electrical and Computer Engineering, The University of Western Ontario, London, ON, Canada, 2012.

[73] F. Solar. (May 2011). *First Solar FS Series 2 PV Module Datasheet* [Online]. Available: http://www.gehrlicher.com/fileadmin/content/downloads/Modules/20110920_DB_FS_Serie_2_EN.pdf

Appendices

Appendix A: Linearized Matrices of State Space Models

A.1 Linearized matrices for Distribution Network Subsystem:

The system matrix A_{11} is a 18 * 18 matrix and is given by:

$A_{11} =$

$$\begin{vmatrix}
\frac{-R_g}{L_g} & \omega_o & \frac{-x_1^2}{L_g} & 0 & 0 & 0 & 0 & 0 & 0 & 0 & 0 & 0 & 0 & 0 & 0 & 0 & 0 & 0 \\
-\omega_o & \frac{-R_g}{L_g} & 0 & \frac{-x_1^2}{L_g} & 0 & 0 & 0 & 0 & 0 & 0 & 0 & 0 & 0 & 0 & 0 & 0 & 0 & 0 \\
\frac{1}{C_1} & 0 & 0 & \omega_o & -\frac{1}{C_1} & 0 & 0 & 0 & 0 & 0 & 0 & 0 & 0 & 0 & 0 & 0 & 0 & 0 \\
0 & \frac{1}{C_1} & -\omega_o & 0 & 0 & -\frac{1}{C_1} & 0 & 0 & 0 & 0 & 0 & 0 & 0 & 0 & 0 & 0 & 0 & 0 \\
0 & 0 & \frac{1}{L_1} & 0 & \frac{-R_1}{L_1} & \omega_o & -\frac{1}{L_1} & 0 & 0 & 0 & 0 & 0 & 0 & 0 & 0 & 0 & 0 & 0 \\
0 & 0 & 0 & \frac{1}{L_1} & -\omega_o & \frac{-R_1}{L_1} & 0 & -\frac{1}{L_1} & 0 & 0 & 0 & 0 & 0 & 0 & 0 & 0 & 0 & 0 \\
0 & 0 & 0 & 0 & \frac{1}{C_{23}} & 0 & 0 & \omega_o & -\frac{1}{C_2} & 0 & 0 & 0 & 0 & 0 & 0 & 0 & 0 & 0 \\
0 & 0 & 0 & 0 & 0 & \frac{1}{C_{23}} & -\omega_o & 0 & 0 & -\frac{1}{C_2} & 0 & 0 & 0 & 0 & 0 & 0 & 0 & 0 \\
0 & 0 & 0 & 0 & 0 & 0 & \frac{1}{L_2} & 0 & \frac{-R_2}{L_2} & \omega_o & -\frac{1}{L_2} & 0 & 0 & 0 & 0 & 0 & 0 & 0 \\
0 & 0 & 0 & 0 & 0 & 0 & 0 & \frac{1}{L_2} & -\omega_o & \frac{-R_2}{L_2} & 0 & -\frac{1}{L_2} & 0 & 0 & 0 & 0 & 0 & 0 \\
0 & 0 & 0 & 0 & 0 & 0 & 0 & 0 & \frac{1}{C_{45}} & 0 & 0 & \omega_o & \frac{-1}{C_{45}} & 0 & 0 & 0 & 0 & 0
\end{vmatrix}$$

$$\begin{vmatrix}
0 & 0 & 0 & 0 & 0 & 0 & 0 & 0 & 0 & \frac{1}{C_{45}} & -\omega_o & 0 & 0 & \frac{-1}{C_{45}} & 0 & 0 & 0 & 0 \\
0 & 0 & 0 & 0 & 0 & 0 & 0 & 0 & 0 & 0 & \frac{1}{L_3} & 0 & \frac{-R_3}{L_3} & \omega_o & \frac{-1}{L_3} & 0 & 0 & 0 \\
0 & 0 & 0 & 0 & 0 & 0 & 0 & 0 & 0 & 0 & 0 & \frac{1}{L_3} & -\omega_o & \frac{-R_3}{L_3} & 0 & \frac{-1}{L_3} & 0 & 0 \\
0 & 0 & 0 & 0 & 0 & 0 & 0 & 0 & 0 & 0 & 0 & 0 & \frac{1}{C_6} & 0 & 0 & \omega_o & \frac{-1}{C_6} & 0 \\
0 & 0 & 0 & 0 & 0 & 0 & 0 & 0 & 0 & 0 & 0 & 0 & 0 & \frac{1}{C_6} & -\omega_o & 0 & 0 & \frac{-1}{C_6} \\
0 & 0 & 0 & 0 & 0 & 0 & 0 & 0 & 0 & 0 & 0 & 0 & 0 & 0 & \frac{1}{L_L} & 0 & \frac{-R_L}{L_L} & \omega_o \\
0 & 0 & 0 & 0 & 0 & 0 & 0 & 0 & 0 & 0 & 0 & 0 & 0 & 0 & 0 & \frac{1}{L_L} & -\omega_o & \frac{-R_L}{L_L}
\end{vmatrix}$$

(A.1)

Matrix B_{11} is a 18 * 2 matrix and is given by,

$B_{11} =$

$$\begin{vmatrix}
0 & 0 \\
0 & 0 \\
0 & 0 \\
0 & 0 \\
0 & 0 \\
0 & 0
\end{vmatrix}$$

$$\begin{vmatrix} 0 & 0 \\ 0 & 0 \\ 0 & 0 \\ 0 & 0 \\ \frac{1}{C_{45}} & 0 \\ 0 & \frac{1}{C_{45}} \\ 0 & 0 \\ 0 & 0 \\ 0 & 0 \\ 0 & 0 \\ 0 & 0 \\ 0 & 0 \end{vmatrix} \quad \text{(A.2)}$$

Matrix B_{12} is a 18 * 2 matrix and is given by,

$B_{12} =$

$$\begin{vmatrix} 0 & 0 \end{vmatrix}$$

0	0
0	0
0	0
0	0
0	0
$\frac{1}{C_{23}}$	0
0	$\frac{1}{C_{23}}$
0	0
0	0
0	0
0	0
0	0
0	0
0	0
0	0
0	0
0	0
0	0

(A.3)

Matrix B_{13} is a 18 * 2 matrix and is given by,

$B_{13} =$

$\frac{x_1}{L_g}\widehat{V_g}\sin(\theta_o - \frac{\pi}{2} - \rho_o)$	i_{1qo}
$\frac{-x_1}{L_g}\widehat{V_g}\cos(\theta_o - \frac{\pi}{2} - \rho_o)$	$-i_{1do}$
0	V_{1qo}
0	$-V_{1do}$
0	i_{12qo}
0	$-i_{12do}$
0	V_{s1qo}
0	$-V_{s1do}$
0	i_{23qo}
0	$-i_{23do}$
0	V_{s2qo}

$$\begin{vmatrix} 0 & -V_{s2do} \\ 0 & i_{34qo} \\ 0 & -i_{34do} \\ 0 & V_{Lqo} \\ 0 & -V_{Ldo} \\ 0 & i_{Lqo} \\ 0 & -i_{Ldo} \end{vmatrix}$$

(A.4)

Matrix C_{311} is a 2 * 18 matrix and is given by,

$C_{311} =$

$$\begin{vmatrix} 0 & 0 & 0 & 0 & 0 & 0 & 1 & 0 & 0 & 0 & 0 & 0 & 0 & 0 & 0 & 0 & 0 & 0 \\ 0 & 0 & 0 & 0 & 0 & 0 & 0 & 1 & 0 & 0 & 0 & 0 & 0 & 0 & 0 & 0 & 0 & 0 \end{vmatrix}$$

(A.5)

A.2 Linearized matrices for PV Subsystem:

The system matrix A_{22} is a 7 * 7 matrix and is given by:

$A_{22} =$

$$
\begin{array}{|cccccc|}
\frac{-R_f}{L_f} & \omega_o & -\frac{1}{L_f} & 0 & \frac{R_c}{xL_f} & 0 \\
-\frac{R_c}{L_f} & & & & & \\
-\omega_o & \frac{-R_f}{L_f} & 0 & -\frac{1}{L_f} & 0 & \frac{R_c}{xL_f} \\
 & -\frac{R_c}{L_f} & & & & \\
\frac{1}{C_f} & 0 & 0 & \omega_o & \frac{-1}{xC_f} & 0 \\
0 & \frac{1}{C_f} & -\omega_o & 0 & 0 & \frac{-1}{xC_f} \\
\frac{R_c}{xL_t} & 0 & \frac{1}{xL_t} & 0 & \frac{-R_c}{x^2L_t} & \omega_o \\
0 & \frac{R_c}{xL_t} & 0 & \frac{1}{xL_t} & -\omega_o & \frac{-R_c}{x^2L_t} \\
\frac{-3m_{do}}{4C_{dc}} & \frac{-3m_{qo}}{4C_{dc}} & 0 & 0 & 0 & 0 \\
\end{array}
\quad
\begin{array}{|c|}
\hline
\frac{m_{do}}{2L_f} \\
\\
\frac{m_{qo}}{2L_f} \\
\\
0 \\
0 \\
0 \\
0 \\
\frac{-a_2a_3e^{a_3V_{dco}+a_4I_{pvo}}}{C_{dc}} \\
-\frac{a_2a_4e^{a_3V_{dco}+a_4I_{pvo}}Ipvvo}{C_{dc}} \\
-\frac{a_5}{C_{dc}} \\
\hline
\end{array}
\tag{A.6}
$$

Where

$$
I_{pvvo} = \frac{-a_2a_3e^{a_3V_{dco}+a_4I_{pvo}} - a_5}{1 + a_2a_4e^{a_3V_{dco}+a_4I_{pvo}}} \tag{A.7}
$$

Matrix B_{21} is a 7 * 2 matrix and is given by,

$B_{21} =$

$$\begin{vmatrix} 0 & 0 \\ 0 & 0 \\ 0 & 0 \\ 0 & 0 \\ \frac{-1}{L_t} & 0 \\ 0 & \frac{-1}{L_t} \\ 0 & 0 \end{vmatrix}$$

(A.8)

Matrix B_{22} is a 7 * 1 matrix and is given by,

$B_{22} =$

$$\begin{vmatrix} 0 \\ 0 \\ 0 \\ 0 \end{vmatrix}$$

$$\begin{vmatrix} 0 \\ 0 \\ \frac{a_1}{C_{dc}} \\ -\frac{a_2 a_4 e^{a_3 V_{dco} + a_4 I_{pvo}} Ipvgo}{C_{dc}} \end{vmatrix} \tag{A.9}$$

Where,

$$I_{pvgo} = \frac{a_1}{1 + a_2 a_4 e^{a_3 V_{dco} + a_4 I_{pvo}}} \tag{A.10}$$

Matrix B_{231} is a 7 * 2 matrix and is given by,

$B_{231} =$

$$\begin{vmatrix} \frac{V_{dco}}{2L_f} & 0 \\ 0 & \frac{V_{dco}}{2L_f} \\ 0 & 0 \\ 0 & 0 \\ 0 & 0 \\ 0 & 0 \\ \frac{-3i_{tdo}}{4C_{dc}} & \frac{-3i_{tqo}}{4C_{dc}} \end{vmatrix} \tag{A.11}$$

Matrix B_{232} is a 7 * 1 matrix and is given by,

$B_{232} =$

$$\begin{vmatrix} i_{tqo} \\ -i_{tdo} \\ V_{cfqo} \\ -V_{cfdo} \\ i_{s1qo} \\ -i_{s1do} \\ 0 \end{vmatrix}$$

(A.12)

Matrix C_{22} is a 2 * 7 matrix and is given by,

$C_{22} =$

$$\begin{vmatrix} 0 & 0 & 0 & 0 & 1 & 0 & 0 \\ 0 & 0 & 0 & 0 & 0 & 1 & 0 \end{vmatrix}$$

(A.13)

Matrix C_{322} is a 7 * 7 matrix and is given by,

$C_{322} =$

$$\begin{vmatrix} 0 & 0 & 1 & 0 & 0 & 0 & 0 \\ 0 & 0 & 0 & 1 & 0 & 0 & 0 \\ 1 & 0 & 0 & 0 & 0 & 0 & 0 \\ 0 & 1 & 0 & 0 & 0 & 0 & 0 \\ 0 & 0 & 0 & 0 & 1 & 0 & 0 \\ 0 & 0 & 0 & 0 & 0 & 1 & 0 \\ 0 & 0 & 0 & 0 & 0 & 0 & 1 \end{vmatrix}$$

(A.14)

A.3 Linearized matrices for Controller Subsystem

As pointed out in section 2.6.3, the rows and columns to be removed from the matrices in order to eliminate the state x_7 have been shown boxed in black using dotted lines in the following matrices. For obtaining model for Full PV mode operation, the rows and columns to be removed are highlighted in yellow.

The system matrix A_{33} is a 11 * 11 matrix and is given by:

$A_{33} =$

$$\begin{vmatrix} 0 & 0 & 0 & b_2 & 0 & 0 & 0 & 0 & 0 & 0 & 0 \\ 1 & 0 & 0 & b_1 & 0 & 0 & 0 & 0 & 0 & 0 & 0 \end{vmatrix}$$

0	0	$\frac{-1}{\tau_2}$	0	0	0	0	0	0	0	0
0	0	0	$\frac{-1}{\tau_2}$	0	0	0	0	0	0	0
0	0	0	0	$\frac{-1}{\tau_1}$	0	0	0	0	0	0
0	0	0	0	0	$\frac{-1}{\tau_1}$	0	0	0	0	0
0	0	0	0	0	0	0	$K_{ii1}K_{iv}$	$K_{ii1}K_{pv}$	0	0
0	0	0	0	0	0	0	0	1	0	0
0	0	0	0	0	0	0	0	$\frac{-1}{\tau_{Vdc}}$	0	0
0	0	$\frac{-3K_{ii2}K_{pvs}K_{droop}i_{tqo}}{2}$	0	$\frac{K_{ii2}K_{pvs}V_{s1do}}{\sqrt{V_{s1do}^2+V_{s1qo}^2}}$	$\frac{K_{ii2}K_{pvs}V_{s1qo}}{\sqrt{V_{s1do}^2+V_{s1qo}^2}}$	0	0	0	0	$-K_{ii2}K_{ivs}$
0	0	$\frac{3K_{droop}i_{tqo}}{2}$	0	$\frac{-V_{s1do}}{\sqrt{V_{s1do}^2+V_{s1qo}^2}}$	$\frac{-V_{s1qo}}{\sqrt{V_{s1do}^2+V_{s1qo}^2}}$	0	0	0	0	0

(A.15)

Matrix B_{331} is a 11 * 2 matrix and is given by,

$B_{331} =$

0	0
0	0
0	0
0	0
$\frac{1}{\tau_1}$	0

$$\begin{bmatrix} 0 & \frac{1}{\tau_1} \\ 0 & 0 \\ 0 & 0 \\ 0 & 0 \\ 0 & 0 \\ 0 & 0 \end{bmatrix} \tag{A.16}$$

Matrix B_{332} is a 11 * 7 matrix and is given by,

$B_{332} =$

$$\begin{bmatrix} 0 & 0 & 0 & 0 & 0 & 0 & 0 \\ 0 & 0 & 0 & 0 & 0 & 0 & 0 \\ \frac{1}{\tau_2} & 0 & \frac{R_c}{\tau_2} & 0 & \frac{-R_c}{x\tau_2} & 0 & 0 \\ 0 & \frac{1}{\tau_2} & 0 & \frac{R_c}{\tau_2} & 0 & \frac{-R_c}{x\tau_2} & 0 \\ 0 & 0 & 0 & 0 & 0 & 0 & 0 \\ 0 & 0 & 0 & 0 & 0 & 0 & 0 \\ 0 & 0 & -K_{ii1} & 0 & 0 & 0 & 0 \\ 0 & 0 & 0 & 0 & 0 & 0 & 0 \\ 0 & 0 & 0 & 0 & 0 & 0 & \frac{1}{\tau_{Vdc}} \end{bmatrix}$$

0	0	0	$\frac{-3K_{ii2}K_{pvs}K_{droop}V_{cdo}}{2} - K_{ii2}$	0	0	0
0	0	0	$\frac{3K_{droop}V_{cdo}}{2}$	0	0	0

(A.17)

Matrix B_{333} is a 11 * 2 matrix and is given by,

$B_{333} =$

0	0
0	0
0	0
0	0
0	0
0	0
0	0
0	0
$\frac{-1}{\tau_{Vdc}}$	0
0	$-K_{ii2}K_{pvs}$
0	1

(A.18)

Matrix $B_{33\omega}$ is a 11 * 1 matrix and is given by

$B_{33\omega} =$

$$\begin{vmatrix} 0 \\ 0 \\ 0 \\ 0 \\ 0 \\ 0 \\ 0 \\ 0 \\ 0 \\ 0 \\ 0 \end{vmatrix}$$

(A.19)

Matrix C_{13} is a 2 * 11 matrix and is given by,

$C_{13}=$

$$\begin{vmatrix} 0 & 1 & 0 & 0 & 0 & 0 & 0 & 0 & 0 & 0 & 0 \\ 1 & 0 & 0 & b_1 & 0 & 0 & 0 & 0 & 0 & 0 & 0 \end{vmatrix}$$

(A.20)

Matrix C_{23m} is a 2 * 11 matrix and is given by,

C_{23m}=

$$\begin{bmatrix} 0 & 0 & \frac{2}{V_{dco}} & 0 & 0 & 0 & \frac{2}{V_{dco}} & \frac{2K_{pi1}K_{iv}}{V_{dco}} & \frac{2K_{pi1}K_{pv}}{V_{dco}} & 0 & 0 \\ 0 & 0 & \frac{-3K_{pi2}K_{pvs}K_{droop}i_{tqo}}{V_{dco}} & \frac{2}{V_{dco}} & \frac{2K_{pi2}K_{pvs}V_{s1do}}{V_{dco}\sqrt{V_{s1do}^2+V_{s1qo}^2}} & \frac{2K_{pi2}K_{pvs}V_{s1qo}}{V_{dco}\sqrt{V_{s1do}^2+V_{s1qo}^2}} & 0 & 0 & 0 & \frac{2}{V_{dco}} & \frac{-2K_{pi2}K_{ivs}}{V_{dco}} \end{bmatrix}$$

(A.21)

Matrix C_{ω} is a 1 * 11 matrix and is given by

C_{ω} =

$$\begin{bmatrix} 1 & 0 & 0 & b_1 & 0 & 0 & 0 & 0 & 0 & 0 & 0 \end{bmatrix}$$

(A.22)

Matrix D_{231} is a 2 * 2 matrix and is given by

D_{231} =

$$\begin{bmatrix} 0 & 0 \\ 0 & 0 \end{bmatrix}$$

(A.23)

Matrix D_{232} is a 2 * 7 matrix and is given by

D_{232} =

$$\begin{vmatrix} 0 & 0 & \frac{-2K_{pi1}}{V_{dco}} & \frac{-2L_f\omega_o}{V_{dco}} & 0 & 0 & -\frac{1}{V_{dco}^2}\{2K_{pi1}K_{pv}x_{6o} + 2K_{pi1}K_{iv}x_{5o} - 2K_{pi1}i_{tdo} + 2x_{3o} - 2L_f\omega_o i_{tqo} + 2V_{cdo}\} \\ 0 & 0 & \frac{2L_f\omega_o}{V_{dco}} & \frac{-3K_{pi2}K_{pvs}K_{droop}V_{cdo}}{V_{dco}} - \frac{2K_{pi2}}{V_{dco}} & 0 & 0 & -\frac{1}{V_{dco}^2}\{-2K_{pi2}K_{pvs}V_{pccref} + 2K_{pi2}K_{pvs}\sqrt{V_{s1do}^2 + V_{s1qo}^2} - 3K_{pi2}K_{pvs}K_{droop}V_{cdo}i_{tqo} - 2K_{pi2}K_{ivs}x_{7o} - 2K_{pi2}i_{tqo} + 2x_{4o} + 2L_f\omega_o i_{tdo} + 2V_{cqo}\} \end{vmatrix}$$

(A.24)

Where,

$$x_{3o} = u_{do} \tag{A.25}$$

$$x_{4o} = u_{qo} \tag{A.26}$$

$$x_{5o} = \frac{i_{tdo}}{K_{iv}} \tag{A.27}$$

$$x_{6o} = 0 \tag{A.28}$$

$$x_{7o} = -\frac{K_{pvs}V_{pccref}}{K_{ivs}} + \frac{K_{pvs}\sqrt{V_{s1do}^2 + V_{s1qo}^2}}{K_{ivs}} - \frac{3K_{pvs}K_{droop}V_{cdo}i_{tqo}}{2K_{ivs}} - \frac{i_{tqo}}{K_{ivs}} \tag{A.29}$$

Matrix D_{233} is a 2 * 2 matrix and is given by

$D_{233} =$

$$\begin{vmatrix} 0 & 0 \\ 0 & \dfrac{-2K_{pi2}K_{pvs}}{V_{dco}} \end{vmatrix}$$

Matrix $D_{23\omega}$ is a 2 * 1 matrix and is given by

$D_{23\omega} =$

$$\begin{vmatrix} \dfrac{-2L_f i_{tqo}}{V_{dco}} \\ \dfrac{2L_f i_{tdo}}{V_{dco}} \end{vmatrix}$$

(A.30)

Appendix B: Study System Parameters

Table B. 1 Parameters of the distribution network and PV STATCOM

Component	Parameter	Value
Distribution Network	$\widehat{V_g}$	99.06 kV
	r	0.1691 Ω/km
	x_l	0.4182 Ω/km
	b	3.954 $\mu S/km$
	f_s	60 Hz
	ω_o	376.8 rad/sec
	x_1	115 kV / 27.6 kV
	L_t	0.0548 H
	R_g	0.0277 Ω
	L_G	2.28 mH
Load parameters for peak daytime load (	R_L	130.7933 Ω
	L_L	0.1584 H
PV Panel	$I_{sc(STC)}$	8.43 A
	K_i	0.06 % / ℃
	T_s	25 ℃ (298.15 K)
	n_s	60
	$I_{mp(STC)}$	7.88 A

	$V_{mp(STC)}$	29.3 V
	n_p	1
	R_{sh}	2344.42 Ω
	R_S	0.00527 Ω
	$V_{oc(STC)}$	36.9 V
	K_v	-0.33 % / ℃
	n	1.21328
	k	1.38064 X 10^{-23} m^2 Kg $s^{-2}K^{-1}$
	G_{nom}	1 kW/m^2
	N_p	1056
	N_s	35
Inverter, Filter and Coupling Transformer	R_{on}	1 mΩ
	C_{dc}	25000 μF
	L_f	30 μH
	C_f	500 μF
	V_{dc}	1.0255 kV
	R_{fL}	1 mΩ
	R_c	0.1 Ω
	L_t	0.0201 H (referred to HV side)

	x	0.48 kV/ 27.6 kV
	f_{sw}	5940 Hz
Measurement Filter	τ_1	0.002 sec (starting value)
	τ_2	0.002 sec (starting value)
DC-Link voltage controller	τ_{Vdc}	0.001 sec
Thevenin inductance	$L_{thevenin}$	0.0381 H

Table B. 2 Operating point data for DC-Link Voltage Controller design

Parameter	Value
G	0.85 kW/m^2
P_{pvo}	7.225 MW
V_{dco}	1.0255 kV
I_{pvo}	7.04 kA
V_{cdo}	0.3918 kV
I_{tdo}	12.294 kA
m_{do}	0.7968

Calculation of per unit voltage:

$$\text{Per Unit (pu)Voltage} = \frac{\text{Actual Voltage}}{\text{Base Voltage}} \quad \text{(B.1)}$$

Base Voltage is chosen as the peak value of phase voltage at PCC which is 22.53 kV.

Table B. 3 Calculation of parameters of Volt/Var curve for $V_d = 1.06$ pu

Parameter	Value
P_N	8.5 MW
$\tan \varphi_{max}$	0.3286
ΔV_{droop}	1.3158 kV
V_{cdo}	0.3919 kV

Transfer Function from i_{tqref} to V_{pcc} about the operating G = 0.85 is,

$$\frac{\widetilde{V_{pcc}}(s)}{\widetilde{i_{tqref}}(s)} = \frac{num\ (s)}{den\ (s)} \tag{B.2}$$

Where for proportional controller:

num (s) = 1.054e11 s^30 + 3.888e15 s^29 + 3.519e21 s^28 + 1.287e26 s^27 + 4.271e31 s^26 + 1.536e36 s^25 + 2.393e41 s^24 + 8.321e45 s^23 + 7.038e50 s^22 + 2.289e55 s^21 + 1.124e60 s^20 + 3.271e64 s^19 + 9.32e68 s^18 + 2.263e73 s^17 + 3.488e77 s^16 + 6.095e81 s^15 + 4.827e85 s^14 + 6.111e89 s^13 + 4.424e93 s^12 + 1.79e97 s^11 + 4.647e100 s^10 + 8.445e103 s^9 + 1.126e107 s^8 + 1.125e110 s^7 + 8.458e112 s^6 + 4.736e115 s^5 + 1.929e118 s^4 + 5.47e120 s^3 + 1.001e123 s^2 + 1.005e125 s + 3.115e126

den (s) = s^33 + 4.824e04 s^32 + 3.556e10 s^31 + 1.655e15 s^30 + 4.75e20 s^29 + 2.091e25 s^28 + 3.076e30 s^27 + 1.241e35 s^26 + 1.091e40 s^25 + 3.891e44 s^24 + 2.223e49 s^23 + 6.685e53 s^22 + 2.587e58 s^21 + 6.123e62 s^20 + 1.614e67 s^19 + 2.716e71 s^18 + 4.697e75 s^17 + 5.068e79 s^16 + 5.576e83 s^15 + 3.754e87 s^14 + 2.428e91 s^13 + 9.153e94 s^12 + 2.268e98 s^11 + 4.117e101 s^10 + 5.749e104 s^9 + 6.315e107 s^8 + 5.498e110 s^7 + 3.771e113 s^6 + 1.993e116 s^5 + 7.825e118 s^4 + 2.164e121 s^3 + 3.872e123 s^2 + 3.838e125 s + 1.19e127

Where for PI controller:

num (s) = 1.063e11 s^30 + 3.933e15 s^29 + 3.55e21 s^28 + 1.302e26 s^27 + 4.31e31 s^26 + 1.554e36 s^25 + 2.416e41 s^24 + 8.416e45 s^23 + 7.11e50 s^22 + 2.315e55 s^21 + 1.136e60 s^20 + 3.311e64 s^19 + 9.443e68 s^18 + 2.293e73 s^17 + 3.546e77 s^16 + 6.19e81 s^15 + 4.927e85 s^14 + 6.209e89 s^13 + 4.491e93 s^12 + 1.82e97 s^11 + 4.733e100 s^10 + 8.612e103 s^9 + 1.148e107 s^8 + 1.145e110 s^7 + 8.584e112 s^6 + 4.789e115 s^5 + 1.943e118 s^4 + 5.49e120 s^3 + 1.001e123 s^2 + 1.003e125 s + 3.107e126

den (s) = s^33 + 4.824e04 s^32 + 3.556e10 s^31 + 1.655e15 s^30 + 4.75e20 s^29 + 2.091e25 s^28 + 3.076e30 s^27 + 1.241e35 s^26 + 1.091e40 s^25 + 3.891e44 s^24 + 2.223e49 s^23 + 6.685e53 s^22 + 2.587e58 s^21 + 6.123e62 s^20 + 1.614e67 s^19 + 2.716e71 s^18 + 4.697e75 s^17 + 5.068e79 s^16 + 5.575e83 s^15 + 3.754e87 s^14 + 2.428e91 s^13 + 9.151e94 s^12 + 2.268e98 s^11 + 4.116e101 s^10 + 5.748e104 s^9 + 6.314e107 s^8 + 5.498e110 s^7 + 3.77e113 s^6 + 1.992e116 s^5 + 7.819e118 s^4 + 2.161e121 s^3 + 3.861e123 s^2 + 3.823e125 s + 1.185e127

Table B. 4 DC-link voltage controller parameters and operating point data for Full STATCOM operation

Parameter	Value
m_{do}	0.7446
K_{iv}	8100
n_o	4.9
z_o	93.89
p_o	2253.5

Appendix C: Parameters used for simulation in Chapter 4

Table C. 1 Parameters of 9.9 MW PV system

Parameter	Value
N_p	1076
N_s	40
V_{dc}	1.172 kV
C_{dc}	25000 μF
L_t	0.0168 H (referred to HV side)

Table C. 2 DC-link voltage controller parameters of 9.9 MW PV system

Parameter	G=0.85 kW/m^2
K_{pv}	21.70
K_{iv}	4822.3
τ_{Vdc}	1 ms

Appendix D: Parameters used for simulation in Chapter 5

Table D. 1 Parameters of PV array designed using FS 272 PV panel

Parameter	8.5 MW PV system	9.9 MW PV system
N_p	7238	7587
N_s	16	18
V_{dc} (Maximum power point voltage for G = 1 kW/m^2)	1.0656 kV	1.1988 kV
C_{dc}	25000 μF	25000 μF
V_{dc} (Open circuit voltage of PV array)	1.4192 kV	1.5966 kV

Calculation of proportional gain based on required reactive current injection:

$$\mathrm{K_{pvs}} = \frac{\text{Peak Current Rating of inverter in kA}}{(1 - \mathrm{x_v}) * 22.53} \quad \text{(D.1)}$$

Where x_v is the maximum value of voltage (in pu) beyond which 100 % reactive current injection is required as per the German grid code.

The peak current rating of inverter is 14.45 kA for 8.5 MW PV system and 16.84 kA for 9.9 MW PV system.

Curriculum Vitae

Name:	Sridhar Bala Subramanian
Post-secondary Education and Degrees:	SSN College of Engineering (affiliated to Anna University) Tamil Nadu, India 2007-2011 B.E. The University of Western Ontario London, Ontario, Canada 2014-2016 M.E.Sc.
Honours and Awards:	Natural Sciences and Engineering Research Council of Canada Industrial Postgraduate Scholarship 1 (NSERC IPS 1) 2015, Co-funded by Bluewater Power Corporation, Sarnia Merit Scholarship from SSN Institutions, India 2007-2008
Related Work Experience:	Management Trainee - System & Support Design Engineer SWELECT Energy Systems Limited, India 2013-2014 Officer – Electrical Maintenance ITC Limited (Paperboards & Specialty Papers Division), India 2011-2012

Publications (tentative details subject to change)

[1] R. K. Varma and Sridhar.BS, “Smart PV Inverter Voltage Control Strategies”, Paper under preparation to be submitted to *IEEE Transactions on Sustainable Energy*.